MONASH University

Chemokine Recognition and Signalling by the Chemokine Receptor CCR1

Julie Sanchez

B.Sc., M.E.

A thesis submitted for the degree of *Doctor of Philosophy* at

Monash University in *2017*

Department of Biochemistry and Molecular Biology

The Faculty of Medicine, Nursing and Health Sciences

Copyright notice

Abstract

Inflammation is a natural response of our bodies to injury or infection. This protective mechanism involves the recruitment of leukocytes to the damaged area and is driven in part by chemokines expressed by the affected tissues. Chemokines are small soluble proteins that stimulate leukocyte recruitment by activation of chemokine receptors, a subfamily of G protein-coupled receptors (GPCRs) expressed on leukocytes. Chemokine:receptor interactions play critical roles in a wide range of inflammatory diseases, such as multiple sclerosis and asthma, as well as in HIV, cancer and diabetes.

To describe chemokine:receptor interactions, the two-site model was developed in 1997 by Crump *et al.* In this model, two sites of interaction are separated both spatially and functionally. Site 1, involving the N-terminus of the receptor and a small groove on the chemokine core, is considered to provide the dominant interactions required for binding, whereas site 2, involving the N-terminus of the chemokine and the receptor transmembrane bundle, is involved only in receptor activation.

Among the chemokine receptor family, CCR1 is particularly interesting because it is recognised as a drug target for multiple sclerosis and rheumatoid arthritis but is a highly promiscuous receptor, as it can recognise more than nine CC chemokines, including HCC-2/CCL15, MCP-3/CCL7 and MCP-2/CCL8. The existence of multiple ligands for the same receptor was once considered to be redundancy. However, it is now recognised that receptors can exhibit biased agonism, the ability to give different signalling responses depending on which ligand it is bound to. In Chapter 3, we characterised biased agonism at CCR1 by measuring activation of several signalling pathways (ERK1/2 phosphorylation, inhibition of cAMP production, β-arrestin recruitment and G protein activation). Bias factors calculated from these data showed that CCR1 exhibits biased agonism. To further investigate this phenomenon, we studied the effects of post-translational tyrosine sulfation of the receptor and N-terminal modifications of the chemokines. Our results showed that the chemokine N-terminus is crucial for receptor activation as predicted by the two-site model. However, it might not be the only important region.

The results of Chapter 3 led us to explore the two-site model further, as it seemed not to be entirely applicable to CCR1. In Chapter 4, we studied site 1 interactions by comparing the affinities of chemokines for CCR1 and for peptides with the sequence of the CCR1 N-terminus. The data showed that the receptor N-terminus was not sufficient to account for the total binding affinity or

chemokine selectivity. In addition, to investigate site 2 interactions, ten chimeric chemokines between MCP-1 and MCP-3 were tested for CCR1 activation, showing that the important regions of the chemokine for CCR1 activation were the N-terminus as expected, but also the N-loop, which was unexpected. Based on these results, we proposed an elaboration of the two-site model, which is discussed in Chapter 6.

A significant effort has been made to develop chemokine receptor antagonists that inhibit pathological leukocyte trafficking. However, it has proved to be a huge challenge due the complexity of the chemokine:receptor network. Thus, there is much interest in developing new ways of modulating leukocyte recruitment, including the use of chemokine antagonists. Previously, chemokine-inhibitory activity in the saliva of one tick species has been attributed to three small proteins called evasins. These evasins are thought to enable the tick to avoid immune detection by its host, thus prolonging blood feeding. In Chapter 5, we hypothesised that other ticks also produce evasins to disrupt the host immune system so we set out to identify more members of the evasin family from a variety of tick species. We used sequence-based searches and bioinformatic tools to identify 257 putative members from three tick genera. Twelve promising candidates were expressed and screened for chemokine-binding activity using a fluorescence anisotropy assay. Eight candidates bound to chemokines and three out of four candidates tested showed chemokine-inhibitory activity.

Overall, this project provides novel information in the chemokine and evasin fields. We characterised CCR1 biased agonism and proposed an extended model to describe chemokine:receptor interactions. In addition, we identified novel evasins able to inhibit chemokine activity. These results will contribute to ongoing efforts to improve our understanding of the chemokine:receptor network and will help the development of chemokine antagonists as therapeutics for inflammatory diseases.

Declaration

This thesis contains no material which has been accepted for the award of any other degree or diploma at any university or equivalent institution and that, to the best of my knowledge and belief, this thesis contains no material previously published or written by another person, except where due reference is made in the text of the thesis.

Signature:  ……

Print Name: …Julie Sanchez…

Date: ……..18/12/2017…

Publications during enrolment

Hayward J.*, **Sanchez J.***, Perry, A., Huang, C., Rodriguez Valle M., Canals M., Payne R. J & Stone M. J. (2017). Ticks from diverse genera encode chemokine-inhibitory evasin proteins. *J. Biol. Chem. 292*(38), 15670-15680. *, these authors contributed equally to this work.

Huma, Z. E., **Sanchez, J.**, Lim, H. D., Bridgford, J. L., Huang, C., Parker, B. J., Pazhamalil J. L., Porebski B. T., Pfleger K. D. G., Lane J. R., Canals M. & Stone, M. J. (2017). Key determinants of selective binding and activation by the monocyte chemoattractant proteins at the chemokine receptor CCR2. *Sci Signal, 10*(480).

Wang, X., **Sanchez, J.**, Stone, M. J., & Payne, R. J. (2017). Sulfation of the Human Cytomegalovirus Protein UL22A Enhances Binding to the Chemokine RANTES. *Angew Chem Int Ed Engl, 56*, 1-6.

Stone, M. J., Hayward, J. A., Huang, C., Z, E. H., & **Sanchez, J.** (2017). Mechanisms of Regulation of the Chemokine-Receptor Network. *Int J Mol Sci, 18*(2).

Isahak, N., **Sanchez, J.**, Perrier, S., Stone, M. J., & Payne, R. J. (2016). Synthesis of polymers and nanoparticles bearing polystyrene sulfonate brushes for chemokine binding. *Org Biomol Chem, 14*(24), 5652-5658.

Thesis including published works declaration

I hereby declare that this thesis contains no material which has been accepted for the award of any other degree or diploma at any university or equivalent institution and that, to the best of my knowledge and belief, this thesis contains no material previously published or written by another person, except where due reference is made in the text of the thesis.

This thesis includes one original paper published in peer reviewed journals. The core theme of the thesis is chemokine receptor interactions. The ideas, development and writing up of all the papers in the thesis were the principal responsibility of myself, the student, working within the Department of Biochemistry and Molecular Biology under the supervision of Associate Professor Martin J. Stone.

The inclusion of co-authors reflects the fact that the work came from active collaboration between researchers and acknowledges input into team-based research.

In the case of *Chapter 5* my contribution to the work involved the following:

- *Expression and purification of various evasin and chemokine proteins*
- *Collection and analysis of the chemokine binding data*
- *Collection and analysis of the chemokine inhibition data*
- *Interpretation of data*
- *Manuscript preparation, figure generation and writing of the first draft.*

Thesis Chapter	Publication Title	Status	Nature and % of student contribution	Co-author name(s) Nature and % of Co-author's contribution*	Co-author(s), Monash student Y/N
5	Ticks from diverse genera encode chemokine-inhibitory evasin proteins	Published	50% Research design, data collection and analysis, and writing of first draft	1) Jenni Hayward, research design, bioinformatic searches, data collection and analysis and first draft writing 40% 2) Andrew Perry, bioinformatics searches 2% 3) Cheng Huang, collection and analysis of mass spectrometry data 1% 4) Manuel Rodriguez Valle, collection of transcriptomics data 1% 5) Meritxell Canals, design and supervision of inhibition assays 1% 6) Richard J. Payne, study concept and experiment design and interpretation 1% 7) Martin J. Stone, study concept, experiment design and interpretation and manuscript writing 4%	Yes No Yes No No No No

I have not renumbered sections of submitted or published papers in order to generate a consistent presentation within the thesis.

Student signature:  **Date: 18/12/2017**

The undersigned hereby certify that the above declaration correctly reflects the nature and extent of the student's and co-authors' contributions to this work. In instances where I am not the responsible author I have consulted with the responsible author to agree on the respective contributions of the authors.

Main Supervisor signature:  **Date: 18/12/2017**

Acknowledgements

My acknowledgements could not start with anyone else than my primary supervisor Associate Professor Martin J. Stone. This project would not have been possible without you. I have learnt and grown so much over the last four years, both professionally and personally. You have always been supportive and available when I needed help. You are an exceptional scientist, inspiring teacher and a wonderful mentor. I cannot thank you enough for this amazing and challenging opportunity and I am grateful to have found such a rewarding collaboration.

I also would like to thank my secondary supervisor Professor Richard J. Payne and his laboratory (Eileen, Johnny, Eric) at The University of Sydney. It has been inspiring to see you strive for excellence and encourage everyone in your group including me, to achieve their best and more. You kept my inner chemist content and provided a fruitful environment to work in.

Another invaluable collaboration to this project was with Dr. Meritxell Canals at Monash Institute of Pharmaceutical Sciences. You allowed me to discover the fantastic work performed at Drug Discovery Biology. You always found some time to help me, although it was never easy between Jack and Columbia University. I have gained new and valuable skills under your supervision and I could not be happier to have joined your group. I take this opportunity to thank the entire "CaHaLa" group: Dr. Michelle L. Halls, Dr J. Robert Lane, Dr Srgjan Chivchiristov, Dr Herman Lim, Alastair Keen and Maxine Roberts for their generous support and time in the final stages of this project.

As studying has its ups and downs, I would like to thank my fellow students from our international office B109 who I shared this journey with: Cheng (Enzo) Huang, Zil E Huma, Nathan Habila, Baydaa Hirmiz, Sayeeda T. Chowdhury, Melissa Honeydew and particularly Jenni A. Hayward who worked with me on the evasin project. We learnt a lot from each other and you became a great friend and support. You did an amazing job and this project would not have been the same without you.

Over the years, I received great insight and advice from many people. I acknowledge my PhD committee: Professor Marie-Isabel Aguilar, Associate Professor Jacqueline A. Wilce and Associate Professor Michelle A. Dunstone who agreed to follow the progress of my candidature and dedicated their time, experience and guidance. In addition, I appreciate the help I received from all our collaborators, co-authors and people who contributed to the success of this project, especially our

former neighbours from the Wilce laboratory and Professor Matthew C.J. Wilce for sharing some crystallography wisdom with me.

I am thankful for my family and friends who are always there for me, particularly my sister, Laura Sanchez, who is a great moral booster and biology expert. It means a lot to know that I have people I can count on, no matter how far or close I am.

Finally, I would like to thank my fiancé and partner of six years, Akshar Apte, who encouraged, helped and believed in me throughout this challenging process. You were always positive when it was tough for me and I am glad to have you by my side.

Table of Contents

Table of Contents

List of General Abbreviations

β-arr	β-arrestin
AC	Adenylyl cyclase
AFU	Arbitrary fluorescence unit
AIDS	Acquired immune deficiency syndrome
ANOVA	Analysis of variance
ATP	Adenosine triphosphate
BCA	Bicinchoninic acid
BRET	Bioluminescence resonance energy transfer
cAMP	Cyclic adenosine monophosphate
CCR1	CC chemokine receptor 1
CHAPS	3-[(3-Cholamidopropyl)dimethylammonio]-1-propanesulfonic acid
Da	Dalton
DMEM	Dulbecco's modified eagle medium
DNA	Deoxyribose nucleic acid
dNTPs	Deoxynucleotide triphosphates
DSS	4,4-dimethyl-4-silapentane-1-sulfonic acid
ECL	Extracellular loop
EDTA	Ethylenediaminetetraacetic acid
ELISA	Enzyme linked immunosorbent assay
Epac	Exchange factor activated by cAMP
ERK1/2	Extracellular signal regulated kinase 1/2
Ev	Evasin
FAA	Fluorescence anisotropy assay
FBS	Fetal bovine serum
Fl	Fluorescein
FRET	Fluorescence resonance energy transfer
Fsk	Forskolin
GAG	Glycosaminoglycan
GDP	Guanosine diphosphate
GEF	Guanine nucleotide exchange factor
GFP	Green fluorescent protein
GPA	G protein activation
GPCR	G protein-coupled receptor
GRK	G protein-coupled receptor kinase
GTP	Guanosine triphosphate

HBSS	Hanks' balanced salt solution
HEK 293	Human embryonic kidney 293 cell line
HIV	Human immunodeficiency virus
ICL	Intracellular loop
IMAC	Immobilised metal affinity chromatography
IP3	Inositol triphosphate
IPTG	Isopropyl β-D-1-thiogalactopyranoside
LB	Luria-Bertani
MALDI-TOF	Matrix-assisted laser desorption/ionisation-time of flight
MAPK	Mitogen activated protein kinases
MCP	Monocyte chemoattractant protein
MOPS	3-(N-morpholino)propanesulfonic acid
MS	Multiple sclerosis
NK	Natural killer
NMR	Nuclear magnetic resonance
PAPS	3'-phosphoadenosine-5'-phosphosulfate
PBS	Phosphate buffered saline
PCR	Polymerase chain reaction
PDB	Protein data bank
pEC_{50}	-$\log_{10}EC_{50}$ where EC_{50} is the concentration of compound required for 50% activation
PEG	Polyethylene glycol
PEI	Polyethylenimine
pERK	Phosphorylated ERK
pIC_{50}	-$\log_{10}IC_{50}$ where IC_{50} is the concentration of compound required for 50% inhibition
PKA	Protein kinase-A
pK_d	-$\log_{10}K_d$ where K_d is the dissociation constant
PLC	Phospholipase C
PMSF	Phenylmethane sulfonyl fluoride
ppm	Parts per million
PSEC	Preparative size exclusion chromatography
RA	Rheumatoid arthritis
RGS	Regulators of G protein signalling
Rluc	Renilla luciferase
RNA	Ribonucleic acid
RP-HPLC	Reverse phase high-performance liquid chromatography
RSA	Rhipicephalus sanguineus
RT	Room temperature
SDS-PAGE	Sodium dodecyl sulfate polyacrylamide gel electrophoresis

SECRET	Smallpox virus-encoded chemokine receptor
SEM	Standard error of the mean
SFM	Serum-free media (DMEM)
SPPS	Solid-phase peptide synthesis
TEMED	Tetramethylethylenediamine
TEV	Tobacco etch virus
TM	Transmembrane
TPST	Tyrosylprotein sulfotransferase
T-Rex	Tetracycline-regulated expression
YFP	Yellow fluorescent protein

Chapter 1. Introduction

1.1. Biological Background

1.1.1. Inflammation and Diseases

Inflammation is a healthy reaction of our body to various types of trauma, such as pathogens, damaged cells or irritants, and is part of a highly complex biological response of vascular tissues to these harmful stimuli. Inflammation is a protective attempt by an organism to remove the source of trauma and initiate the healing process. This process involves the activation and maturation of our immune system for it to be ready to fight any invader recognised as foreign. The five common expressions of inflammation are heat, redness, swelling, pain and loss of function [1]. Inflammation can be classified as either acute or chronic depending on the duration of the disease development, acute conditions being sudden and chronic conditions being, by contrast, long-developing syndromes. Without inflammatory responses, wounds and infections would never heal and progressive destruction of the tissue would compromise the survival of the organism.

Acute inflammation is the initial response of the body to a sudden threat, including pathogen infection or tissue damage and it involves the increased movement of plasma and leukocytes from the blood to the site of inflammation [2]. In order to recruit efficiently all the different players of this immune response, a series of biochemical events takes place involving the local vascular system, the immune system and various cells within the injured tissue. Inflammation is not a synonym of infection, but they can be related, as infection might generate an immune response.

Chronic or prolonged inflammation features similar biological processes as acute inflammation but over longer and repeated stages. This causes a progressive change in the type of cells present at the site of inflammation and generates the simultaneous destruction and repair of the tissue. Chronic inflammation can lead to various diseases, such as atherosclerosis, rheumatoid arthritis (RA), diabetes, allergies, hay fever, asthma, periodontitis and even cancer. In some cases, our normally helpful immune system is mistakenly activated when there is no invader to combat and starts degrading healthy surrounding tissues that are wrongly recognised as foreign. This type of malfunction can lead to auto-immune diseases [3] such as multiple sclerosis (MS) or lupus.

1.1.2. Leukocyte Recruitment

During an inflammatory response, different physiological events are necessary to allow leukocytes to travel from the blood to the site of inflammation [4]. The leukocyte recruitment is driven, in part, by small proteins known as chemokines, which are secreted by the injured tissues and form a concentration gradient to guide the leukocytes [5]. This leukocyte migration involves a multi-step process that is summarised in Figure 1.1. Upon injury or infection, damaged extravascular cells secrete chemokines (dark blue half-circles) as an alarm signal. These chemokines accumulate on glycosaminoglycans (GAGs) [6-8] to form a chemokine gradient that reaches the blood vessels, which provides directional signals for migrating cells. Leukocytes present in blood vessels, naturally circulate in the blood and roll along the endothelium using interactions with adhesion molecules called selectins (orange and green) in order to sense and probe their microenvironment. The interactions between selectin and leukocyte are labile and do not prevent leukocyte

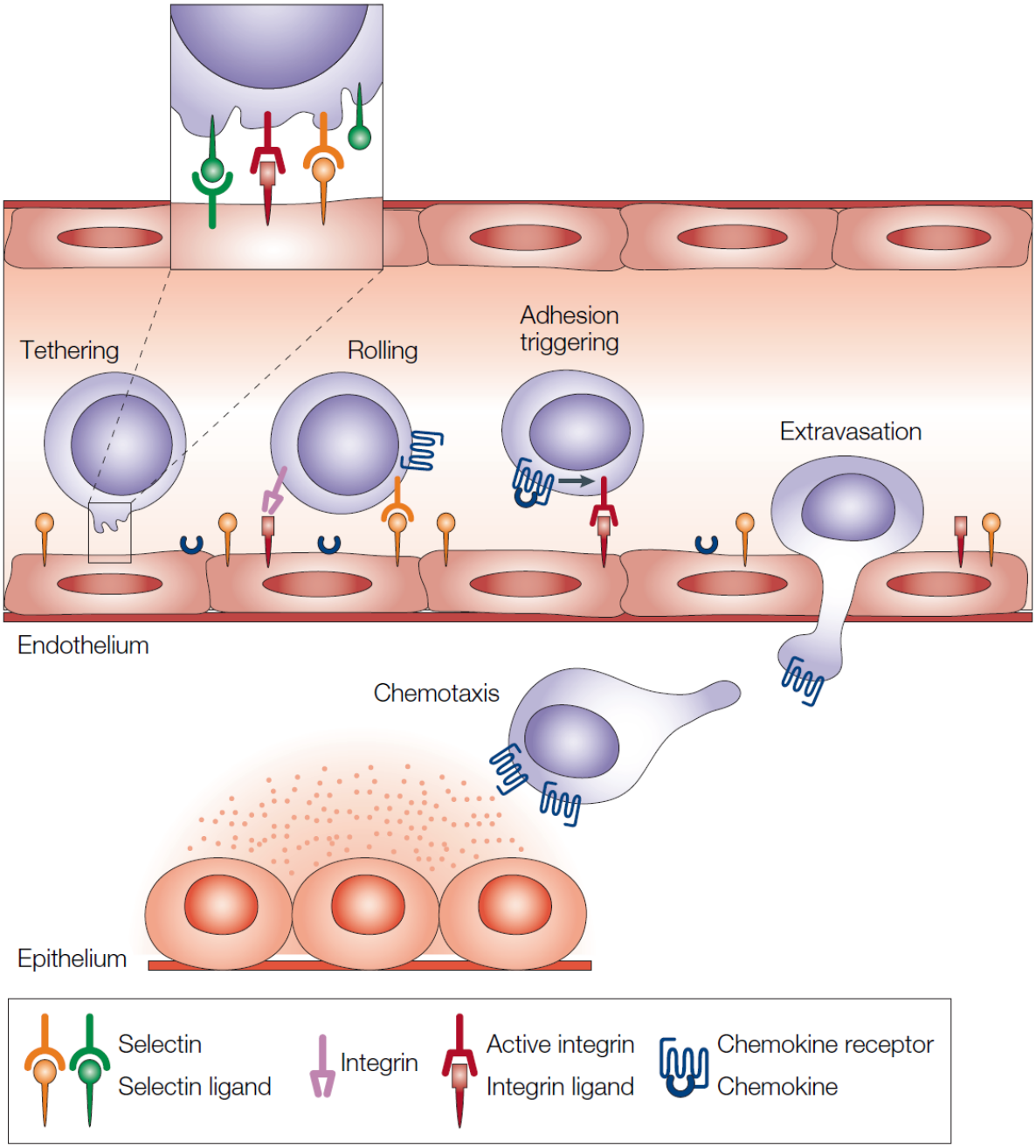

Figure 1.1: Leukocyte Trafficking Process [5]. This scheme describes the different stages involved in leukocyte recruitment by chemokines. Chemokine ligands are shown as dark blue half-circles, the receptors are shown in dark blue and leukocytes are shown as purple cells. Leukocytes, naturally tethering and rolling in the blood vessels, start to firmly adhere and ultimately migrate through the endothelium when activated by chemokines through chemokine receptors expressed on the surface of leukocytes. Once out of the blood vessel, leukocytes migrate to the site of inflammation by following the chemokine gradient.

movement. However, when the leukocytes encounter GAG-immobilised chemokines, the chemokines can bind to their cognate G protein-coupled receptors (GPCRs) on the leukocyte surface, which leads to the activation of another type of adhesion molecules named integrins (pink and dark red). This phase, which marks the end of the rolling phase, is called firm adhesion. Once arrested on the endothelium and still under chemokine activation, leukocytes undergo complex shape modifications [9] to extravasate between endothelial cells into the surrounding tissue. The final phase of the leukocyte journey is the chemotaxis along the chemokine gradient to the site of tissue injury.

1.2. Chemokines

1.2.1. Biological Function

Chemokines are chemotactic cytokines that participate in both innate and adaptive immunity. They form a family of small soluble proteins (8–12 kDa) that play essential roles in leukocyte recruitment to the site of inflammation [10]. They are indeed responsible for the trafficking and activation of leukocytes through interactions with their receptors [11]. They mainly act on monocytes, lymphocytes, basophils, eosinophils and neutrophils and play a pivotal role in host defence mechanisms. Over 50 chemokines have been identified in humans [12] and the sequence identity between chemokines varies from 20 to 90%. The recognition of chemokines as chemotactic molecules came after the detailed study of interleukin 8 (IL-8 or CXCL8) in 1987 [13], despite the fact that the first chemokine discovered was platelet factor 4 (PF4 or CXCL4) [14] a decade before. Since then, chemokines have become best known for their roles in immune surveillance and defence to resolve physiological abnormalities. As the chemokine:chemokine receptor interactions are highly complex, it is challenging to describe their involvement in disease mechanisms. However, incorrect regulation of these proteins can lead to an extraordinary number of diseases including inflammatory allergies, asthma, atherosclerosis, cancer and AIDS. Hence it is of significant interest to understand better how these small proteins function in order to develop better drugs to block or regulate their activities.

1.2.2. Classification

Chemokines are divided into four subfamilies, two major subfamilies CC and CXC (previously known as β and α chemokines respectively), and two minor subfamilies C and CX_3C (previously known as γ and δ chemokines respectively). The classification is based on the relative position of their highly conserved amino-terminal cysteine residues [15]. These cysteine residues are one amino acid apart for the CXC family or directly adjacent to each other for the CC family. The chemokines used to be named and classified according to their main biological functions but as more chemokines were discovered, this traditional classification became confusing, which is why the systematic nomenclature was introduced. In this thesis, abbreviated common names are used to name chemokines, although full common names, abbreviated names and systematic names will be given when chemokines are mentioned for the first time. In addition, a correspondence table providing all three chemokine names is available in Appendix I, Table 1.

Chemokines can also be classified according to their predominant patterns of expression, depending on their inducible or constitutive nature. Pro-inflammatory or inducible chemokines control the activation and

migration of leukocytes in case of sudden invasion [16]. On the other hand, homeostatic or constitutive chemokines interact with leukocytes for general immune surveillance and maintenance of healthy tissues and during induction of adaptive immune responses [17]. Some more recent studies suggest that some chemokines are involved in both functions [18].

1.2.3. Structure

Despite some variety in their primary structures, chemokines share highly similar secondary and tertiary structures. The three-dimensional general fold of chemokines is well known and is usually solved using NMR spectroscopy or X-ray crystallography. This structure illustrated in Figure 1.2, consists of an unstructured and highly flexible N-terminus (magenta), conserved mono- or di-cysteine motif (yellow) followed by an irregularly structured region called the N-loop (green), a 3_{10}-turn and a triple-stranded antiparallel β-sheet (cyan) packed against a C-terminal α-helix (red). Most chemokines also have two disulfide bonds formed by four conserved cysteine residues. However some chemokines, such as hemofiltrate CC chemokine 2 (HCC-2 or CCL15), have an additional disulfide bond. The first cysteine residue (conserved cysteine motif) of the sequence is linked to the third one (30s loop, between β1 and β2 strands) and the second cysteine residue (conserved cysteine motif) binds to the fourth one (β3 strand) to form the disulfide bridges.

Whereas some chemokines are constitutively monomeric, most chemokines have the ability to oligomerise in solution and form dimers, tetramers and higher order oligomers. The structures of oligomers differ between families although the monomeric fold of all chemokines is very similar. As shown in Figure 1.3, the CXC chemokines dimerise with structures similar to IL-8 [19], generating a globular dimer, with the dimer interface involving the β1-strands. By contrast, the CC chemokines dimerise by forming elongated structures like monocyte chemoattractant protein 1 (MCP-1 or CCL2 [20], with the dimer interface involving the N-termini. Several chemokines such as hemofiltrate CC chemokine 1 (HCC-1 or CCL14) [21] have been reported as tetramers in solution. The tetramers are generally the result from dimerisation of dimers, although other possibilities are not excluded. Even higher order oligomers can be formed but are harder to study because of their higher molecular weight and heterogeneity.

Although chemokines are present in various oligomeric forms in our bodies, it is mainly the monomeric form that binds to the receptor to induce chemotaxis [22]. Despite the fact that oligomerisation is not required for receptor activation, it is still a highly important phenomenon as it is required for *in vivo* function [23]. Oligomerisation is involved in GAG binding [24] which promotes chemokine localisation and chemokine gradient formation, which is vital for leukocyte trafficking. In fact, some mutational studies revealed that engineered monomers that could activate receptors but not bind to GAGs were non-functional *in vivo*.

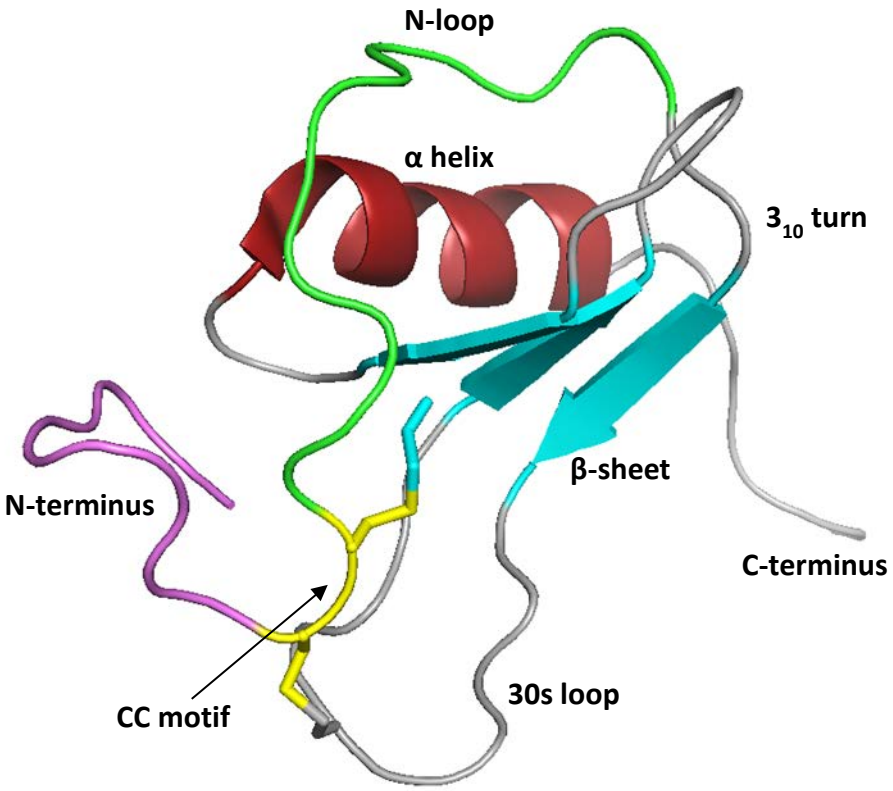

Figure 1.2: Typical Tertiary Structure of Chemokines. Structure of monocyte chemoattractant protein 3 (MCP-3 or CCL7) showing the location of structural elements labelled in bold (PDB ID: 1ncv [25]). The N-terminus is shown in magenta, the CC motif and two disulfide bridges are in yellow, the N-loop in green, the three-stranded β-sheet in cyan and the α-helix in red.

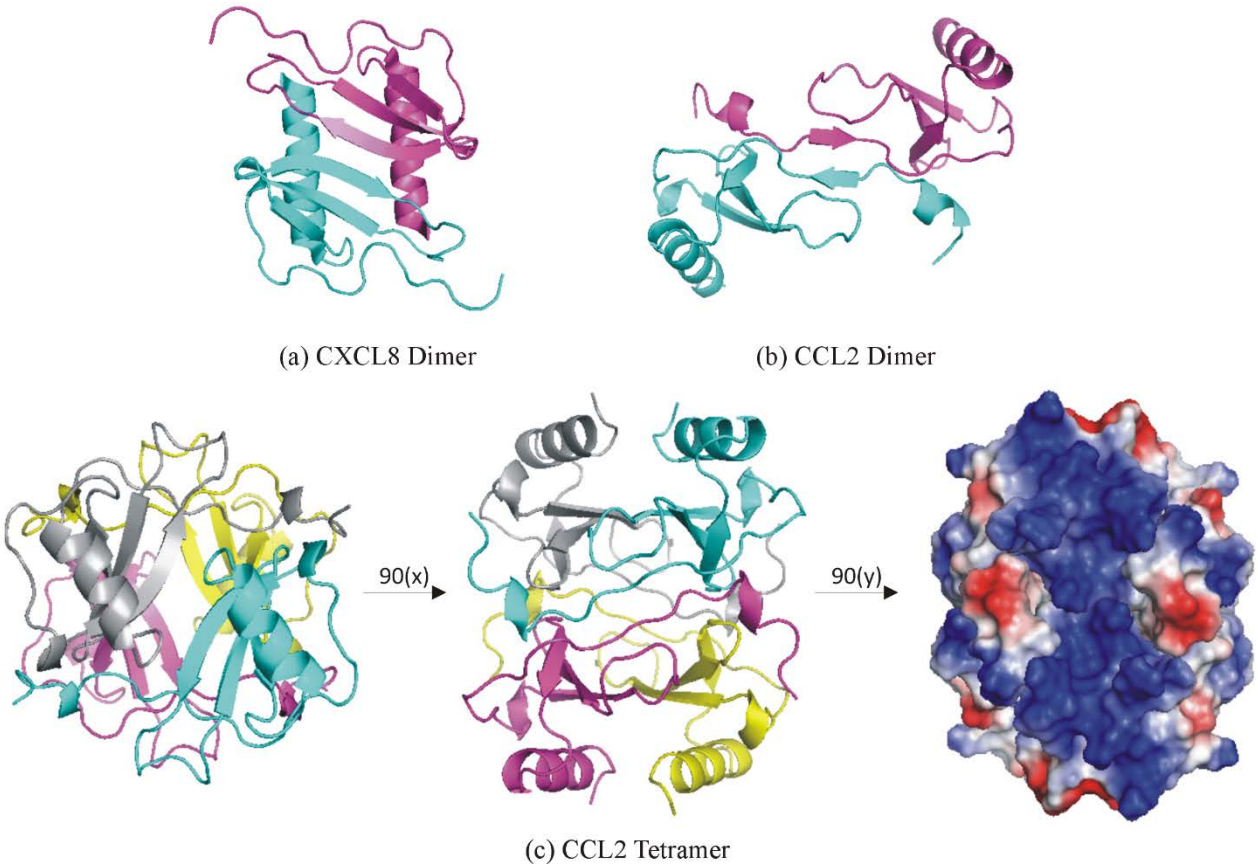

Figure 1.3: Oligomeric Structures of Chemokines [26]. (a,b) Dimer structures of (a) IL-8 and (b) MCP-1, highlighting the distinct dimer interfaces for CXC and CC chemokines, respectively. (c) Tetramer structure of MCP-1, highlighting: (left) the CXC-type dimer interfaces (cyan to grey and magenta to yellow protomers); (centre) the CC-type dimer interfaces (cyan to magenta and yellow to grey protomers); and (right) the highly electropositive (dark blue) surface involved in GAG binding.

1.2.4. Post-Translational Modifications

As secreted proteins, chemokines can be post-translationally modified in different ways, including glycosylation [27-29], citrullination [30, 31], oxidation [32] or proteolytic processing [33, 34]. Proteolytic processing affects biological functions of most chemokines in a crucial way. This can be explained by the fact that the N-terminal part of chemokines is a key region for receptor activation [35-37]. Structure-function studies have highlighted how damaging N-terminal modifications can be for chemokine function [38, 39]. However, this is not always the case and some natural N-terminal truncations can actually increase the activity of chemokines at their receptors by removing a long signal peptide for example. The intricacy of chemokine N-terminal truncation is particularly obvious when considering the two chemokines HCC-1 and HCC-2. Full-length HCC-1(1-74) and HCC-2(1-92) are weak agonists of the receptor CCR1 but are later cleaved to give HCC-1(9-74) and HCC-2(27-92), both potent agonists of CCR1 [40, 41]. However, further processing produces biologically inactive HCC-1(11-74) [42] or lower affinity truncated HCC-2 proteins (HCC-2(28-92), (29-92), (30-92) and (31-92)). This illustrates the importance of optimum N-terminal processing to yield the most efficacious version of each chemokine.

1.3. Chemokine Receptors

1.3.1. Biological Function

Chemokine receptors belong to the G protein-coupled receptor (GPCR) superfamily, more particularly to the rhodopsin-like class (Class A) [43]. Since the cloning of the first chemokine receptor (IL-8 receptor) in 1991 [44], they have been implicated in a very large number of diseases such as cancer [45], atherosclerosis [46] or type 1 diabetes [47]. Most of these diseases are inflammatory diseases [48], chronic or acute, involving inappropriate regulation of leukocyte trafficking, creating a lack or an accumulation of these cells in specific tissues. However, a significant amount of work has been directed towards the receptors CXCR4 and CCR5 because they are also involved as co-receptors for HIV infection [49, 50]. The fact that individuals who lack CCR5 are naturally resistant to HIV infection and do not present any apparent health problems [51], was an interesting starting point. It was then reported that the receptors assist viral entry by interacting with the viral surface glycoprotein gp120 [52, 53]. These results opened the door for CXCR4 and CCR5 antagonist design as it seemed that blocking the function of these receptors by using antagonists, or even promoting receptor internalisation, may provide an effective way of fighting viral entry without significantly affecting the health of patients [54, 55].

1.3.2. Classification

Around 25 chemokine receptors have currently been identified and they are classified according to the chemokines they recognise [56]. Like the chemokine family, they are divided into four subfamilies, two major subfamilies CC and CXC, and two minor subfamilies C and CX_3C. In addition to these active mammalian chemokine receptors, there are some atypical receptors, such as Duffy Antigen and Receptor for Chemokines (DARC) and D6, which are structurally similar to chemokine receptors but do not signal upon binding to chemokines [57] and some virus-encoded chemokine decoy receptors [58].

1.3.3. Chemokine:Chemokine Receptor Network

As mentioned earlier, the chemokine receptor and chemokine families include around 25 receptors and 50 ligands. Whereas some receptor:ligand interactions are specific, a majority of the receptors recognise several chemokines and most chemokines activate multiple receptors [59]. The chemokine:chemokine receptor binding selectivities are illustrated in Figure 1.4. Despite a lack of consistency in the literature, as different articles can report different selectivities especially among the shared receptors, it gives a good idea of how complex this binding network can be. The complexity of this network used to be seen as representing redundancy, which was consistent with the idea that GPCRs have only two conformations, one active and one inactive. However, this on-off switch model for the GPCRs is no longer valid, as it is now known that GPCRs are highly dynamic proteins. They can be stabilised in several conformations and therefore the idea that two ligands might activate the same receptor in two different ways is increasingly accepted.

1.4. G Protein-Coupled Receptors

1.4.1. The GPCR Superfamily

Chemokine receptors are members of the GPCR superfamily. GPCRs, also known as seven transmembrane (7TM) receptors, constitute the largest family of cell surface receptors. There are over 800 members in this superfamily that are expressed in numerous cell types throughout the human body and they play a crucial role in communication processes by transmitting extracellular information into the cell. GPCRs can detect a diverse array of extracellular stimuli or ligands, including hormones, neurotransmitters, metabolites, peptides, chemokines, ions and photons [60, 61]. Because of this variety of ligands, GPCRs are involved in regulating almost all biological processes in our bodies, which reinforces the importance of improving our knowledge in this field.

GPCRs are divided into five major families based on sequence similarity: class A (rhodopsin), class B (secretin), class C (glutamate), class F (frizzled) and class G (adhesion) [62]. The most obvious way to distinguish between families is to examine the length, structure and function of the N-terminal extracellular domain of the receptors. The class A GPCRs have small extracellular domains which mainly help receptor folding and trafficking to the plasma membrane [63]. They form the largest family and are further divided into four subfamilies and various subgroups [64]. All four remaining families have large extracellular domains which mainly differ by their structure and function [65-68].

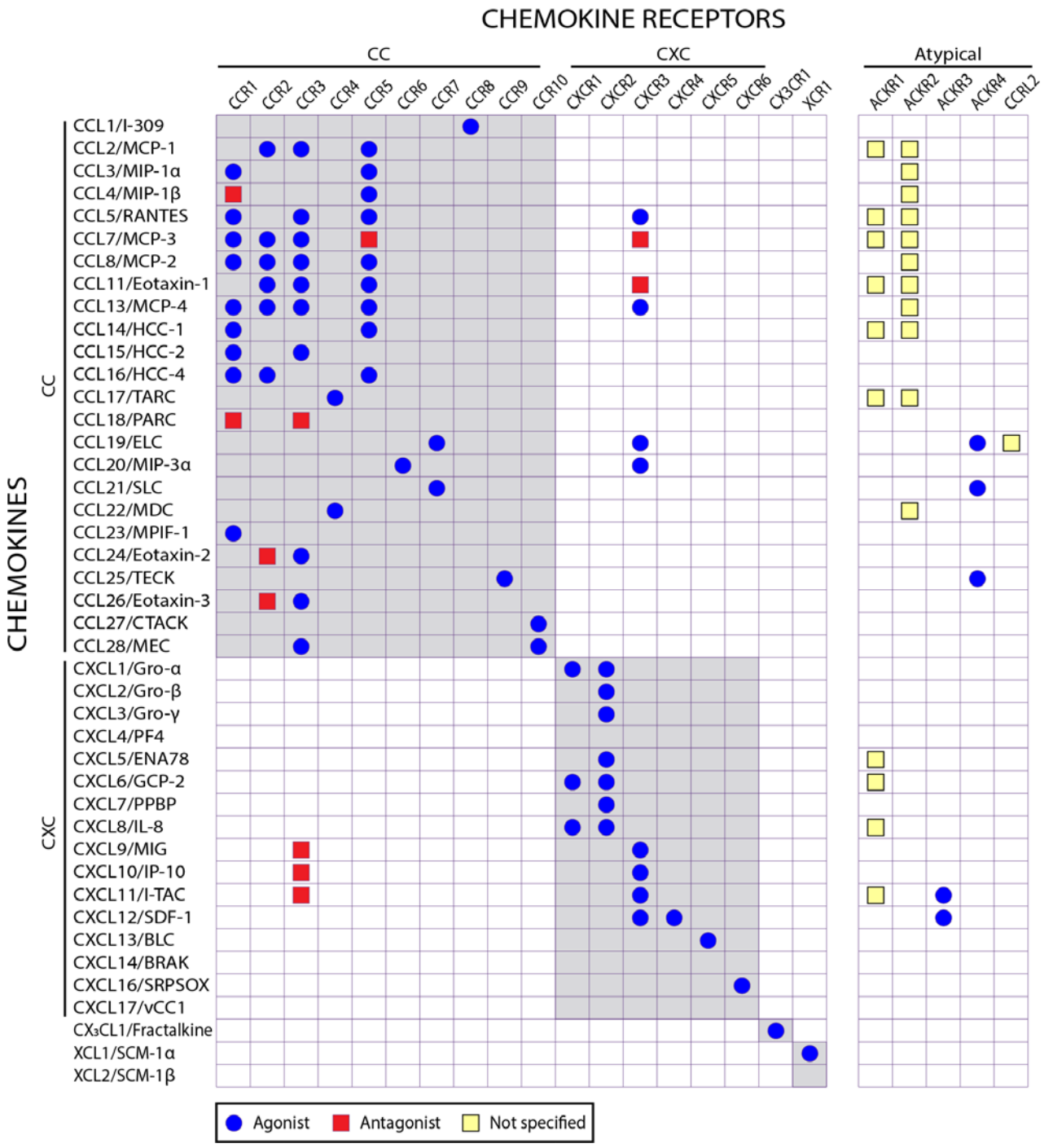

Figure 1.4: The Human Chemokine:Receptor Network [26]. Human chemokines and receptors are listed with symbols indicating whether they are specified as agonists or antagonists (or not specified) in the IUPHAR database. Note that, although CXCL1 is listed as a CXCR1 agonist in IUPHAR, the database reference suggests that it is actually an antagonist [69].

1.4.2. Structure

All GPCRs share the same basic structure shown in Figure 1.5. They are made of a single protein chain that starts with an extracellular N-terminal region, then forms a bundle of seven α-helical transmembrane (TM) regions linked by alternating intracellular (ICL1-3) and extracellular loops (ECL1-3) and ends with an intracellular C-terminal region, which usually contains a small α-helix anchored to the plasma membrane [70-72]. The TM helices are numbered from TM1 to TM7 with the small C-terminal α-helix called helix-8. Another common structural feature of the GPCR structure is the presence of a disulfide bridge between the extracellular end of TM3 and ECL2, which contributes to receptor stability [73]. The extracellular ends of the TM domains along with the ECLs of the receptor form a cavity that, in the majority of class A GPCRs, serves as the binding site for the endogenous ligand, also known as the orthosteric binding site [74, 75]. Similarly, the intracellular ends of the TM domains along with the ICLs and the C-terminus form a cavity that serves as the binding site for intracellular signalling proteins which enables signal transduction into the cell. The main family of intracellular signalling effectors that bind and are activated by GPCRs is the heterotrimeric guanine nucleotide binding protein family, or G protein family, hence the names of the receptor superfamily. Interactions between GPCRs and G proteins are complex and may slightly vary between receptors and G proteins. However, the main interaction site involves the ICL2 and intracellular ends of TM5 and TM6 of the receptor [76, 77].

1.4.3. Function and Signalling

In order to transmit the extracellular signal into the cell and initiate multiple signalling pathways (Figure 1.6), GPCRs have to interact with intracellular effectors, which are mainly heterotrimeric G proteins. The three G protein subunits are Gα, Gβ and Gγ [78]. Upon activation, GPCRs function as guanine nucleotide exchange factors (GEFs) which allows the α subunit of the heterotrimeric G protein to transition from inactive (GDP-bound) to active (GTP-bound) [79, 80] and to dissociate from the βγ subunits [81, 82]. Both Gα and Gβγ are able to interact with other effectors to generate signal transduction [83].

The Gα proteins are divided into four major classes based on their sequence and function: $G\alpha_s$ stimulates the production of cAMP by activating adenylyl cyclase (AC) [84, 85]; $G\alpha_{i/o}$ inhibits the production of cAMP by inhibiting AC [86]; $G\alpha_{q/11}$ activates phospholipase C β, generating second messengers like IP_3 [87] to ultimately upregulate the level of intracellular calcium [88]; and finally $G\alpha_{12/13}$ is related to Rho signalling, which is mainly linked to cytoskeletal rearrangements needed for cell growth [89, 90].

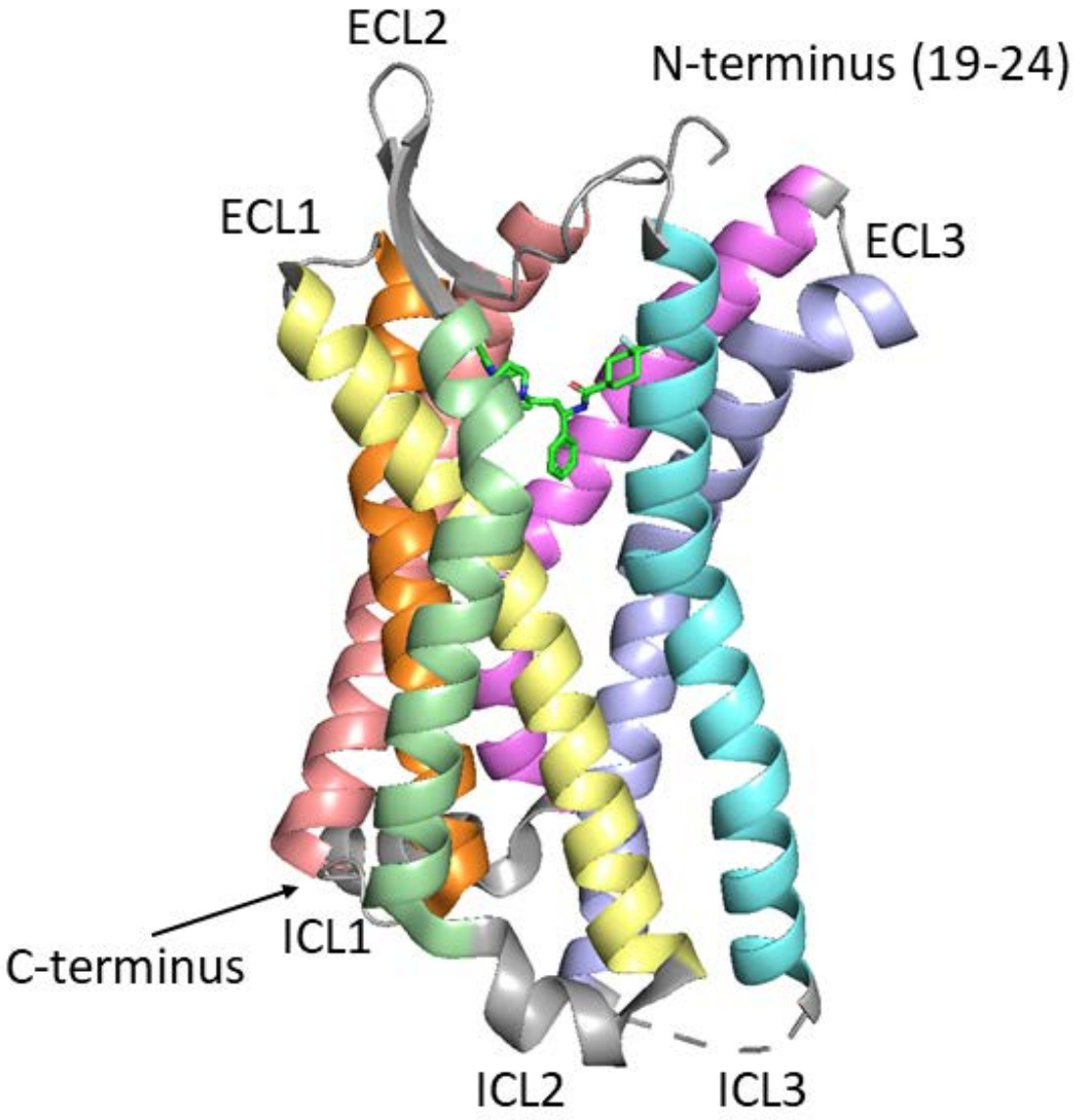

Figure 1.5: Typical Chemokine Receptor Structure. Structure of one monomer unit of the chemokine receptor CCR5 bound to the drug maraviroc (PDB ID: 4mbs [91]). Transmembrane helices are coloured salmon (TM1), orange (TM2), yellow (TM3), green (TM4), cyan (TM5), violet (TM6) and magenta (TM7) and maraviroc is shown as sticks. The N-terminus is extracellular and the C-terminus is intracellular. They are shown in grey along with the three extracellular and intracellular loops (ECLs and ICLs respectively).

The Gβγ dimer can act as a Gα inhibitor when bound to a Gα subunit, because it favours the interaction between Gα and GDP. However, when the Gβγ complex is dissociated from Gα, it can also participate in the signalling cascade [92]. For example, Gβγ can regulate ion channels [93] and is also involved in phosphorylation of the extracellular signal–regulated kinases 1 and 2 (ERK1/2) via the protein kinase C/protein kinase A pathway [94]. Furthermore, the Gβγ dimer is involved in receptor phosphorylation mediated by G protein-coupled receptor kinases (GRKs) [95]. This leads to uncoupling from the G protein and recruitment of β-arrestins, which is known as receptor desensitisation [96].

The arrestin family also includes four subtypes. Arrestin-1 (visual arrestin) and arrestin-4 (cone arrestin) are located exclusively in retinal rods and cones. Arrestin-2 (or β-arrestin 1) and arrestin-3 (or β-arrestin 2) are non-visual arrestins that are expressed in numerous cell types. The affinity of β-arrestins for the non-phosphorylated (inactive) receptor is low which limits any basal activity [97, 98]. When the receptor is activated, β-arrestins are able to displace the G protein before it is activated giving rise to G protein-independent β-arrestin signalling [99, 100]. On the other hand, when β-arrestins compete with the G protein after its activation, this leads to G protein-dependent β-arrestin signalling. The latter signalling has been well studied and includes ERK phosphorylation through the MAPK cascade [101] and receptor internalisation in clathrin coated pits [102, 103].

Regulation of chemokine receptor (and other GPCR) signalling pathways being a highly complex phenomenon, it has to be considered with respect to its cellular context. There are approximately twenty Gα subunits, five Gβ subunits and twelve Gγ subunits [104], resulting in a huge array of possible heterotrimeric G proteins. The expression levels of these various subunits vary between cell types or under different conditions and the different complexes are expected to compete with each other for association with a particular receptor. In addition, the availability of particular G proteins may depend on the presence of other GPCRs in the same cell. Moreover, the ability of a chemokine receptor to signal is also dependent on the presence of other factors such as regulators of G protein signalling (RGS) proteins, which negatively regulate G protein signalling by acceleration of GTP hydrolysis by Gα [105-107], or lipids, such as cholesterol, which can potentially influence receptor oligomerisation and conformational changes [108, 109]. Considering these potential variations in signalling pathways between cells, perhaps it should not be surprising that the literature describing chemokine:chemokine receptor signalling is full of apparent inconsistencies. As one example, different studies have concluded that eotaxin-1 is a partial agonist and an antagonist of CCR2 [110-112]. Thus, although detailed mechanistic studies of chemokine:receptor interactions typically require carefully controlled experimental conditions using immortalised cell lines, it is important to validate the biological relevance of results using primary cells.

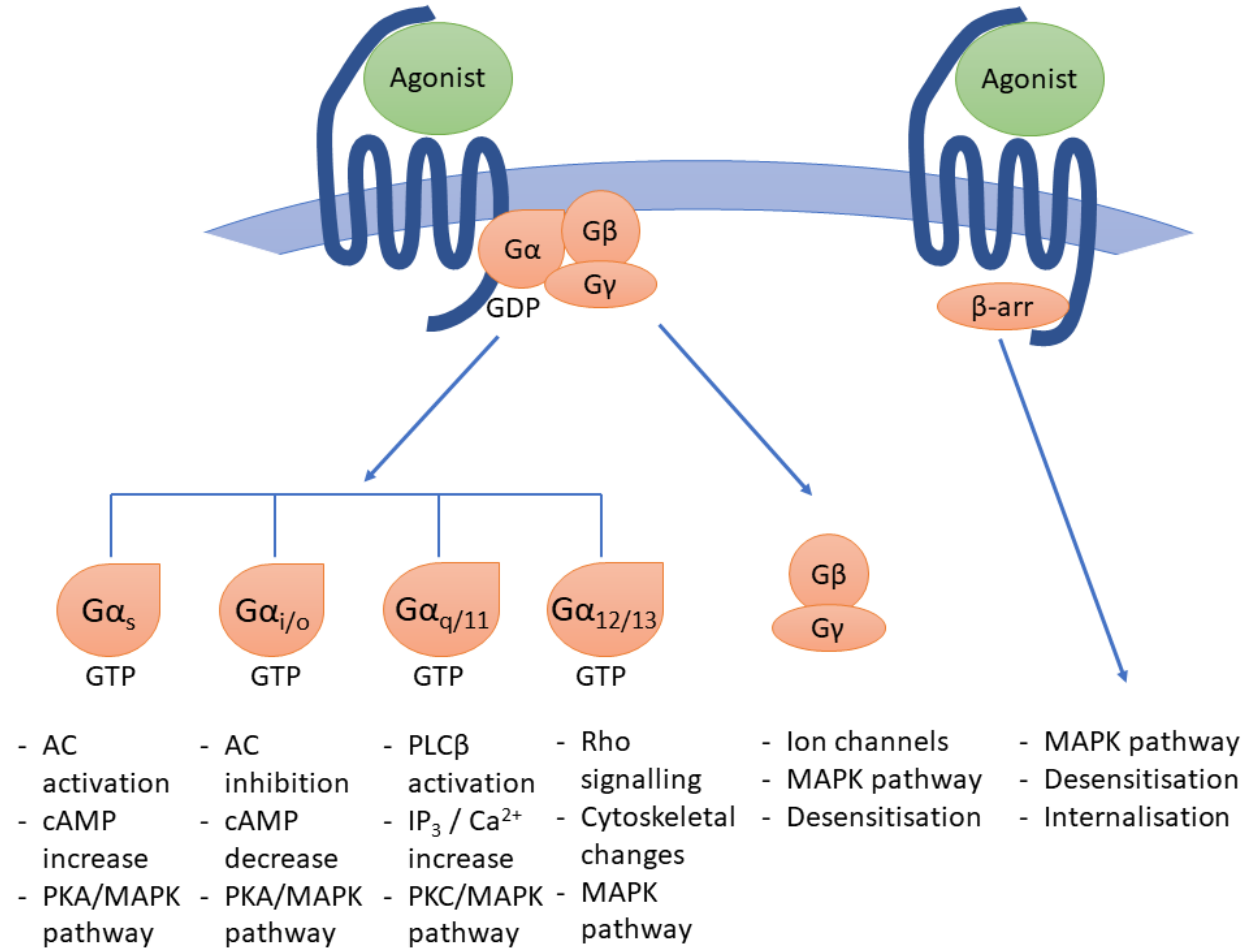

Figure 1.6: Common GPCR Signalling Pathways. The conformation of the GPCR depends on the agonist bound on the extracellular side and determines which intracellular effector can bind to the GPCR to generate further downstream signalling. The most common GPCR pathways are G protein-mediated and vary depending on the Gα subtype or β-arrestin-mediated.

1.4.4. Biased Agonism

As it is now thought that the GPCRs are highly dynamic machines that can be activated in several different ways, the traditional notion of a simple on/off switch to represent the active and inactive states of a GPCR seems to no longer stand. Biased agonism, also known as functional selectivity or agonist-selective signalling, is an increasingly developed concept based on the idea that agonists acting at the same receptor can have different abilities to activate different signalling pathways, as shown schematically in Figure 1.7. This natural phenomenon has been observed for a variety of GPCRs and the first reported case of biased agonism was described for an acetylcholine receptor to pilocarpine and carbachol in 1994 [113]. Following this study, biased agonists have been identified for several therapeutically important GPCRs [114] such as μ-opioid receptors [115, 116], β2 adrenergic receptor [117], dopamine receptors [118], 5-HT_2 and $5HT_{1A}$ serotonin receptors [119, 120] and angiotensin type 1A (AT_{1A}) receptor [121].

Biased agonism is believed to be due, at least in part, to the ability of receptors to adopt multiple active conformations, each leading to a different balance of signalling outcomes and each differentially stabilised by different ligands [122]. The growing thought that it could be possible to design partial or biased ligands for GPCRs, which could activate or inhibit one pathway without altering others, or inhibit the effects of only one ligand, is likely to be of great interest particularly in the pharmaceutical industry. Hence structural information and better understanding of the conformational changes induced by ligands are highly desirable [123]. In order to better understand biased agonism and guide drug development, several models have been proposed to quantify agonist bias [124, 125].

A number of chemokine receptors have been found to display biased agonism. For example, the chemokines Epstein-Barr virus-induced molecule 1 ligand chemokine (ELC or CCL19) and secondary lymphoid tissue chemokine (SLC or CCL21) both activate CCR7 to induce G protein activation and calcium mobilisation but only ELC gives rise to desensitisation of CCR7, which is mediated by β-arrestin recruitment [126]. In a systematic study of G protein versus β-arrestin bias for three CC and three CXC chemokine receptors, Rajagopal *et al*. found significant levels of signalling bias for CCR1, CCR10, and CXCR3 [127]. Similarly, Corbisier *et al*. found significant levels of signalling bias for CCR2, CCR5, and CCR7 in comparisons of G protein activation using several Gα subtypes as well as β-arrestin 2, cAMP and Ca^{2+} signalling [128]. These recent studies suggest that biased signalling responses to chemokine ligands may be a rather general phenomenon contributing to the different downstream cellular outcomes of chemokine receptor activation, enabling fine tuning of each individual inflammatory response.

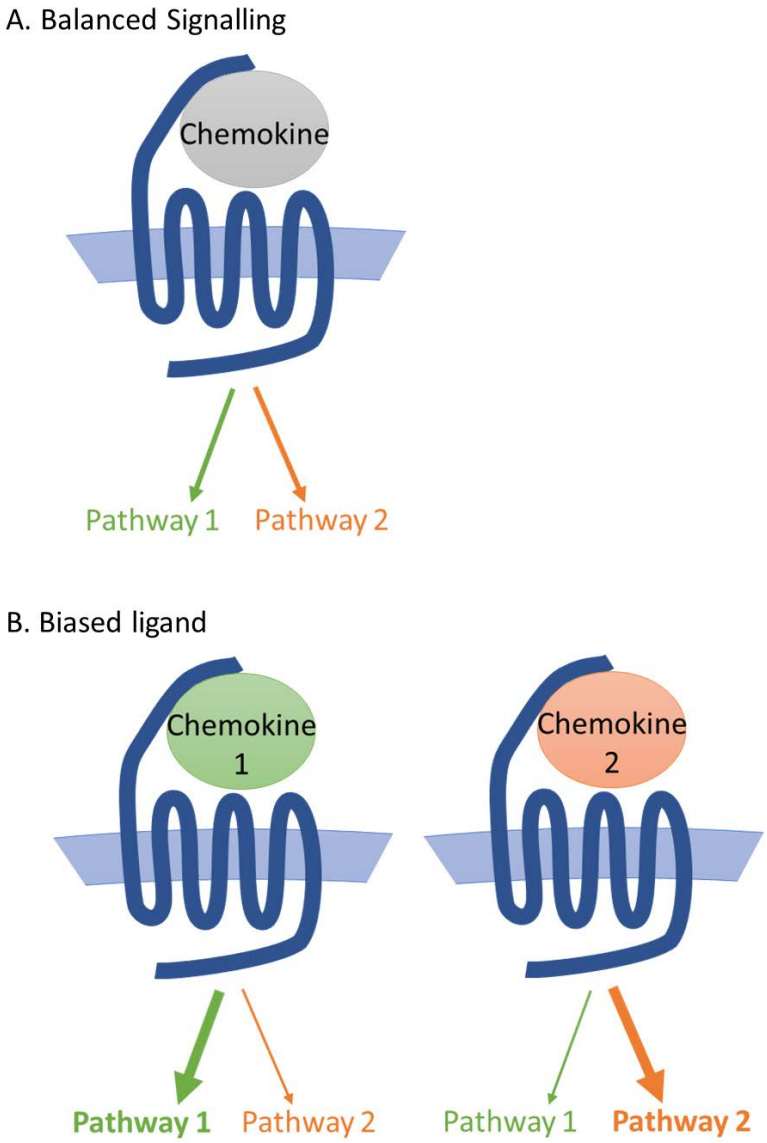

Figure 1.7: Schematic Representation of Biased Agonism. (A) The grey chemokine induces balanced signalling. **(B)** The green chemokine (left) selectively activates pathway 1, whereas the orange chemokine (right) selectively activates pathway 2.

1.4.5. Post-Translational Tyrosine Sulfation

GPCRs can be post-translationally modified in various ways, the most common being the ligand-induced reversible receptor phosphorylation at the intracellular C-terminal part of the receptor. This post-translational modification is integral to GPCR signalling and also enables receptor desensitisation and internalisation (see section 1.3.3 for details). In addition to phosphorylation, GPCRs can be glycosylated [129, 130], palmitoylated [131, 132], ubiquitinated [133] or sulfated [134]. This section focuses on tyrosine sulfation, the effects of which are investigated in experiments described in this thesis.

Tyrosine sulfation is a common post-translational modification in secreted and transmembrane proteins; over 1 % of the human proteome has been suggested to possess sulfated tyrosine residues [135]. The transfer of a sulfate group from 3'-phosphoadenosine 5'-phosphosulfate (PAPS) to the hydroxyl group of a tyrosine residue is catalysed by either of two isoforms of an enzyme called tyrosylprotein sulfotransferase (TPST-1 or -2) [136] (Figure 1.8). The TPST enzymes are localised to the trans-Golgi network [137] and are selective for tyrosine residues close in sequence to acidic amino acids, a motif found in the N-terminal (chemokine-binding) regions of most chemokine receptors [138].

Nowadays, it is well established that tyrosine sulfation is present in many chemokine receptors [137], as shown in Table 1.1. However, the precise sulfation state of these receptors remains largely unknown as tyrosine sulfation is hard to characterise, often heterogeneous and difficult to control [139]. It has been shown that tyrosine sulfation of chemokine receptors can enhance chemokine affinity [140], influence chemokine selectivity [141], as well as modulate chemokine oligomerisation state [142, 143], but once again the structural changes responsible for these results remain difficult to assess. This is why it is crucial to find a way of studying these interactions in more detail. One strategy recently developed by our group as well as several other groups, is to use sulfopeptides as receptor N-terminal mimics [144-146]. Sulfopeptides are indeed proposed to be a good model for the N-terminal part of the chemokine receptors, because the receptor N-terminus is a highly flexible region. Moreover, such sulfopeptides are easier to work with as they can be synthetised homogeneously, with a controlled sulfation pattern [147]. However, the question of whether they are good models open as their ability to mimic the receptor binding selectivity has never been tested directly.

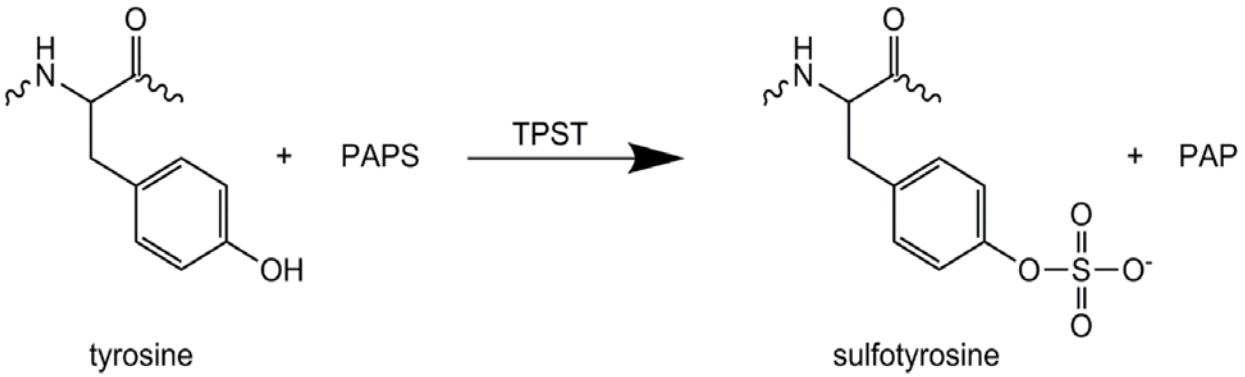

Figure 1.8: General Scheme of Tyrosine Sulfation [138]. The addition of a sulfate group and a negative charge to the phenolic hydroxyl of the tyrosine side chain is catalysed by TPST enzymes and the sulfate group is provided by PAPS.

Table 1.1: Chemokine Receptors known to be Sulfated and their Cognate Chemokines [138].

Receptor	Chemokine Ligands[1]	Receptor N-terminal Amino Acid Sequence[2]	Key Findings	References
CCR2	CCL2/MCP-1 CCL7/MCP-3 CCL8/MCP-2 CCL11/eotaxin-1 CCL13/MCP-4 CCL16/HCC-4	$_{1}$MLSTSRSRFIRNTNESGEEVTTFFDYDYGAPC$_{32}$	• Y26 is sulfated • Y26A mutant has reduced receptor binding/activation • Mutation of D25 reduces sulfation	[145, 148]
CCR3	CCL11/eotaxin-1 CCL13/MCP-4 CCL15/HCC-2/Lkn-1 CCL24/eotaxin-2 CCL26/eotaxin-3 CCL28	$_{1}$MTTSLDTVETFGTTSYYDDVGLLC$_{24}$	• CCR3 is Tyr-sulfated • Tyrosine sulfation enhances receptor activity	[149]
CCR5	CCL3/MIP-1α CCL4/MIP-1β CCL5/RANTES CCL8/MCP-2 CCL11/eotaxin-1 CCL14/HCC-1 CCL16/HCC-4	$_{1}$MDYQVSSPIYDINYYTSEPC$_{20}$	• CCR5 is Tyr-sulfated • Sulfated Tyr residues contribute to binding of MIP-1α, MIP-1β and HIV-1 surface proteins	[150]
CCR8	CCL1/I-309 CCL4/MIP-1β CCL16/ HCC-4 CCL17/TARC	$_{1}$MDYTLDLSVTTVTDYYYPDIFSSPC$_{25}$	• N-terminal Tyr residues are sulfated • Sulfated Tyr residues contribute to binding of I-309	[151]
CXCR3	CXCL9/MIG CXCL10/IP-10 CXCL11/I-TAC	$_{1}$MVLEVSDHQVLNDAEVAALLENFSSSYDYGENESDSC$_{37}$	• Y27 and Y29 or CXCR3 are sulfated • Mutation of Y27 or Y29 reduces binding and activation by MIG, IP-10 and I-TAC	[152, 153]
CXCR4	CXCL12/SDF-1	$_{1}$MEGISIYTSDNYTEEMGSGDYDSMKEPC$_{28}$	• N-terminal Tyr residues are sulfated • Mutation of N-terminal Tyr residues reduces SDF-1binding	[154]
CX_3CR1	CX_3CL1/fractalkine	$_{1}$MDQFPESVTENFEYDDLAEACYIGDIV$_{27}$	• Mutation of N-terminal Tyr residues or sulfatase treatment reduces fractalkine binding affinity	[155]
DARC	Many CC and CXC chemokines	$_{1}$MGNCLHRAELSPSTENSSQLDFEDVWNSSYGVNDSFPDGDYDANLEAAAPCHSCNLLDDS$_{60}$	• Y30 and Y41 are sulfated • Mutation of Y30 and Y41 reduces binding to different chemokines • Mutation of Y41 reduces binding to *Plasmodium vivax* Duffy binding protein	[156]

[1]Chemokine ligands are those listed in [157]

[2]Potentially sulfated Tyr residues are shown in red; acidic residues are underlined

1.5. Chemokine:Receptor Interactions

1.5.1. Chemokine Receptor Structure

Chemokine receptors, as a subfamily of the GPCR family, are seven-transmembrane helix receptors [158] expressed on the cell surface of leukocytes. Their structure determination, just like any other membrane proteins, has proven to be a very challenging task and the main issues that scientists have to address include expression of sufficient quantities of receptors, purification, reconstitution of functional receptors in artificial membranes, and crystallisation of these dynamic proteins. The chemokine receptor structure shown in Figure 1.9 illustrates features common to all chemokine receptors, including seven transmembrane α-helices, the extracellular N-terminus (mostly not visible in the figure as it is a highly flexible region, generally not observed in structures), the intracellular C-terminus (mostly not visible on the figure and in structures, but expected to contain an additional α-helix, helix-8) and six loops (three extracellular loops (ECL) and three intracellular loops (ICL)) making the links between helices. ECL2, which is the longest loop, contains a β-hairpin structure. Disulfide bridges are also highly important features, as some studies have proven their roles in receptor function [159, 160]. Chemokine receptors usually have one cysteine residue in each ECL and form two disulfide bridges. The first one involves the two cysteine residues present on the N-terminus and ECL3 and is specific to chemokine receptors [157]. The second one links the two cysteine residues of TM3 and ECL2, and is common to all rhodopsin-like GPCRs [161].

Until now, structures of five chemokine receptors have been solved, the receptors being unbound or bound to small molecules (CXCR1 [162], CXCR4:IT1t [163] CCR2:BMS-681 [164], CCR5:maraviroc [91] and CCR9:vercirnon [165]). In addition, three more structures of a chemokine receptor bound to a chemokine have been solved (CXCR4:vMIPII [166], CCR5:5P7-CCL5 [167] and US28:CX3CL1 [168]). However, no structure of a chemokine:receptor complex in the activated state is available to date, so the structural basis of transmembrane signalling remains to be established.

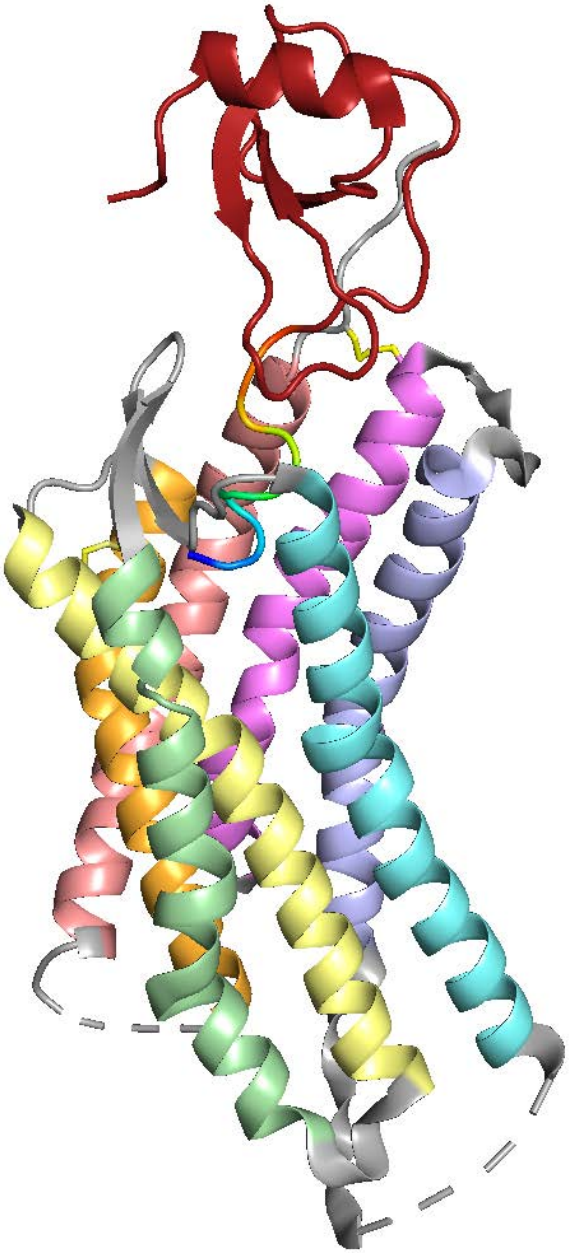

Figure 1.9: Crystal Structure of the CXCR4–vMIP-II Complex (PDB ID: 4rws [166]). Transmembrane helices are coloured salmon (TM1), orange (TM2), yellow (TM3), green (TM4), cyan (TM5), violet (TM6) and magenta (TM7), the disulfide bridges are shown as yellow sticks and the N-terminus, ECLs and ICLs are in grey. The viral chemokine vMIP-II is shown in dark red except for its N-terminus which is highlighted in rainbow colours.

1.5.2. Structural Model for Chemokine Receptor Activation by Chemokines

To improve our understanding of chemokine:chemokine receptor interactions, numerous studies have been conducted to investigate which particular regions of chemokines and their receptors are significant for binding and activation [169, 170]. Collectively, these studies of structure-activity relationship showed that chemokines have two major sites of interaction with their receptors, which resulted in Crump *et al.* proposing in 1997 a general model for chemokine:receptor interaction, called the "two-site model" [171]. The first site circled in black on Figure 1.10, involves the N-terminal region of the receptor and a shallow groove formed by the N-loop and β3-strand of the cognate chemokine, whereas the second site circled in orange involves the N-terminal part of the chemokine and a more buried region of the receptor, which could include one or more of the ECLs and some residues in the transmembrane helices and causes the receptor to change conformation and become activated [169].

The two-site model is generally accepted, as it is consistent with most published mutational data. A recent shotgun mutagenesis study of CXCR4 also provides insight into receptor structure and activation [172]. Moreover, the recent structures of chemokine-bound receptors [166, 173], in addition to several structures of chemokines bound to receptor fragments [149, 174, 175], have confirmed the two central aspects of the two-site model. However, this model may be an oversimplification as it does not account for subtle changes occurring after post-translational modification of the receptor for example. In addition, the two-site model implies that the two steps of the interaction occur sequentially as two separate steps, step one representing initial binding and step two representing subsequent activation. The spatial and functional independence of the two sites is another aspect of this model that is being challenged and needs to be addressed to fully characterise chemokine recognition by their receptors. An additional model was recently proposed based on the structure of CXCR4 in complex with a viral chemokine [166]. This model is derived from the two-site model but introduces a chemokine recognition site called CRS 1.5, located between CRS 1 (N-terminus) and 2 (N-loop and β3-strand groove) to account for interactions observed between CXCR4 and chemokine residues separating the N-terminus and N-loop, particularly the two cysteines residues in the CC motif. Although this model implies that the chemokine regions involved in binding and activation are not clearly spatially separated, it still assumes that binding and activation occur as sequential steps, so it presents many of the same limitations as the conventional two-site model.

In summary, the two-site model is a basic frame work that has proved useful over many years. However, advances in the GPCR signalling field have rendered this model insufficient to explain recent subtle results. Although it is a good starting point and still guides traditional result interpretation, refining it is required to gain more detailed mechanistic insights.

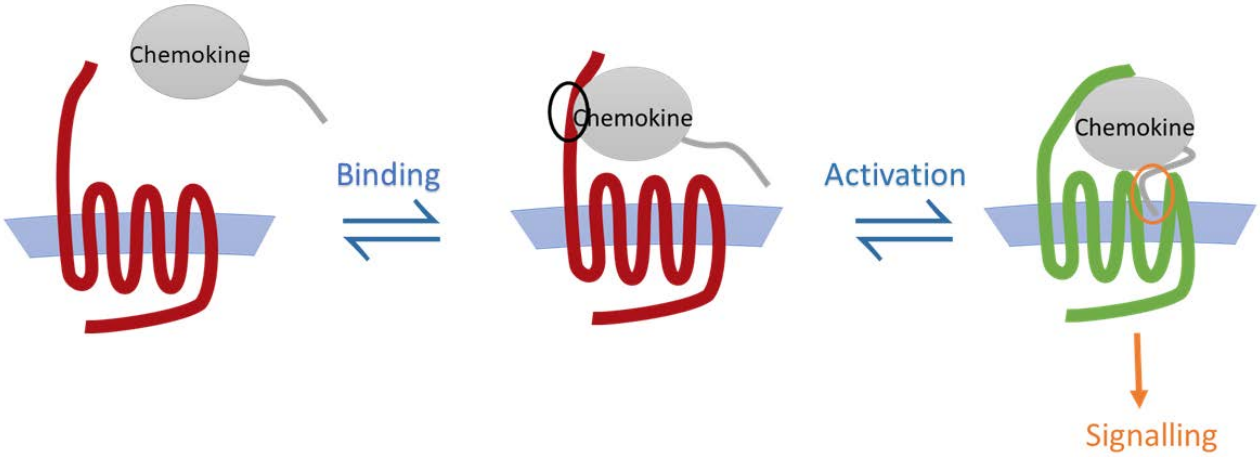

Figure 1.10: Proposed Two-site Model for Chemokine:Chemokine Receptor Interaction [176]. The first species represents the receptor in an inactive state (red) and the ligand prior to any interaction between the two. The second species represents the interaction of the chemokine N-loop and β3-turn with the N-terminal segment of the receptor (site 1 circled in black). Interactions in site 1 are considered to be driving binding only; thus, the receptor is still in an inactive state (red). The third species represents the interaction between the N-terminal region of the chemokine and the receptor TM bundle (site 2 circled in orange). Insertion of the N-terminal region of the chemokine results in activation of the receptor (active state in green) and interactions in site 2 are considered to be driving activation only.

1.6. CC Chemokine Receptor 1 (CCR1)

1.6.1. Biological Function

CCR1 is a member of the CC chemokine receptor subfamily and, like the other chemokine receptors, belongs to the GPCR family. It is a seven-transmembrane helical cell surface receptor, which upon activation triggers several physiological responses. It was the first CC receptor to be identified, in 1993 [177], and is mainly expressed on the cell surface of monocytes, natural killer (NK) cells and immature myeloid cells [178]. It has been linked to a large variety of diseases [179], particularly inflammatory diseases and diseases that involve malfunction in leukocyte recruitment.

Rheumatoid arthritis (RA) is an autoimmune disease that mainly results in pain and chronic inflammation of the flexible joints, although other tissue or organs can be affected too. Joints become painful and swollen due to an inflammatory response of the capsule around the joints, and mobility may be reduced. Although the causes of RA are still unknown, autoimmunity plays a big part and some studies have shown that CCR1 is involved in the disease development [180]. CCX354-C, a CCR1 antagonist, was administrated to some patients in a clinical trial and reduced joint swelling.

Multiple sclerosis (MS) is another autoimmune disease involving the inflammation and destruction of the myelin sheaths located in the brain and spinal cord. This damage disrupts communication between parts of the central nervous system and gives rise to a wide range of symptoms, including physical, mental and sometimes psychiatric problems. Although the causes and mechanisms accountable for MS are not currently known, they are most likely mediated, in part, by leukocyte trafficking and some studies have shown that CCR1 plays a role in the disease development [181]. This conclusion comes from the analysis of the expression of CCR1 on circulating cells. The analysis suggests that the monocytes able to enter and be retained in the central nervous system derive from a minority of CCR1-positive cells, which were also found in active MS lesions.

The role of CCR1 in cancer has also been investigated, especially for cancer metastasis and multiple myeloma [182, 183]. Furthermore CCR1 appears to play key roles in transplant rejection [184], diabetes [185], osteopenia [186], as well as in progressive kidney disease [187].

CCR1 is reported to recognise several CC chemokines [188], the most common ones being HCC-1, -2 and -4, myeloid progenitor inhibitory factor 1 (MPIF-1 or CCL23), regulated upon activation, normally T cell expressed and secreted (RANTES or CCL5), macrophage inflammatory protein 1α (MIP-1α or CCL3) and MCP-2, -3 and -4. The CCR1 signalling profile has been studied by different groups [189] and is similar to other chemokine receptors, including calcium mobilisation, β-arrestin recruitment, and cAMP signalling, leading to a variety of downstream cellular effects, including receptor internalisation and leukocyte chemotaxis.

The CCR1 three-dimensional structure remains unknown, however a predicted topology has been reported using its sequence and the general GPCR structure [190]. Another predicted structure of CCR1 bound to BX 471, a CCR1 small molecule antagonist, was also described [191] but no structural data have been

generated yet. Apart from the lack of structural information available on CCR1, another challenge faced by scientists is the investigation of the post-translational state of the receptor, including tyrosine sulfation and glycosylation. There are two tyrosine residues in the CCR1 N-terminal sequence, in positions 10 and 18. These residues are surrounded by acidic residues which makes them potential sulfation sites. As mentioned in section 1.3.5, tyrosine sulfation can influence different aspects of chemokine:receptor interaction such as binding or differential agonism, which provides a strong incentive for further studies on CCR1 tyrosine sulfation.

1.6.2. CCR1 as a Drug Target

Chemokine receptors have been the targets of numerous drug discovery programs and clinical trials. Only two receptor antagonists have reached the market: Maraviroc, a CCR5 antagonist, used as an antiviral agent in HIV infection [192, 193] and Plerixafor, a CXCR4 inhibitor, used during hematopoietic stem cell collection for later transplantation [194]. Although there is no approved CCR1 blockade available to date, CCR1 is recognised as a promising drug target because of the various diseases in which it is involved [195]. Gene deletion of CCR1 is not lethal [196] but knockout of CCR1 revealed both beneficial effects, including the suppression of tissue allograft rejection [197] and detrimental effects, including the development of osteopenia [186]. This is why targeting CCR1 has to be done in a highly controlled and selective way, to avoid any undesired side effects.

Several strategies targeting CCR1 have been used to design and test new drugs blocking CCR1-mediated responses, including small molecule antagonists, as well as anti-CCR1 antibodies [198]. One of the most potent CCR1 antagonists is the compound BX 471, developed by Berlex [199]. It has a 50 % inhibitory concentration (IC_{50}) of 2 nM (in human), is able to efficiently displace MIP-1α, RANTES and MCP-3 in CCR1 competition binding assays and also inhibits a number of CCR1 signalling pathways, including calcium mobilisation and leukocyte migration. It shows a greater than 10,000-fold selectivity for CCR1 compared to 28 different GPCRs. In a rat model of MS, BX 471 appeared to reduce the impact of the autoimmune disease which was the first time this effect was observed for a non-peptide antagonist. This compound was tested against other diseases and demonstrated efficacy in a rat heterotopic heart transplant rejection model [184] and a mice renal fibrosis model [200, 201].

Other small molecule antagonists have been developed and reported by several companies, including Merck, Pfizer and Millennium Pharmaceuticals. CCR1 blockade demonstrated efficacy in animal models in suppressing colon cancer liver metastasis (BL5923, [202]), treatment of RA (BX 471 and anti-CCR1 antibodies, [203]), treatment of multiple myeloma and associated osteolytic bone disease (CCX721, [204]) and treatment of eosinophil-mediated inflammatory disorders, such as asthma (UCB35625, [205]). Some compounds went through clinical trials (phase I or II) testing efficacy against MS or RA, the most promising compound being CP-481715, a CCR1 antagonist developed by Pfizer [206]. Unfortunately, no CCR1 antagonist demonstrated sufficient efficacy in RA and MS clinical trials [207, 208]. Numerous other clinical trials have also been unsuccessful due to side effects or lack of efficacy. This highlights the importance of better understanding the intricacies of the chemokine:receptor network. Despite previous unsuccessful

attempts, inhibition of CCR1 or its ligands may still prove to be an effective strategy, potentially in combination with other chemokine receptor antagonists [209].

1.6.3. Cognate Chemokines

As mentioned above, CCR1 is reported to recognise several CC chemokines, the most common ones being HCC-1, -2 and -4, MPIF1, RANTES, MIP1α and MCP-2, -3 and -4. In this study, four of the CCR1 cognate chemokines are of particular interest, HCC-1, HCC-2, MPIF-1 and MCP-3, as they each activate a different subset of CC chemokine receptors.

Unlike most chemokines, HCC-1 (CCL14) is constitutively expressed in human plasma and tissues including spleen and liver [210]. It is present in our bodies in different forms as it can be post-translationally modified by glycosylation or truncation [211], the N-terminally truncated form of HCC-1 [9-74] being the most potent form. HCC-1 is structurally related to MIP-1α. It can form higher molecular weight assemblies, is stable as a tetramer at high concentrations and its structure was solved using X-ray crystallography in 2007 [21]. It is a chemoattractant for leukocytes [212] and signals through CCR1 and CCR5 receptors.

Similar to HCC-1, HCC-2 (CCL15) is a constitutive chemokine, expressed in the gut and liver [213]. It also has a long N-terminus that can be truncated to give rise to a more active form of the chemokine [41]. Its solution structure was reported in 1999, using nuclear magnetic resonance (NMR) spectroscopy [214]. It revealed that HCC-2 shares the same general structure as the other chemokines and is mainly monomeric, but has a third disulfide bond. Functionally similar to MIP-1α, HCC-2 induces chemotaxis on monocytes, T-lymphocytes and eosinophils by signalling through CCR1 and CCR3 receptors [215].

MPIF-1 (CCL23) is a constitutive chemokine expressed in the liver, lung and bone marrow [216]. Its solution structure was solved in 2001, using NMR spectroscopy [217]. Like HCC-2, MPIF-1 is monomeric and has an additional disulfide bond. While some chemokines can interact with several receptors, MPIF-1 binds specifically to CCR1. It is involved in chemotaxis of monocytes [218] and cytoskeletal remodelling [219].

MCP-3 (CCL7) is a pro-inflammatory chemokine expressed by mononuclear leukocytes, fibroblasts and osteosarcoma cells. It activates a large variety of immune cells such as monocytes, T-lymphocytes, NK cells, dendritic cells, eosinophils, neutrophils and basophils [220, 221] through activation of CCR1, CCR2 or CCR3 [222] and is one of the four members of the human MCP family. Structurally MCP-3 is monomeric [223] and is closely related to MCP-1 with 71% sequence identity [224], although MCP-1 does not activate CCR1.

1.7. Natural and Synthetic Chemokine Inhibitors

1.7.1. Targeting Chemokines

Knowing that chemokines and their receptors are involved in numerous diseases, particularly inflammatory and autoimmune diseases, it is not surprising that a considerable effort has been made to develop chemokine receptor antagonists [225, 226]. These chemokine receptor antagonists are usually small molecules and as mentioned in section 1.5.2, only Maraviroc and Plerixafor have reached the market. However, some antibodies have also been developed, such as Mogamulizumab (targets CCR4 and is used to treat T-cell lymphoma [227]) or a human single domain antibody called "i-body" (targets CXCR4 [228]). Some viral chemokines, such as vMIP-II, have also been established as chemokine receptor antagonists [166]. However, viral chemokines can be promiscuous or behave as agonists depending on the receptor they interact with [229].

Despite a few successes, numerous chemokine receptor antagonists have failed in clinical trials mainly due to a lack of efficacy [230, 231], which can be explained by the promiscuity of the chemokine network. Using a combination of antagonists and blocking several receptors at the same time has also been considered but this approach presents significant risks as it could result in a loss of beneficial immune responses. Thus, targeting chemokines themselves could be an alternative therapeutic approach. For example, it has been shown that macrophages present in MS brain lesions come from a subset of CCR1 expressing macrophages [181]. Based on this result, CCR1 antagonists were expected to reduce myelin degradation and disease severity which was not the case in clinical trials [54]. CCR1 was indeed activated by MIP-1α, which is also a CCR5 ligand, and as the macrophages present in the MS lesions also expressed CCR5, they were still recruited despite administering a CCR1 antagonist. In this situation, targeting MIP-1α instead of its receptors seems like a better strategy, especially as removal of MIP-1α using monoclonal antibodies proved to decrease MS disease severity [232].

1.7.2. Small Molecules, Synthetic Polymers and Nanoparticles

Small molecules used as chemokine antagonists are not as common as chemokine receptor antagonists because chemokines do not have a clearly defined small molecule binding site like receptors do. Thus, chemokine antagonists may suffer from fast clearance rates or relatively low specificity, leading to off-target effects. However, this idea was still considered because small molecules often have the advantage of high oral bioavailability and small molecules that bind (μM affinities only) and antagonise chemokines were discovered. For instance, the structure of chemokine stromal cell-derived factor 1 (SDF-1 or CXCL12) in complex with an antagonist was determined, showing that this antagonist occupies the site normally bound by the N-terminal regions of the receptor CXCR4 [233].

To decrease clearance rate and increase affinity and specificity, bigger molecules were investigated, particularly among polymers. Having long and extended molecules that could wrap around chemokines and resembles the chemokine receptor N-termini or the GAGs used to form chemokine gradients could be a successful strategy to antagonise chemokines. For example, conjugation of heparin to a polymer backbone

provided a polymer able to bind to CCL7 [234] and a polystyrene derivative, polystyrene sulfonate, was able to bind to MCP-1 [235].

Nanoparticles are another useful tool that could be used along with polymer chemistry to either release [236] or reduce the concentrations of chemokines in the body. For the example, the polystyrene sulfonate brushes mentioned above were attached to silica nanoparticles to maintain the benzenesulfonic acid groups, that resemble sulfated tyrosine residues, close to each other and mimic GAGs. The nanoparticles retained their chemokine binding ability, binding MCP-1 with a higher affinity than the polymer alone for the short-length brushes [235]. However, it is difficult to envisage how such nanoparticles would accomplish high specificity for a particular chemokine over all the other possible targets.

1.7.3. Antibodies, Viral Proteins and Decoy Receptors

Alternately, several larger biomolecules have also been developed, particularly in the antibody family that is known for its specificity. An anti-IL-8 antibody is currently marketed in China for the treatment of psoriasis and antibodies targeting MCP-1, RANTES and 10 kDa interferon gamma-induced protein (IP-10 or CXCL10) are in clinical trials [237, 238]. Finally, an L-stereoisomer oligonucleotide aptamer targeting MCP-1 has progressed to a Phase IIa clinical trial in diabetic nephropathy patients [239].

Strategies to disrupt the host immune system can be observed in large DNA viruses. One such strategy is molecular mimicry of chemokines and chemokine receptors to modulate the chemokine signalling network [240-242]. Viruses such as herpesviruses and poxviruses can express receptors that interact directly with human chemokines. For example, US28 is a CX_3CR1 homologue encoded by human cytomegalovirus that binds chemokines from both the CC and CX_3C subfamilies. The crystal structure of US28 bound to a human chemokine (fractalkine or CX_3CL1) has been determined [173]. Similarly, the UL21.5 glycoprotein, encoded by human cytomegalovirus has been reported as a decoy receptor binding specifically to RANTES, although only a limited number of chemokines were tested [243, 244]. The poxvirus also encodes chemokine-binding proteins such as VEGF coregulated chemokine 1 (vCCI or CXCL17), which binds with high affinity to nearly all CC chemokines and with only low affinity to the CXC chemokines IL-8 and melanoma growth stimulatory activity α (Gro-α or CXCL1) [245]. The structures of the vCCI protein both free and bound to macrophage inflammatory protein 1β (MIP-1β or CCL4) were solved [246, 247] and found to be conserved with several other viral chemokine-binding proteins, including A41 [248], the SECRET (smallpox virus-encoded chemokine receptor) domain of CrmD [249] and the herpesvirus encoded M3 protein [58].

1.7.4. Tick Evasins

In the same way as viruses, parasites have evolved and developed various sophisticated ways to evade detection by their host immune system. Thus, chemokine-binding proteins can be found in worms [250] and ticks. Ticks are small ectoparasitic arachnids that are divided in two major families: *Ixodidae* (hard ticks) and *Argasidae* (soft ticks) [251]. The hard tick family counts around 700 different species [252].

Ticks express a variety of immunomodulatory compounds to avoid immune detection by the host and prolong feeding [253, 254]. Recently, the chemokine-binding activity detected in tick saliva was linked to small soluble secreted proteins, that were identified in the hard tick species *Rhipicephalus sanguineus* (RSA) [255]. This species produces three chemokine-binding proteins, named evasins [256, 257]. Evasins-1 and -4 have similar sequences and bind exclusively to CC chemokines while evasin-3 binds only CXC chemokines. Evasins-1 and -4 differ in selectivity, with evasin-1 binding to three CC chemokines with high affinity and evasin-4 binding to approximately 20 CC chemokines [258]. The structure of evasin-1 has been determined both free and bound to MIP-1α (Figure 1.11), revealing a novel fold different from that of viral chemokine-binding proteins [259]. The evasin-3 structure was reported in the same article but is not available in the PDB database. The bound structure of evasin-1 showed that although evasins are small proteins (8-11 kDa) and about the same size as their binding partners, they can wrap around chemokines and interact with the chemokine regions that are known to be crucial for chemokine receptor interactions, thus preventing chemokines from interacting with and activating their cognate receptors.

From a therapeutic perspective, there is a particular interest in studying ticks for two main reasons. Firstly, ticks carry a range of diseases that can be transmitted to humans when ticks bite and feed off their host [260, 261]. Secondly, when it comes to targeting chemokines, tick evasins, in their natural forms or after appropriate modifications, could potentially be used as therapeutics. Unlike most viral chemokine-binding proteins, they already show some selectivity in the subset of chemokines to which they bind with high affinity. In addition, evasins have already been tested in a range of inflammatory disease models. For example, evasin-1 was successfully tested as a MIP-1α/MIP-1β antagonist in murine models of pulmonary fibrosis [262] and psoriasis [256]; evasin-4 as an eotaxin-1 (CCL11) antagonist in a murine model of inflammatory bowel disease [263]; and evasin-3 as a CXC chemokine antagonist in murine models of arthritis [256] and acute pancreatitis [264]. Another possible advantage of using evasins as therapeutics is that their immunogenicity is expected to be low, based on their low number of predicted $CD4^+$ T-cell epitopes and high degree of glycosylation [265], although this prediction will have to be experimentally tested. Despite evasins presenting a very promising alternative for treatment involving chemokine inhibition, they have not yet progressed from animal models to human clinical trials [266]. The evasin field is still young and additional knowledge is needed before considering clinical trials. In addition, several clinical trials targeting chemokines have previously failed mainly because of the ambivalent or redundant roles chemokines play [267], which adds another degree of difficulty when designing trials.

In summary, evasin proteins are extremely promising as a starting point for selective chemokine-binding proteins. Prior to the work described in this thesis, there were only three known evasins, all from the same tick species. However, it seemed highly likely that other species also produce evasins in order to evade immune detection. Recent efforts in sequencing tick genomes have helped developing multiple databases, which makes looking for evasins in other tick species more accessible. It is indeed crucial to identify more evasins and test them for chemokine-binding activity. This will lead to a larger variety of selectivity profiles, which would facilitate the development of therapeutic agents.

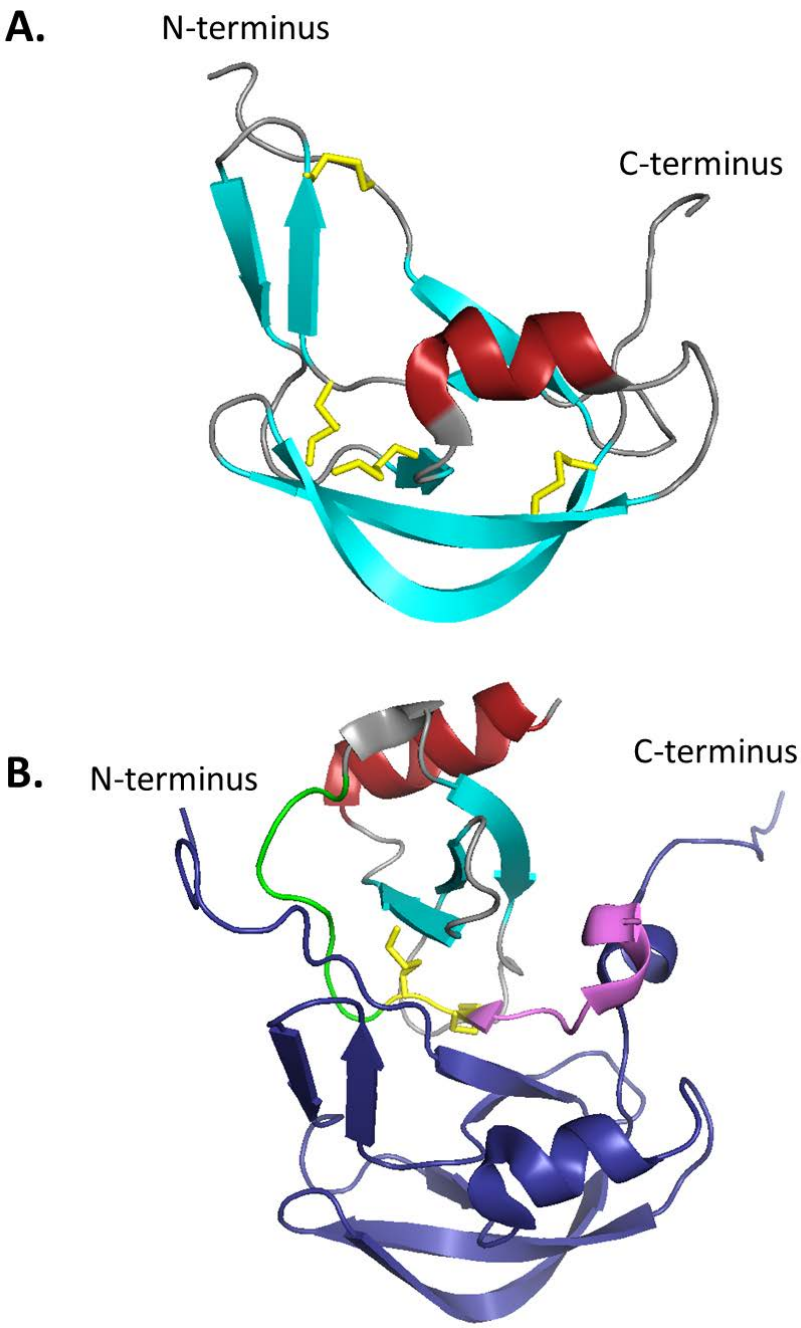

Figure 1.11: Structures of Evasin-1 in Free and MIP-1α-bound Forms [259]. (A) The structure of unbound evasin-1 (PDB ID: 3fpr). The N- and C-termini are labelled, the seven β-strands are shown in cyan, the α-helix in red and the four disulfide bridges in yellow. Evasin-1 fold is new and has a boat-like shape. **(B)** The structure of evasin-1 bound to MIP-1α (PDB ID: 3fpu). N- and C-termini of evasin-1 are labelled and evasin-1 is shown in dark blue. The structural elements of MIP-1α are colour-coded in the same way as Figure 1.2. The N-terminus is shown in magenta, the CC motif and two disulfide bridges are in yellow, the N-loop in green, the three-stranded β-sheet in cyan and the α-helix in red. This shows that evasin-1 interacts mainly with the N-terminus and N-loop of the chemokine which are the main regions involved in chemokine receptor binding.

1.8. Hypotheses

After reviewing the literature in the chemokine field, we can see that chemokines and their receptors play major roles in inflammatory processes whether they are healthy or pathological. Considering the limited success of clinical trials for drugs targeting chemokine receptors, there is a need for more detailed understanding of chemokine:receptor signalling networks. Structural data have been difficult to obtain but mutational data have yielded the two-site model, which describes the binding and activation of chemokine receptors by their cognate chemokines. Although the central features of this widely accepted model provide a reasonable representation of chemokine:receptor interactions, the model does not account for some aspects of receptor activity, including biased agonism and the role of tyrosine sulfation. The project described in this thesis was designed to address three hypotheses related to the two-site model and the various factors that could influence chemokine receptor signalling and chemokine activity:

a. When activated by cognate chemokines, CCR1 exhibits biased agonism that is dependent on receptor tyrosine sulfation.

b. CCR1 activation follows the two-site model, where the receptor N-terminus is responsible for binding and binding selectivity and the chemokine N-terminus is responsible for receptor activation.

c. Novel evasins with selective chemokine-binding profiles can be identified in a variety of tick species.

1.9. Project Aims

1.9.1. Aim 1: To determine whether the CC chemokine receptor CCR1 exhibits biased agonism in response to cognate chemokine ligands and to assess the influence of receptor tyrosine sulfation

Biased agonism has been observed in several GPCRs and chemokine receptors. CCR1 is one of the most promiscuous chemokine receptors, with at least nine cognate chemokines, so it could exhibit biased agonism. In addition, the CCR1 N-terminus has two potential sulfation sites (tyrosine residues surrounded by acidic residues). Prior to this work, it was not known whether these residues are sulfated and whether the sulfation state of CCR1 has an influence on its signalling.

This aim was designed to characterise CCR1 signalling profile by measuring several signalling readouts such as β-arrestin recruitment, G protein activation, cAMP inhibition and ERK1/2 phosphorylation. Biased agonism was then quantified using the operational model of agonism and the same dataset was collected for the non-sulfated CCR1 receptor (cells treated with sodium chlorate) to allow for comparison. Further investigation of CCR1 biased agonism was performed using N-terminally modified HCC-2 chemokines and HCC-2/MCP-3 chimeric proteins.

1.9.2. Aim 2: To investigate the two-site model at the chemokine receptor CCR1

The two-site model is a well-accepted model that was developed in 1997 by Crump *et al.* and that is currently used to describe the interaction between chemokines and their receptors. Although very useful for a number of years, this simple model might need to be refined to account for more recent findings such as biased agonism or post-translational modifications.

This aim involved the study of each site of the two-site model using the chemokine receptor CCR1. Site 1, which involves the receptor N-terminus and is believed to control binding, was investigated by comparing chemokine binding to sulfopeptides derived from the N-terminal sequence of CCR1 with chemokine binding to the full-length receptor. Peptide binding was assessed in solution using a competitive fluorescence anisotropy assay and whole receptor binding was measured using a radioligand displacement assay. Site 2 which involves the chemokine N-terminus and is believed to control receptor activation was investigated using a set of chimeric chemokines between MCP-1 and -3 and measuring the same signalling readouts as in Aim 1. Since MCP-3 is a potent CCR1 agonist whereas MCP-1 is not, the chimeras enabled us to identify the key regions require for CCR1 activation.

1.9.3. Aim 3: To identify novel evasins with chemokine-binding and -inhibitory activity

Three evasin proteins have been identified in the brown dog tick species and are responsible for the chemokine-binding activity observed in the tick saliva. These evasins bind to a specific subset of chemokines, each evasin having a different binding profile. Evasins have a huge potential for therapeutic applications as they already showed some selectivity unlike other viral chemokine-binding proteins. Furthermore, they were efficacious in reducing disease severity in several murine inflammatory disease models and are expected to have a low immunogenicity. The hard tick subfamily alone has around 700 species, which opens up the possibility to identify many chemokine binding proteins.

This aim was set up to identify novel evasins using bioinformatic methods and sequence-based searches. The most promising evasin candidates from several genera were expressed, partially purified and screened for chemokine-binding abilities. The best candidates were fully purified and tested for chemokine-binding and -inhibitory activities.

1.10. Thesis Outline

The results of Aim 1, 2, 3 are presented in Chapters 3, 4 and 5 respectively. The results from Aim 3 were published as a research article in the *Journal of Biological Chemistry* (2017). Hence, this published article is included in this thesis as Chapter 5 and the supplementary material associated with this article are provided in Appendix V.

Chapter 2. Materials and Methods

2.1. Materials

Oligonucleotides designed for recursive PCR or plasmid amplification were purchased from Geneworks (Australia). Clones encoding evasin candidates were purchased from GenScript® (USA). Deoxynucleotide triphosphates (dNTPs) and all the enzymes required for cloning were purchased from NEB (Ipswich, MA) or Promega (Madison, WI, USA). Dulbecco's Modified Eagle Medium (DMEM) and Hanks's balanced salt solution (HBSS) were purchased from Invitrogen. Blasticidin and Hygromycin B were from InvivoGen (San Diego, CA). Foetal bovine serum (FBS) was purchased from In Vitro Technologies (Noble Park, VIC, Australia). Polyethyleneimine (PEI) was purchased from Polysciences, Inc. (Warrington, PA). Coelenterazine h was purchased from NanoLight (Pinetop, AZ). HisTrap HP nickel affinity columns (5 mL volume) and a HiLoad 16/60 Superdex 75 preparative grade size exclusion column (PSEC) were purchased from GE Healthcare. Unless otherwise noted, all other chemicals/reagents were purchased from Sigma-Aldrich.

2.2. Media, Buffers and Solutions

LB media (1 L): 10 g tryptone, 5 g peptone (yeast extract), 10 g NaCl, 1 mL of 1 M NaOH

LB plates: 15 mL of LB media containing 0.23 g agar

Ampicillin: 50 μg/mL in milliQ H_2O

Kanamycin: 30 μg/mL in milliQ H_2O

Lysis buffer: 20 mM Tris.HCl, pH 8.5, 500 mM NaCl, 5 mM imidazole, 0.02 % (w/v) NaN_3

Inclusion body wash buffer: 20 mM Tris.HCl, pH 8.5, 500 mM NaCl, 5 mM imidazole, 0.5 % (v/v) TX-100, 2 mM DTT and 0.02 % (w/v) NaN_3

Refolding buffer: 20 mM Tris. HCl, pH 8.0, 400 mM NaCl, 2.0 mM reduced glutathione (GSH), 0.5 mM oxidised glutathione (GSSG), 0.02 % (w/v) NaN_3

IMAC denaturing load buffer: 6 M Gdn.HCl, 20 mM Tris, pH 8.0, 20 mM imidazole and 20 mM β-mercaptoethanol (β-ME)

IMAC denaturing elution buffer: 6 M Gdn.HCl, 20 mM Tris, pH 8.0, 200 mM imidazole, 20 mM β-ME

Thrombin cleavage buffer: 20 mM Tris.HCl, pH 8.5, 400 mM NaCl, 2.5 mM $CaCl_2$

TEV cleavage buffer: 50 mM Tris.HCl, pH 8.0, 0.5 mM EDTA, 1 mM DTT, 0.02 % (w/v) NaN_3

HisTrap column buffers:

- Buffer A: 20 mM Tris.HCl, pH 8.0, 500 mM NaCl, 20 mM imidazole
- Buffer B: 20 mM Tris.HCl, pH 8.0, 500 mM NaCl, 200 mM imidazole
- HisTrap stripping buffer: 20 mM NaH_2PO_4, 0.5 M NaCl, 50 mM EDTA

Anion exchange buffers:

- Buffer A: 20 mM Bis-Tris (pH 6.5), pH 8.0
- Buffer B: 20 mM Bis-Tris (pH 6.5), 1 M NaCl, pH 8.0

Cation exchange buffers:

- Buffer A: 20 mM Tris.HCl, pH 8.0
- Buffer B: 20 mM Tris.HCl, 2 M NaCl

Size exclusion chromatography buffer: 10 mM HEPES, pH 7.4, 150 mM NaCl, 0.02 % (w/v) NaN_3

SDS-PAGE solutions:

- Running gel buffer: 1.5 M Tris.HCl, pH 8.8
- Stacking gel buffer: 0.5 M Tris.HCl, pH 6.8
- Tank buffer: 0.025 M Tris.HCl, 0.192 M glycine, 3.5 mM SDS
- Gel drying solution: 4 % (v/v) glycerol, 30 % (v/v) EtOH
- Non-reducing loading dye (2X): 0.5 M Tris.HCl, pH 6.8, 2.5 mL glycerol, 0.5 % (w/v) bromophenol blue, 10 % (w/v) SDS
- Reducing loading dye (2X): 0.5 M Tris.HCl, pH 6.8, 2.5 mL glycerol, 0.5 % (w/v) bromophenol blue, 10 % (w/v) SDS, 0.5 mL β-ME
- Fixing solution: 40 % (v/v) methanol, 13.5 % (v/v) formalin in milliQ H_2O
- Developing solution: 3 % (w/v) Na_2CO_3, 0.05 % (v/v) formalin, 0.000016 % (w/v) $Na_2S_2O_3$

Phosphate buffered saline (PBS): 137 mM NaCl, 2.7 mM KCl, 10 mM Na_2HPO_4, 2 mM KH_2PO_4, pH 7.4

Hank's Balanced-Salt Solution (HBSS): 137 mM NaCl, 5.36 mM KCl, 1.3 mM $CaCl_2.2H_2O$, 0.5 mM $MgCl_2.6H_2O$, 0.4 mM $MgSO_4.7H_2O$, 0.34 mM $Na_2HPO_4.7H_2O$, 0.44 mM KH_2PO_4, 4.2 mM $NaHCO_3$, 5.5 mM glucose, pH 7.4

Radioligand buffer: 50 mM MOPS, pH 7.4, 5 mM $MgCl_2$

Radioligand wash buffer: 50 mM MOPS, pH 7.4, 0.05 % (w/v) CHAPS, 0.5 M NaCl

TAE buffer: 2 M Tris, pH 8.0, 5.71 % (v/v) glacial acetic acid, 50 mM EDTA

2.3. Bacterial Strains

The genotypes of competent cells (Invitrogen ™) used in this study are as follows:

- DH5α strain: DH5α™ - Φ80*lac*ZΔM15 Δ(*lac*ZYA-*arg*F) U169 *rec*A1 *end*A1 *hsd*R17 (rK–, mK+) *pho*A *sup*E44 λ– *thi*-1 *gyr*A96 *rel*A1
- BL21 (DE3) strain: BL21 (DE3) - *omp*T *hsd*SB (rB–, mB–) *gal dcm* (DE3)

Competent cells were prepared as follows: A single colony from a plate of freshly grown cells, DH5α or BL21 (DE3), was selected and transferred into 5 mL of LB media. Cells were grown at 37 °C overnight. 2 mL of this overnight culture was used to inoculate 200 mL of LB media in a 500-mL flask. The cells were grown at 37 °C, 180 rpm until the OD_{600} reached ~0.3-0.35. Cells were then harvested by centrifugation at 3000 g for 5 min at 4 °C. The pellet was resuspended gently in 50 mL of 0.1 M $CaCl_2$ (sterile-filtered and chilled on ice), followed by incubation on ice for 20 minutes. Cells were harvested again by centrifugation at 3000 g for 5 min. The pellet was resuspended gently in 4 mL of ice-cold 0.1 M $CaCl_2$. Competent cells were either used immediately at this stage or frozen. For storage in a freezer, a sterile-filtered solution of 75 % (v/v) glycerol was added to give a final concentration of 15 % (v/v) glycerol and aliquots (50 µL) were stored at -80 °C until needed.

2.4. Plasmid Synthesis and Cloning

2.4.1. Recursive PCR and Clone Insertion

Genes encoding chemokine sequences of the chemokines HCC-1/CCL14, HCC-2/CCL15 and MPIF-1/CCL23, each with a N-terminal His_6-tag and a TEV protease cleavage site, were synthesised using recursive polymerase chain reaction (PCR). The oligonucleotides were obtained from Geneworks (Australia) and dissolved to stock concentrations of 100 µM. One full length gene construct was synthesised from six overlapping oligonucleotides, the first three oligonucleotides going in the forward direction and the last three going in the reverse direction. The ratios in which each oligonucleotide is added determines which PCR product prevails in solution. Recursive PCR reactions (total volume 50 µL) contained: oligonucleotides 3 and 4 (0.02 µM each), 2 and 5 (0.1 µM each) and 1 and 6 (1 µM each); dNTPs (0.2 mM each); Pfu buffer and Pfu polymerase (0.204 U/µL, Promega, Madison, WI, USA). Reaction mixtures were heated at 95 °C for 5 minutes and then subjected to 30 cycles of 1 min at 95 °C (denaturation), 1 min at 60 °C (annealing) and 2 min at 72 °C (elongation) using a Minicycler™ (MJ Research). The PCR products were purified by using a QIAquick PCR purification kit (QIAGEN) according to manufacturer's instructions then digested and ligated into the NdeI/XhoI restriction sites of the pET28a plasmid and transformed into DH5α cells. The colonies were further screened for gene insertion using colony PCR and 2 % agarose gel electrophoresis. Recombinant plasmids were prepared and sequenced using the procedures described in 1.4.3. and 1.4.5.

2.4.2. Transformation of DH5α Cells

50 µL of competent *E. coli* DH5α cells were transformed as follows. DNA (1-5 µL) was added to the cells and incubated on ice for 30 minutes. The cell mixture was then heat shocked at 42 °C for 45 seconds and placed on ice for 1-2 min. Subsequently, 450 µL of LB media was added and the cultures incubated in a shaker at 37 °C for 60 min. Cultures were then spread onto LB agar plates containing selection antibiotic and incubated overnight at 37 °C.

2.4.3. Preparation of DNA

A single colony was selected from a plate of transformed DH5α cells and used to inoculate 5 mL of LB media containing the corresponding selection antibiotic. The culture was incubated overnight in a shaker

at 37 °C, 180 rpm. Plasmid DNA was isolated from the cells using a QIAprep Spin Miniprep Kit (QIAGEN) according to manufacturer's instructions. The concentration of plasmid DNA was determined by spectrophotometric analysis from its absorbance at 260 nm, using the formula for double-stranded DNA and a path of 1 cm:

$$[DNA] = 50\ \mu g/mL \times OD_{260} \times \text{dilution factor} \qquad \text{(Equation 1)}$$

The purity of the DNA sample was estimated from the ratio of A_{260}/A_{280}. Generally, ratios in the range of 1.65-1.85 were considered acceptable for DNA sequencing reactions. Higher value ratios indicated RNA contamination, whereas lower values indicated protein contamination. Plasmid samples were stored at -20 °C in a 10 mM Tris.HCl buffer, pH 8.5 for later use.

2.4.4. Agarose Gel Electrophoresis

Agarose gel electrophoresis was used throughout the preparation of any clone to analyse and assess the purity of each sample. To prepare a TAE agarose gel, 2 % (w/v) agarose was added to the TAE buffer and the mixture was heated until the agarose was all dissolved. RedSafe Nucleic Acid staining (20,000x solution, iNtRON Biotechnology) or ethidium bromide (final concentration of 0.5 µg/mL) was added to the agarose mixture and the mixture was set in a cast. Samples were combined with 10X loading dye and loaded on the gel together with a 1kb DNA ladder (Promega) for molecular weight comparison. TAE buffer was used as the tank buffer and the electrophoresis was performed at 100 V until the low molecular weight dye was close to the end of the gel.

2.4.5. DNA Sequencing

DNA samples (5 µL of sample at 200 µM for each reaction) were submitted to Micromon, Monash University, for sequencing. Sequence analysis was performed using the software Sequence Scanner 2.0 (Applied Biosystems).

2.5. Protein Production and Purification

2.5.1. General Methods

The following procedure was used for production of all wild type and chimeric chemokines as well as evasin proteins.

BL21 (DE3) competent cells were transformed with the desired expression plasmid and screened for optimal protein expression. A single colony was used to inoculate the starter culture, 50 mL of LB media containing kanamycin (30 µg/mL) or ampicillin (50 µg/mL). The culture was grown overnight in a shaker incubator at 37 °C, 180 rpm. For large-scale growth, 4 x 2 L flasks, each containing 1 L of LB/antibiotic media, were inoculated with 10 mL of the overnight starter culture and grown at 37 °C, 180 rpm until the optical density (OD_{600}) reached ~0.6-0.7. The expression of the desired protein was induced by addition of isopropyl β-D-1-thiogalactopyranoside (IPTG) to each flask at a final concentration of 1 mM. Protein expression was allowed overnight at 37 °C, 180 rpm.

Cells were harvested the next day via centrifugation (Sorvall Evolution RC-SLC 6000 rotor, 5000 rpm, 20 min, 4 °C). The resultant pellet was resuspended in lysis buffer (60 mL) and hen egg white lysozyme (20 mg) was added. The mixture was incubated for 30 min at RT, followed by sonication of the cells with 6 x 30 sec bursts at 10 Amp, with 1 min incubation on ice between bursts (MSE Soni prep 150 plus). The insoluble fraction was separated by centrifugation (Sorvall Evolution SS-34 rotor, 15000 rpm, 20 min, 4 °C) and resuspended in lysis buffer (60 mL). DNase I (20 µg) was added to degrade the genomic DNA and the mixture was incubated for 30 min at RT. The inclusion bodies were washed at least twice with the inclusion body wash buffer (2 x 60 mL or until the supernatant was not brown in colour anymore) and left to denature overnight in the IMAC denaturing load buffer (60 mL). The denatured inclusion bodies were purified by immobilised metal affinity chromatography (IMAC) using Ni-NTA agarose affinity resin (QIAGEN/Sigma; ~10 mL wet volume). The denatured protein was loaded on the beads (1 h incubation), the resin was then washed twice with the IMAC denaturing load buffer (40 mL each time) and the protein was then removed from the beads using the IMAC denaturing elution buffer (20 mL, 20 min incubation). The desired protein was then refolded by rapid dilution (0.1 mL/min dropwise addition) into the refolding buffer (2 L). The solution was left overnight at 4 °C to ensure the refolding equilibrium had been reached. The refolded protein solution was filtered and degassed using a SPARMAX pump then loaded (5 mL/min) onto a 5 mL HisTrap nickel affinity column using an AKTA purifier chromatography system (GE). The column was washed with HisTrap buffer A and the purified protein was eluted at 5 mL/min using a stepwise isocratic gradient with HisTrap buffer B. The fractions showing UV absorbance were further analysed on SDS-PAGE under reducing and non-reducing conditions.

Unless stated otherwise, the next step of the purification process was the removal of the N-terminal His_6 tag. For this the eluted protein was dialyzed against TEV protease or thrombin cleavage buffer overnight at room temperature using snakeskin dialysis tubing (3500 Da molecular weight cut off (MWCO)). The amount of protein present in the dialysis tube was determine using spectrophotometry (280 nm) and the Beer-Lambert law:

$$\text{mass} = A/\varepsilon \times l \times Mw \times V \qquad \text{(Equation 2)}$$

where A is the observed UV absorbance (280 nm); ε is the molar absorptivity coefficient for each protein; l is the length of the cuvette (1 cm); Mw is the molecular weight of the protein to cleave and V is the total volume of the sample. Samples were then incubated with TEV protease or thrombin (0.02 mg/mg of protein or 10 U/mg of protein respectively) overnight at 34 °C and 37 °C respectively to remove the N-terminal His_6-tag. To stop the thrombin cleavage reaction, phenylmethanesulfonylfluoride (PMSF) was added at a final concentration of 200 µM. The protein was again loaded on a 5 mL HisTrap column to remove the His_6 tag, as well as any remaining uncleaved protein and the His-tagged TEV protease when relevant. The flow-through containing the cleaved protein was collected, concentrated down to 2 mL and loaded onto a Hi-load 16/60 Superdex 75 preparative grade size exclusion chromatography (PSEC) column attached to an AKTA purifier FPLC system (GE). The protein was eluted using the size exclusion chromatography buffer at 0.3 mL/min. The fractions showing UV absorbance were further analysed on SDS-PAGE under reducing and non-reducing

conditions to evaluate disulfide formation and purity. If the protein was not pure, it was further purified by ion exchange chromatography using 5 mL HiTrap Q HP (anion exchange) or HiTrap SP HP (cation exchange) columns eluted at a 5 mL/min flow rate, a salt gradient with anion or cation exchange buffers and an AKTA purifier chromatography system(GE). The fractions showing UV absorbance were further analysed on SDS-PAGE under reducing and non-reducing conditions to evaluate folding and purity. Protein integrity was confirmed by MALDI-TOF mass spectrometry. Fractions containing the desired protein were pooled, concentrated and stored at -20 °C until further use.

2.5.2. SDS-PAGE Gel Electrophoresis

A 15 % crosslinking polyacrylamide running gel was prepared and polymerisation initiated with 0.1 % ammonium persulfate (APS), stabilised by 0.01 % TEMED. This was immediately poured between the plates of a Mini-Protean II SDS-PAGE apparatus (Bio-Rad®). When the running gel had polymerised, a 4 % crosslinking stacking gel was prepared with 0.1 % APS, 0.01 % TEMED and poured on top of the running gel. A comb was added into the top of the stacking gel to form wells, and the gel allowed to polymerise. Once the gel had polymerised, samples were boiled for 5 minutes and then loaded into the wells alongside protein markers (Bio-Rad®) and electrophoresis was performed at 120 V through the stacking gel and 150 V through the separating gel in a Mini-Protean II assembly (Bio-Rad®) with SDS-PAGE tank buffer until the dye front migrated to the bottom of the gel.

2.5.3. Silver Staining

To stain the gel, the running gel was removed from the glass plates and incubated at room temperature for 10 minutes in fixing solution, followed by washing with milliQ water, 1 min in 0.02 % $Na_2S_2O_3$, followed by another wash with milliQ water, and then 10 minutes in 0.1 % silver nitrate solution. The gel was then washed twice with milliQ water and incubated in developing solution (approx. 1-3 min) until protein bands were visible. Citric acid (2.3 M) was used to stop the colour development and the gel was then washed a further 3 times in milliQ water.

2.6. Nuclear Magnetic Resonance (NMR)

NMR experiments were conducted at 25 °C on a Bruker Avance 600 MHz NMR spectrometer equipped with a triple-resonance cryoprobe. Chemical shifts were referenced to external 4,4-dimethyl-4-silapentane-1-sulfonic acid (DSS). Protein samples were exchanged into 20 mM sodium acetate-d_4, pH 7.0 containing 5% D_2O. 1D ^1H experiments were recorded using 128 scans using gradient water suppression. NMR data was processed and analysed using Bruker TopSpin software.

2.7. Fluorescence Anisotropy Assay (FAA)

All FAA were performed at 25 °C using a PHERAstar plate reader (BMG Labtech, Ortenberg, Germany) equipped with a fluorescence polarisation module with dedicated excitation and emission wavelengths of 485 and 520 nm respectively. All sulfopeptides were synthesised in the laboratory of A/Prof Richard Payne (The University of Sydney) using solid phase peptide synthesis (SPPS) [147]. Sulfopeptide concentrations were determined using UV spectrophotometry and RP-HPLC [141]. Due to the absorbance at

280 nm of sulfotyrosine being too weak to assess concentrations directly, the non-sulfated peptide was used to build a standard curve at 214 nm and determine the concentrations of the corresponding sulfated peptides. The assay is a two-step process in which the first step, called direct binding assay, determines the affinity of a chemokine for a fluorescein-tagged sulfopeptide (Fl-R2D) used as a probe. The second step, called competitive binding assay, determines the affinity of a chosen competitor (non-fluorescent sulfopeptide or evasin) for the chemokine by measuring its ability to displace the chemokine from the fluorescein-tagged probe. The samples were prepared in 50 mM MOPS buffer (pH 7.4) using Greiner non-binding, black, flat-bottomed, 96-well microplates (catalogue no. 655900) or Greiner non-binding, black, flat-bottom, small volume, 384-well microplates (catalogue no. 784900) coated with 0.001 % poly-L-lysine. Final volumes of 200 and 20 µL per well were used for the 96-well and 384-well plates, respectively. A separate well containing free fluorescein (5 nM) was used as a reference for focal height adjustment and intensity and anisotropy calibration. The direct binding assays were performed using a chemokine solution which was serially 2-fold diluted on the plate with MOPS buffer (final concentrations from 2000 to 31 nM). A solution of Fl-R2D was then added to all the wells (final concentration of 10 nM). The competitive binding assays were performed using invariable final concentrations of the chemokine (100 nM) and Fl-R2D (10 nM) and with a range of concentrations for the competitor (non-fluorescent sulfopeptides R2A-R2D, R1A-R1D or evasin candidates) which were serially 2-fold diluted on the plate using the highest final concentrations of 100 µM (for R1A and R2A), 50 µM (for R1B, R1C, R2B and R2C), 10 µM (for R1D and R2D), 1 µM (for the evasin candidates) and 300 nM (for evasin-4 with a 1.33 dilution factor). The plates were read after 5 min to measure fluorescence anisotropy and assays were performed in duplicate, three times independently.

2.8. Cell-Based Assays

2.8.1. Mammalian Cell Line and Culture

All experiments used human embryonic kidney 293 (HEK 293) cells stably transfected with the Flp-In™ T-REx™ vector expression system (Flp-In™ T-REx™ 293, Invitrogen™). The Flp-In expression system ensures that a single copy of the receptor transgene is incorporated into the same position of the genome in each cell, maintaining equal receptor expression levels across cells. The T-REx (tetracycline-regulated expression) system places the receptor gene under transcriptional control of the tetracycline-repressor gene that allows transcription only in the presence of tetracycline. The receptors used for the evasin candidate assays were cMyc-FLAG-(human)CCR2 and cMyc-FLAG-(human)CCR3, stably transfected into HEK 293 cells. The rest of the assays were performed using His_6-cMyc-(human)CCR1 stably transfected into HEK 293 cells, except for the β-arrestin recruitment assay in which the transfection is transient. Cells were grown and maintained in full media comprised of Dulbecco's modified eagle medium (DMEM, Gibco®) supplemented with 5 % (v/v) tetracyclin-free fetal bovine serum (FBS, Gibco), 5 µg/mL blasticidin (Invitrogen) to maintain selection of cells stably transfected with the tetracyclin repressor gene (tetR) and 200 µg/mL hygromycin B (Invitrogen) to maintain selection of cells stably transfected with the gene of interest. Cells were grown and maintained at 37 °C in 5 % CO_2 in 175 cm^2 flasks and were detached from the flask by washing with versene (PBS/EDTA), followed by incubation in 1 % (w/v) trypsin in versene for 5 minutes. Tyrosine sulfation was

inhibited 48 hours prior to each experiment by addition of 30 mM sodium chlorate ($NaClO_3$) to cell media. Receptor expression was induced 24 hours prior to each experiment by addition of 10 µg/mL tetracycline to cell media.

2.8.2. Generation of Stable Cell Lines

Correctly sequenced plasmids were used to generate stable cell lines. 2.5 x 10^6 HEK 293 Flp-In T-Rex cells were plated in a T25 flask. The DNA (10 µg in total: 1 µg pcDNA5/FRT/TO-gene of interest + 9 µg pOG44 Flp-recombinase expression vector) was diluted in 625 µL of reduced serum media (Opti-MEM). 25 µL Lipofectamine 2000 (Invitrogen™) was mixed with 600 µL Opti-MEM and incubated at RT for 5 min and then was added to the DNA tubes, which were then incubated for 20 min at RT. The old media from the cells was replaced by Opti-MEM. This was followed by the addition of (1.25 mL) complexes (Lipofectamine and DNA) to the cells and plates were incubated at 37 °C, 5 % CO_2. The media was changed after 4-6 h to Dulbecco's Modified Eagle Medium (DMEM) supplemented with 5 % (v/v) tetracycline-free FBS. Cells were split 48 h post-transfection. Selection of the cells was started using the media containing hygromycin B (200 µg/mL) and blasticidin (5 µg/mL). The cells were fed with the selective medium every 3-4 days until foci were visible. This process was repeated until a stable cell-line was achieved.

2.8.3. ERK1/2 Phosphorylation Assay

HEK 293 cells stably transfected with His_6-cMyc-(human)CCR1 were seeded in a poly-D-lysine-coated 96-well plate in full media containing 10 µg/mL of tetracycline (around 5 x 10^5 cells per well) and grown overnight at 37 °C in 5 % CO_2. Cells were then washed twice with PBS and serum starved overnight to minimise basal levels of phosphorylation by incubating in serum-free media (SFM) containing 10 µg/mL of tetracycline. The cells were stimulated with chemokines in SFM to a total volume of 100 µL per well. Initially a time-course experiment was conducted over an hour which determined that peak levels of ERK1/2 phosphorylation were achieved at 5 minutes after the addition of chemokine. In subsequent concentration response experiments, cells were stimulated with chemokines for 5 minutes at 37 °C. The reaction was stopped by removing the media and adding 100 µL of SureFire lysis buffer per well. Lysis of cells was assisted by shaking the plate on a plate shaker at 600 rpm for 5 minutes. ERK1/2 phosphorylation was detected in cell lysates using the AlphaScreen®35 SureFire® pERK1/2 Assay Kit (PerkinElmer, TGR biosciences). 5 µL of lysate from each well was transferred to a white 384-well Proxiplate™ and 8 µL of SureFire AlphaScreen detection mix (240:1440:7:7 v/v dilution of SureFire activation buffer: Surefire reaction buffer: AlphaScreen acceptor beads: AlphaScreen donor beads) was added to each well in green light conditions. This detection mix contains antibodies that form complexes with phosphorylated ERK1/2. AlphaScreen donor and acceptor beads are brought closer by binding the antibody complexes, allowing energy transfer from the donor to the acceptor bead which increases the fluorescence of the acceptor beads with increasing pERK (Figure 3.1). The plate was incubated in the dark at 37 °C for 1.5 hour after which an Envision® plate reader (PerkinElmer) was used to measure fluorescence signal using standard AlphaScreen settings. The data were normalised between the fluorescence emitted without chemokine (0 % response) and in the presence of 10 % (v/v) FBS (100 %

response) which non-specifically increases ERK1/2 phosphorylation. All experiments were performed in duplicate and at least three times independently.

2.8.4. Inhibition of Forskolin-Induced cAMP Production

HEK 293 cells stably transfected with the desired receptor were plated in a Petri dish (about 2.5 x 10^6 cells per dish) and allowed to grow overnight in full media at 37 °C, 5 % CO_2. The following day, cells were transfected in full media with the cAMP BRET biosensor CAMYEL. This biosensor consists of Renilla luciferase (Rluc) and yellow fluorescent protein (YFP), which are linked by a polypeptide corresponding to Epac (exchange protein activated by cAMP) (Figure 3.1) and allows detection of relative cAMP levels by measurement of a BRET signal [268]. For transfection, 2 µg of CAMYEL DNA was diluted in 150 mM NaCl and added to an equal volume of 150 mM NaCl containing 12 µg of PEI (1:6 DNA to PEI ratio). The transfection mixture was vortexed immediately for 5 seconds, incubated at RT for 10 minutes and then added to the cells in full media. Cells were allowed to grow in transfection media mix for 24 hours at 37 °C, 5 % CO_2. Cells were then replated in a poly-D-lysine-coated 96-well white-bottom Culturplate (PerkinElmer) in full media containing 10 µg/mL tetracycline and cells were incubated for a further 24 hours. Cells were washed once with 100 µL per well of HBSS and incubated in fresh HBSS for approximately 30 min at 37 °C. Cells were stimulated in HBSS to a total volume of 100 µL per well. The Rluc substrate coelenterazine h was added to each well (final concentration of 5 µM) and cells were incubated for 5 minutes at 37 °C. After 5 minutes, cells were stimulated with chemokines and incubated for a further 5 minutes at 37 °C. Forskolin, which stimulates the production of cAMP via adenylate cyclase (AC), was then added to each well (final concentration of 10 µM) and cells incubated for a final 5 minutes before detection. YFP and Rluc emission signals (535 and 475 nm respectively) were measured using a PHERAstar plate reader (BMG Labtech, Ortenberg, Germany) and the ratio of YFP:Rluc was used to quantify the relative cAMP level in each well. Data were normalised between the YFP:Rluc value in the absence of chemokine and forskolin (low cAMP, 100 % inhibition) and the YFP:Rluc in the presence of 10 µM forskolin and absence of chemokine (high cAMP, 0 % inhibition). All experiments were performed in duplicate and at least three times independently.

2.8.5. β-arrestin 2 Recruitment

Parental HEK 293 cells were plated in a Petri dish (about 2.5x10^6 cells per dish) and allowed to grow overnight in full media at 37 °C, 5 % CO_2. The following day, cells were transfected in full media with CCR1-Rluc DNA and β-arrestin-2-YFP DNA. 1 µg of CCR1-Rluc and 4 µg of β-arrestin-2-YFP were diluted in 150 mM NaCl and added to an equal volume of 150 mM NaCl containing 30 µg of PEI (1:6 total DNA to PEI ratio) and vortexed for 5 seconds immediately. The transfection mixture was incubated at RT for 10 minutes and then added to the cells in full media. Cells were allowed to grow in transfection media mix for 24 hours at 37 °C, 5 % CO_2. Cells were then replated in a poly-D-lysine-coated 96-well white-bottom Culturplate in full media and allowed to grow for another 24 hours. Cells were then washed once with 100 µL per well of HBSS and incubated in fresh HBSS for approximately 30 min at 37 °C. Cells were stimulated in HBSS to a total volume of 100 µL per well. The Rluc substrate coelenterazine h was added to each well (final concentration of 5 µM) and cells were incubated for 5 minutes at 37 °C. After 5 minutes, cells were stimulated with

chemokines and incubated for a further 10 minutes at 37 °C. YFP and Rluc emission signals (535 and 475 nm respectively) were measured using a PHERAstar plate reader and the ratio of YFP:Rluc was used to quantify β-arrestin-2 recruitment in each well. Data were normalised by subtracting the YFP:Rluc ratio measured in the absence of chemokine. All experiments were performed in duplicate and at least three times independently.

2.8.6. G Protein Activation

HEK 293 cells stably transfected with His_6-cMyc-(human)CCR1 were plated in a Petri dish and allowed to grow in full media at 37 °C in 5 % CO_2 overnight. The following day, cells were transfected in full media with 2 µg of $G_{\alpha i}$, 1 µg $G_{\beta\text{-Venus(C-terminus)}}$, 1 µg of $G_{\gamma\text{-Venus(N-terminus)}}$ and 1 µg of masGRK3-ct-Rluc [269] were diluted in 150 mM NaCl and added to an equal volume of 150 mM NaCl containing 30 µg of PEI (1:6 total DNA to PEI ratio) and vortexed for 5 seconds immediately. The transfection mixture was incubated at RT for 10 minutes and then added to the cells in full media. Cells were allowed to grow in transfection media mix for 24 hours at 37 °C, 5 % CO_2. Cells were then replated in a poly-D-lysine-coated 96-well white-bottom Culturplate in full media containing 10 µg/mL tetracycline and allowed to grow for another 24 hours. Cells were then washed once with 100 µL of HBSS and incubated in fresh HBSS for approximately 30 min at 37 °C. Cells were stimulated in HBSS to a total volume of 100 µL per well. The Rluc substrate coelenterazine h was added to each well (final concentration of 5 µM) and cells were incubated for 5 minutes at 37 °C. After 5 minutes, cells were stimulated with chemokines and incubated for a further 10 minutes at 37 °C. Venus and Rluc emission signals (535 and 475 nm respectively) were measured using a PHERAstar plate reader and the ratio of Venus:Rluc was used to quantify relative levels of trimeric G protein dissociation in each well. Data were normalised by subtracting the Venus:Rluc ratio measured in the absence of chemokine. All experiments were performed in duplicate and at least three times independently.

2.8.7. Receptor Binding Assay using a Radioligand Probe

Radioligand displacement assay was performed as described by Zweemer et al. [270] using ^{125}I-CCL3 purchased from PerkinElmer (Product number: NEX298005UC). Labelled chemokines were stored for less than a week before use to avoid decay. Cell membranes were prepared by centrifuging CCR1 or CCR2 expressing cells for 5 minutes at 3000 g. The pellet was resuspended in ice-cold radioligand buffer and homogenised by sonication. Membranes and the cytosolic fraction were separated by centrifugation at 40,000 g at 4 °C for 20 minutes. The pellet was resuspended in 10 mL of radioligand buffer, and the homogenisation and centrifugation steps were repeated. Finally, the membrane pellet was resuspended in radioligand buffer and aliquoted for storage at -20 °C. Membrane protein concentration was measured using a BCA protein determination [271]. ^{125}I-CCL2 or ^{125}I-CCL3 binding assays were performed in a 100 µL reaction volume containing radioligand buffer and 10 µg of membrane protein. For competition experiments, increasing concentrations of non-labelled chemokines were incubated with 50 pM of ^{125}I-CCL2 or ^{125}I-CCL3 for 2 hours at RT. At this concentration, total radioligand binding did not exceed 10 % of the amount added to prevent ligand depletion. Nonspecific binding was determined with 10 µM INCB3344 or BX471 (CCR2 and CCR1 antagonist, respectively). Separation of bound from free radioligand was performed by rapid filtration through a 96-well GF/B filter plate precoated with 0.25 % PEI using a Filtermate-harvester (PerkinElmer, Groningen,

The Netherlands). Filters were washed 3 times with ice-cold radioligand wash buffer and dried at 50 °C for 1 hour. 25 µL of MicroScint-O scintillation cocktail (PerkinElmer) was added to each well and the filter-bound radioactivity was determined by using a MicroBeta2 LumiJET 2460 Microplate Counter (PerkinElmer). All experiments were performed in duplicate at least three independent times.

2.9. Data Analysis and Statistics

2.9.1. Fluorescence Anisotropy

All data points represent the mean and error bars represent the standard error of the mean (SEM) of at least three independent experiments. The results were analysed using Prism 6.0 (GraphPad Software Inc., San Diego, CA). The direct binding data were fitted with a non-linear 1:1 binding equilibrium model described by the following equation:

$$Y = \mathrm{Y}_i + \left(\mathrm{Y}_f - \mathrm{Y}_i\right) \times \left(\frac{1}{2\mathrm{P}_t}\right)\left[(\mathrm{P}_t + \mathrm{L}_t + \mathrm{K}_d) - \sqrt{((P_t + L_t + K_d)^2 - 4\mathrm{P}_t\mathrm{L}_t)}\right] \qquad \text{(Equation 3)}$$

in which: Y is the observed anisotropy; Y_i and Y_f are the initial and final anisotropy, respectively; P_t is the total concentration of Fl-R2D; L_t is the total concentration of the chemokine and K_d is the fitted equilibrium dissociation constant.

The competitive binding data were fitted with a non-linear 1:1 competitive displacement equation derived by Huff et al. [272], where the concentration of the non-fluorescent peptide was the independent variable while the dependent variable was the observed anisotropy; fixed input parameters were the total concentrations of Fl-R2D and chemokine, the final anisotropy value which corresponds to the anisotropy of the free Fl-R2D and the affinity between Fl-R2D and chemokine (K_d value obtained from the direct binding assay). The fitted parameters were the initial anisotropy and the K_d between the competitor and the chemokine.

2.9.2. Receptor Binding Assay using a Radioligand Probe

All data points represent the mean and error bars represent the standard error of the mean (SEM) of at least three independent experiments. The results were analysed using Prism 6.0 (GraphPad Software Inc., San Diego, CA). The concentration of agonist that inhibited half of the ^{125}I-CCL3 binding (IC_{50}) was determined using a non-linear one site competitive binding fit described by the following equation:

$$Y = \frac{Top - Bottom}{1 + 10^{(X - logIC_{50})}} + Bottom \qquad \text{(Equation 4)}$$

in which X denotes the concentration of unlabeled ligand, Y denotes the percentage-specific binding, *Top* and *Bottom* denote the maximal and minimal asymptotes, respectively and IC_{50} denotes the X-value when the response is midway between *Bottom* and *Top*.

2.9.3. Concentration-Response Curves

All data points represent the mean and error bars represent the standard error of the mean (SEM) of at least three independent experiments. The results were analysed using Prism 6.0 (GraphPad Software Inc., San Diego, CA). All data from concentration-response curves for signalling responses (β-arrestin 2, ERK1/2 phosphorylation, cAMP production and G protein activation) were normalised as outlined above and fitted using the following three parameter equation:

$$Y = bottom + \frac{top - bottom}{1 + 10^{(\log EC_{50} - \log[A])}} \quad \text{(Equation 5)}$$

in which *top* and *bottom* represent the maximal and minimal asymptote of the concentration–response curve, [*A*] is the molar concentration of agonist and EC_{50} is the molar concentration of agonist required to give a response half way between *bottom* and *top*.

2.9.4. Quantification of the Signalling Bias

Each individual concentration–response curve was also fitted to the following form of the operational model of agonism [273] to allow the quantification of biased agonism:

$$Y = basal + \frac{(E_m - basal)\left(\frac{\tau}{K_A}\right)^n [A]^n}{[A]^n\left(\frac{\tau}{K_A}\right)^n + \left(1 + \frac{[A]}{K_A}\right)^n} \quad \text{(Equation 6)}$$

in which E_m is the maximal possible response of the system, *basal* is the basal level of response, *[A]* is the molar concentration of each agonist, K_A represents the equilibrium dissociation constant of the agonist and τ is an index of the signalling efficacy of the agonist that is defined as R_T/K_E, where R_T is the total number of receptors and K_E is the coupling efficiency of each agonist-occupied receptor, and *n* is the slope of the transducer function that links occupancy to response. The analysis assumes that the transduction machinery used for a given cellular pathway are the same for all agonists, such that the E_m and transducer slope *(n)* are shared between agonists. Data for all chemokines for each pathway were fitted globally, to determine values of K_A and τ. Biased agonism was quantified as previously described [124]. In short, to exclude the impact of cell-dependent and assay-dependent effects on the observed agonism at each pathway, the $\log(\tau/K_A)$ value of a reference agonist, in this case HCC-2, is subtracted from the $\log(\tau/K_A)$ value of the other chemokines to yield $\Delta\log(\tau/K_A)$. The relative bias can then be calculated for each chemokine at the two different signalling pathways by subtracting the $\Delta\log(\tau/K_A)$ of one pathway from the other to give a $\Delta\Delta\log(\tau/K_A)$ value, which is a measure of bias. A lack of biased agonism will result in values of $\Delta\Delta\log(\tau/K_A)$ not significantly different from 0 between pathways. To account for the propagation of error associated with the determination of composite parameters, the following equation was used:

$$Pooled\_SEM = \sqrt{(SEj1)^2 + (SEj2)^2} \quad \text{(Equation 7)}$$

Where *pooled_SEM* is the calculated error for the difference and SE_j1 and SE_j2 is the individual uncorrelated/random error values used to propagate the pooled SEM value.

2.9.5. Statistical Analysis

All affinity (pIC_{50}), potency (pEC_{50}) and transduction ratio ($\log(\tau/K_A)$) parameters were estimated as logarithms. Christopoulos *et al*. have previously demonstrated that the logarithm of the measure is

approximately Gaussian [274] and, as the application of t-tests and analyses of variance assume Gaussian distribution, estimating the parameters as logarithms allows valid statistical comparison.

Multiple t-test comparison with Holm-Sidak correction or one way ANOVA were used as stated in figure legends. Significance is defined as * for $p< 0.05$, ** for $p<0.01$ and *** for $p < 0.001$ for the comparison graphs.

Chapter 3. Characterisation of Biased Agonism at the Chemokine Receptor CCR1

3.1. Background

CCR1 is a member of the CC chemokine receptor subfamily and is mainly expressed on the cell surface of monocytes, natural killer (NK) cells and immature myeloid cells [178]. It has been linked to a large variety of diseases [179], particularly inflammatory diseases such as multiple sclerosis [181] and rheumatoid arthritis [203] and plays a role in transplant rejection [197] and cancer [182, 275]. It is a highly promiscuous receptor that interacts with at least nine CC chemokines and is already recognised as a drug target. Small molecule inhibitors for CCR1 have been developed, the most common one being BX471 [200]. However, no CCR1 inhibitor is currently approved for treatment mainly due to a lack of efficacy in clinical trials [209].

The chemokine:receptor network is highly complex. Most chemokines bind and activate several chemokine receptors. Correspondingly, most chemokine receptors bind and respond to multiple chemokines. Previously, the existence of several ligands for the same receptor was considered as redundancy [276, 277]. However, it is now well accepted that different chemokines can activate the same receptor in different ways, leading to different signalling and cellular effects. This suggests that the network is even more complex than it was once thought to be and that there is an opportunity for fine-tuning the receptor's responses to selectively recruit leukocytes depending on the type of inflammatory stimuli the tissues are exposed to.

Biased agonism, also known as functional selectivity, has recently attracted a lot of interest in the GPCR field. It is defined by the fact that different ligands activate a shared receptor differentially, leading to the stabilisation of different active conformations of the receptor [278]. This causes the receptor to interact with different effectors, ultimately giving rise to different signalling and cellular outcomes [279]. Biased agonism has already been reported among chemokine receptors. For example, Kohout et al. have reported that ELC and SLC have shown biased agonism with CCR7, both ligands being equally potent for calcium mobilisation, but ELC showing a 4-fold increase in ERK phosphorylation compared to SLC [126]. In addition, Rajagopal *et al.* demonstrated that cutaneous T-cell attracting chemokine (CTACK or CCL27) and mucosae-associated epithelial chemokine (MEC or CCL28) were biased when activating CCR10, both chemokines signalling through G protein-mediated pathways but only CTACK promoting receptor internalisation through β-arrestin-mediated pathways [127]. In the same article, CCR1 was shown to exhibit biased agonism when activated by various CC chemokines (MIP-1α, RANTES, HCC-1, HCC-2 and MPIF-1). Similarly, Corbisier et al. reported biased agonism in CCR2 and CCR5 between G protein subtypes [128], which shows an extreme degree of complexity in the chemokine network.

To better understand the mechanisms regulating the interactions between chemokines and their receptors, the two-site model was developed by Crump *et al.* in 1997 [280]. This widely cited model is a good working model as it accounts for the results of numerous previous structure-function studies. This model identifies two distinct sites, one involving interactions between the N-loop and β3 regions of the chemokine and the N-terminus of the receptor, controlling receptor binding, the second involving the N-terminus of the chemokine interacting with transmembrane helices of the receptor, controlling receptor activation and signalling. Despite being a useful tool, this model may not be detailed enough to account for some more refined concepts that

have emerged more recently such as biased agonism or the influence of post-translational modifications on signalling responses.

Several post-translational modifications can happen on both chemokine and receptor and have the potential to influence the signalling responses engendered by the interaction between chemokines and receptors. On the receptor side, one of the main post-translational modifications is tyrosine sulfation. Several chemokine receptors have already been proven to be sulfated [138] and although CCR1 is not among those, it has two tyrosine residues in a relatively acidic environment which makes them good candidates for sulfation. Tyrosine sulfation has been reported to increase binding affinity of chemokines for the receptors as well as potency [145], so it could potentially influence biased agonism.

On the chemokine side, an important post-translational modification that has a major impact on receptor activation is N-terminal truncation. Chemokines are originally expressed with a signal sequence that gets cleaved off to produce a mature protein. However some chemokines, such as the CCR1 ligand HCC-2, can be further processed on their N-termini by proteases, which generates an array of chemokines with N-terminal regions of various lengths. The chemokine N-terminus being the main region governing receptor activation, varying its length usually leads to inactive mutants. However, HCC-2, which initially has a long N-terminus (31 residues before the CC motif), is only partially active in its full-length form whereas removal of 24 or 26 residues (HCC-2(Δ24) and HCC-2(Δ26), respectively) converts it into its most potent forms [41]. HCC-2(Δ12) has also been reported to activate CCR1, which is surprising considering that numerous studies have shown how sensitive chemokine N-termini are to mutations or truncations.

Considering the ability of CCR1 to be activated by a variety of chemokine ligands and the potential of both the receptor and its ligands to undergo post-translational modifications, we hypothesised that differential signalling responses of CCR1 may be influenced by those modifications. To this end, we undertook a systematic study of CCR1 biased agonism, as described in this chapter. In addition to comparing the CCR1 signalling profiles in response to several chemokines, we also investigated the influences of various factors, including receptor tyrosine sulfation and chemokine N-terminal modifications, and characterised the kinetics of the CCR1 signalling.

3.2. CCR1 Signalling Responses

Binding of chemokines to their cognate receptor results in activation of several downstream pathways that can be monitored to determine whether the different ligands are biased towards one pathway relative to another. There are many options in the readouts that can be measured. For this study we selected two proximal, non-amplified assays (recruitment of β-arrestin 2 (β-Arr2) and G protein activation (GPA)) and two downstream, amplified signals (inhibition of adenosine 3',5'-monophosphate (cAMP) production and phosphorylation of ERK1/2). For the proximal signals, the best-coupled ligand will be the most efficacious ligand. However, for the amplified signals, maximal efficacies are similar for differently-coupled ligands because the signals are amplified to the full capacity of the pathway even when the receptor is not fully activated. In this case, strongly coupled ligands are expected to exhibit higher potency than weakly coupled ligands [281]. Initially, three chemokines (HCC-2(Δ26), MCP-2 and MCP-3) were used to activate CCR1 and compared to assess for biased agonism at CCR1.

Binding between CCR1 and the chemokines was measured using a radioligand displacement assay (Figure 3.1A). Membranes of HEK 293 cells overexpressing CCR1 were incubated with ^{125}I-MIP-1α and increasing concentrations of non-labelled chemokines. HCC-2 had the highest affinity for CCR1 (pIC_{50} = 10.2 ± 0.2), followed by MCP-3 (pIC_{50} = 9.6 ± 0.2) and MCP-2 (pIC_{50} = 8.7 ± 0.1). HCC-2 having the highest affinity for CCR1, it was chosen as a reference for the bias factor calculations.

The first proximal signal that was measured was β-Arr2 recruitment. This assay used CCR1-Rluc8 and β-Arr2-YFP constructs in HEK293 cells (see Chapter 2, section 2.7.5 for details). β-Arr2 recruitment to the receptor brings the YFP and Rluc8 proteins close to each other which enables the BRET signal to be detected. The three chemokines induced β-Arr2 recruitment with different potencies, HCC-2 being the most potent, followed by MCP-3 and then MCP-2 (Figure 3.1B). However, HCC-2 and MCP-2 had similar efficacies (around 0.08 AFU above the baseline) and MCP-3 had a significantly lower efficacy (around 0.03 AFU above the baseline). The order of efficacies for this assay was different from what would have been expected if coupling to the β-arr2 pathway was simply a reflection of ligand binding affinity. This difference is an early indication of biased agonism.

The second proximal signal that was measured was G protein activation (GPA). This assay used a wild-type Gα subunit (which allows for Gα screening), a Gβ subunit tagged with the C-terminal part of a Venus protein, a Gγ subunit tagged with the N-terminal part of a Venus protein and a GRK3-Rluc8 construct that is embedded in the cell membrane [269]. When the receptor is activated, the trimeric G protein is separated in two parts and the Gβγ subunit is recruited to GRK3, which brings the Venus and Rluc8 proteins close to each other and enables the BRET signal to be detected (Figure 3.1C). The order of potencies was the same as the β-arr2 assay but the order of efficacies was different. MCP-3 and MCP-2 were the most efficacious agonists. This swap in the order of efficacies between proximal signals can best be explained by the agonists being biased towards different pathways.

To further investigate biased agonism at CCR1, two important downstream signals were chosen. The first assay focuses on the regulation of the activity of the enzyme adenylyl cyclase (AC). This enzyme is responsible for the production of the second messenger cAMP. CCR1 is mainly coupled to the $G\alpha_i$ subunit, which, after dissociation from the receptor and Gβγ subunits, directly inhibits the activity of AC [282]. To measure the levels of cAMP present in the cells, a CAMYEL biosensor was used (Figure 3.1D). In this assay, a BRET signal is detected when the biosensor is free from cAMP. The more cAMP is produced within the cell, the lower the BRET signal is. For this pathway, HCC-2 and MCP-3 were the most potent agonists which is different from the two previous results and supports the biased agonism hypothesis.

The other important downstream event that was investigated was phosphorylation and activation of the ERK1/2, which involves several distinct and overlapping signalling pathways. The coupling of CCR1 to either $G\alpha_i$ or Gβγ subunits or β-arrestins leads to phosphorylation of ERK1/2. The levels of phosphorylated ERK1/2 were detected in cell lysates using AlphaScreen technology (streptavidin donor beads and protein A acceptor beads) (Figure 3.1E). For this pathway, HCC-2 was the most potent ligand and MCP-3 the most efficacious. The potency and efficacy values for the three ligands in all assays are listed in Table 3.1.

3.3. Influence of Tyrosine Sulfation on CCR1 Signalling

The previous results suggest that CCR1 exhibits biased agonism in response to chemokine ligands. CCR1 has two potential tyrosine sulfation sites in its N-terminal part, which is known to be critical for chemokine:chemokine receptor interaction. It is not currently known whether CCR1 N-terminus is sulfated or not, however sulfation has already been proven to be an important factor for chemokine receptor signalling, as it increases receptor affinity for chemokines and can influence selectivity as well as chemokine oligomerisation. Therefore, we hypothesised that tyrosine sulfation may influence biased agonism at CCR1. To test this hypothesis, the same set of experiments described in section 3.2 was performed on cells treated with sodium chlorate and compared to the results for non-treated cells. Chlorate inhibits tyrosine sulfation by competing with sulfate ions when binding to ATP–sulfurylase, the enzyme that initiates the formation of PAPS [283]. PAPS is used by TPST as a source of sulfate groups to transfer onto tyrosine residues and therefore preventing its formation results in inhibition of tyrosine sulfation within the cells.

Results are shown in Figure 3.2 and Table 3.2 and revealed that sulfation did not have any effect on chemokine binding affinities for CCR1 which was unexpected. The effect on signalling responses was also very subtle. Potencies remained similar for all assays although some pERK data were difficult to fit. Efficacy values remained similar for β-Arr2 recruitment and cAMP inhibition. GPA efficacies showed a slight increase but the main effect was on the decrease in pERK efficacy values. We are not sure how to explain this result because ERK phosphorylation seems to be the only response significantly affected. If this effect is due to differences in receptor sulfation, it would be expected that other responses upstream from ERK phosphorylation would also be affected. As this was not the case, it is worth noting that the chlorate treatment could be responsible for the change in ERK phosphorylation. Although the positive controls for pERK using FBS did not vary upon chlorate treatment, it would be useful to perform more controls as FBS is not specific.

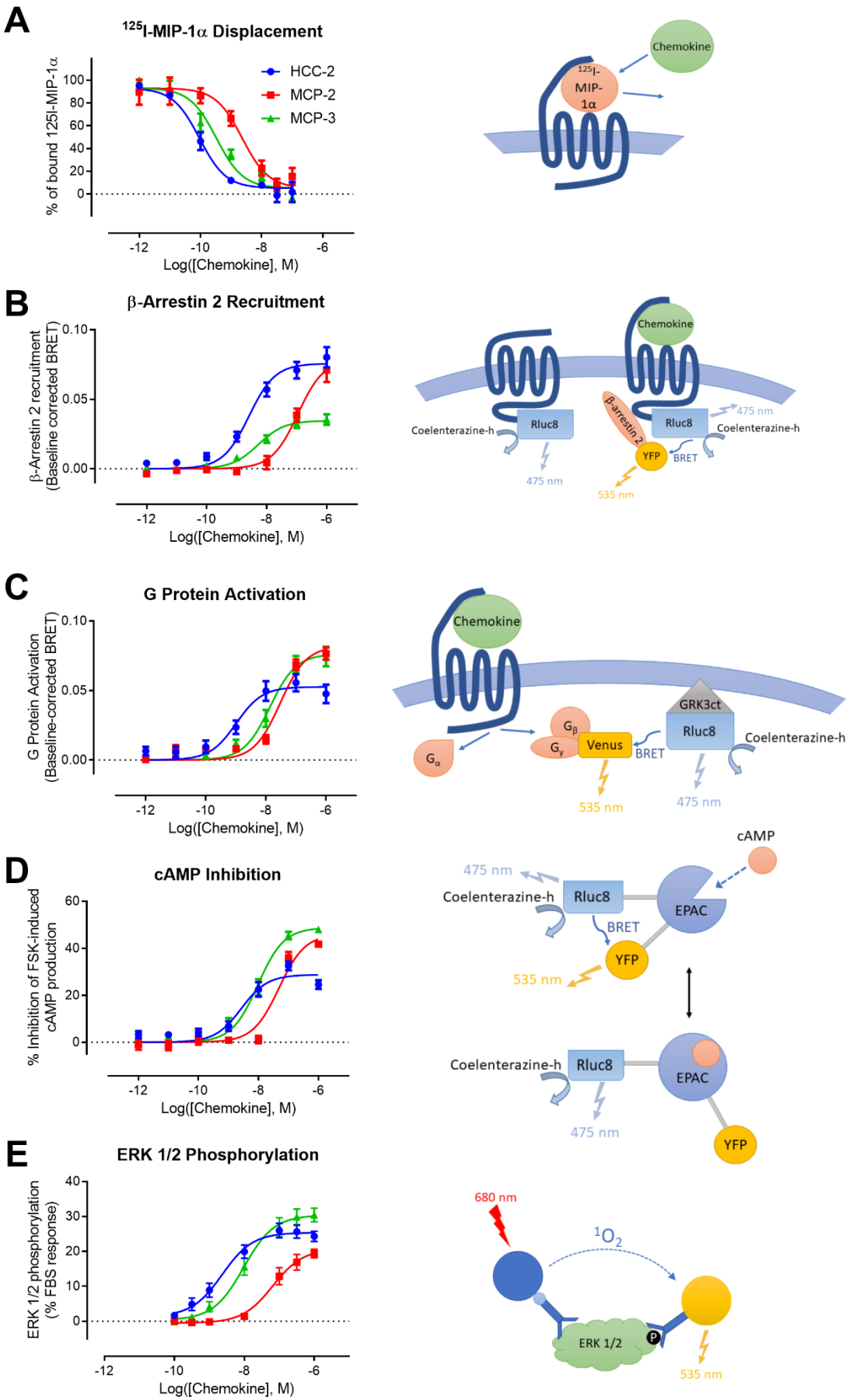
A
125I-MIP-1α Displacement
% of bound 125I-MIP-1α
HCC-2
MCP-2
MCP-3
Log([Chemokine], M)
Chemokine
125I-MIP-1α
B
β-Arrestin 2 Recruitment
β-Arrestin 2 recruitment (Baseline corrected BRET)
Log([Chemokine], M)
Chemokine
Coelenterazine-h
Rluc8
β-arrestin 2
YFP
BRET
475 nm
535 nm
C
G Protein Activation
G Protein Activation (Baseline-corrected BRET)
Log([Chemokine], M)
Chemokine
GRK3ct
Rluc8
Gβ
Gγ
Gα
Venus
BRET
Coelenterazine-h
535 nm
475 nm
D
cAMP Inhibition
% Inhibition of FSK-induced cAMP production
Log([Chemokine], M)
cAMP
475 nm
Coelenterazine-h
Rluc8
EPAC
BRET
YFP
535 nm
E
ERK 1/2 Phosphorylation
ERK 1/2 phosphorylation (% FBS response)
Log([Chemokine], M)
680 nm
1O2
ERK 1/2
P
535 nm

Figure 3.1: Chemokines Display Different Efficacies and Affinities at CCR1. Each experiment is represented by two figures. On the left-hand side, a graph shows the concentration-response data for three chemokines HCC-2, MCP-2 and MCP-3. Data points represent means ± SEM of at least three independent experiments performed in duplicate. On the right-hand side is a schematic representation of the assay. **(A)** Competitive displacement was measured using membrane preparations of His_6-cMyc-CCR1 Flp-In T-REx HEK 293 cells and ^{125}I-MIP-1α as a probe. **(B)** β-arr2 recruitment was measured using parental HEK 293 cells transiently transfected with plasmids encoding CCR1-RLuc8 and β-arr2-YFP. **(C)** GPA was measured using His_6-cMyc-CCR1 Flp-In T-REx HEK 293 cells and $G\alpha_{i1}$. Transfections were performed as described in Chapter 2, section 2.7.6. **(D)** cAMP inhibition was measured using His_6-cMyc-CCR1 Flp-In T-REx 293 cells transiently transfected with a BRET-based cAMP biosensor. **(E)** ERK1/2 phosphorylation assay was performed using His_6-cMyc-CCR1 Flp-In T-REx HEK 293 cells and the amount of phosphorylated ERK1/2 was measured by AlphaScreen detection.

CCR1	MW	Radioligand Binding	pERK		β-Arr2		cAMP		GPA	
	Predicted Mass (Da)	pIC_{50}	pEC_{50}	E_{max} (%)	pEC_{50}	E_{max} (AFU)	pEC_{50}	E_{max} (%)	pEC_{50}	E_{max} (AFU)
HCC-2(Δ26)	7212.4	10.2 ± 0.2	8.6 ± 0.2	25.4 ± 1.0	8.6 ± 0.1	0.076 ± 0.003	8.6 ± 0.2	28.7 ± 1.6	9.0 ± 0.2	0.053 ± 0.004
MCP-2	8914.4	8.7 ± 0.2	7.0 ± 0.2	20.8 ± 1.5	7.0 ± 0.1	0.079 ± 0.006	7.3 ± 0.1	46.0 ± 3.0	7.5 ± 0.1	0.082 ± 0.004
MCP-3	8956.4	9.6 ± 0.2	8.0 ± 0.1	30.4 ± 1.2	8.3 ± 0.1	0.035 ± 0.002	8.0 ± 0.1	48.8 ± 1.8	7.9 ± 0.1	0.076 ± 0.004

Table 3.1: Affinity, Potency and Efficacy Values of Various Chemokines at the Receptor CCR1 for Radioligand Binding, ERK Phosphorylation, β-arrestin 2 Recruitment, cAMP Inhibition and G Protein Activation Assays. Data represent mean ± SEM of at least three independent experiments performed in duplicate. Assays were performed using non-treated cells, which means that the receptor could be sulfated.

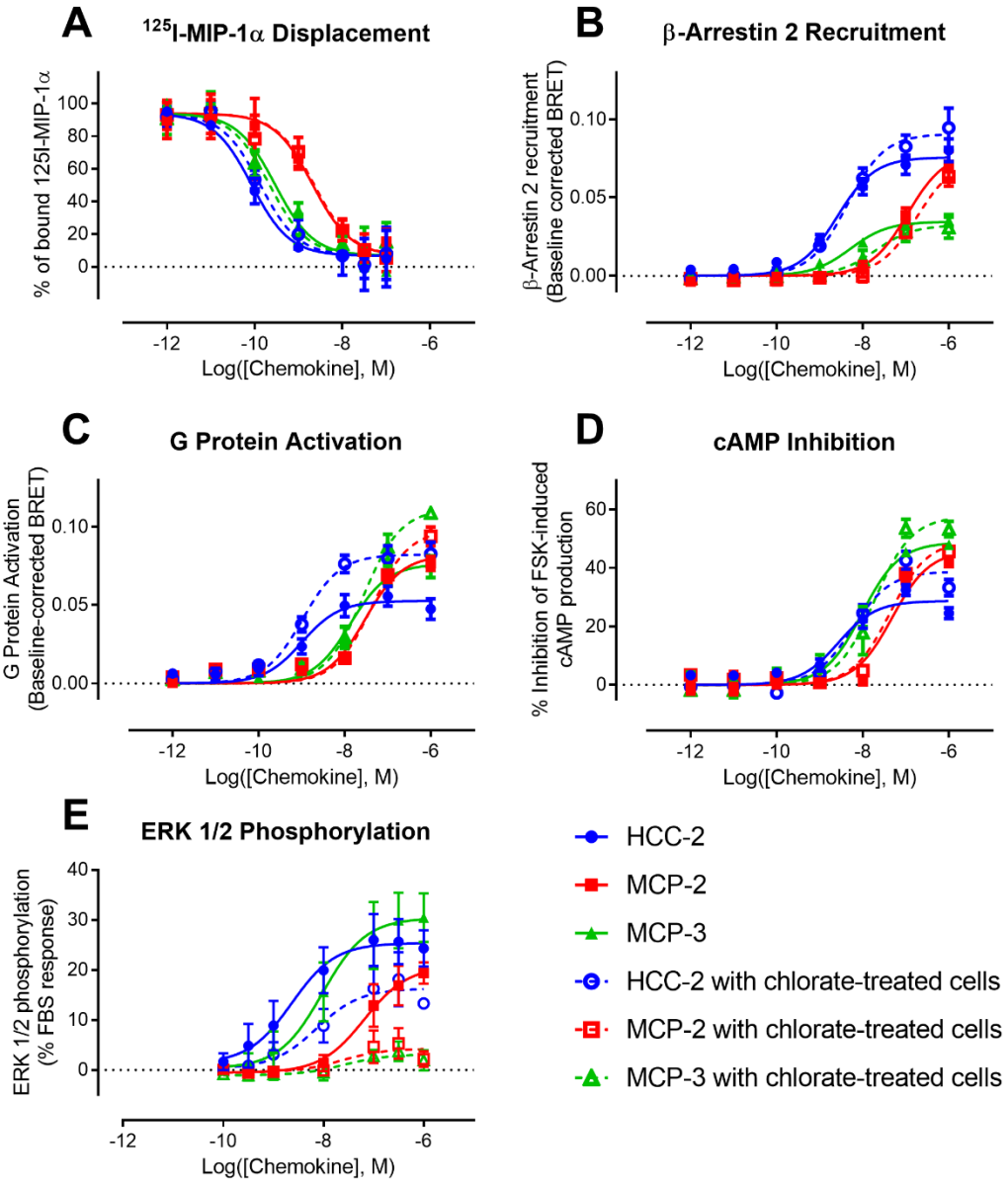

Figure 3.2: Influence of Tyrosine Sulfation on CCR1 Signalling Responses. (A) Competitive displacement was measured using membrane preparations of His_6-cMyc-CCR1 Flp-In T-REx HEK 293 cells and ^{125}I-MIP-1α as a probe. **(B)** β-arr2 recruitment was measured using parental HEK 293 cells transiently transfected with plasmids encoding CCR1-RLuc8 and β-arr2-YFP. **(C)** GPA was measured using His_6-cMyc-CCR1 Flp-In T-REx HEK 293 cells and $G\alpha_{i1}$.Transfections were performed as described in Chapter 2, section 2.7.6. **(D)** cAMP inhibition was measured using His_6-cMyc-CCR1 Flp-In T-REx 293 cells transiently transfected with a BRET-based cAMP biosensor. **(E)** ERK1/2 phosphorylation assay was performed using His_6-cMyc-CCR1 Flp-In T-REx HEK 293 cells and the amount of phosphorylated ERK1/2 was measured by AlphaScreen detection. Each graph shows the concentration-response data for three chemokines HCC-2, MCP-2 and MCP-3, using cells grown in the absence (filled symbols and solid lines) or presence (open symbols and dashed lines) of 30 mM sodium chlorate. Data points represent means ± SEM of at least three independent experiments performed in duplicate.

CCR1	MW	Radioligand Binding		pERK			
	Predicted Mass (Da)	Without chlorate	With chlorate	Without chlorate		With chlorate	
		p*IC* $_{50}$	p*IC* $_{50}$	p*EC* $_{50}$	E_{max} (%)	p*EC* $_{50}$	E_{max} (%)
HCC-2(Δ26)	7212.4	10.2 ± 0.2	10.0 ± 0.1	8.6 ± 0.2	25.4 ± 1	8.1 ± 0.2	16.3 ± 1.2
MCP-2	8914.4	8.7 ± 0.2	8.7 ± 0.1	7.0 ± 0.2	20.8 ± 1.5	7.4 ± 0.4	4.3 ± 0.9
MCP-3	8956.4	9.6 ± 0.2	9.8 ± 0.1	8.0 ± 0.1	30.4 ± 1.2	7.3 ± 0.5	3.2 ± 0.7

CCR1	B-Arr2				cAMP			
	Without chlorate		With chlorate		Without chlorate		With chlorate	
	p*EC* $_{50}$	E_{max} (AFU)	p*EC* $_{50}$	E_{max} (AFU)	p*EC* $_{50}$	E_{max} (%)	p*EC* $_{50}$	E_{max} (%)
HCC-2(Δ26)	8.6 ± 0.1	0.076 ± 0.003	8.4 ± 0.1	0.091 ± 0.004	8.6 ± 0.2	28.7 ± 1.6	8.2 ± 0.1	38.8 ± 2.1
MCP-2	7.0 ± 0.1	0.079 ± 0.006	6.7 ± 0.1	0.075 ± 0.006	7.3 ± 0.1	46.0 ± 3.0	7.4 ± 0.1	49.5 ± 2.4
MCP-3	8.3 ± 0.1	0.035 ± 0.002	7.7 ± 0.2	0.032 ± 0.004	8.0 ± 0.1	48.8 ± 1.8	7.7 ± 0.1	57.7 ± 3.2

CCR1	GPA			
	Without chlorate		With chlorate	
	p*EC* $_{50}$	E_{max} (AFU)	p*EC* $_{50}$	E_{max} (AFU)
HCC-2(Δ26)	9.0 ± 0.2	0.053 ± 0.004	9.0 ± 0.1	0.082 ± 0.003
MCP-2	7.5 ± 0.1	0.082 ± 0.004	7.4 ± 0.1	0.098 ± 0.006
MCP-3	7.9 ± 0.1	0.076 ± 0.004	7.6 ± 0.1	0.11 ± 0.005

Table 3.2: Affinity, Potency and Efficacy Values of Various Chemokines at the Receptor CCR1 for Radioligand Binding, ERK Phosphorylation, β-arrestin 2 Recruitment, cAMP Inhibition and G Protein Activation Assays. Data represent mean ± SEM of at least three independent experiments performed in duplicate. Assays performed using non-treated cells characterise a potentially sulfated receptor (probably a mixture of heterogeneous sulfation states) and assays performed using chlorate-treated cells characterise a non-sulfated version of the receptor.

ERK phosphorylation assays using HEK cells expressing a receptor that cannot be sulfated could be performed in the presence or absence of chlorate treatment to make sure chlorate does not affect the ability of cells to signal through ERK phosphorylation. As the influence of receptor sulfation was subtle and restricted to ERK phosphorylation results, it is difficult to conclude on the sulfation state of CCR1. Thus, additional experiments should be performed to investigate further. For example, using a proteomic approach could be envisaged where a methylation step could be performed before submitting samples to mass spectrometry. This could allow for identification of tyrosine residues that were originally sulfated in case the sulfate groups are too volatile to be seen directly in mass spectrometry. In addition, this method could answer several questions on the location of sulfation sites and heterogeneity of sulfated receptor population across cells types and tissues.

3.4. Determination of Bias Factors

To quantify the biased agonism observed in CCR1 signalling and to assess the effect of tyrosine sulfation, we analysed our data using a derivation of the Black and Leff operational model of agonism [273]. This model was used to fit each concentration-response experiment and yielded a "transduction coefficient" $\log(\tau/K_A)$ as a measure of intrinsic activity of an agonist at a given pathway. The two parameters in the transduction coefficient are the equilibrium dissociation constant of the agonist for the form of the receptor coupled to the relevant pathway (K_A) and an operational measure of signal efficacy (τ), which is ligand and pathway dependent [124].

Transduction coefficient values were obtained for each chemokine, each pathway and each individual experiment at the receptor CCR1, averaged and then normalised to the values of the chosen reference, HCC-2 in this case (with and without chlorate treatment). This first normalisation removes any system (that is cell background dependent) and observational (that is assay dependent) bias. It is worth noting that ERK phosphorylation assays are performed with a five-minute activation time instead of ten minutes for the other assays. This is due to the transient nature of the ERK phosphorylation response with a maximal signal five minutes after addition of chemokines. This could have an influence on the calculated transduction coefficients but further kinetic studies would have to be performed to answer this question. Comparison of these normalised values across the different pathways (Figure 3.3) revealed that MCP-2 and MCP-3 displayed biased agonism relative to HCC-2 when activating CCR1. This is the most obvious when comparing the inhibition of forskolin-induced cAMP production to β-arrestin 2 recruitment (Figure 3.3B). MCP-2 and -3 are both biased towards cAMP inhibition and away from β-arrestin 2 recruitment compared to HCC-2. This result is comparable to results published by Rajagopal *et al.* in 2013 [127] where different CCR1 ligands were used to activate cAMP inhibition and β-arrestin 2 recruitment and compared using MIP-1α as a reference for the bias factor calculations. HCC-2 was found biased towards β-arrestin recruitment and RANTES and MPIF-1 were found biased towards cAMP inhibition. These two signalling events are well characterised and occur through distinct pathways. The receptor is interacting with different intracellular proteins, which is consistent with the receptor adopting different conformations when activated by different ligands.

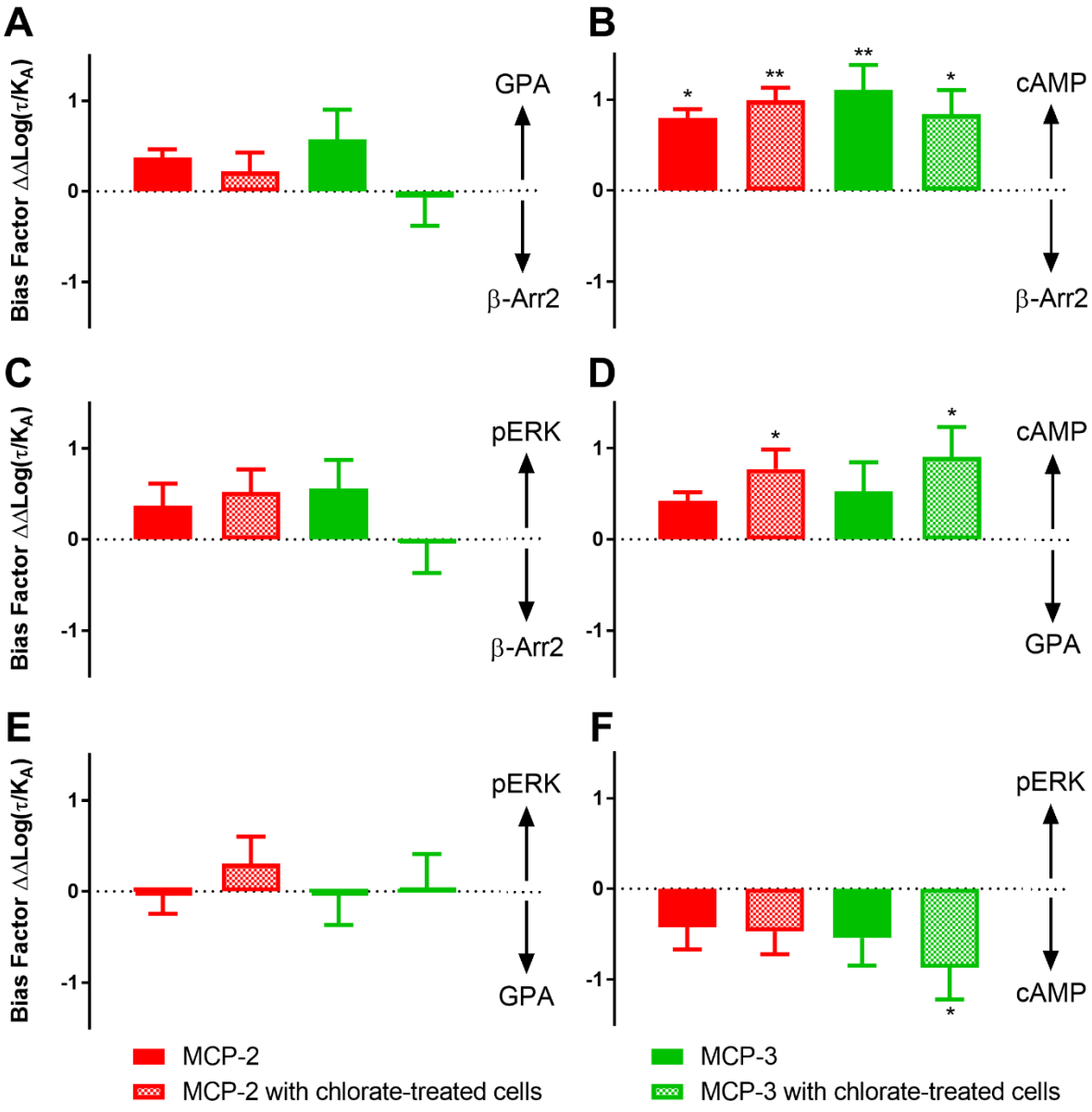

Figure 3.3: Bias Factor Plots. Each graph shows the bias factors relative to HCC-2 for the chemokines MCP-2 and MCP-3 with and without chlorate treatment on the cells 48 h prior to the experiments. Bias factors were calculated according to the Black and Leff operational model of agonism. Data points represent means ± SEM of at least three independent experiments performed in duplicate. Statistical analysis was performed using one-way ANOVA with Tukey's multiple comparison correction. * $p < 0.05$, ** $p < 0.01$, *** $p < 0.001$.

However, bias between two G protein-mediated pathways was also observed. MCP-2 and -3 were both biased towards cAMP inhibition and away from G protein activation (Figure 3.3D), in the absence of sulfation. This result could potentially be explained by the hypothesis that cAMP inhibition occurs through a different Gα subunit from the Gαi1 that was used in the G protein activation assay. Our investigation of this hypothesis is described in the following section.

3.5. Timecourses and Gα Proteins Screen

To explore the possibilities of bias between two G protein-mediated pathways, we decided to use the same G protein activation assay as previously (Figure 3.2C), in which wild type Gα subunits are transfected into the cells, to screen several Gα subunits and see if any bias could be detected between Gα proteins. Five inhibitory subunits, known to inhibit AC and interact with chemokine receptors were chosen (i_1, i_2, i_3, o_A and o_B) and experiments were performed using non-treated and chlorate-treated cells because the previous bias observed seemed to be affected by receptor sulfation. We also decided to add RANTES as a fourth chemokine to increase the likelihood of observing bias and to perform a timecourse as biased agonism has been shown to be time-dependent for the dopamine D_2 receptor [284]. Kinetic studies are important because most assays are performed under pseudo-equilibrium conditions where the receptor occupancy of an agonist may differ depending on the time at which the measurement is taken. This may affect agonist potency and, if there are marked differences in binding kinetics within a subset of ligands, this could be misinterpreted as biased agonism.

A subset of data from the Gα screen and timecourse is shown in Figures 3.4 to 3.6 and the full data set is available in Appendix II, Figures 1 to 5. Figure 3.4 represents the concentration-response curves for HCC-2, MCP-2, MCP-3 and RANTES using different wild-type Gα subunits, 10 minutes after the addition of chemokines. It shows that all Gα subunits tested are activated in a similar way. HCC-2 is the most potent chemokine and RANTES the most efficacious while MCP-2 is the least potent and efficacious chemokine. When analysing this data set with the Black and Leff operational model of agonism and calculating the bias factors for each Gα protein and chemokine at 10 minutes, it turned out that no bias between G protein could be observed.

Figure 3.5 shows the timecourse data for $G\alpha_{i2}$ and the same four chemokines. This shows that the concentration-response curves do not change significantly over time. There is a slight loss in efficacies over time, however, as it is consistent for all chemokines, it did not affect bias factors. Similarly, Figure 3.6 shows the influence of tyrosine sulfation on the receptor ability to dissociate trimeric G proteins. As previously observed, and regardless of the Gα subtype, preventing tyrosine sulfation did not influence signalling or bias.

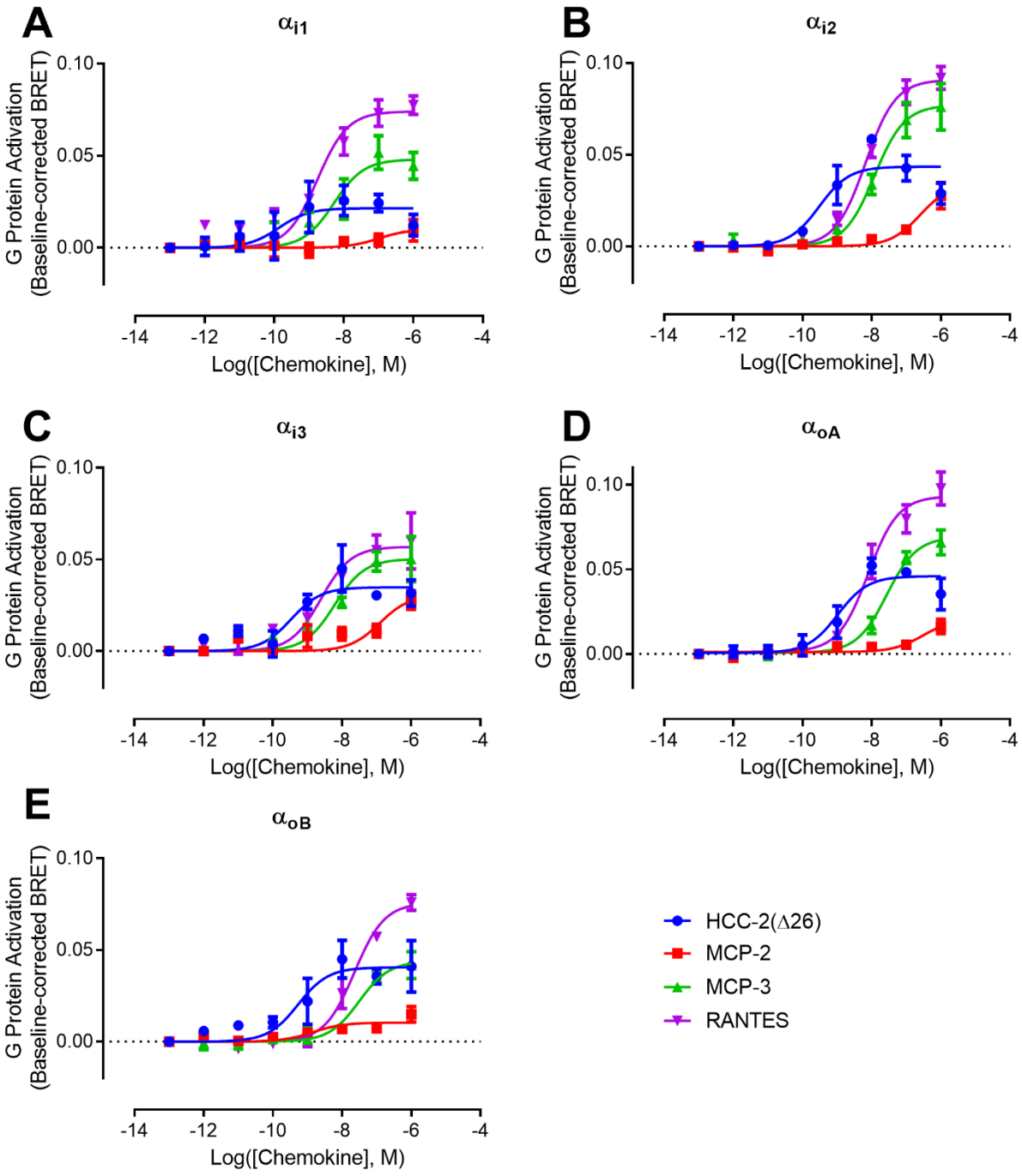

Figure 3.4: Concentration-response Curves for Gα Screen. GPA was measured using His_6-cMyc-CCR1 Flp-In T-REx HEK 293 cells and five different wild-type Gα subunits. Transfections were performed as described in Chapter 2, section 2.7.6. In each graph, a different Gα subunit is used and the concentration-response curves of four chemokines HCC-2, MCP-2, MCP-3 and RANTES, are shown ten minutes after the addition of chemokines. Data points represent means ± SEM of at least three independent experiments performed in duplicate.

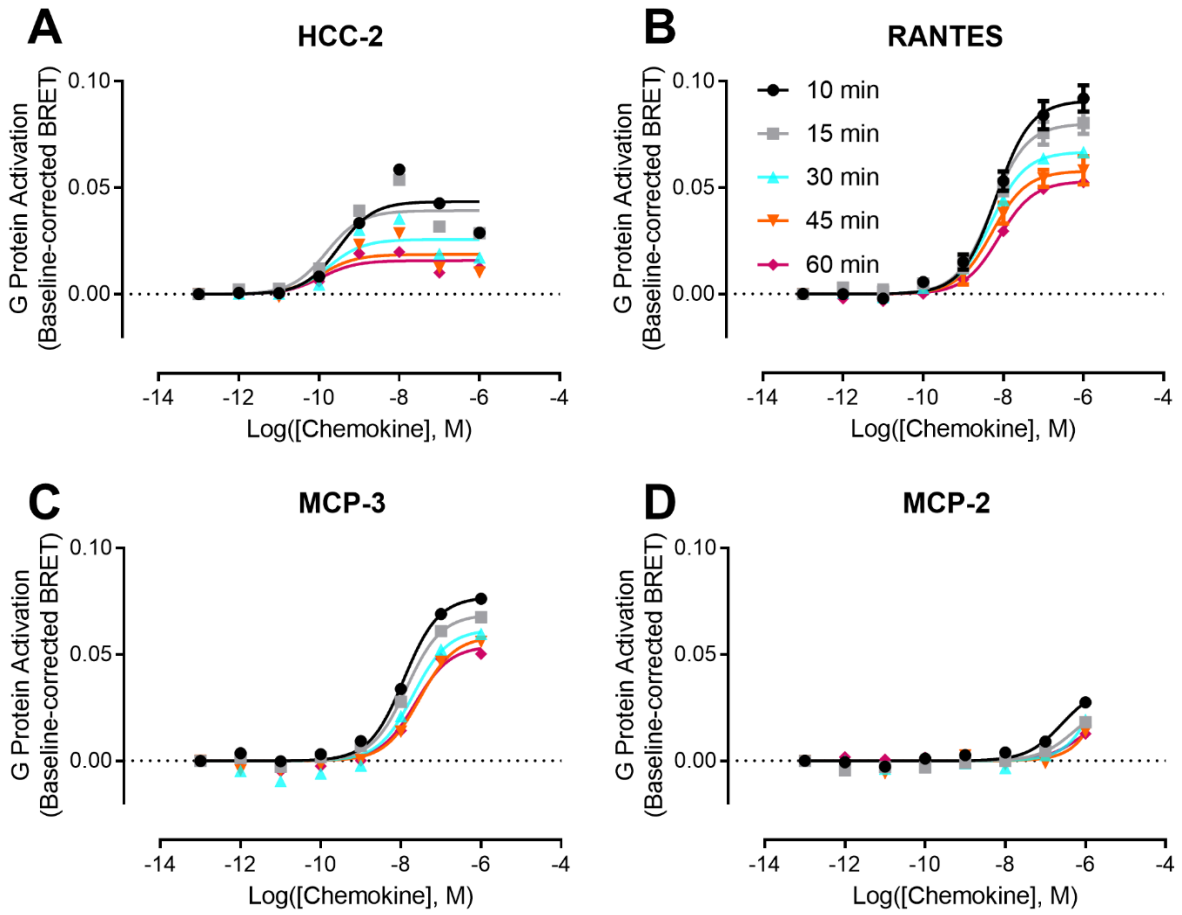

Figure 3.5: Concentration-response Curves and Timecourse. GPA was measured using His_6-cMyc-CCR1 Flp-In T-REx HEK 293 cells and $G\alpha_{i2}$. Transfections were performed as described in Chapter 2, section 2.7.6. Each graph shows, for a chemokine, the concentration-response data for five time points using $G\alpha_{i2}$ as an example. Data points represent means ± SEM of at least three independent experiments performed in duplicate.

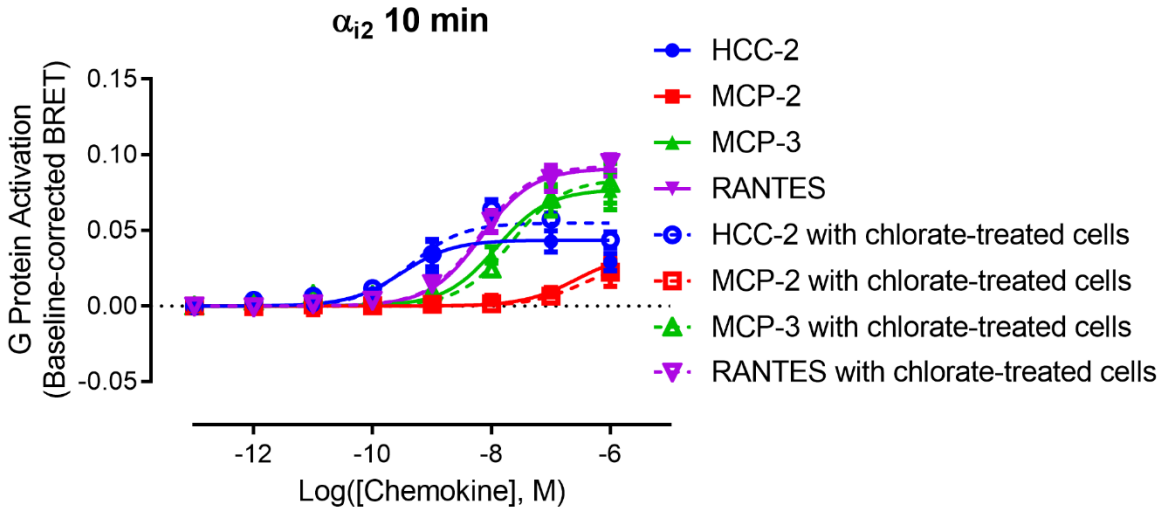

Figure 3.6: Concentration-response Curves and Receptor Tyrosine Sulfation. GPA was measured using His_6-cMyc-CCR1 Flp-In T-REx HEK 293 cells and $G\alpha_{i2}$. Transfections were performed as described in Chapter 2, section 2.7.6. Each graph shows, ten minutes after the addition of chemokines, the concentration-response data for four chemokines HCC-2, MCP-2, MCP-3 and RANTES using non-treated and chlorate-treated cells. Data points represent means ± SEM of at least three independent experiments performed in duplicate.

3.6. Design of HCC-2/MCP-3 Chimeric Chemokines and CCR1 Signalling

The previous results in this chapter suggest that HCC-2 and MCP-3 both activate CCR1 but in different ways. This made us wonder which differences between MCP-3 and HCC-2 could result in biased agonism. The two-site model hypothesised that the N-terminal part of the chemokine is the main region of chemokines that controls receptor activation. Therefore, we chose to alter this region of the chemokines, as HCC-2 and MCP-3 have different N-termini and it is likely to have an effect on receptor activation. As mentioned in the introduction of this chapter, several chemokines can be naturally N-terminally truncated, generating an array of chemokines with various lengths N-termini, that are more or less able to activate their cognate receptors. HCC-2 being one of these processed chemokines, it became of interesting to assess whether the length or the nature of the N-terminus had an influence on CCR1 biased agonism.

A set of five chimeric and truncated chimeras was designed by swapping the N-termini between HCC-2 and MCP-3 and by varying the length of the HCC-2 N-terminus (Figure 3.7A-B). Clones corresponding to each chimera were ordered from GenScript and each clone was expressed in *E. coli* BL21 (DE3). Expression levels were sufficient for all proteins and each protein was purified using the process described in Chapter 2, section 1.5. HCC-2(N-MCP-3) and HCC-2(Δ28) were successfully purified and the final size exclusion chromatograms and SDS-PAGE gels are presented in Figure 3.7C-D. However, HCC-2(Δ12) was very insoluble due to its longer N-terminus and could not be refolded. MCP-3(N-HCC-2) and HCC-2(Δ24) were successfully refolded but the affinity tag attached to the N-terminus could not be cleaved off despite several attempts under various conditions. Therefore, the CCR1 signalling experiments were performed using only HCC-2(N-MCP-3) and HCC-2(Δ28) and HCC-2 (also called HCC-2(Δ26)) and MCP-3 as references.

The same signalling readouts as section 3.2 were measured using BRET-based detection for β-arrestin 2 recruitment, G protein activation and cAMP inhibition and AlphaScreen detection for ERK1/2 phosphorylation assays. The concentration-response curves from these experiments are presented in Figure 3.8 and the derived parameters are listed in Table 3.3. Both chimeras were active at CCR1 and presented different signalling profiles from HCC-2 and MCP-3. The ability of HCC-2(Δ28), which is two residues shorter than HCC-2, to activate CCR1 is in agreement with previously published results [285]. However, it is unusual for chemokines to be able to signal with such a short N-terminus because the N-terminus is expected to reach deeper into the receptor transmembrane helices, which does not seem possible with a three-residue N-terminus. For HCC-2(N-MCP-3), the results were expected to be very similar to MCP-3 because according to the two-site model, the N-terminus of the chemokine governs the receptor activation and thus, the signalling outcomes. However, HCC-2(N-MCP-3) had an intermediate profile. This mutant behaves like HCC-2 for pERK and GPA readouts (Figure 3.8B,C and E) and similarly to HCC-2 in the β-Arr2 assay (Figure 3.8A), albeit with reduced efficacy. In contrast, in the cAMP inhibition assay, this mutant is more potent than HCC-2 or MCP-3 and has an intermediate efficacy value between the two parental chemokines.

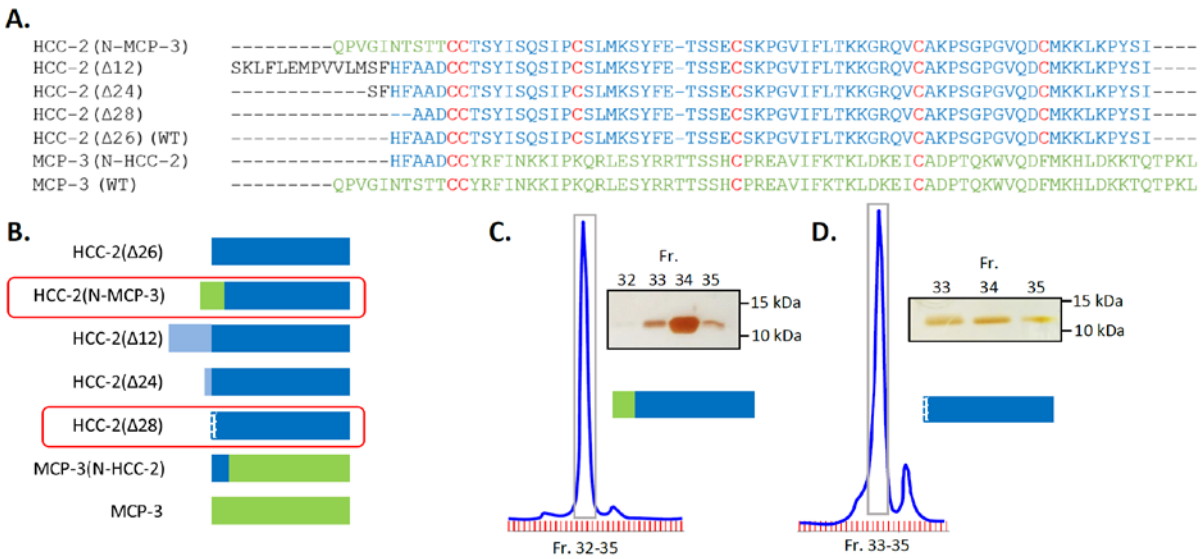

Figure 3.7: HCC-2/MCP-3 Chimeras. (A) Sequence alignment for the set of five chimeras and the two original chemokines (WT). **(B)** Schematic representation of the five truncated and chimeric chemokines with the two original chemokines at the top (HCC-2 in blue) and the bottom (MCP-3 in green). The two proteins that were successfully expressed and purified are circled in red. **(C)** HCC-2(N-MCP-3) purification: preparative size exclusion chromatogram and SDS-PAGE gel of the desired fractions under non-reducing conditions. **(D)** HCC-2(Δ28) purification: preparative size exclusion chromatogram and SDS-PAGE gel of the desired fractions under non-reducing conditions.

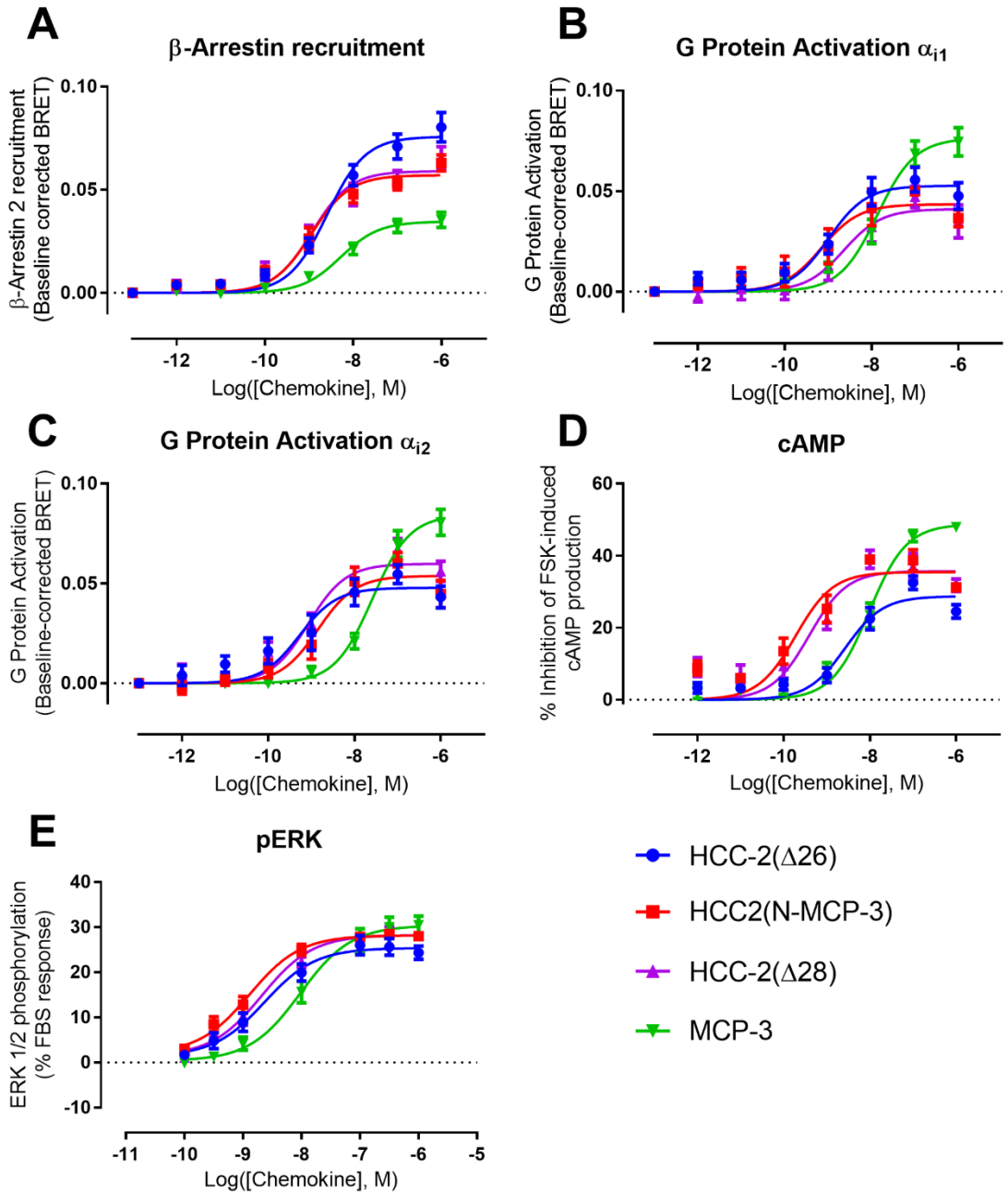

Figure 3.8: Influence of Chimeric HCC-2/MCP-3 Chemokines on CCR1 Signalling Responses. (A) β-arr2 recruitment was measured using parental HEK 293 cells transiently transfected with plasmids encoding CCR1-RLuc8 and β-arr2-YFP. **(B-C)** GPA was measured using His_6-cMyc-CCR1 Flp-In T-REx HEK 293 cells and $G\alpha_{i1}$ **(B)** and $G\alpha_{i2}$ **(C)** constructs (as described in Chapter 2, section 2.7.6). **(D)** cAMP inhibition was measured using His_6-cMyc-CCR1 Flp-In T-REx 293 cells transiently transfected with a BRET-based cAMP biosensor. **(E)** ERK1/2 phosphorylation assay was performed using His_6-cMyc-CCR1 Flp-In T-REx HEK 293 cells and the amount of phosphorylated ERK1/2 was measured by AlphaScreen detection. Each graph shows the concentration-response data for a different signal readout. Data points represent means ± SEM of at least three independent experiments performed in duplicate.

CCR1	MW	pERK		B-Arr2		cAMP		GPA α_{i1}		GPA α_{i2}	
	Predicted Mass (Da)	p*EC* $_{50}$	E_{max} (%)	p*EC* $_{50}$	E_{max} (AFU)	p*EC* $_{50}$	E_{max} (%)	p*EC* $_{50}$	E_{max} (AFU)	p*EC* $_{50}$	E_{max} (AFU)
HCC-2(Δ26)	7212.4	8.6 ± 0.2	25.4 ± 1.0	8.6 ± 0.1	0.076 ± 0.003	8.6 ± 0.2	28.7 ± 1.6	9.0 ± 0.2	0.053 ± 0.003	9.3 ± 0.2	0.048 ± 0.004
HCC-2(N-MCP-3)	7670.0	8.9 ± 0.1	28.2 ± 0.6	9.0 ± 0.1	0.057 ± 0.002	9.7 ± 0.2	35.5 ± 1.9	9.2 ± 0.2	0.043 ± 0.004	8.9 ± 0.2	0.054 ± 0.003
HCC-2(Δ28)	6928.1	8.7 ± 0.1	28.3 ± 0.8	8.9 ± 0.1	0.059 ± 0.003	9.4 ± 0.2	35.7 ± 2.2	8.6 ± 0.3	0.041 ± 0.004	9.1 ± 0.1	0.060 ± 0.003
MCP-3	8956.4	8.0 ± 0.1	30.4 ± 1.2	8.3 ± 0.1	0.035 ± 0.002	8.0 ± 0.1	48.8 ± 1.8	7.9 ± 0.1	0.076 ± 0.004	7.6 ± 0.1	0.084 ± 0.004

Table 3.3: Potency and Efficacy Values of Chimeric HCC-2/MCP-3 Chemokines at the Receptor CCR1 for ERK Phosphorylation, β-arrestin-2 Recruitment, cAMP Production Inhibition and G Protein Activation Assays. Data represent mean ± SEM of at least three independent experiments performed in duplicate.

Bias factors were calculated using the same method as in section 3.4, based on the operational model of agonism developed by Black and Leff. Results (Figure 3.9) show that the previously observed bias of MCP-3 towards cAMP inhibition and away from β-Arr2 when compared to HCC-2 remained and that swapping the HCC-2 N-terminus and replacing by the N-terminus of MCP-3 makes HCC-2(N-MCP-3) also biased towards cAMP inhibition and away from β-Arr2 when compared to HCC-2 (Figure 3.9C). Other biases resulted from the N-terminal modifications, such as bias towards cAMP inhibition and away from pERK for both HCC-2(N-MCP-3) and HCC-2(Δ28) when compared to HCC-2 (Figure 3.9J) and bias towards cAMP inhibition or GPA α_{i2} and away from GPA α_{i1} for HCC-2(Δ28) (Figure 3.9E, F). This shows bias between G protein-mediated pathways but also between Gα proteins, which is novel.

3.7. Discussion

CCR1 is a very promiscuous receptor, expressed on the surface of monocytes, lymphocytes and dendritic cells. CCR1+ cells and ligands of this receptor are increased in numerous inflamed tissues. CCR1 blockade has been effective in animal models of rheumatoid arthritis (RA), multiple sclerosis (MS) and several other diseases [209]. However, in clinical trials for RA, MS and chronic obstructive pulmonary disease, CCR1 antagonists did not demonstrate significant efficacy [208, 286]. Thus, it is essential to understand CCR1 signalling better to improve our strategies to treat these diseases.

In this chapter, we showed that CCR1 exhibits biased agonism when activated by HCC-2, MCP-2 and MCP-3. This result was not surprising, knowing that CCR1 can be activated by at least nine CC chemokines and it already exhibited biased agonism when activated by some other chemokines. The strongest bias was observed with MCP-3 biased towards cAMP inhibition and away from β-arrestin 2 recruitment in comparison to HCC-2. These two pathways involve different signalling proteins interacting with the intracellular side of the receptor. This is consistent with the idea that different ligands can stabilise different active conformations of the same receptor, favouring interactions with β-arrestin 2 when the receptor is bound to HCC-2 and favouring interactions with G proteins when the receptor is bound to MCP-3. In addition to this expected result, the initial biased agonism study suggested that bias could be seen between pathways that both involve G proteins interacting with the receptor and that this bias may be dependent on the sulfation state of the receptor.

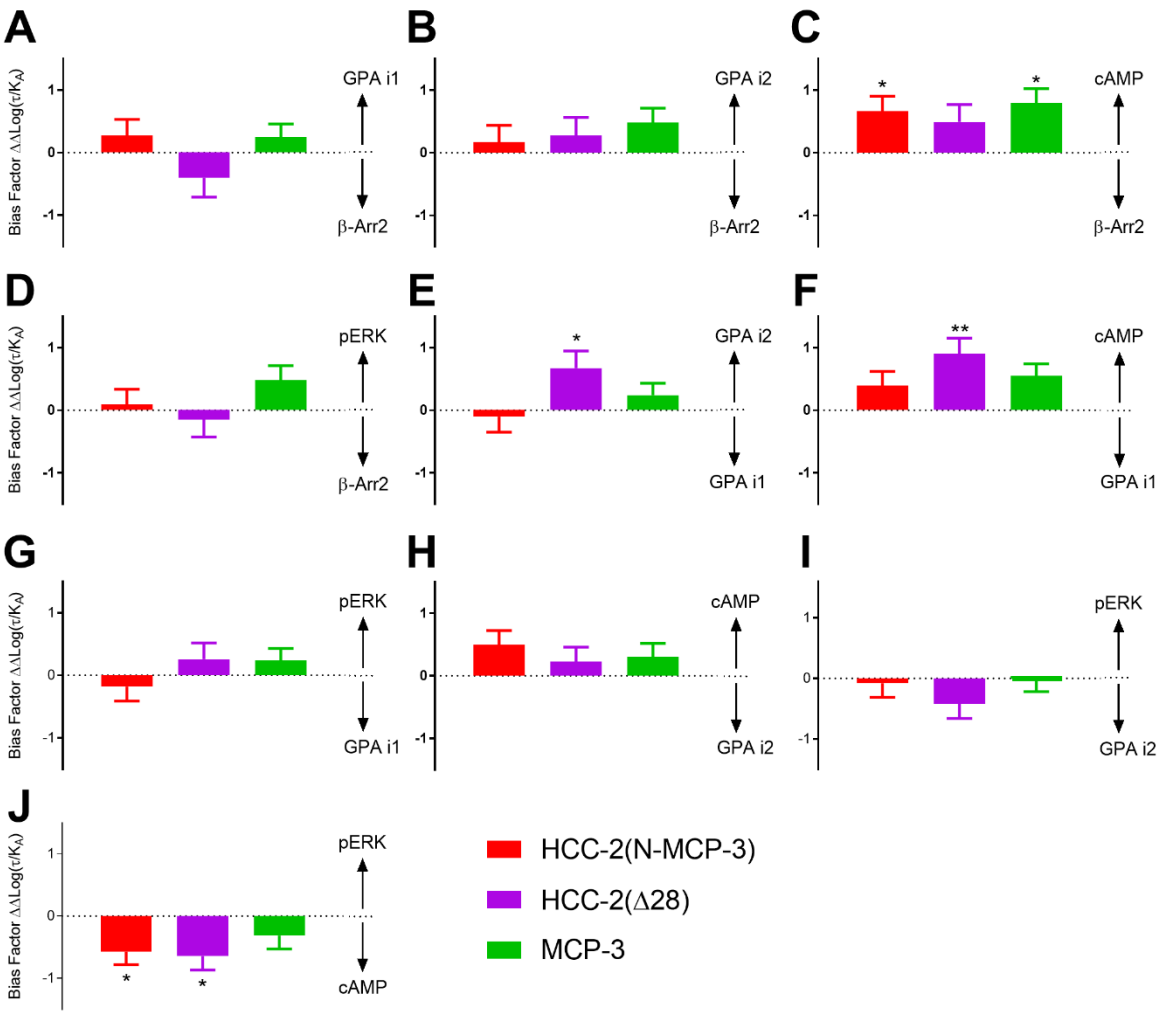

Figure 3.9: Bias Factor Plots. Each graph shows the bias factors for three chemokines HCC-2(N-MCP-3), HCC-2(Δ28) and MCP-3 relative to HCC-2(Δ26). Bias factors were calculated according to the Black and Leff operational model of agonism. Data points represent means ± SEM of at least three independent experiments performed in duplicate. Statistical analysis was performed using one-way ANOVA with Tukey's multiple comparison correction. * $p < 0.05$, ** $p < 0.01$, *** $p < 0.001$.

Therefore, we decided to investigate further by performing a Gα screen and it was expected that tyrosine sulfation would have some influence on CCR1 binding affinities and/or on its biased agonism, which was not the case. This result could be explained by the inefficacy of the chlorate treatment. However, this hypothesis is less likely as controls were performed on cMyc-FLAG-hCCR2 expressing HEK 293 Flp-In Trex cells. An anti-FLAG antibody which recognises only the non-sulfated version of the FLAG tag, was used in ELISA assays to assess the efficacy of the chlorate treatment. cMyc-FLAG-hCCR2 could not be detected by the anti-FLAG antibody in the absence of chlorate treatment because the FLAG tag was sulfated. In addition, treating the cells with chlorate enabled the detection of the receptor. Although this is not a direct measurement of the receptor sulfation state of the receptor, it is a proof of principle that chlorate treatment inhibits tyrosine sulfation. A similar experiment could be performed using a FLAG-tagged CCR1 construct. Although no effect of sulfation was observed in the current study suggesting that CCR1 was probably not sulfated when overexpressed in HEK cells, it may not be the same for an endogenously expressed receptor. Therefore, it remains possible that sulfation may influence the activity of endogenous CCR1. However, this would have to be tested using THP-1 cells for example. In addition, the population of sulfated receptors could vary from one tissue to another and from one condition to another (for example, in the presence or absence of inflammatory stimuli). This could provide a customisable response adapted to specific needs. Future studies will be needed to investigate these possibilities.

To increase our understanding of the mechanisms involved in CCR1 biased agonism, we designed chimeras between HCC-2 and MCP-3. The N-terminal part of the chemokines was chosen to be modified. Based on the two-site model, the N-terminus of the chemokine is the main region directly activating the receptor and generating cellular responses. Thus, according to this model, we predicted that swapping the N-terminus of HCC-2 and replacing by the N-terminus of MCP-3 should result in a chimera biased towards cAMP inhibition and away from β-Arr2. This was indeed the case because HCC-2(N-MCP-3), like wild type MCP-3, exhibits bias towards cAMP inhibition and away from β-Arr2 recruitment (Figure 3.9C). However, when looking at the individual concentration response curves, it can be seen that despite the final bias being the same, HCC-2(N-MCP-3) does not have a similar signalling profile to MCP-3 (Figure 3.8A-D). This result indicates that the N-terminus is not the only region of the chemokine influencing receptor activation and that other parts are also important when it comes to controlling signalling responses. To test this hypothesis, more HCC-2/MCP-3 chimeras could be designed where other regions, particularly the N-loop, are swapped and tested for CCR1 activation.

Truncating HCC-2(Δ26) also resulted in alteration of bias. HCC-2(Δ28) became biased towards GPA α_{i2} and away from GPA α_{i1}, as well as biased towards cAMP inhibition and away from GPA α_{i1} when compared to HCC-2. This suggests that the length of the N-terminus is important for activation, but also biased agonism and it would be of interest to explore this result in more details by making more truncated variant of HCC-2. It is already known that even the longer N-terminal variant of HCC-2 can activate CCR1 but biased agonism has not been tested yet.

When considering the two most amplified pathways, cAMP inhibition and ERK phosphorylation, both modified chemokines were significantly biased towards cAMP inhibition and away from ERK phosphorylation when compared to HCC-2, which was not the case with MCP-3. Thus, modifying the N-termini of both proteins, resulting in one longer and one shorter N-terminus, made them both about 10-fold more potent for cAMP inhibition than any of the two wild-type chemokines (Figure 3.8D and Table 3.3). This is where the two-site model is not sufficient to understand and explain this result.

In summary, the results presented in this Chapter argue in favour of parts of the chemokines other than the N-terminus being involved in controlling CCR1 signalling. This is different from recent results obtained in our laboratory for CCR2 signalling where the main interactions between the MCP family and CCR2 were primarily located within the N-terminus [287]. CCR2 was not found to exhibit biased agonism but partial agonism instead when activated by the MCP family. So, it is possible that when biased agonism is observed more regions of the chemokine are needed to interact with the receptor to stabilise various active conformations. On the other hand, considering a particular pathway, a partial agonist could stabilise the same conformation as a full agonist but to a lesser extent. Thus, no new interactions have to be formed which is likely to be different for a biased agonist.

Chapter 4. Exploring the Two-site Model at the Chemokine Receptor CCR1

4.1. Background

Based on the results from the previous chapter as well as other published results [127], CCR1 exhibits biased agonism when activated by different cognate chemokines. However, it is unknown at this stage how CCR1 signalling is controlled. According to the two-site model (Figure 4.1), swapping N-termini between HCC-2 and MCP-3 should have been sufficient to make them signal like each other, but this was not the case. This raised several questions, in particular; which other regions of the chemokine are involved in controlling CCR1 signalling and how can the two-site model be further developed to account for our more recent results? To explore these questions, we decided to investigate CCR1 binding and activation by studying both proposed sites of interactions.

Mutational and structural studies have previously identified the N-terminus of chemokine receptors (receptor site 1) as the initial chemokine binding site [288, 289]. If this region actually contributes to the dominant chemokine binding interactions then peptides with the same sequence as the receptor N-terminus should mimic the receptor binding behaviour (affinity and selectivity). These N-terminal peptides are often used as simplified models of chemokine receptors [145] but their ability to mimic receptors has not carefully been assessed. In most cases, these peptides also contain the potential sulfation sites of the receptor, which makes the issue more complex. To further explore the site 1 interactions that contribute to chemokine binding by CCR1, we designed a series of sulfopeptides which have the CCR1 N-terminal sequence and display different sulfation patterns. In the first part of this chapter, we compared the chemokine-binding affinities and selectivities of these peptides to those of the corresponding intact receptor.

While the two-site model emphasises the above site 1 interactions in the initial binding step, it also proposes that the interactions of the chemokine N-terminus with the receptor transmembrane bundle (site 2 interactions) are responsible for subsequent activation of the receptor. The previous chapter of this thesis suggested that the chemokine N-terminus is not the only region involved in receptor activation. To improve our understanding of site 2 interactions and propose a more detailed model, more information is needed on the site 2 interactions and particularly on the regions of the chemokine that have a major influence. This question can be addressed by comparing two chemokines that have similar sequences and structures but distinct effects on activation of the same receptor. Thus, we decided to use two closely related chemokines, MCP-1 and MCP-3 which share 71% sequence identity and have similar structures, but only MCP-3 is a CCR1 agonist. Considering that MCP-1 and MCP-3 have a high degree of similarity but still behave differently at CCR1, they serve as an excellent model to identify the chemokine features required for CCR1 activation. Thus, the second part of this chapter describes a study of CCR1 signalling and site 2 interactions that was carried out using MCP-1/3 chimeras.

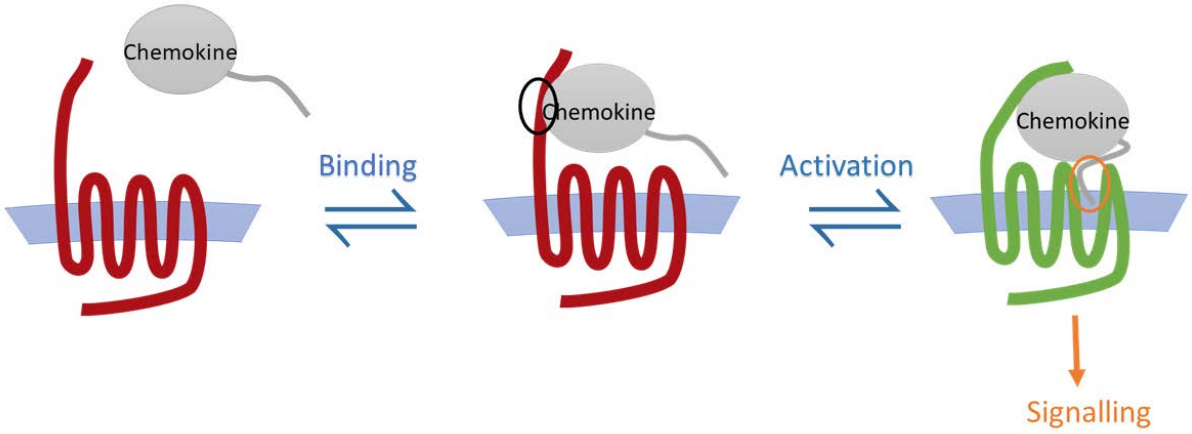

Figure 4.1: Proposed Two-site Model for Chemokine:Chemokine Receptor Interaction [176]. The first species represents the receptor in an inactive state (red) and the ligand prior to any interaction between the two. The second species represents the interaction of the chemokine N-loop and β3 turn with the N-terminal segment of the receptor (site 1 circled in black). Interactions in site 1 are considered to be driving binding only; thus, the receptor is still in an inactive state (red). The third species represents the interaction between the N-terminal region of the chemokine and the receptor TM bundle (site 2 circled in orange). Insertion of the N-terminal region of the chemokine results in activation of the receptor (active state in green) and interactions in site 2 are considered to be driving activation only.

4.2. Contribution of CCR1 N-Terminus to Chemokine Binding

4.2.1. Sulfopeptides: Design and Synthesis

To design and synthesise the CCR1 sulfopeptides, we collaborated with Prof. Richard J. Payne and his laboratory at The University of Sydney. Peptides were all synthesised and purified by one of his PhD students, Xuyu (Johnny) Liu. The peptide sequence is the same for all four CCR1 sulfopeptides and it corresponds to the first twenty-nine residues of CCR1, with the cysteine (residue 24) mutated to a serine residue to avoid intermolecular disulfide bond formation. In this sequence, there are two tyrosine residues, in positions 10 and 18, that are potential sulfation sites, particularly as they are close to several acidic residues [290]. The native sulfation state of CCR1 being unknown, we decided to make a set of four sulfopeptides R1A-D, where R1A is not sulfated, R1B is sulfated on tyrosine 10, R1C is sulfated on tyrosine 18 and R1D is sulfated on both tyrosine residues (sequences shown in Figure 4.2). One additional peptide was needed to use as a fluorescent probe for fluorescence anisotropy measurements. This peptide needs to be labelled with fluorescein, which is easy to add at the N-terminus, and doubly-sulfated to enhance its affinity for chemokines. We fortuitously found that peptide Fl-R2D (sequence shown in Figure 4.2), which was already available in our laboratory, served this purpose well.

4.2.2. Chemokine:Sulfopeptide Binding using Fluorescence Anisotropy

To measure binding between chemokines and sulfopeptides, a fluorescence anisotropy assay was developed [291]. Fluorescence anisotropy can be measured in solution and in a given environment (pH, temperature) mainly depends on the size of the fluorescent molecule [292]. Anisotropy uses polarised light to excite a fluorophore and compares the polarisation of the emitted light to the source. During the delay between excitation and emission (the fluorescence lifetime), small fluorophores will rotate fast in solution which will randomise the orientation of the emitted signal, leading to small anisotropy values. On the other hand, large fluorophores (or those attached to large molecules or complexes) will rotate less during the time between excitation and emission. This means that the orientation of the emitted light will be similar from one molecule to the other. This leads to a more polarised emitted signal and high anisotropy values. Therefore, anisotropy measurements are well suited to binding studies. As a complex between a fluorescent probe and another molecule forms, the size of the fluorescent species increases and so does the anisotropy. To have access to K_d values for unlabelled peptides, without interference from the fluorophore, we designed a displacement assay, where one peptide Fl-R2D is labelled and used as a probe and unlabelled peptides are used as competitors. The principle of the assay is described in Figure 4.3. Firstly, a direct binding assay is performed to measure the affinity of a chemokine for the fluorescent probe. The probe goes from a free state to a bound state, which increases its size, hence the increasing anisotropy values (Fig 4.3A and C). Secondly, a competitive binding assay is performed where increasing concentrations of an unlabelled peptide are added to a solution containing the chemokine:probe complex. If the peptide displaces the probe, the probe goes from a bound state to a free state, hence the decrease in anisotropy (Fig 4.3B and D). Binding curves can be fitted using the chemokine:probe affinity measured in the direct binding step to obtain the affinity between chemokine and unlabelled peptide [272].

R1A METPNTTED**Y**DTTTEFD**Y**GDATPSQKVNE
R1B METPNTTED**Y**DTTTEFD**Y**GDATPSQKVNE
R1C METPNTTED**Y**DTTTEFD**Y**GDATPSQKVNE
R1D METPNTTED**Y**DTTTEFD**Y**GDATPSQKVNE
Fl-R2D Fl-EEVTTFFD**Y**D**Y**GAP

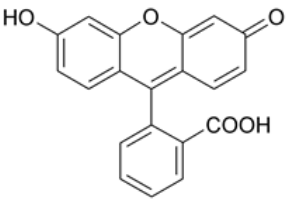

Fluorescein (Fl)

Figure 4.2: Sequences of Sulfopeptides R1A-D and Fl-R2D. On the left-hand side, sulfopeptide sequences with sulfated tyrosine residues in bold red (**Y**) and non-sulfated tyrosine residues in bold blue (**Y**) are shown. On the right-hand side, the chemical structure of fluorescein is shown.

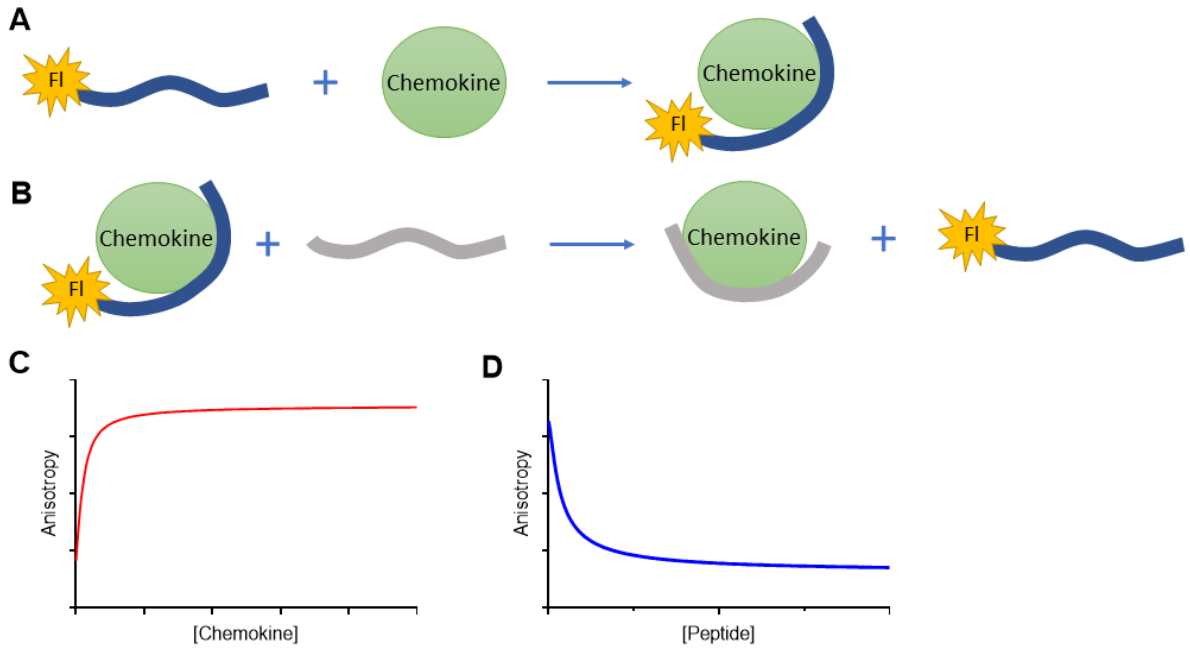

Figure 4.3: Fluorescence Anisotropy Assay Principle. (A) Schematic representation of the direct binding assay. A fluorescent peptide (blue) binds to the chemokine (green) to form a complex which makes the size of the fluorescent species increase hence the increase in anisotropy. **(B)** Schematic representation of the competitive binding assay. This assay starts with a solution containing the chemokine:fluorescent peptide complex to which is added a competitor such as non-fluorescent peptides R1A-D (grey). The competitor displaces the fluorescent peptide from the chemokine which makes the size of the fluorescent species decrease, hence the decrease in anisotropy. **(C)** Theoretical anisotropy data obtained from a direct binding experiment between a chemokine and Fl-R2D. **(D)** Theoretical anisotropy data obtained from a competitive binding experiment between a chemokine and a sulfopeptide, using Fl-R2D as a fluorescent probe.

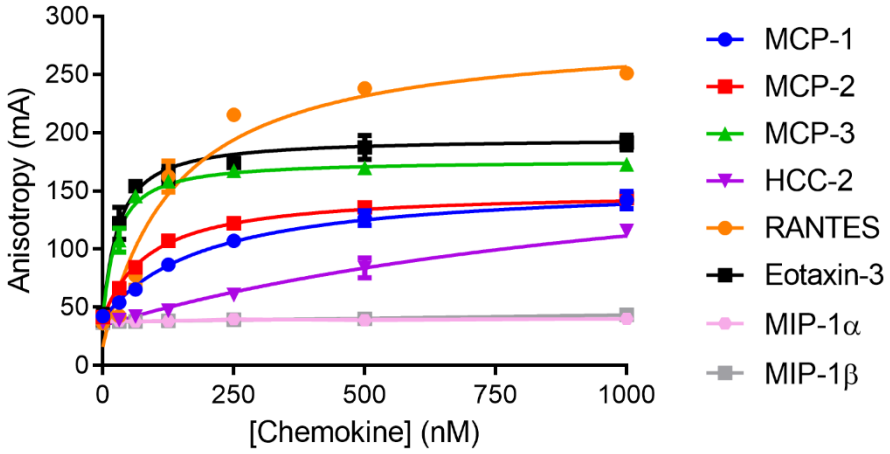

Figure 4.4: Direct Binding of Various CC Chemokines with Fl-R2D. Chemokines display different affinities for the fluorescent peptide Fl-R2D. The final concentration of Fl-R2D was 10 nM and the K_d values range from 21.3 nM to 1.2 μM with MIP-1α and MIP-1β not binding this peptide at all. Data points represent mean ± SEM of at least three independent experiments performed in duplicate.

Chemokine	pK_d	K_d (nM)
MCP-1	6.73 ± 0.04	186
MCP-2	7.09 ± 0.03	82.3
MCP-3	7.67 ± 0.04	21.3
HCC-2	5.90 ± 0.05	1245
RANTES	6.89 ± 0.06	129
Eotaxin-3	7.61 ± 0.05	24.5
MIP-1α	No binding	
MIP-1β	No binding	

Table 4.1: Affinity of Various CC Chemokines at Fl-R2D using FAA. Data represent mean ± SEM from at least three independent experiments performed in duplicate.

Direct binding assays were performed with eight CC chemokines and results are presented in Figure 4.4 and Table 4.1. Unfortunately, MIP-1α and MIP-1β did not bind the probe which prevented any competition assay from being performed. This is probably due to the fact that these two chemokines are not CCR2 ligands, Fl-R2D being a doubly-sulfated peptide with the N-terminal sequence of CCR2 (residues 18 to 31). The other chemokines tested did bind to Fl-R2D with affinities ranging from 21 nM to 1.2 μM, MCP-3 and eotaxin-3 (CCL26) having the highest affinity and HCC-2 having the lowest.

Competitive binding assays were then performed with the remaining six CC chemokines and the CCR1 sulfopeptides and results are presented in Figure 4.5 and Table 4.2. It is worth noting that displacement graphs are shown on a linear scale to avoid confusion between IC_{50} and K_d. As shown by simulated displacement curves (Appendix V, Figure S1), the shape of the curve is indicative of the equilibrium dissociation constant (K_d) between unlabelled R1A-D peptide and chemokine, although the concentration of unlabelled peptide required for 50 % displacement of the fluorescent peptide is substantially higher than the K_d; this difference is related to the concentrations of the chemokine and fluorescent peptide used in the assay and their affinity for each other. Sulfopeptides R1A-D displaced Fl-R2D from all six chemokines. We can easily see that tyrosine sulfation increases the peptide affinity for the chemokines, R1D being a better competitor than R1A, with R1B and R1C being intermediate in most cases. This result was expected as previous results in our laboratory led to the same conclusion. The only exceptions to this pattern are RANTES for which, all three sulfated peptides have similar affinities and MCP-2 for which, R1D and R1C have the same affinities.

The highest affinity chemokine for both R1A and R1B was RANTES with affinities of 1.7 μM and 0.25 μM respectively. For R1C and R1D, the highest affinity chemokine was MCP-2 with affinities of 83 nM and 42 nM respectively. It was not surprising to find RANTES, along with MCP-3 among the high affinity ligands for the CCR1 sulfopeptides as RANTES is a common CCR1 ligand. MCP-2 however, is a weaker CCR1 agonist which mainly activates CCR2, so it was unexpected to find it among the high affinity ligands especially for the peptides with sulfated tyrosine 18. The lowest affinity chemokine turned out to be HCC-2 with affinities between 24 and 2.3 μM, which was also unexpected and might be due to HCC-2 and Fl-R2D interacting in a non-specific manner, generating systematic error in the competition assay.

When looking at correlations between peptides (Table 4.3), the best pairs are R1A:R1B and R1C:R1D with R^2 values at 98 and 94 % respectively. This suggests that the sulfation of tyrosine 10 does not have a high impact on binding. One possible explanation for this result is that this residue does not interact directly with the chemokines, so modifying it has little effect. The two tyrosine residues are further apart in the CCR1 N-terminal sequence, compared to CCR2 or CCR3 where the tyrosine residues are around the 20^{th} to 30^{th} position. If the chemokines bind around the same positions in CCR1, this would suggest that tyrosine 18 interacts more with the chemokine than tyrosine 10.

In order to assess the ability of the CCR1 sulfopeptides to mimic CCR1, binding measurements to the full receptor in absence and presence of sodium chlorate (to prevent receptor sulfation) had to be performed, then affinity and selectivity could be compared.

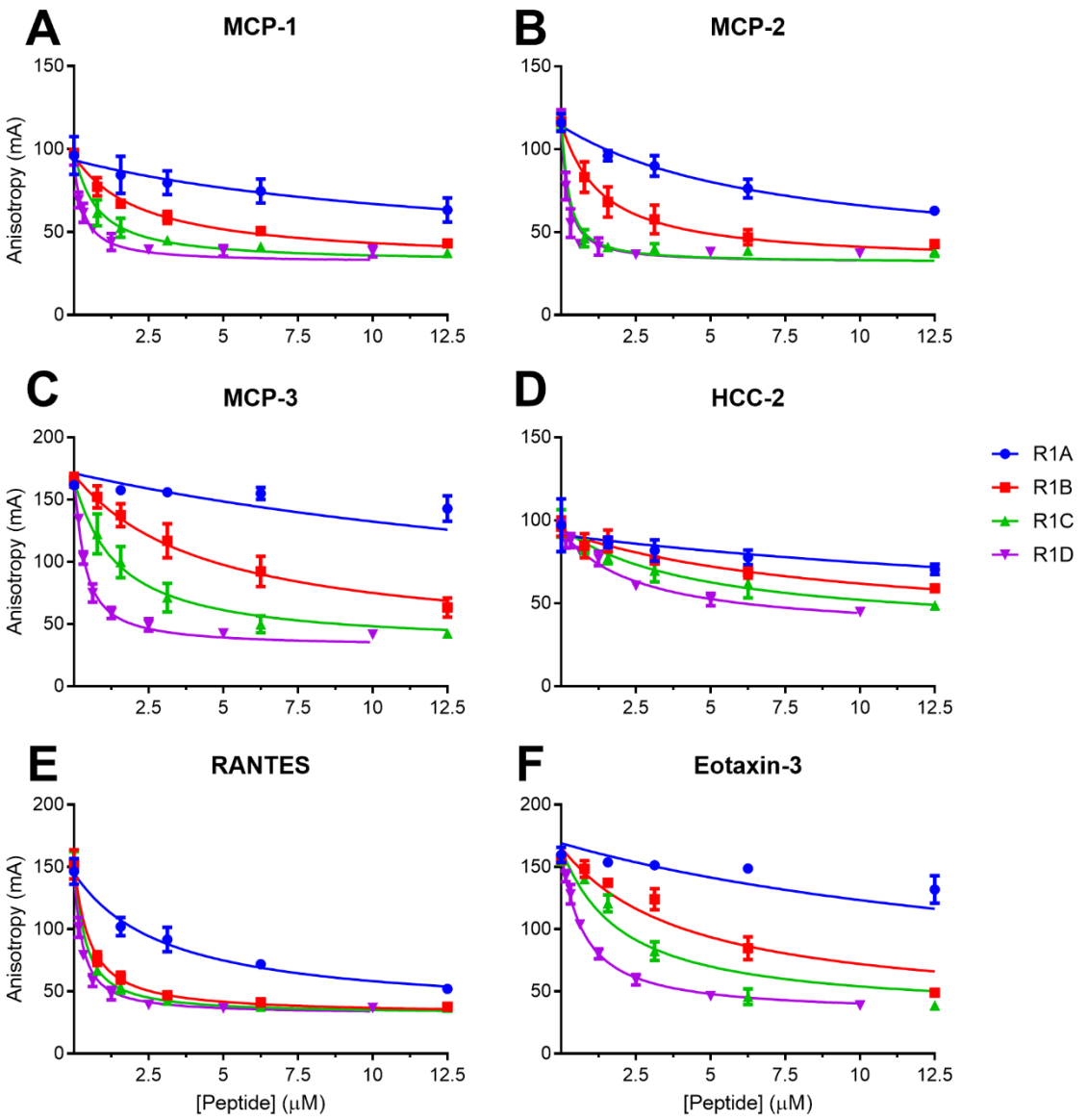

Figure 4.5: Competitive Binding of R1A-D to Various CC Chemokines. Each panel shows the competitive displacement of one chemokine and four sulfopeptides R1A-D: **(A)** MCP-1, **(B)** MCP-2, **(C)** MCP-3, **(D)** HCC-2, **(E)** RANTES and **(F)** Eotaxin-3. R1A-D peptides have different sulfation patterns, R1A being non-sulfated, R1B and C being singly-sulfated on tyrosine 10 and 18, respectively, and R1D being doubly-sulfated. The final concentrations of Fl-R2D and the chemokine were 10 and 100 nM, respectively. Data points represent mean ± SEM of at least three independent experiments performed in duplicate.

Chemokine	Competitive Binding pK_d				K_d (μM)			
	R1A	R1B	R1C	R1D	R1A	R1B	R1C	R1D
MCP-1	5.1 ± 0.07	5.8 ± 0.03	6.4 ± 0.04	6.9 ± 0.05	9.1	1.4	0.4	0.1
MCP-2	5.5 ± 0.03	6.2 ± 0.04	7.1 ± 0.01	7.4 ± 0.04	3.2	0.6	0.1	0.04
MCP-3	5.3 ± 0.05	6.1 ± 0.03	6.6 ± 0.04	7.3 ± 0.02	4.7	0.8	0.2	0.1
HCC-2	4.6 ± 0.06	5.1 ± 0.05	5.4 ± 0.05	5.6 ± 0.04	23.9	8.8	4.3	2.3
RANTES	5.8 ± 0.03	6.6 ± 0.03	6.8 ± 0.02	7.1 ± 0.03	1.7	0.2	0.2	0.1
Eotaxin-3	5.4 ± 0.06	6.1 ± 0.05	6.4 ± 0.05	6.8 ± 0.02	4.0	0.8	0.4	0.1

Table 4.2: Affinity of Various CC Chemokines for the CCR1 Sulfopeptides R1A-D. Values were measured using a fluorescent anisotropy assay. Affinities are reported as pK_d values (-$\log_{10}$ of the K_d; in M). Data are mean and SEM from at least 3 independent experiments performed in duplicate. The corresponding K_d values (in μM) are shown in the adjacent column.

RSQ values

R1A	R1B	0.98
R1A	R1C	0.81
R1A	R1D	0.70
R1B	R1C	0.86
R1B	R1D	0.78
R1C	R1D	0.94

Sulfation patterns

	sY^{10}	sY^{18}
R1A	N	N
R1B	Y	N
R1C	N	Y
R1D	Y	Y

Table 4.3: Coefficients of Determination (RSQ or R^2 Values) and CCR1 Peptides Sulfation Patterns. RSQ values indicate how well the two data sets that are compared match with one another. The sulfation pattern table indicates which tyrosine residues are sulfated in each peptide (N=No and Y=Yes).

4.2.3. Chemokine:Chemokine Receptor Binding Using Radioligand Displacement

To assess receptor binding and selectivity, a radioligand displacement assay was performed using eight CC chemokines: MIP-1α, HCC-2, RANTES, MCP-2 and MCP-3 which are known to be CCR1 agonists, MIP-1β which is a CCR1 antagonist and MCP-1 and eotaxin-3 which are not expected to bind CCR1. The radioligand displacement assay was performed, as described by Zweemer *et al.* [270], using ^{125}I-MIP-1α as a probe. Membranes of CCR1 expressing HEK 293 cells were prepared as described in Chapter 2, section 2.7.7, both in the absence or presence of sodium chlorate, which prevents receptor sulfation. For competition experiments, membranes were incubated with increasing concentrations of non-labelled chemokines and 50 pM ^{125}I-MIP-1α for 2 hours at RT. At this concentration, total radioligand binding did not exceed 10 % of the amount of radioligand added, thus avoiding ligand depletion effects. Nonspecific binding was determined in the presence of 10 μM BX471 (CCR1 antagonist) [201]. Separation of bound from free radioligand was performed by rapid filtration and a scintillation cocktail was used to measure filter-bound radioactivity.

The results are shown in Figure 4.6A for the potentially sulfated receptor and Figure 4.6B for the non-sulfated receptor. MIP-1α (pink) proved to have the highest affinity for CCR1, closely followed by HCC-2 (purple) (Table 4.4). MCP-3 (green) and RANTES (orange) are the next two CCR1 ligands and their affinities were slightly improved when receptor sulfation was prevented, which was unexpected. Receptor sulfation did not have an influence on affinity order. However, while the non-sulfated receptor has similar affinities for the four best CCR1 agonists, the receptor on non-treated membranes can distinguish between chemokines better. MCP-2 (red) and MIP-1β (grey) had lower affinities than the other CCR1 ligands, and sulfation did not influence their binding. In addition, we tested two chemokines that are not reported to bind CCR1: MCP-1 (blue) and eotaxin-3 (black). As expected, eotaxin-3 hardly bound to the potentially sulfated receptor. MCP-1 affinity was closer to that of MIP-1β, especially in the absence of sulfation, which suggests that MCP-1 may be able to activate (or inhibit) CCR1 to some extent.

Overall, preventing receptor sulfation did not have a major influence on chemokine affinities. The binding results established the expected selectivity for CCR1, especially between the cognate and non-cognate chemokines. By comparing these results to the sulfopeptide binding results we could then assess how well sulfopeptides can mimic CCR1 binding and selectivity.

The influence of tyrosine sulfation in chemokine binding can be assessed by comparing binding data between chlorate-treated and non-treated cells. Our results show that the two data sets correlate well with each other (R^2=0.95, Fig 4.7) which can mean either that the sulfation does not influence binding or that the receptor is not sulfated. Another explanation for these results could be that the chlorate treatment of the cells was not efficient in preventing receptor sulfation. However, this possibility was excluded as controls were run on HEK cells expressing cMyc-FLAG-hCCR2 to confirm that the chlorate treatment was working. An anti-FLAG antibody which recognises only the non-sulfated version of the FLAG tag, was used in ELISA assays to assess the efficacy of the chlorate treatment. An anti-cMyc antibody was used to detect the total amount of CCR2, which did not vary with the chlorate treatment.

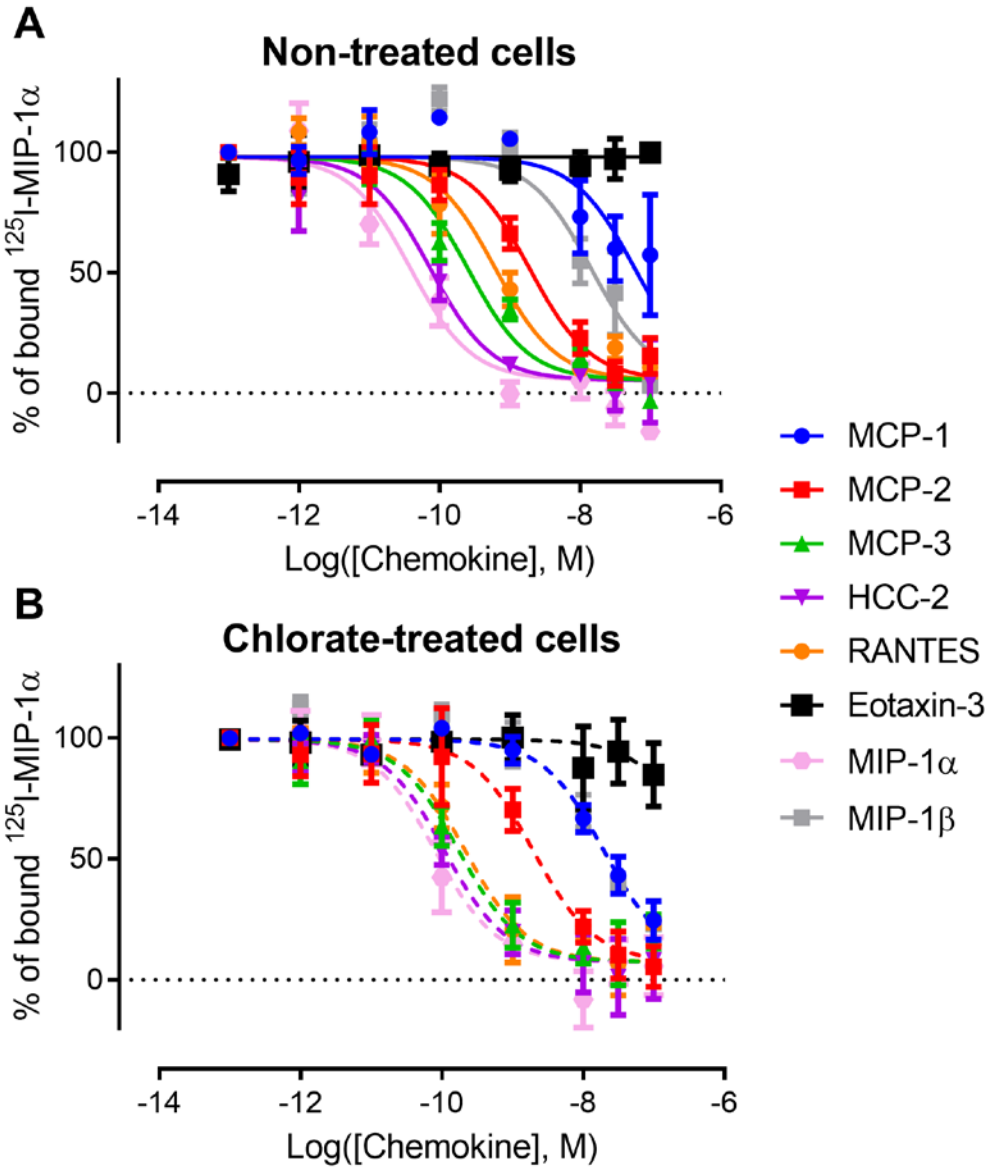

Figure 4.6: Affinities of Various CC Chemokines at the Receptor CCR1. The radioligand displacement assay was performed using membrane preparations of His_6-cMyc-CCR1 and ^{125}I-MIP-1α as a probe. **(A)** Affinities for the receptor without chlorate treatment (potentially sulfated CCR1). **(B)** Affinities for the receptor with 30 mM chlorate treatment (non-sulfated CCR1). Data points represent means ± SEM of at least three independent experiments performed in triplicate.

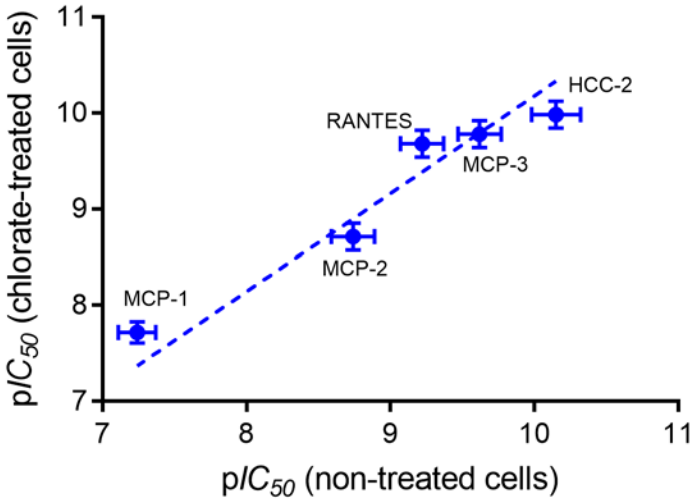

Figure 4.7: Correlation Graph between Potentially Sulfated CCR1 Binding and Non-sulfated CCR1 Binding. The pIC_{50} values for the potentially sulfated receptor with several chemokines are on the x-axis and the pIC_{50} values for the non-sulfated receptor with the same set of chemokines are on the y-axis. If the data sets were matching well, the correlation would be linear (x=y), which is the case here (R^2=0.95; slope = 1.02). Eotaxin-3 was excluded from this graph because no value was obtained for eotaxin-3 binding to non-treated CCR1.

Chemokine	Radioligand Binding pIC_{50}		IC_{50} (nM)	
	CCR1 (no chlorate)	CCR1 (chlorate)	CCR1 (no chlorate)	CCR1 (chlorate)
MCP-1	7.2 ± 0.1	7.7 ± 0.1	57.5	19.1
MCP-2	8.7 ± 0.2	8.7 ± 0.1	1.8	1.9
MCP-3	9.6 ± 0.1	9.8 ± 0.1	0.4	0.2
Eotaxin-3	no binding	6.3 ± 0.2	no binding	457.1
HCC-2	10.1 ± 0.2	10.0 ± 0.1	0.07	0.1
RANTES	9.2 ± 0.2	9.7 ± 0.1	0.6	0.2
MIP-1α	10.4 ± 0.2	10.1 ± 0.2	0.04	0.08
MIP-1β	7.9 ± 0.1	7.7 ± 0.1	13.8	19.1

Table 4.4: Affinity of Various CC Chemokines at the CCR1 Receptor using a Radioligand Displacement Assay. Data represent mean ± SEM from at least three independent experiments performed in triplicate. The chlorate treatment was performed on the cells 48 h prior to the experiments.

cMyc-FLAG-hCCR2 could not be detected by the anti-FLAG antibody in the absence of chlorate treatment because the FLAG tag was sulfated. However, treating the cells with chlorate enabled the detection of around half the amount of receptor that was detected by the anti-cMyc antibody. Although this is not a direct measurement of the receptor sulfation state of the receptor, it is a proof of principle that chlorate treatment inhibits tyrosine sulfation. As the data sets are similar, the non-sulfated data set will be used for comparisons, mainly because eotaxin-3 did not bind the potentially sulfated receptor.

4.2.4. Comparison of Sulfopeptide and Chemokine Receptor Binding

To assess the contribution of the receptor N-terminus to overall binding affinity, sulfopeptide data were correlated with the whole receptor data. Figure 4.8 shows a correlation graph between non-sulfated CCR1 (y axis) and R1A-D (x axis). Coefficients of determination or R^2 values have been calculated between the receptors and the different sulfopeptide data sets and are presented in Table 4.5. This shows that the highest correlation is only 16% between non-treated CCR1 cells and R1D, which indicates that there is no substantial correlation. This result contradicts the two-site model and argues that the N-terminus contributes only a small amount to the selectivity (= *relative* binding affinity) of receptor amongst chemokine ligands. Moreover, the peptides bind with substantially lower affinities than the intact receptor. Therefore, it seems likely that other receptor regions contribute to chemokine binding and selectivity. If this proposal is correct, results coming from studies using N-terminal peptides as models for chemokine receptors have to be interpreted in a careful manner.

Although N-terminal peptides might not be good models to use when trying to replicate chemokine receptor selectivity, they still bind chemokines with mid to low micromolar affinities. In addition, several groups have observed interactions between chemokines and receptor N-termini. Thus, the N-terminal region of the receptor is still likely to form an initial, relatively low affinity complex with the chemokine and interactions described between peptide residues and chemokines, deduced from structural studies for example, might still be an accurate representation of interactions made in the low affinity complex between receptors and chemokines although this remains to be experimentally verified. This initial binding could then be followed by the formation of a tighter, more specific complex involving other parts of the receptor in addition to the N-terminal region. To test the contribution of other receptor regions, binding studies could be performed using a receptor where the N-terminus has been truncated. Binding affinity would be expected to be much lower than binding affinity to the full-length receptor [293, 294] but could still indicate that additional interactions contribute to the overall affinity and the receptor's selectivity.

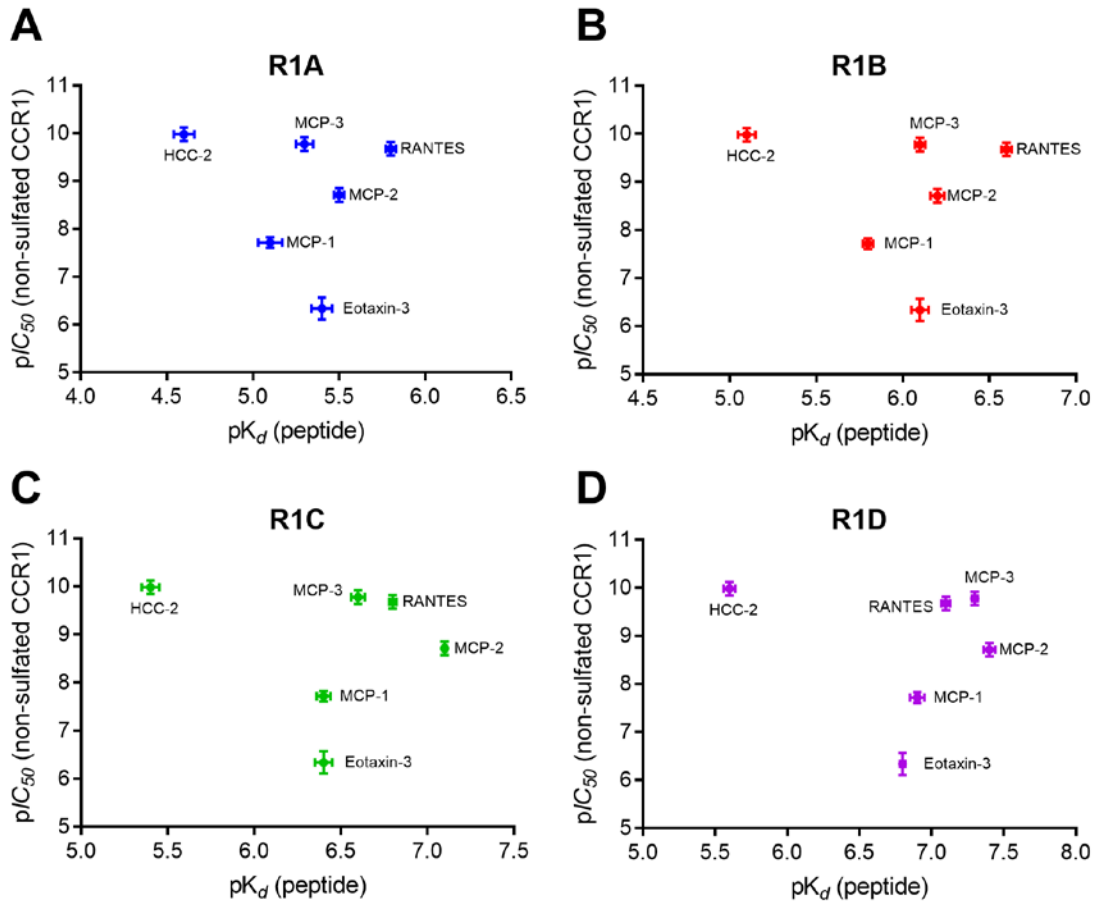

Figure 4.8: Correlation Graphs between Non-sulfated CCR1 Binding and Peptide Binding. The pIC_{50} values for the non-sulfated receptor with several chemokines are on the y-axis and the pK_d values for the CCR1 sulfopeptides with the same set of chemokines are on the x-axis. Each panel represents a different sulfopeptide: **(A)** R1A, **(B)** R1B, **(C)** R1C and **(D)** R1D. If the data sets were matching well, the correlation would be linear (x=y), which is not the case here.

RSQ values

CCR1 (no chlorate)	CCR1 (chlorate)	0.95
CCR1 (no chlorate)	R1A	0.03
CCR1 (no chlorate)	R1B	0.07
CCR1 (no chlorate)	R1C	0.13
CCR1 (no chlorate)	R1D	0.16
CCR1 (chlorate)	R1A	0.02
CCR1 (chlorate)	R1B	0.02
CCR1 (chlorate)	R1C	0.02
CCR1 (chlorate)	R1D	0.04

Table 4.5: Coefficients of Determination (RSQ or R^2 Values). RSQ values indicate how well the two data sets that are compared match with one another. The chlorate treatment was performed on the cells 48 h prior to the experiments.

4.3. Contribution of Chemokine N-Termini to CCR1 Activation

4.3.1. MCP-1/MCP-3 Chimeras: Design and Synthesis

Mutational and structural studies have previously identified three regions of chemokines that interact with receptors [280, 294]. The so-called "N-loop" (a ~twelve residue sequence between the conserved CC/CXC motif and the first β-strand) and the β3 region (third β-strand and preceding turn) form the two sides of a shallow groove that binds to the flexible N-terminal tail of the receptor. The N-terminal region of the chemokine (preceding the CC/CXC motif) penetrates into the transmembrane helical bundle of the receptor. To further investigate the structural elements of chemokines that contribute to CCR1 activation, we designed a series of chimeric proteins in which these three regions of MCP-1 and MCP-3 were swapped between the two chemokines.

The chimeras were originally designed to investigate the structural basis of CCR2 binding and activation [287]. However, the chimeras could also be used to investigate the structural basis of CCR1 activation as MCP-3 is a potent CCR1 agonist but MCP-1 is not. The chimeras were designed and synthesised together with another doctoral student Zil E Huma who was working on the CCR2 receptor project. MCP-1 and -3 were chosen as parent chemokines because their sequences are closely related (71% identity), allowing us to more easily draw conclusions about the roles of specific residues and both MCP-3 and the MCP-1(P8A) mutant used here are monomeric. Human MCP-1 and MCP-3 protein sequences were aligned and the three receptor-binding regions were identified (Fig 4.8C). The sequences were compared and 13 possible mutations (of each chemokine) were identified. Each of these was individually analysed, considering the chemical properties of each amino acid, the relative position of that amino acid in the chemokine and the structural changes which could arise after replacing that residue with the one at the same position from the other chemokine. Two potential mutations (V22K and I46K) were anticipated to disturb the core structure of the chemokine and therefore were not introduced. All other potential mutations, which are present on the surface and not predicted to destabilise the structure, were considered suitable. Each chimera was named according to the parental chemokine from which it is derived, followed by a sequence of three numbers representing the origin of the N-terminal, N-loop and β3 elements, respectively; for example, MCP1-311 is a chimera derived from MCP-1 and containing the N-terminal region of MCP-3, the N-loop of MCP-1 and the β3 region of MCP-1.

Ten chimeras were prepared (schematic diagrams and sequences shown in Fig 4.9) out of the possible 14 combinations. Some chimeras with two regions swapped (MCP1-331, MCP1-313, MCP3-113 and MCP3-131) were not prepared, as the N-terminus was thought to be independent from the other two regions and involved in receptor activation but not binding. Five chimeras are on the MCP-1 background with three regions (N-terminus, N-loop and β3-turn) replaced, individually or in combination, with the corresponding regions of MCP-3 (except the two excluded residues). The other five chimeras are on the MCP-3 background with the three important regions of MCP-1 introduced. All MCP-1 chimeras have the P8A mutation in their sequence (monomeric mutants).

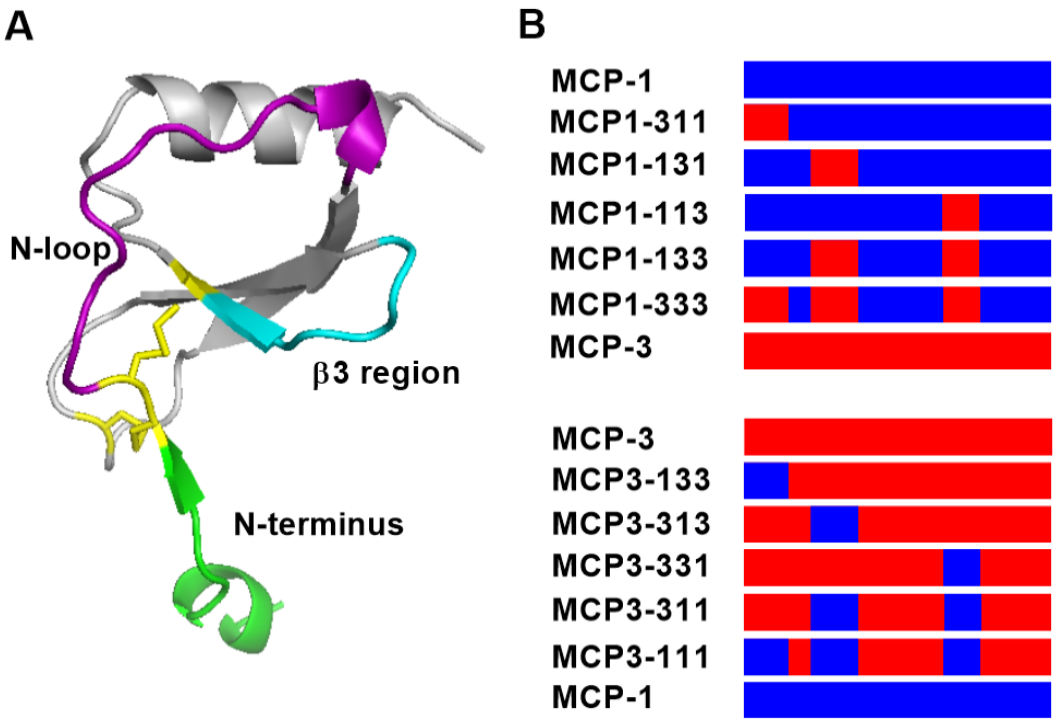

C

```
      N-terminal  N-loop                          β3 region
       1        10  13          24                46    52
MCP-1:QPDAINAAVTCCYNFTNRKISVQRLASYRRITSSKCPKEAVIFKTIVAKEICADPKQKWVQDSMDHLDKQTQTPKT
1-311:QPVGINTSTTCCYNFTNRKISVQRLASYRRITSSKCPKEAVIFKTIVAKEICADPKQKWVQDSMDHLDKQTQTPKT
1-131:QPDAINAAVTCCYRFINKKIPVQRLASYRRITSSKCPKEAVIFKTIVAKEICADPKQKWVQDSMDHLDKQTQTPKT
1-113:QPDAINAAVTCCYNFTNRKISVQRLASYRRITSSKCPKEAVIFKTILDKEICADPKQKWVQDSMDHLDKQTQTPKT
1-133:QPDAINAAVTCCYRFINKKIPVQRLASYRRITSSKCPKEAVIFKTILDKEICADPKQKWVQDSMDHLDKQTQTPKT
1-333:QPVGINTSTTCCYRFINKKIPVQRLASYRRITSSKCPKEAVIFKTILDKEICADPKQKWVQDSMDHLDKQTQTPKT

MCP-3:QPVGINTSTTCCYRFINKKIPKQRLESYRRTTSSHCPREAVIFKTKLDKEICADPTQKWVQDFMKHLDKKTQTPKL
3-133:QPDAINAAVTCCYRFINKKIPKQRLESYRRTTSSHCPREAVIFKTKLDKEICADPTQKWVQDFMKHLDKKTQTPKL
3-313:QPVGINTSTTCCYNFTNRKISKQRLESYRRTTSSHCPREAVIFKTKLDKEICADPTQKWVQDFMKHLDKKTQTPKL
3-331:QPVGINTSTTCCYRFINKKIPKQRLESYRRTTSSHCPREAVIFKTKVAKEICADPTQKWVQDFMKHLDKKTQTPKL
3-311:QPVGINTSTTCCYNFTNRKISKQRLESYRRTTSSHCPREAVIFKTKVAKEICADPTQKWVQDFMKHLDKKTQTPKL
3-111:QPDAINAAVTCCYNFTNRKISKQRLESYRRTTSSHCPREAVIFKTKVAKEICADPTQKWVQDFMKHLDKKTQTPKL
```

Figure 4.9: Design, Schematics and Sequences of MCP-1/MCP-3 Chimeras. (A) Structure of MCP-1 showing the three important regions (PDB ID: 1DOK) highlighting the regions swapped in the chimeras. **(B)** Schematic diagrams of the chimeras with regions from MCP-1 and MCP-3 in blue and red respectively. **(C)** Sequences of the chimeras. The green highlighted regions correspond to the N terminus (1-10), N loop (12 - 24) and β3 strand (46-52) in MCP-1 and MCP-3. The yellow highlighted regions correspond to the regions that are mutated (from MCP-1 to MCP-3 in the five chimeras on MCP-1 background and from MCP-3 to MCP-1 in the five chimeras on MCP-3 background) and the red, underlined residues are the specific mutations made.

Cloning and protein production were mainly done by Zil E Huma, following the method described in Chapter 2, section 2.4 and 2.5 Briefly, genes were made using recursive PCR and cloned into pET28a vectors. After correct sequencing, plasmids were transformed into BL21(DE3) *E.coli* cells and the N-terminal His_6-tagged protein was expressed after IPTG induction. Inclusion bodies containing the fusion proteins were isolated, dissolved in denaturing buffer and purified by Ni^{2+}-affinity chromatography. The fusion proteins were refolded by rapid dilution. The His_6-tag was removed using human thrombin and the untagged protein (containing the native N-terminus) was further purified by size exclusion chromatography. ^1H NMR spectra were collected for all the chimeras along with the parent chemokines to confirm correct folding (Figure 4.10) [287]. Methyl groups in unstructured peptides resonate close to 1 ppm, while in these spectra, the resonances around -0.5 ppm indicate a folded tertiary structure. The most upfield peak in each spectrum (lower than -0.5 ppm) is shifted further for MCP-3 compare to MCP-1. This peak is present in all five chimeras in the MCP-3 background around the same chemical shift as MCP-3 and similarly in the MCP-1 background chimeras around the chemical shift of MCP-1. The downfield regions also show well resolved peaks between 6.5 to 10 ppm. Thus, the NMR data indicate that all the chimeras are well folded and adopt the expected native 3D structures.

4.3.2. Assessment of Receptor Activation

To investigate CCR1 activation, the same signalling readouts used in Chapter 3 were measured: β-arrestin 2 recruitment, G protein activation, inhibition of cAMP production and ERK1/2 phosphorylation. Flp-In T-Rex HEK 293 cells stably expressing an N-terminally tagged human CCR1 receptor (His_6-cMyc-hCCR1) were used. Binding assays have not been performed yet, as we initially focused on receptor activation. However, binding will be assessed at a later stage because it is a necessary information to fully understand and characterise the way chemokines act at CCR1. Considering that MCP-1 is not a CCR1 cognate chemokine, biased agonism quantification was not considered, unlike the HCC-2/MCP-3 chimera set where HCC-2 and MCP-3 are both CCR1 ligands. This set of chimeras allows for the distinction between activated and non-activated receptor only.

All ten chimeras together with the two parent chemokines were used in each of the four signalling assays. The full data are presented in the Appendix section (Appendix III) and Table 4.6 and only a subset of the data is shown here in Figures 4.11 to 4.14. Figure 4.11 shows four graphs, one for each assay, with the parent chemokines (MCP-1 and MCP-3) and the N-terminal swap chimeras (MCP1-311 and MCP3-133). MCP1-311 (dotted blue curve) is indeed better than MCP-1 (full blue curve) at activating CCR1 in all four readouts and, in the same way, the ability of MCP3-133 (dotted red curve) to activate CCR1 decreases compared to MCP-3 (full red curve). This confirms that the N-terminus is an important region of the chemokines for receptor activation. However, both chimeras have intermediate CCR1 activation abilities (potency and efficacy) between MCP-1 and MCP-3, whereas the two-site model would predict MCP1-311 to behave like MCP-3 and MCP3-133 like MCP-1. This suggests that the chemokine N-terminus is not the only region involved in controlling receptor activation.

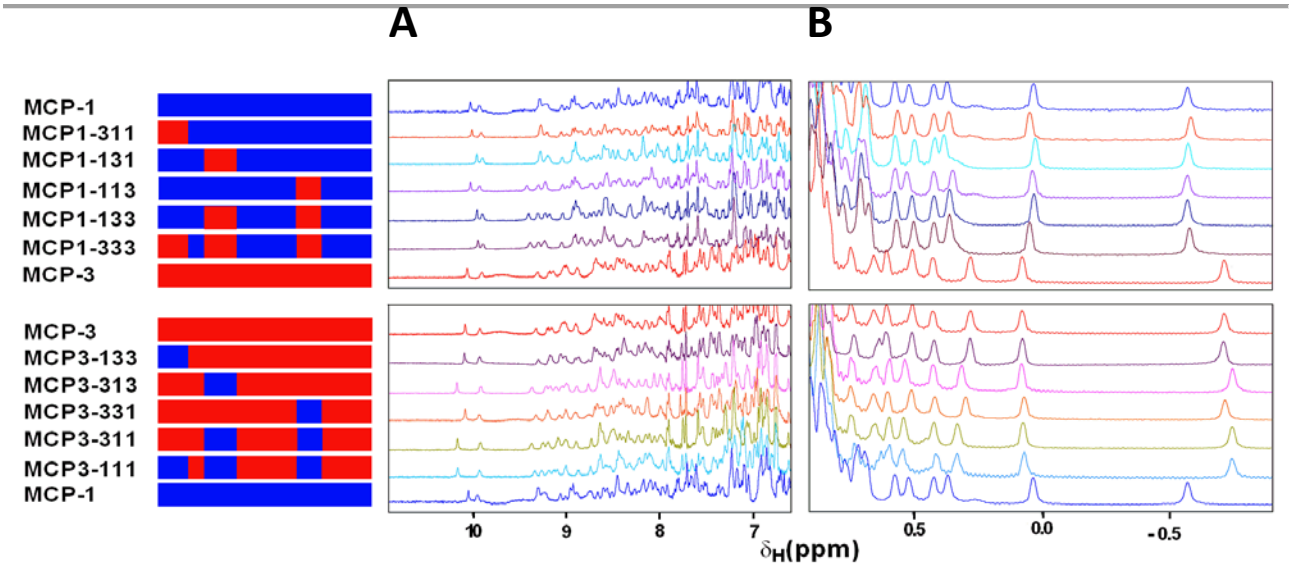

Figure 4.10: Structure Validation of MCP-1/MCP-3 Chimeras. 1D ^{1}H NMR spectra of all the ten chimeras showing **(A)** the downfield (amide and aromatic) region and **(B)** the upfield (methyl) region of the spectra. Both regions showed well-dispersed peaks indicative of correct folding of protein. Several peaks characteristic of MCP-1 or MCP-3 background can be seen in the chimeras with MCP-1 or MCP-3 background respectively, confirming that chimeras have similar structures to the parent chemokine. Names and schematic diagrams of the chemokines and chimeras are shown on the left. All protein samples were in 20 mM sodium acetate-d_4, pH 7.0 containing 5 % D_2O. ^{1}H NMR spectra were recorded at 25 °C and referenced to external DSS.

Figure 4.12 shows the N-loop swap chimeras MCP1-131 and MCP3-313. Just like the N-terminal swap chimeras, the potency and efficacy of both chimeras are intermediate between the parent chemokines. This implies that the N-loop is important for CCR1 activation. The two-site model does not predict this result directly. However, this is where the binding results will help our understanding. If MCP3-313 binds CCR1 with a weaker affinity than MCP-3, which is predicted by the two-site model, it is then expected that it will have decreased potency but not efficacy at CCR1. At this stage, it is not possible to say whether this result disagrees with the model or not but it is clear that the N-loop is another region to consider when it comes to CCR1 activation.

Figure 4.13 shows the β3 region swap chimeras MCP1-113 and MCP3-331. This region proved not to be involved in CCR1 activation as MCP1-113 behaves like MCP-1 and MCP3-331 like MCP-3. This result was confirmed by the fact that MCP1-133 behaves like MCP1-131 and MCP3-311 like MCP3-313 (see Appendix III) and agrees with the two-site model.

According to the results from single region swap chimeras, the chemokine N-terminus and N-loop are two regions to consider for CCR1 activation. If these regions are the only ones involved, it would then be expected that by mutating both regions together, the mutants will behave differently from the background chemokine and more like the chemokine from which the mutated regions are derived. As we did not make a N-terminus/N-loop mutant, we answered this question using the triple mutants. The β3 region having no influence on CCR1 activation, it is reasonable to assume that MCP1-333 and MCP1-331 would behave similarly. Figure 4.14 shows the results for the triple mutants MCP1-333 and MCP3-111 and as predicted, MCP1-333 behaves like MCP-3 and MCP3-111 like MCP-1. So, the conclusions made from the single region mutation held true when mutating multiple regions and confirmed that the chemokine N-terminus and N-loop are the two main regions controlling CCR1 activation.

	Mass Spectrometry		pERK Assay		cAMP Assay		GPA Assay (αi2)		β-Arrestin-2 Assay	
	Predicted Mass (Da)	Observed Mass (Da)	p*EC* $_{50}$	E_{max}	p*EC* $_{50}$	E_{max}	p*EC* $_{50}$	E_{max}	p*EC* $_{50}$	E_{max}
MCP-1	8658.9	8659.4	6.9 ± 0.1	24.2 ± 2	6.3 ± 0.4	41.9 ± 14.2	did not fit		7.8 ± 0.3	0.023 ± 0.003
MCP1-311	8677.0	8676.3	7.6 ± 0.2	33.7 ± 2	6.9 ± 0.2	38.4 ± 5.1	6.2 ± 0.3	0.095 ± 0.01	7.8 ± 0.2	0.029 ± 0.002
MCP1-131	8695.1	8696.1	7.7 ± 0.2	31.4 ± 2	7.3 ± 0.1	42.5 ± 3.2	6.9 ± 0.1	0.067 ± 0.01	7.8 ± 0.1	0.028 ± 0.002
MCP1-113	8717.0	8717.8	7.0 ± 0.1	27.1 ± 2	5.9 ± 0.8	49.5 ± 55.6	6.1 ± 0.5	0.046 ± 0.02	7.0 ± 0.2	0.033 ± 0.004
MCP1-133	8753.1	8751.1	7.8 ± 0.2	22.4 ± 1	7.4 ± 0.2	38.5 ± 3.4	7.0 ± 0.1	0.063 ± 0.01	8.1 ± 0.2	0.031 ± 0.002
MCP1-333	8771.2	8769.7	7.8 ± 0.1	37.8 ± 2	7.6 ± 0.1	49.5 ± 3.1	7.3 ± 0.1	0.099 ± 0.01	8.3 ± 0.1	0.042 ± 0.002
MCP-3	8956.4	8952.7	8.2 ± 0.2	43.7 ± 2	7.9 ± 0.2	44.2 ± 2.8	7.4 ± 0.1	0.110 ± 0.01	8.3 ± 0.1	0.039 ± 0.002
MCP3-133	8938.4	8936.1	7.2 ± 0.2	32.3 ± 3	7.5 ± 0.2	37.9 ± 2.6	6.8 ± 0.1	0.057 ± 0.01	8.2 ± 0.2	0.030 ± 0.003
MCP3-313	8920.2	8920.3	7.6 ± 0.1	40.5 ± 1	7.2 ± 0.1	39.7 ± 2.7	6.5 ± 0.2	0.097 ± 0.01	8.2 ± 0.2	0.033 ± 0.003
MCP3-331	8898.4	8902.7	8.2 ± 0.1	50.2 ± 2	7.9 ± 0.1	50.3 ± 2.3	7.6 ± 0.1	0.098 ± 0.01	8.7 ± 0.2	0.039 ± 0.003
MCP3-311	8862.2	8860.1	7.5 ± 0.1	41.5 ± 2	7.7 ± 0.2	35.7 ± 2.4	7.3 ± 0.3	0.081 ± 0.01	7.3 ± 0.1	0.068 ± 0.004
MCP3-111	8844.2	8844.4	6.5 ± 0.1	22.1 ± 3	6.5 ± 0.1	51.2 ± 4.3	did not fit		did not fit	

Table 4.6: Potency and Efficacy of the Different MCP-1/3 Chimeras at the CCR1 Receptor in β-arrestin Recruitment, G Protein Activation, cAMP Inhibition and ERK1/2 Phosphorylation Assays. Data are mean and SEM from at least 3 independent experiments performed in duplicate.

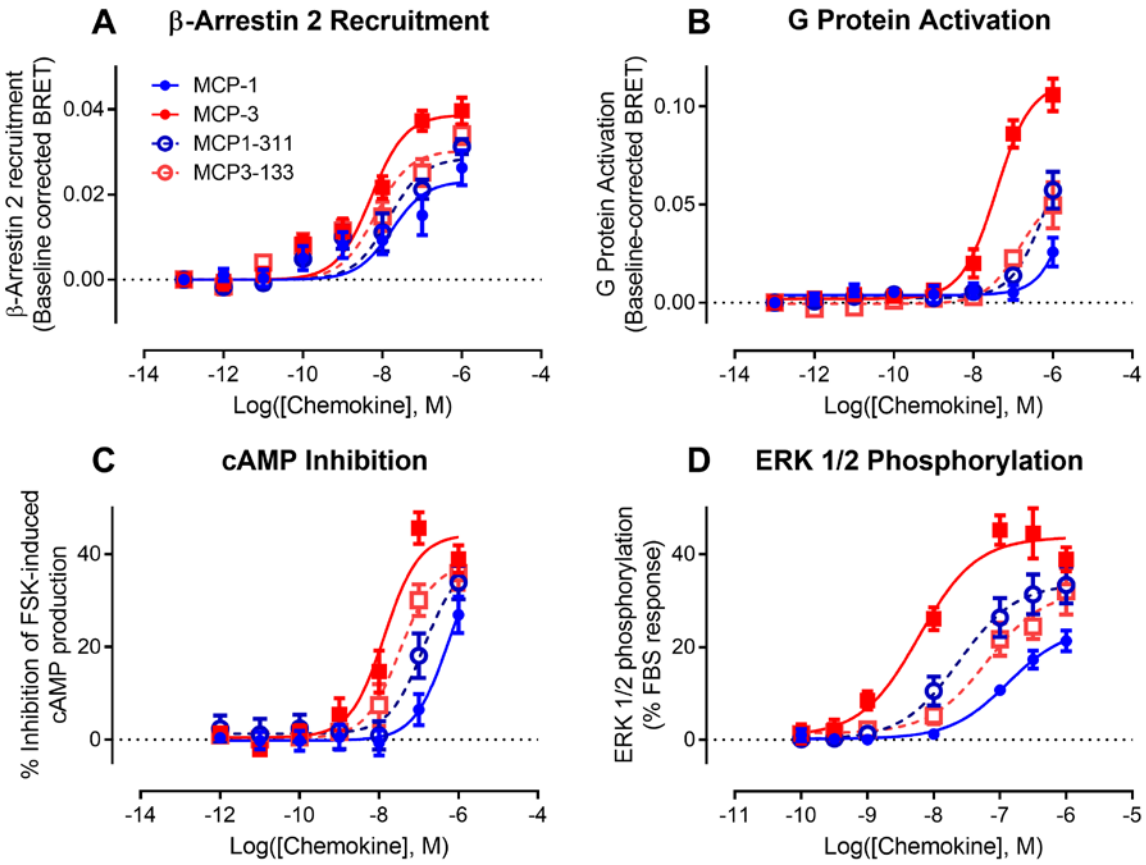

Figure 4.11: Activation of CCR1 by MCP-1/3 N-terminal Swap Chimeras. (A) β-arr2 recruitment was measured using parental HEK 293 cells transiently transfected with plasmids encoding CCR1-RLuc8 and β-arr2-YFP. **(B)** GPA was measured using His_6-cMyc-CCR1 Flp-In T-REx HEK 293 cells and $G\alpha_{i2}$. Transfections were performed as described in chapter 2, section 2.7.6. **(C)** cAMP inhibition was measured using His_6-cMyc-CCR1 Flp-In T-REx 293 cells transiently transfected with a BRET-based cAMP biosensor. **(D)** ERK1/2 phosphorylation assay was performed using His_6-cMyc-CCR1 Flp-In T-REx HEK 293 cells and the amount of phosphorylated ERK1/2 was measured by AlphaScreen detection. Data points represent means ± SEM of at least three independent experiments performed in duplicate.

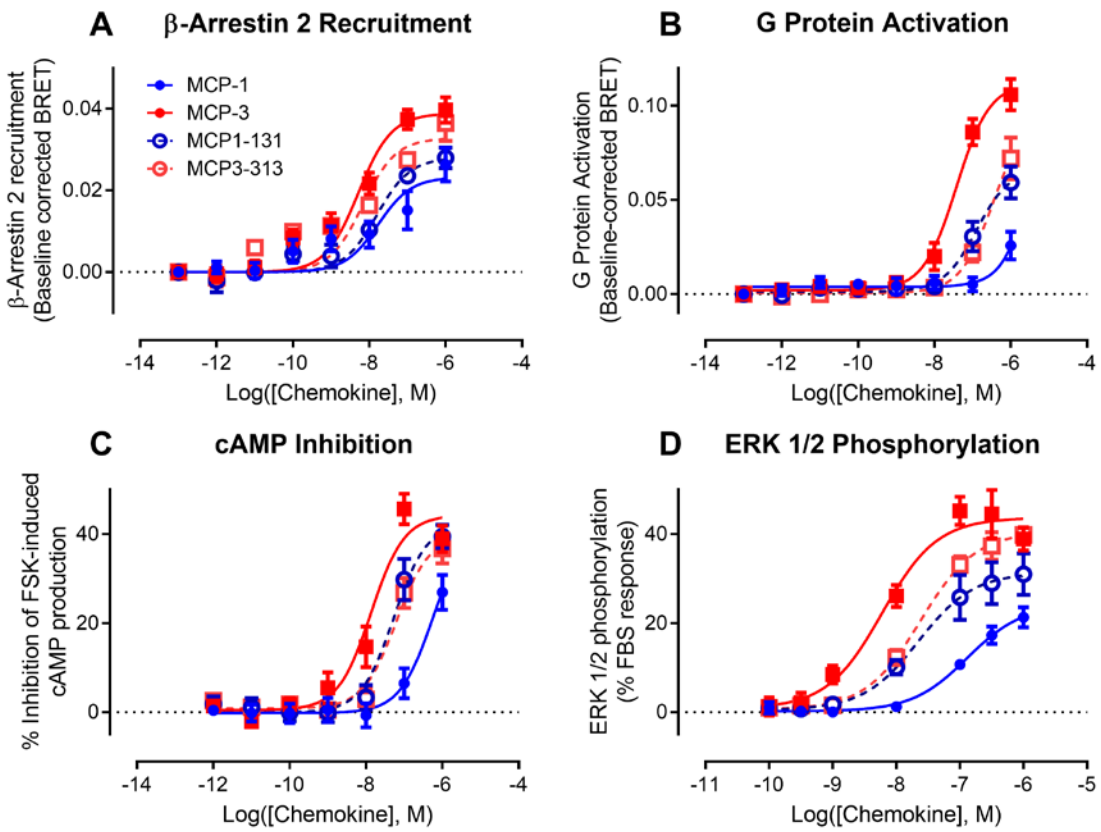

Figure 4.12: Activation of CCR1 by MCP-1/3 N-loop Swap Chimeras. (A) β-arr2 recruitment was measured using parental HEK 293 cells transiently transfected with plasmids encoding CCR1-RLuc8 and β-arr2-YFP. **(B)** GPA was measured using His_6-cMyc-CCR1 Flp-In T-REx HEK 293 cells and $G\alpha_{i2}$. Transfections were performed as described in chapter 2, section 2.7.6. **(C)** cAMP inhibition was measured using His_6-cMyc-CCR1 Flp-In T-REx 293 cells transiently transfected with a BRET-based cAMP biosensor. **(D)** ERK1/2 phosphorylation assay was performed using His_6-cMyc-CCR1 Flp-In T-REx HEK 293 cells and the amount of phosphorylated ERK1/2 was measured by AlphaScreen detection. Data points represent means ± SEM of at least three independent experiments performed in duplicate.

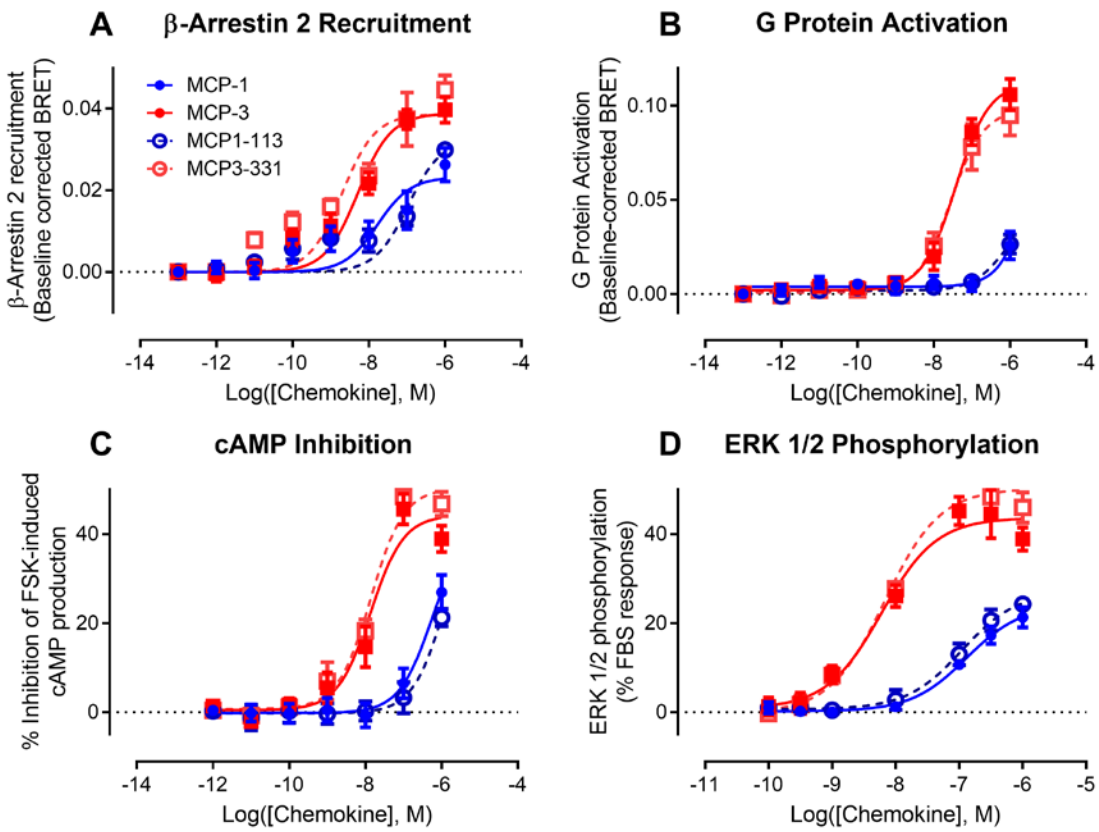

Figure 4.13: Activation of CCR1 by MCP-1/3 β3-turn Swap Chimeras. (A) β-arr2 recruitment was measured using parental HEK 293 cells transiently transfected with plasmids encoding CCR1-RLuc8 and β-arr2-YFP. **(B)** GPA was measured using His_6-cMyc-CCR1 Flp-In T-REx HEK 293 cells and $G\alpha_{i2}$. Transfections were performed as described in chapter 2, section 2.7.6. **(C)** cAMP inhibition was measured using His_6-cMyc-CCR1 Flp-In T-REx 293 cells transiently transfected with a BRET-based cAMP biosensor. **(D)** ERK1/2 phosphorylation assay was performed using His_6-cMyc-CCR1 Flp-In T-REx HEK 293 cells and the amount of phosphorylated ERK1/2 was measured by AlphaScreen detection. Data points represent means ± SEM of at least three independent experiments performed in duplicate.

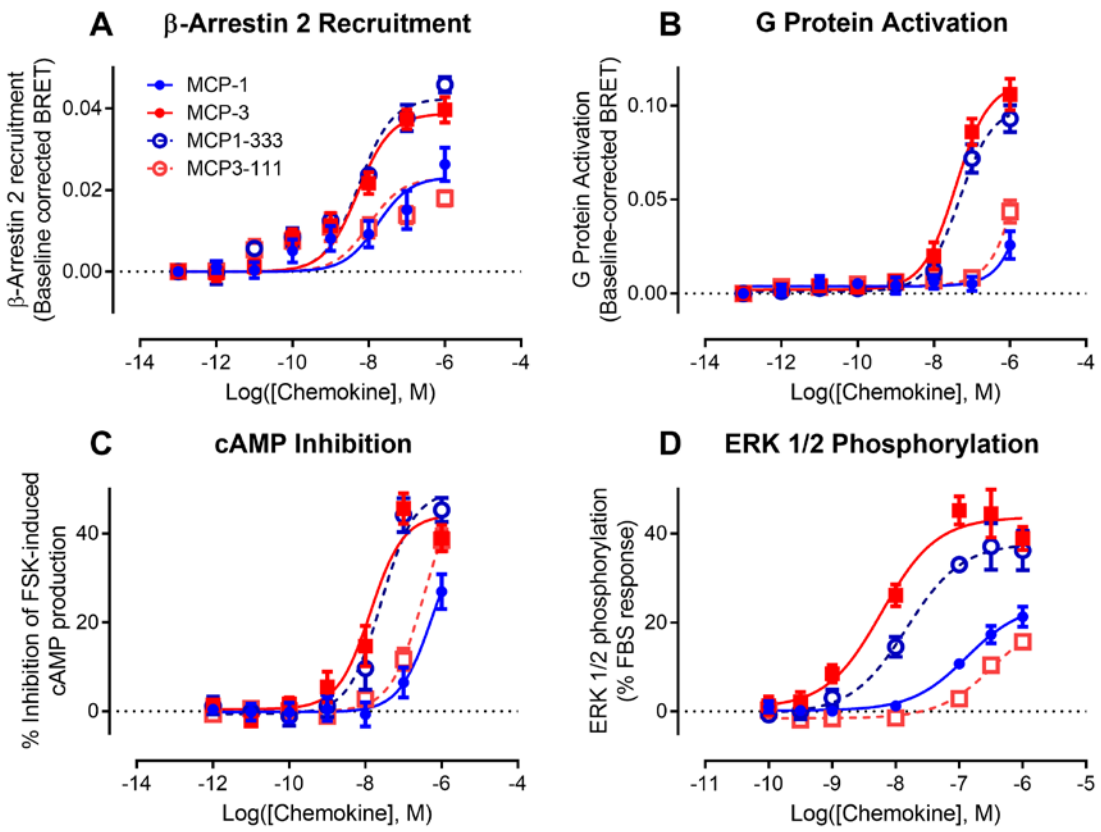

Figure 4.14: Activation of CCR1 by MCP-1/3 Triple Swap Chimeras. (A) β-arr2 recruitment was measured using parental HEK 293 cells transiently transfected with plasmids encoding CCR1-RLuc8 and β-arr2-YFP. **(B)** GPA was measured using His_6-cMyc-CCR1 Flp-In T-REx HEK 293 cells and $G\alpha_{i2}$. Transfections were performed as described in chapter 2, section 2.7.6. **(C)** cAMP inhibition was measured using His_6-cMyc-CCR1 Flp-In T-REx 293 cells transiently transfected with a BRET-based cAMP biosensor. **(D)** ERK1/2 phosphorylation assay was performed using His_6-cMyc-CCR1 Flp-In T-REx HEK 293 cells and the amount of phosphorylated ERK1/2 was measured by AlphaScreen detection. Data points represent means ± SEM of at least three independent experiments performed in duplicate.

4.4. Discussion

Chemokine:receptor interactions have been studied for over 20 years and despite a significant effort, the mechanisms regulating chemokine receptor signalling still remain incompletely characterised. This is due, in part, to a very complex network comprising over 50 chemokines and 25 receptors. Most receptors and chemokines are promiscuous [295], which was originally interpreted as functional redundancy but is now increasingly recognised as a way to generate a diverse array of fine-tuned signalling responses. The concept of biased agonism or functional selectivity, which has been observed for several chemokine receptors [296, 297], demonstrates the intricacy of the chemokine:receptor system.

To investigate these interactions further, numerous structural and mutational studies have been performed [298] and a model based on these studies was proposed in 1997 by Crump *et al.* [280]. This model defines two sites that are distinct both spatially and functionally. Site 1 involves the receptor N-terminus and the chemokine N-loop and β3 regions and accounts for chemokine:receptor binding. Site 2 involves the chemokine N-terminus and some receptor transmembrane helices and is responsible for receptor activation. This simple model has proven very useful over the years and was consistent with most results that were available at the time. However, as techniques and knowledge improve, we now have access to new results that either are hard to explain using the two-site model only or directly challenge the two-site concept [299]. Therefore, we decided to explore the implications of this model and study interactions involved on both sites using the CCR1 receptor as well as the influence of tyrosine sulfation on the site 1 interactions.

4.4.1. Site 1 Interactions

The first part of this chapter reports the strategy we developed to assess site 1 interactions. We used peptides with the CCR1 N-terminal sequence and various tyrosine sulfation patterns to compare chemokine binding between a whole receptor and its N-terminus. The two-site model predicts that binding between N-terminal peptides and whole receptor should correlate, yet we found that it was not the case. A fluorescence anisotropy assay was developed for peptide binding measurements and a radioligand displacement assay was performed for whole receptor binding and correlation did not exceed 16%, regardless of the sulfation pattern.

Several hypotheses can be proposed to explain this result. Firstly, the receptor N-terminus could be in a different structure (or structural environment) in the intact receptor compared to the peptides. Although it is reasonable to assume that the receptor N-terminus is elongated like the peptides might be, it could still have a different structure when attached to the entire receptor. Secondly, the membrane could play a role in chemokine:receptor interaction, either interacting with the receptor N-terminus or bringing chemokines closer to the receptor. Thirdly, other post-translational modifications could contribute to chemokine binding in the intact receptor. Although these hypotheses are possible, the most reasonable explanation for our results is that other regions of the receptor are involved in chemokine binding by CCR1. This hypothesis is supported by the fact that peptides binding is much weaker than receptor binding and does not correlate with the selectivity of the receptor. In addition, the recent structures of chemokine:receptor complexes show interactions in site 2

between an inactive conformation of the receptor and chemokines, which suggests that these are binding interactions, as they cannot contribute to activation.

Another aspect of this site 1 study was the influence of tyrosine sulfation on chemokine binding. Sulfation has been shown to enhance chemokine binding in several chemokine receptors [144]. This result was confirmed in the peptide binding assay. However, inhibiting CCR1 sulfation did not have a major influence on CCR1 radioligand binding results. This suggests that CCR1 might not have been sulfated under the conditions used for the radioligand displacement assay. Although the idea that CCR1 was sulfated and sulfation does not affect binding is also possible, the lack of sulfation seems more likely, knowing that sulfation usually influences binding [139, 145]. Results from Chapter 3 were also inconclusive regarding the effect of sulfation because no change was observed when HCC-2, MCP-2 and MCP-3 were assessed in CCR1 binding and activation of β-arr2 recruitment, G protein activation, cAMP inhibition and ERK1/2 phosphorylation using chlorate-treated and non-treated cells. Thus, it appears that in HEK 293 cells, CCR1 may not be sulfated. However, CCR1 could still be sulfated in a different context. Sulfation patterns are indeed likely to vary depending on tissue type [300] or the surrounding conditions (pro- or anti-inflammatory). To investigate these results, it would be interesting to develop a method that can assess the receptor sulfation directly. This could be done by using mass spectrometry techniques or anti-tyrosine antibodies that would be sensitive to tyrosine sulfation. It would also be advantageous to perform experiments using cells that endogenously express CCR1. This would provide insight on whether the CCR1 sulfation state varies across cell types or tissues and could be of interest when targeting specific cells or areas in the body.

4.4.2. Site 2 Interactions

The second part of this chapter was set out to explore the site 2 interactions. The two-site model predicts that only the interactions of the chemokine N-terminus control receptor activation. Based on this hypothesis, we chose to design and synthesise chimeras between MCP-1 and MCP-3. These two chemokines are closely related (71% sequence identity), which makes it easier to swap regions without disturbing their structure too much and interpret results, but only MCP-3 activates CCR1. We then measured four different signalling responses to assess for receptor activation.

As the two-site model predicted, the chemokine N-terminus is involved in receptor activation, although the results indicate that it is not the only region. Swapping N-termini between MCP-1 and -3 was not sufficient to make MCP-1 behave like MCP-3 and vice versa. Results revealed that the N-loop is also involved in receptor activation. It is unclear at this stage if it is a direct implication in receptor activation and binding studies will have to be performed to address this question. If the N-loop influences binding as predicted by the two-site model, it should impact the potency in a similar way. This indirect effect would not be due to the N-loop directly contributing to activation, it would be a consequence of a change in binding affinity. On the other hand, if a change in efficacy is observed, it cannot be linked to binding and would imply a direct role of the N-loop in receptor activation. Regardless, this result challenges the two-site model as well, either by adding a chemokine region to consider when assessing receptor activation or by questioning the independence of the

two sites. It is worth mentioning that this result is also different from the results obtained on CCR2. Our laboratory recently published a similar study [287] using CCR2 and the same set of MCP-1/3 chimeras and established the chemokine N-terminus as the main region controlling both relative binding affinity and full versus partial activation of CCR2. The differences between CCR1 and CCR2 activation by MCP-1/3 is further discussed in Chapter 6, section 6.3. As these results do not completely correlate with the two-site model predictions, it suggests that it is time to reassess the two-site model, which might avoid overlooking more complex aspects of chemokine receptor signalling. It is worth noting that up until this point, all our results can be explained by considering only the two sites. However, their functions are not clearly separated between binding (site 1) and activation (site 2). This is why we envisioned an extension of the current two-site model, which has an additional state where the inactive conformation of the receptor is fully bound to its cognate chemokine (site 1 and site 2 binding interactions) and eliminates the spatial separation between binding and activation. This extended model is presented in Chapter 6, section 6.2.1

Chapter 5. Targeting Chemokines using Tick Evasins

5.1. Preface to Chapter 5

As discussed in the introduction of this thesis, targeting chemokine receptors using small molecule inhibitors has proven to be very challenging [54, 301]. Several clinical trials have failed over the years mainly because of a lack of efficacy from the antagonist [302]. Although it is hard to explain why the trials were unsuccessful, one reason could be the complexity of the chemokine:receptor network. Most immune cells express several chemokine receptors on their surfaces [181, 226] and blocking one receptor might not be sufficient to stop chemotaxis or any other undesirable effect, as chemokines can activate a different receptor potentially leading to similar signalling outcomes. Blocking chemokine receptors also leads to a partial loss of immune protection which presents a risk when our body is infected.

To avoid the downfalls of blocking chemokine receptors, we and other groups have considered targeting chemokines instead [303, 304]. A variety of chemokine-binding proteins have already been identified [305-307] and our group recently reported two studies using nanoparticles bearing sulfonated polystyrene brushes [235] or using a protein produced by the human cytomegalovirus [243] to bind chemokines. We then focused on another family of proteins expressed by ticks, called evasins, that were discovered in 2007 [256, 308] and allow ticks to avoiding immune detection by their hosts. The first evasins were found in the saliva of the species *Rhipicephalus sanguineus* (brown dog tick). Although no evasin protein had been reported in any other tick species, it seemed likely that such proteins would exist. Therefore we decided to use bioinformatic methods to identify other evasin proteins that we could test for chemokine-binding and -inhibitory activity.

This chapter is comprised of a published manuscript (Hayward J.*, **Sanchez J**.*, Perry A., Huang C., Valle M. R., Canals M., Payne R. J. and Stone M. J., Ticks from Diverse Genera Encode Chemokine-Inhibitory Evasin Proteins. J. Biol. Chem. 2017; DOI: 10.1074/jbc.M117.807255; *, these authors contributed equally to this work) in which we described the discovery of several evasins and assessed their ability to bind and inhibit CC chemokines. Working together with Honours student Jenni Hayward, I expressed and purified these proteins and measured their chemokine binding. I also performed the cell-based assays to determine chemokine inhibition. The supplementary data are included as Appendix V. The results have been reprinted with permission from the journal.

JBC ARTICLE

Ticks from diverse genera encode chemokine-inhibitory evasin proteins

Received for publication, July 18, 2017 Published, Papers in Press, August 4, 2017, DOI 10.1074/jbc.M117.807255

Jenni Hayward[‡1], Julie Sanchez[‡1], Andrew Perry[§], Cheng Huang[‡], Manuel Rodriguez Valle[¶], Meritxell Canals[‖2], Richard J. Payne[**], and Martin J. Stone[‡3]

From the [‡]Infection and Immunity Program, Monash Biomedicine Discovery Institute, and Department of Biochemistry and Molecular Biology and the [§]Monash Bioinformatics Platform, Monash University, Clayton, Victoria 3800, Australia, [¶]Department of Veterinary Biosciences, Faculty of Veterinary and Agricultural Sciences, The University of Melbourne, Parkville, Victoria 3010, [‖]Drug Discovery Biology, Monash Institute of Pharmaceutical Sciences, Monash University, Parkville, Victoria 3052, and the [**]School of Chemistry, The University of Sydney, New South Wales 2006, Australia

Edited by Luke O'Neill

To prolong residence on their hosts, ticks secrete many salivary factors that target host defense molecules. In particular, the tick *Rhipicephalus sanguineus* has been shown to produce three salivary glycoproteins named "evasins," which bind to host chemokines, thereby inhibiting the recruitment of leukocytes to the location of the tick bite. Using sequence similarity searches, we have identified 257 new putative evasin sequences encoded by the genomes or salivary or visceral transcriptomes of numerous hard ticks, spanning the genera *Rhipicephalus*, *Amblyomma*, and *Ixodes* of the Ixodidae family. Nine representative sequences were successfully expressed in *Escherichia coli*, and eight of the nine candidates exhibited high-affinity binding to human chemokines. Sequence alignments enabled classification of the evasins into two subfamilies: C_8 evasins share a conserved set of eight Cys residues (four disulfide bonds), whereas C_6 evasins have only three of these disulfide bonds. Most of the identified sequences contain predicted secretion leader sequences, *N*-linked glycosylation sites, and a putative site of tyrosine sulfation. We conclude that chemokine-binding evasin proteins are widely expressed among tick species of the Ixodidae family, are likely to play important roles in subverting host defenses, and constitute a valuable pool of anti-inflammatory proteins for potential future therapeutic applications.

Ticks are hematophagous arachnids that parasitize humans, livestock, and both domestic and wild animals. Many ticks are vectors of pathogenic microorganisms that cause disease when transmitted to the host, including anaplasmosis, ehrlichiosis, babesiosis, and Lyme disease (1–3). In particular, several species of hard tick (family Ixodidae) from the genera *Amblyomma*, *Ixodes*, and *Rhipicephalus* have been studied extensively due to their medical and veterinary significance (4).

Mammals respond to tick bites and other injuries or infections by mounting a complex inflammatory response, a key feature of which is the recruitment of circulating leukocytes to the site of the affected tissues. Leukocyte recruitment is mediated by chemokine proteins, which are secreted into the vasculature at the site of the injury. There, they bind to chemokine receptors on circulating leukocytes and thereby stimulate leukocyte trafficking to the damaged tissue (5, 6). Humans and other mammals produce an array of chemokines and chemokine receptors, which collectively orchestrate the migration of different types of leukocytes in response to different inflammatory stimuli (7, 8).

As an evolutionary strategy to prolong blood feeding and survival, ticks have developed an extensive repertoire of secreted, biologically active salivary factors that compromise host defenses, including vasodilators, blood coagulation inhibitors, and immunomodulatory proteins (9–12). In particular, the brown dog tick (*Rhipicephalus sanguineus*) has been found to produce three salivary glycoproteins, named "evasins," which are secreted during a blood meal and bind to host chemokines, thus inhibiting the host inflammatory response (13, 14). Evasin-1 and evasin-4 are homologous with 27% amino acid sequence identity and a conserved core of eight Cys residues that form four disulfide bonds (15, 16). Evasin-3 has an unrelated sequence (16). The gene encoding a fourth protein, evasin-2, has reportedly been cloned but has not been described in detail (16). In addition, five transcripts encoding proteins with sequence similarity to either evasin-1 and -4 or evasin-3 have been reported in the salivary gland transcriptome of *R. sanguineus* (17). Each evasin characterized to date binds with high affinity to a different but overlapping set of chemokines, thus inhibiting their receptor binding and activation (15, 16, 18).

Prior to the current study, there have been no evasins characterized from other tick species. However, the salivary gland transcriptomes of some tick species have been reported to encode evasin homologues, including several in the genera *Amblyomma* (*Amblyomma americanum* (19, 20), *Amblyomma cajennense*, *Amblyomma parvum*, *Amblyomma triste* (21), and *Amblyomma maculatum* (22)) and *Rhipicephalus* (*Rhipiceph-*

This work was supported in part by Australian Research Council Discovery Grant DP120100194 (to M. J. S. and R. J. P.), the Monash Institute of Pharmaceutical Sciences Large Grant Support Scheme (to M. C.), and ANZ Trustees Grant 12-3831 (to M. J. S. and M. C.). The authors declare that they have no conflicts of interest with the contents of this article.
This article contains supplemental Figs. S1–S4 and Table S1.
[1] Both authors contributed equally to this work.
[2] A Monash Fellow.
[3] To whom correspondence should be addressed: Dept. of Biochemistry and Molecular Biology, Monash University, Clayton, Victoria 3800, Australia. Tel.: 61-3-9902-9246; E-mail: martin.stone@monash.edu.

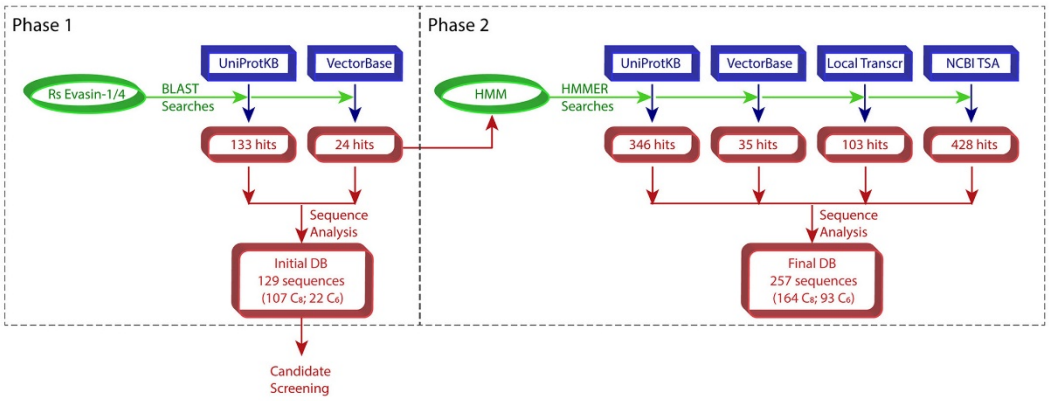

Figure 1. Schematic workflow for identification of evasins by sequence similarity searches. *DB*, database; *Local Transcr*, locally obtained *I. holocyclus* and *R. microplus* transcriptome data sets; *Rs*, *R. sanguineus*; *TSA*, Transcriptome Shotgun Assembly.

alus pulchellus (23) and *Rhipicephalus appendiculatus* (24)). Furthermore, saliva from several species of Ixodidae contains chemokine-binding activity suggested to be similar to that of evasin-3 (25). Thus, it is likely that evasins are ubiquitously expressed by a wide variety of tick species.

In addition to their functions in host defense, the interactions of chemokines with their receptors also contribute to excessive leukocyte recruitment in many inflammatory diseases (7, 8). Thus, chemokine receptors and to a lesser extent chemokines themselves are popular targets for the development of anti-inflammatory therapeutics (26, 27). To this end, Proudfoot and co-workers (16, 28–30) have demonstrated that *R. sanguineus* evasins are efficacious anti-inflammatory agents in animal models of psoriasis (16), lung injury (16, 28), colitis (29), atherosclerosis (30), and ischemic stroke (30).

Motivated by the potential of evasins to inhibit chemokine-mediated inflammation in other diseases, we have explored tick genomic and transcriptomic databases to identify homologues of evasin-1 and evasin-4. Here we describe the identification of more than 250 putative tick evasins, spanning three genera of hard ticks (*Rhipicephalus*, *Amblyomma*, and *Ixodes*), and the validation of representative members of this protein family as binders and inhibitors of human chemokines. We discuss the implications of our findings for evasin evolution and for future development of chemokine-targeted anti-inflammatory therapeutics.

Results

Identification of evasin candidates from gene and transcript databases

To identify predicted tick proteins with high sequence identity to *R. sanguineus* evasin-1 and -4, we initially searched the UniProtKB protein sequence database as well as the tick genomic and transcriptomic data in VectorBase (Fig. 1, *Phase 1*). UniProtKB searches yielded 133 protein sequences with 9–42% sequence identity to *R. sanguineus* evasin-1 and -4. These sequences were derived from one *Rhipicephalus* species (*R. pulchellus*) and five *Amblyomma* species (*A. americanum*, *A. cajennense*, *A. maculatum*, *A. parvum*, and *A. triste*). VectorBase searches yielded 24 sequences from the species *Ixodes ricinus* and one putative evasin from *Ixodes scapularis* with relatively low (9–20%) sequence identity to *R. sanguineus* evasin-1 and -4. To identify additional evasin candidates, we used the aligned sequences of the initial hits to generate a hidden Markov model (HMM)[4] with which we then interrogated four databases: the UniProtKB protein sequence database; the genomic, transcriptomic, and peptide data in VectorBase; data from the NCBI Transcriptome Shotgun Sequence Assembly Database; and salivary gland and viscera transcriptomes from the cattle tick *Rhipicephalus microplus* and the Australian paralysis tick *Ixodes holocyclus* (Fig. 1, *Phase 2*). In combination with the initial search results, these searches identified a total of 428 sequences, which were curated for conserved features (see below) to yield a final database of 257 putative evasins (accession numbers are listed in supplemental Table S1) with 9–46% sequence identity to *R. sanguineus* evasin-1 and -4.

Conserved features of evasin sequences: C_8 and C_6 subfamilies

R. sanguineus evasin-1 and -4 contain several sequence features that are expected to be conserved in orthologous proteins. Eight conserved Cys residues form four disulfide bonds in the structure of evasin-1, most of which should be retained in other evasins. Because evasins are secreted proteins, N-terminal signal sequences are also anticipated to be present. In addition, *R. sanguineus* evasin-1 and -4 contain three conserved potential *N*-linked glycosylation sites (evasin-4 contains four additional sites) and have previously been shown to be glycosylated when expressed in both HEK293 cells and TN5 insect cells (15). Finally, the N-terminal regions of both evasin-1

[4] The abbreviations used are: HMM, hidden Markov model; AAM, *A. americanum*; ACA, *A. cajennense*; AMA, *A. maculatum*; APA, *A. parvum*; ATR, *A. triste*; BRET, bioluminescence resonance energy transfer; BLAST, Basic Local Alignment Search Tool; CCL, CC chemokine ligand; CCR, CC chemokine receptor; EC_{80}, 80% maximal effective concentration; IRI, *I. ricinus*; K_d, equilibrium dissociation constant; MCP, monocyte chemoattractant protein; RPU, *R. pulchellus*; RSA, *R. sanguineus*; Rluc, *Renilla* luciferase; IHO, *I. holocyclus*.

Tick evasins from diverse genera

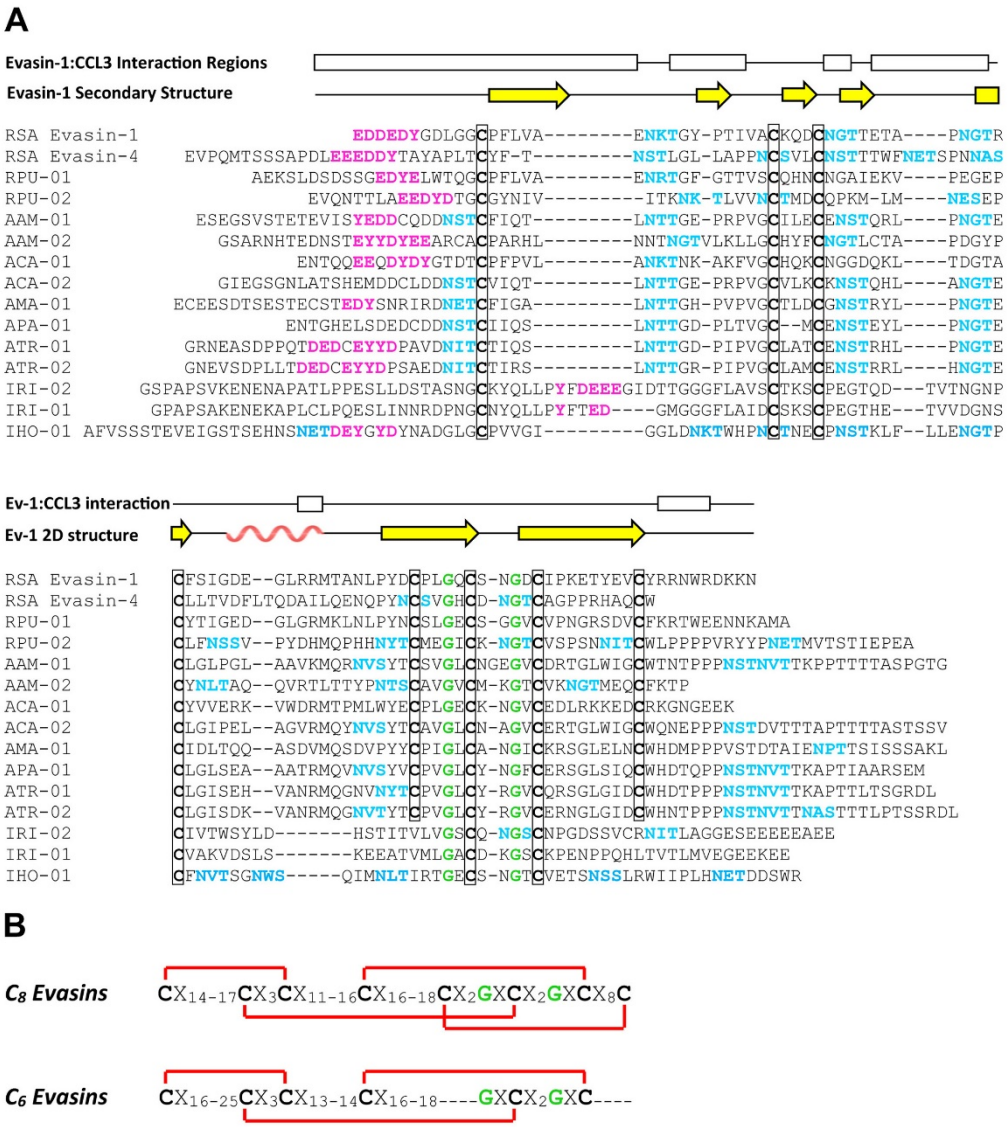

Figure 2. Features of the evasin protein family. *A*, multiple sequence alignment (obtained using MUSCLE) of selected evasin candidates with *R. sanguineus* evasin-1 and -4. Features indicated are conserved cysteines (*bold* and *boxed*) and glycines (*green*), potential *N*-linked glycosylation sites (*cyan*), and putative tyrosine sulfation sites (*magenta*). The secondary structure and regions of evasin-1 that interact with CCL3 in the crystal structure are shown above the alignment; *yellow arrows* indicate β-strands and the *rose wavy line* indicates the α-helix. Abbreviations use for tick species are: *RSA*, *R. sanguineus*; *RPU*, *R. pulchellus*; *AAM*, *A. americanum*; *ACA*, *A. cajennense*; *AMA*, *A. maculatum*; *APA*, *A. parvum*; *ATR*, *A. triste*; *IRI*, *I. ricinus*; *IHO*, *I. holocyclus*. *B*, conserved sequence motifs of the C_8 and C_6 evasins showing (in *red*) the disulfide bond connectivity observed in the structure of *R. sanguineus* evasin-1.

and -4 contain tyrosine residues adjacent to several acidic residues (sequences EDDEDY and EEEDDY, respectively), which we identified as likely to be post-translationally sulfated (12, 31, 32). This feature of evasin sequences has not been identified previously.

All of these sequence features are present in the majority of putative evasin sequences retrieved in the above searches as illustrated for 13 selected sequences in Fig. 2. Although the pattern of Cys residues was completely conserved in putative evasin sequences from *Rhipicephalus* and *Amblyomma* species,

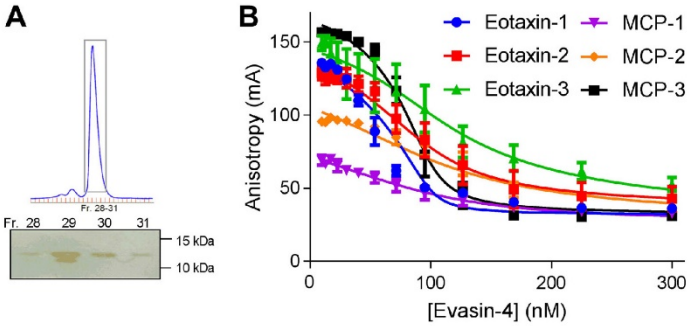

Figure 3. Purification and characterization of recombinant *R. sanguineus* evasin-4. *A*, size exclusion chromatogram for purification of evasin-4 (after His_6 tag removal) with non-reducing SDS-PAGE of fractions (*Fr.*) spanning the main peak (*boxed* on the chromatogram); the molecular weight marker used was Bio-Rad Precision Plus Protein™ unstained standards. *B*, fluorescence anisotropy-binding curves showing displacement of a fluorescent CCR2-derived sulfopeptide from each of six chemokines using purified recombinant evasin-4. Data plotted are the averages of three independent experiments, each recorded in duplicate, and *error bars* represent the S.E. *Solid lines* are fitted binding displacement curves.

all *Ixodes* sequences were missing the fifth and/or eighth Cys, which are disulfide-bonded to each other in evasin-1. Interestingly, the *Ixodes* sequences retain the putative tyrosine sulfation site, but it is located after the first conserved Cys in these sequences in contrast to being before the first conserved Cys in the *Rhipicephalus* and *Amblyomma* sequences. Although the effects of these sequence differences on evasin structure and function remain to be determined, the sequence comparisons led us to propose that there are two distinct subfamilies of evasins homologous to *R. sanguineus* evasin-1 and -4, namely the C_8 evasins (found in *Rhipicephalus* and *Amblyomma*) and the C_6 evasins (found in *Ixodes* species). Both subfamilies are distinct from the evasin-3 type evasins.

Bacterial expression of evasins

Previous studies of recombinant evasin-1 and -4 have used mammalian or insect cell expression systems. To evaluate whether evasins expressed in a bacterial system would be folded and functional, we expressed N-terminally His_6-tagged *R. sanguineus* evasin-1 and -4 in *Escherichia coli*. Evasin-4 was expressed in inclusion bodies but could be renatured under disulfide exchange conditions and purified chromatographically (Fig. 3*A*). Evasin-1 was expressed poorly and was not pursued further.

Binding of purified evasin-4 to each of several chemokines was detected using a competitive fluorescence anisotropy-binding assay (Fig. 3*B*) (33). In this assay, a fluorescein-labeled peptide derived from the N-terminal region of a chemokine receptor is displaced from the chemokine, resulting in decreased fluorescence anisotropy with increased concentration of evasin. As shown by simulated displacement curves (supplemental Fig. S1), the shape of the curve is indicative of the equilibrium dissociation constant (K_d) between evasin and chemokine, although the concentration of evasin required for 50% displacement of the fluorescent peptide is substantially higher than the K_d; this difference is related to the concentrations of the chemokine and fluorescent peptide used in the assay and their affinity for each other. We observed that His_6-tagged evasin-4 bound to each of six chemokines tested with K_d values ranging from ~1 to ~20 nM (Fig. 3*B* and Table 1). These results indicated that glycosylation and/or tyrosine sulfation is not essential for chemokine binding, consistent with previous results showing that deglycosylation of evasin-1 did not affect activity (15). We concluded that the *E. coli* system was appropriate for screening novel evasin candidates.

To determine whether the evasin candidates identified above are able to bind chemokines, we expressed 12 selected sequences in *E. coli*, two each from the species *R. pulchellus*, *A. americanum*, *A. cajennense*, *A. triste*, and *I. ricinus* and one each from *A. maculatum* and *A. parvum*; evasin candidates are identified by the names listed in Fig. 2 (*e.g.* ACA-01 and ACA-02 for the two candidates from *A. cajennense*). Initial expression trials indicated that the majority of candidates were sequestered in inclusion bodies, which were therefore harvested and denatured to allow the His_6-tagged proteins to be partially purified. After renaturation by rapid dilution and subsequent immobilized metal affinity purification, nine of the 12 candidates (all except APA-01, ATR-01, and IRI-02) were isolated in sufficient quantities to screen for chemokine binding.

Evasin candidates bind to chemokines

The competitive fluorescence anisotropy-binding assay was used to assess the binding of the nine isolated evasin candidates to each of five CC chemokines previously expressed and purified in our laboratory (supplemental Fig. S2). With the exception of ACA-02 (from *A. cajennense*), all evasin candidates bound to at least one of the chemokines tested with K_d values of <50 nM (Table 2). We conclude that these eight proteins are chemokine-binding evasins and, by extension, that the majority of evasin candidates identified in our sequence-based searches are also likely to be chemokine binders.

We selected one newly identified evasin from each genus (ACA-01, RPU-01, and IRI-01) and an additional putative evasin (IHO-01; Fig. 2) from the Australian paralysis tick *I. holocyclus* for detailed comparison with *R. sanguineus* evasin-4 in chemokine-binding and inhibition assays. These proteins were expressed, refolded, and purified by size exclusion chromatography (Fig. 4). Non-reducing SDS-PAGE (Fig. 4) indicated that

Tick evasins from diverse genera

Table 1

Affinities for binding of purified evasins to human CC chemokines

Affinities are reported as pK_d values ($-\log_{10}$ of the K_d, in M) ±S.E. The corresponding K_d values (in nM) are in parentheses. The affinity of RSA evasin-4 for MCP-3 (not shown in the table) was $pK_d = 9.21 \pm 0.2$ ($K_d = 0.62$ nM).

Evasin	Chemokine				
	Eotaxin-1	Eotaxin-2	Eotaxin-3	MCP-1	MCP-2
RSA evasin-4	9.25 ± 0.20 (0.57)	8.15 ± 0.10 (7.1)	8.00 ± 0.10 (10)	7.71 ± 0.09 (20)	7.68 ± 0.07 (21)
RPU-01	7.88 ± 0.08 (13)	6.81 ± 0.05 (150)	7.44 ± 0.04 (36)	7.39 ± 0.07 (40)	7.78 ± 0.06 (17)
ACA-01	7.94 ± 0.07 (12)	6.05 ± 0.07 (890)	6.16 ± 0.05 (690)	6.45 ± 0.04 (360)	8.09 ± 0.10 (8.1)
IRI-01	6.76 ± 0.06 (170)	[a]	6.46 ± 0.04 (350)	5.95 ± 0.05 (1100)	5.97 ± 0.04 (1100)
IHO-01	6.90 ± 0.06 (130)	6.48 ± 0.05 (330)	7.08 ± 0.03 (83)	6.04 ± 0.08 (920)	6.10 ± 0.06 (800)

[a] K_d >1 mM (pK_d + S.E. <6).

Table 2

Affinities for binding of nine evasin candidates to six human CC chemokines

Affinities are reported as pK_d values ($-\log_{10}$ of the K_d, in M) ±S.E. The corresponding K_d values (in nM) are in parentheses.

Evasin	Chemokine					
	Eotaxin-1	Eotaxin-2	Eotaxin-3	MCP-1	MCP-2	MCP-3
RPU-01	7.26 ± 0.09 (55)	7.06 ± 0.09 (86)	7.28 ± 0.10 (53)	6.74 ± 0.08 (180)	7.11 ± 0.10 (77)	7.70 ± 0.10 (20)
RPU-02	7.33 ± 0.06 (74)	6.88 ± 0.09 (130)	7.63 ± 0.09 (23)	6.33 ± 0.04 (470)	6.27 ± 0.10 (540)	7.09 ± 0.06 (81)
AAM-01	7.66 ± 0.03 (22)	6.88 ± 0.04 (130)	7.73 ± 0.05 (19)	6.06 ± 0.10 (870)	5.94 ± 0.09 (1100)	6.99 ± 0.04 (100)
AAM-02	7.72 ± 0.09 (19)	6.87 ± 0.09 (130)	7.77 ± 0.07 (170)	5.99 ± 0.10 (1000)	[a]	6.75 ± 0.05 (180)
ACA-01	7.93 ± 0.10 (12)	7.16 ± 0.09 (70)	7.26 ± 0.10 (55)	6.79 ± 0.07 (160)	8.24 ± 0.10 (5.8)	7.76 ± 0.05 (17)
ACA-02	6.73 ± 0.03 (180)	5.94 ± 0.10 (1100)	6.65 ± 0.04 (220)	[a]	[a]	[a]
AMA-01	7.60 ± 0.05 (25)	6.94 ± 0.05 (120)	7.66 ± 0.05 (22)	6.38 ± 0.10 (420)	6.33 ± 0.06 (470)	6.97 ± 0.03 (110)
ATR-02	7.41 ± 0.09 (39)	6.87 ± 0.09 (140)	7.35 ± 0.07 (44)	5.99 ± 0.20 (1000)	6.22 ± 0.08 (610)	7.01 ± 0.07 (98)
IRI-01	7.28 ± 0.10 (53)	6.95 ± 0.10 (110)	6.80 ± 0.10 (160)	6.70 ± 0.06 (200)	6.85 ± 0.09 (140)	7.39 ± 0.09 (41)

[a] K_d >1 mM (pK_d + S.E. <6) or binding not detected.

the purified proteins did not contain intermolecular disulfide bonding, suggesting that they were predominantly correctly folded. These four evasins bound to five CC chemokines tested (Fig. 4) with the K_d values listed in Table 1). Notably, the two C_6 evasins (from *Ixodes* species) bind with lower affinity than the C_8 evasins (from *Rhipicephalus* and *Amblyomma* species) to the chemokines tested here. This may be an indication of differences in target chemokine selectivity, the requirement for post-translational modifications, or simply lower intrinsic affinity.

Evasin candidates inhibit chemokine activity

Chemokines activate their receptors to initiate a variety of G protein-dependent (*e.g.* inhibition of cAMP synthesis) and G protein-independent (*e.g.* β-arrestin recruitment) signaling pathways. To determine whether the newly identified evasins inhibit chemokine signaling via their cognate receptors, we determined the effects of evasins on the inhibition of cAMP production induced by treatment of CCR2-expressing HEK293 cells with the chemokines monocyte chemoattractant protein-1 (MCP-1/CCL2) and MCP-2/CCL8 or by treatment of CCR3-expressing HEK293 cells with the chemokines eotaxin-1/CCL11 and eotaxin-2/CCL24. As shown in Fig. 5 and Table 3, three of the novel evasins (RPU-01, ACA-01, and IHO-01) were able to inhibit the activity of one or more chemokine tested, although again the evasin from the *Ixodes* species exhibited relatively low potency. Notably, the selectivities for chemokine inhibition clearly differ among the evasins, suggesting that it may be possible to identify or engineer evasins for desired inhibitory selectivity against target chemokines.

Discussion

We have shown here that the genomes or transcriptomes of several species of hard ticks, spanning the three genera *Rhipicephalus*, *Amblyomma*, *and Ixodes*, encode numerous proteins with sequences similar to the previously characterized evasin-1 and -4 from *R. sanguineus*. Among 12 of these proteins screened, nine were expressed well in *E. coli* and were sufficiently renatured for binding measurements. Of these nine candidate evasins, eight bound to one or more chemokine(s) tested with affinities of ~50 nM or tighter. Moreover, three of the four fully purified evasins tested were found to inhibit chemokine signaling. These results strongly suggest that many of the proteins identified by our bioinformatics approach are indeed chemokine-inhibitory evasins.

During the final revisions of the current manuscript, a study by Singh *et al.* (34) describing the application of yeast surface display to identify several evasins from ticks in the genera *Rhipicephalus* and *Amblyomma* was published. Among the 10 evasins characterized in that study, two were the same as evasins we have characterized, namely ACA-01 (designated by Singh *et al.* (34) as P974_AMBCA) and RPU-01 (P467_RHIPU).

Considering that the current experiments were limited to a small subset of human chemokines, it seems likely that some of the evasins tested may be more potent inhibitors of different human chemokines or chemokines from other species, such as the natural hosts of the relevant tick species. In addition, it is possible that evasins may inhibit binding of chemokines to not only chemokine receptors but also glycosaminoglycans, which are important for establishment of chemokine gradients required for effective leukocyte trafficking *in vivo* (35). Of course, it also remains possible that evasins may bind to other host proteins in addition to chemokines. Future studies will be needed to investigate these hypotheses.

The new evasins identified here bound to a panel of related CC chemokines with K_d values in the range ~5 nM to ~1 μM. In comparison, *R. sanguineus* evasin-1 and -4 have been reported

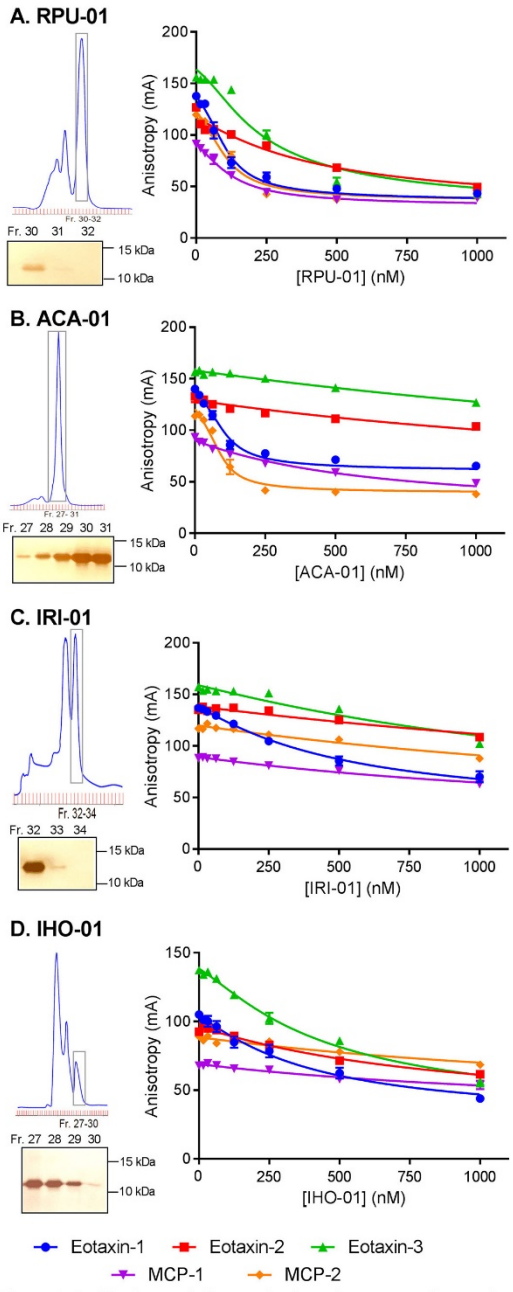

Figure 4. Purification and characterization of representative evasins from three genera. For evasins, ACA-01 from *A. cajennense* (*A*), RPU-01 from *R. pulchellus* (*B*), IRI-01 from *I. ricinus* (*C*), and IHO-01 from *I. holocyclus* (*D*) are shown. *Top left*, the size exclusion chromatogram for purification of the evasin protein (with a C-terminal His_6 tag); *bottom left*, non-reducing SDS-PAGE of fractions (*Fr.*) spanning the main peak (*boxed* on the chromatogram); *right*, competitive fluorescence anisotropy curves for binding of the purified evasin to each of five CC chemokines. The molecular weight marker used for SDS-PAGE was Bio-Rad Precision Plus Protein unstained standards. Binding data represent the average ± S.E. (*error bars*) of values from three independent experiments, each recorded in duplicate. *Solid lines* are fitted binding displacement curves.

to bind various chemokines with K_d values ranging from ~30 pM to ~200 nM, although the reported values varied somewhat depending on the experimental methods used (13, 16) and may also be dependent on expression systems used due to variable post-translational modifications. In addition, the new evasins exhibited distinct binding selectivities to the various chemokines. For example, ACA-01 binds to the chemokines eotaxin-1 and MCP-2 substantially more tightly than to eotaxin-2, eotaxin-3, or MCP-1, whereas RPU-01 has similar affinities for eotaxin-1, eotaxin-3, MCP-1, and MCP-2 and lower affinity for eotaxin-2 (supplemental Fig. S3 and Table 1). The existence of such affinity and selectivity differences is consistent with the sequence variation among the evasins and chemokines tested. In particular, the evasin sequences differ substantially in the regions that interact with the chemokine in the structure of *R. sanguineus* evasin-1 bound to human CCL3 (Fig. 2*A*) and in the few residues of evasin-4 previously found to contribute to binding of CCL5 (36, 37). Similarly, there are numerous differences in the evasin-binding regions of the chemokines, such as the flexible N-terminal region. Future studies will be required to more fully elucidate the structural basis of the selectivity differences.

Despite the sequence variation in chemokine-binding residues, the evasins identified here share several highly conserved features, represented by the sequence motifs in Fig. 2. Like *R. sanguineus* evasin-1 and -4, most of these proteins (dubbed C_8 evasins) share a distinctive pattern of eight core Cys residues, which form four disulfide bonds in *R. sanguineus* evasin-1. *Ixodes* sequences (dubbed C_6 evasins) lack one of these disulfide bonds, suggesting that the missing disulfide may not be critical for folding and stability, but the C_6 evasins also bind more weakly to the chemokines tested here, so the additional disulfide may enhance binding affinity. Additional conserved features are glycine residues, glycosylation sites, and an apparent tyrosine sulfation site, which has not been identified previously.

Future studies will be required to determine whether the conserved post-translational modifications occur *in vivo* and influence the properties of evasins. Previous studies of the *R. sanguineus* evasin-1 and -4 in animal models (16, 28, 29) have utilized proteins produced in eukaryotic cell lines and therefore presumably decorated heterogeneously with various post-translational modifications. We have shown here that homogeneous evasins produced in *E. coli* retain the ability to bind chemokines with high affinity, suggesting that the post-translational modifications are not essential for chemokine binding. However, it remains possible that these modifications influence such properties as binding affinity, selectivity, stability, or pharmacokinetics, thereby affecting the efficacy of evasins in disease models.

Tick evasins from diverse genera

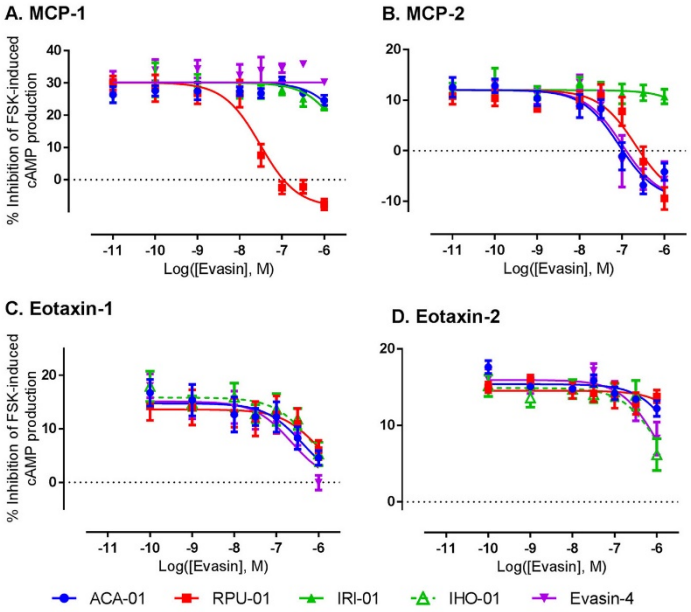

Figure 5. Inhibition of chemokine activity by purified evasins. Shown are concentration-response curves for inhibition of the chemokines MCP-1 (10 nM) (*A*) and MCP-2 (100 nM) (*B*) acting at the receptor CCR2 and for inhibition of the chemokines eotaxin-1 (100 nM) (*C*) and eotaxin-2 (100 nM) (*D*) acting at the receptor CCR3. Chemokine activity was detected as the ability of the chemokine to inhibit forskolin (*FSK*)-induced production of cAMP as detected via a BRET sensor (see "Experimental procedures" for details); thus, evasins inhibit the cAMP-inhibitory activity of the chemokines. Data represent the average ± S.E. (*error bars*) of values from three independent experiments, each recorded in duplicate.

Table 3

Inhibition constants for inhibition of chemokine activity by purified evasins

Inhibition constants are reported as pIC_{50} values ($-\log_{10}$ of the IC_{50}; in M) ±S.E. The corresponding IC_{50} values (in nM) are in parentheses.

	MCP-1	MCP-2	Eotaxin-1	Eotaxin-2
RSA evasin-4	[a]	7.00 ± 0.2 (100)	6.65 ± 0.2 (220)	5.99 ± 0.1 (1000)
RPU-01	7.47 ± 0.3 (34)	6.68 ± 0.1 (210)	6.03 ± 0.3 (940)	[a]
ACA-01	[a]	7.07 ± 0.1 (84)	6.39 ± 0.2 (400)	[a]
IHO-01	[b]	[b]	6.20 ± 0.2 (630)	5.95 ± 0.2 (1100)

[a] IC_{50} >1 μM (pIC_{50} ± S.E. <6) or no inhibition detected.
[b] Not determined.

Previously, the only tick evasins shown to bind and inhibit chemokines were the three *R. sanguineus* evasins. Our results indicate that evasins are likely to be broadly expressed by many hard tick species and therefore that chemokine inhibition has been an advantageous evolutionary strategy for ticks. As all hard ticks are obligatory blood feeders, this may reflect positive selection pressure to maintain immunomodulatory evasin proteins and to evade immune recognition and remain attached to hosts for extended periods to enable continued blood feeding.

Among the 257 putative evasins identified in our bioinformatics searches, there is substantial sequence variation within each tick species and between different species, both common characteristics of tick protein families (11). Within a single species, we identified numerous different evasin-like sequences. For example, we found 13 *R. pulchellus* sequences with pairwise sequence identities ranging from 14 to 50%. Considering the current and previous observations that chemokine selectivity can vary substantially among evasins (15, 16, 18), it seems likely that the expression of several evasins by the same species may be a strategy to more effectively suppress the activities of multiple host chemokines and thereby inhibit the recruitment of their target leukocytes.

Comparison of sequences from different species also indicated a high level of sequence divergence. The average ± S.D. of cross-species pairwise identities was 20.1 ± 6.7%, and pairwise identities were <50% for 99% of cross-species comparisons and <30% for 95% of cross-species comparisons. The maximum identity found to *R. sanguineus* evasin-1 or -4 was 46% (to sequence JAA60818.1 from *R. pulchellus*). These sequence variations suggest that there has been substantial evolutionary pressure for evasin sequences to diverge after tick speciation events. Because speciation of ticks would typically be associated with a new mammalian host, the evolutionary pressure may arise from the different arrays of chemokines expressed by the hosts for the different tick species.

Many tick species are of medical or agricultural importance because they function as vectors for microbial pathogens. Within the genus *Ixodes*, *I. ricinus* and the related *I. scapularis* are of particular interest as vectors of the Lyme disease spirochete *Borrelia burgdorferi* (38–40). Within the genus *Rhipicephalus*, *R. microplus* (previously known as *Boophilus microplus*) is considered the most economically important tick for the United States and Australian cattle industries as it can cause weight loss in host animals and transmit agents of several cattle diseases (41, 42). Based on the prevalence of evasin sequences in the currently available databases, we anticipate that ongoing genome projects for *I. scapularis* and *R. microplus* are likely to reveal additional evasins as a mechanism of host immune evasion by these important tick species.

The numerous tick evasins identified in the current study represent a rich "library" of chemokine-binding proteins from which to identify proteins that selectively inhibit chemokines of interest in specific human or animal diseases. Notably, several of the newly identified evasins have high affinity for the chemokine eotaxin-1, a major chemoattractant for eosinophils and basophils, which play a key role in allergic responses and reactions to parasitic infestations. This is consistent with the role of evasins being to suppress host responses to ticks. However, it also suggests that evasins may be useful therapeutics in human diseases in which these types of leukocytes are involved as observed in a previous study of experimental colitis (29).

Conclusion

Our sequence similarity searches have identified more than 250 predicted tick protein sequences with features similar to *R. sanguineus* evasin-1 and -4 but substantial sequence variation in chemokine recognition residues. Among these sequences, we have identified two distinct subfamilies of evasins (C_8 and C_6). Among nine candidates screened for chemokine binding, eight exhibited nanomolar affinities for one or more chemokine tested. Our results suggest that most hard ticks express chemokine-binding evasins and that these evasins play important roles in evasion of host immune responses. The evasins identified here provide a valuable pool of potential inhibitors for development of chemokine-targeted anti-inflammatory therapies.

Experimental procedures

Media and reagents

Dulbecco's modified Eagle's medium (DMEM) and Hanks' balanced salt solution were from Invitrogen. Fetal bovine serum (FBS) was from *In Vitro* Technologies (Noble Park, Victoria, Australia). Polyethyleneimine (PEI) was from Polysciences, Inc. (Warrington, PA). Coelenterazine h was from NanoLight (Pinetop, AZ). All other reagents were purchased from Sigma-Aldrich.

Bioinformatics and evasin identification

Sequences of the canonical *R. sanguineus* evasin-1 and evasion-4 were retrieved from UniProt (accession numbers P0C8E7 and P0C8E9). These were used as queries against UniProtKB (restricted to Arthropoda; July 20, 2015 release) using the Basic Local Alignment Search Tool (BLAST) (43) with the BLASTp algorithm and against VectorBase (*I. scapularis* and *I. ricinus* transcriptome and genome sequences) (44) using tBLASTn with default parameters. Hits were ranked based on highest pairwise identity to the known evasin sequences using a pairwise identity matrix generated by Clustal Omega (45). The presence of the cysteines conserved in the canonical evasins was assessed. Putative evasin sequences were then analyzed using SignalP (46) to predict signal peptide cleavage sites. The putative evasin sequences with highest pairwise identity to the known evasins for each tick species were selected as candidates for cloning and expression. These candidate sequences were analyzed for the presence of putative sulfation sites using Sulfinator (47) and *N*-linked glycosylation sites by the motif N*(S/T).

Multiple sequence alignments of initial hits were generated using MUSCLE v3.8.31 (48). HMMs were constructed from these MUSCLE alignments using HMMER v3.1b1 (49). The HMMs were used with hmmsearch (default parameters) to identify more distantly related evasin sequences in UniProtKB (version January 11, 2016), NCBI Transcriptome Shotgun Assembly databases (downloaded February 10, 2016), VectorBase (*I. scapularis* and *I. ricinus* transcriptome sets translated with TransDecoder (50) and six-frame translated genome sequences), and *I. holocyclus* and *R. microplus* transcriptome data sets provided by Manuel Rodriguez Valle. Sequences were retained if they contained conserved cysteine residues equivalent to the canonical evasins and a predicted signal sequence and were less than 200 residues long. Hits were compiled into a final non-redundant set of putative evasins.

Cloning, expression, and purification of putative evasins for screening

Plasmids containing the coding sequences of evasin candidates plus a C-terminal His_6 tag in the background expression vector pET28a were ordered from GenScript; codon usage was optimized for expression in *E. coli*. BL21(DE3) *E. coli* cells transformed with these plasmids were grown in 1 liter of LB medium supplemented with kanamycin sulfate (30 μg/ml) until the optical density at 600 nm reached 0.6. Protein expression was initiated by addition of isopropyl β-D-1-thiogalactopyranoside (1 mM), and the culture was grown for either 4 h or overnight. Cells were harvested by centrifugation; resuspended in 15 ml of 20 mM Tris·HCl, 500 mM NaCl, 5 mM imidazole, 0.02% (w/v) NaN_3, pH 8.0; sonicated; and centrifuged to separate the soluble from insoluble (inclusion body) fraction. Inclusion bodies were washed in 20 mM Tris·HCl, 500 mM NaCl, 5 mM imidazole, 0.02% (w/v) NaN_3, 2 mM DTT, 0.5% (v/v) Triton X-100, pH 8.0, and denatured in 20 mM Tris·HCl, 6 M guanidine·HCl, 20 mM imidazole, 20 mM β-mercaptoethanol, pH 8.0, before being added to 15 ml of loose nickel-nitrilotriacetic acid resin (Qiagen) to purify recombinant protein by batch immobilized metal affinity chromatography. Denatured protein was then refolded via rapid dilution (flow rate, 0.1 ml/min) in 2 liters of 20 mM Tris·HCl, 400 mM NaCl, 2 mM reduced glutathione, 0.5 mM oxidized glutathione, 0.02% (w/v) NaN_3, pH 8.0. This was followed by further purification by immobilized metal affinity chromatography (HisTrap HP 5-ml column, GE Healthcare).

Tick evasins from diverse genera

After initial screening, expression of selected evasins was repeated at 4-liter scale, including a final purification step of size exclusion chromatography (HiLoad 16/60 Superdex 75 prep grade column, GE Healthcare). The molecular weights of pure proteins were confirmed by mass spectrometry using an Orbitrap Fusion Tribrid mass spectrometer (Thermo Scientific) in intact protein mode.

Chemokine-binding assay

Competition-binding assays, measuring the displacement of a fluorescent receptor peptide from each of six CC chemokines (CCL2/MCP-1, CCL7/MCP-3, CCL8/MCP-2, CCL11/eotaxin-1, CCL24/eotaxin-2, and CCL26/eotaxin-3), were conducted for each candidate evasin to screen for chemokine-binding ability as described (33). Briefly, a solution of the candidate evasin was prepared in MOPS buffer (50 mM MOPS, pH 7.4), and a serial 2-fold dilution was conducted on a 96-well plate (final concentration range from 1 μM to 15.6 nM). A mixed solution of the fluorescent peptide and chemokine (final concentrations of 10 nM and 100 nM, respectively) was added such that the final volume in each well was 200 μl. Competition-binding assays were also performed using the purified evasins to measure the displacement of a fluorescent receptor peptide from each of five CC chemokines (MCP-1, MCP-2, eotaxin-1, eotaxin-2, and eotaxin-3) under similar conditions. Briefly, a solution of the purified evasin was prepared in MOPS buffer, and a serial 2-fold dilution (1.33-fold dilution for evasin-4) was conducted on a 384-well plate coated with a 0.001% (w/v) solution of poly-L-lysine (final concentration range from 1 μM to 15.6 nM or 300 nM to 9.5 nM for evasin-4). A mixed solution of the fluorescent peptide and chemokine (final concentrations of 10 and 100 nM, respectively) was added such that the final volume in each well was 20 μl. In both cases, fluorescence anisotropy was measured 5 min after plating with excitation and emission wavelengths of 485 and 520 nm, respectively, using a BMG Labtech PHERAstar FS plate reader. Experiments were conducted in duplicate three times independently, and the mean anisotropy was fitted by non-linear regression analysis using GraphPad Prism v.6.0 software to the equation for a 1:1 competitive displacement curve, described previously (51), transformed to enable $-\log K_d$ (pK_d) values ± S.E. to be determined. Multiple *t* tests were conducted to assess significance of the differences in pK_d.

Inhibition of chemokine signaling

Chemokine signaling via the receptor CCR2 or CCR3 was measured using a cAMP biosensor assay developed previously (52). The assay measures the ability of chemokines to inhibit forskolin-induced cAMP production in c-Myc-FLAG-CCR2 or c-Myc-FLAG-CCR3 FlpIn TREx HEK293 cells transiently transfected with the CAMYEL cAMP bioluminescence resonance energy transfer (BRET) biosensor (53). Cells were grown overnight in 10-cm dishes using DMEM + 5% FBS before transfection using 6:1 (w/w) PEI:DNA. Tetracycline (10 μg/ml) was added 24 h after transfection to induce expression of c-Myc-FLAG-CCR2 or c-Myc-FLAG-CCR3, and cells were seeded (25,000 cells/well) in a white, poly-D-lysine-coated 96-well plate (CulturPlates, PerkinElmer Life Sciences) and incubated overnight at 37 °C in 5% CO_2. The following day, cells were washed and equilibrated in Hanks' balanced salt solution for 30 min at 37 °C. Cells were then incubated with the Rluc substrate coelenterazine h (final concentration, 5 μM) for 5 min followed by a further 5-min incubation with a solution containing a fixed concentration of chemokine (10 nM MCP-1, 100 nM MCP-2, 100 nM eotaxin-1, or 100 nM eotaxin-2, corresponding to approximately the EC_{80}, as shown in supplemental Fig. S4) with various concentrations of an evasin candidate that had been preincubated for ~15 min to allow binding of the evasin to the chemokine. A final 5-min incubation step was conducted after addition of forskolin (final concentration, 10 μM), which directly stimulates the production of cAMP via adenylyl cyclase. The Rluc and yellow fluorescent protein (YFP) emissions were then measured at 475 and 525 nm, respectively, using a BMG Labtech PHERAstar FS plate reader. Data are presented as a BRET ratio, calculated as the ratio of YFP to Rluc signals and expressed as the percentage of the forskolin-induced signal.

Author contributions—J. H. and J. S. participated in research design, performed experiments, and conducted data analyses. A. P. and J. H. conducted bioinformatics searches and analyses. C. H. performed and interpreted mass spectrometry experiments. M. R. V. collected transcriptomics data for Australian tick species and contributed to bioinformatics analyses/interpretation. M. C. designed and supervised cell-based assays. R. J. P. and M. J. S. conceived the study and designed and interpreted the experiments. J. H., J. S., and M. J. S. drafted the manuscript, and all authors read and critically reviewed the manuscript.

Acknowledgments—We thank Professor Catherine Hill (Purdue University) for helpful discussions and Natalya Stone for technical assistance.

References

1. Dantas-Torres, F., Chomel, B. B., and Otranto, D. (2012) Ticks and tick-borne diseases: a One Health perspective. *Trends Parasitol.* **28,** 437–446
2. Becker, C. A., Bouju-Albert, A., Jouglin, M., Chauvin, A., and Malandrin, L. (2009) Natural transmission of zoonotic *Babesia* spp. by *Ixodes ricinus* ticks. *Emerging Infect. Dis.* **15,** 320–322
3. de la Fuente, J., Ayoubi, P., Blouin, E. F., Almazán, C., Naranjo, V., and Kocan, K. M. (2006) Anaplasmosis: focusing on host–vector–pathogen interactions for vaccine development. *Ann. N.Y. Acad. Sci.* **1078,** 416–423
4. Fivaz, B., Petney, T., and Horak, I. (1992) *Tick Vector Biology*, Springer-Verlag, Berlin
5. Moser, B., Wolf, M., Walz, A., and Loetscher, P. (2004) Chemokines: multiple levels of leukocyte migration control. *Trends Immunol.* **25,** 75–84
6. Zlotnik, A., and Yoshie, O. (2000) Chemokines: a new classification system and their role in immunity. *Immunity* **12,** 121–127
7. Baggiolini, M. (2001) Chemokines in pathology and medicine. *J. Intern. Med.* **250,** 91–104
8. Gerard, C., and Rollins, B. J. (2001) Chemokines and disease. *Nat. Immunol.* **2,** 108–115
9. Kazimírová, M., and Štibrániová, I. (2013) Tick salivary compounds: their role in modulation of host defences and pathogen transmission. *Front. Cell. Infect. Microbiol.* **3,** 43
10. Rodríguez-Valle, M., Moolhuijzen, P., Piper, E. K., Weiss, O., Vance, M., Bellgard, M., and Lew-Tabor, A. (2013) *Rhipicephalus microplus* lipocalins (LRMs): genomic identification and analysis of the bovine immune response using in silico predicted B and T cell epitopes. *Int. J. Parasitol.* **43,** 739–752

11. Rodriguez-Valle, M., Xu, T., Kurscheid, S., and Lew-Tabor, A. E. (2015) *Rhipicephalus microplus* serine protease inhibitor family: annotation, expression and functional characterisation assessment. *Parasit. Vectors* **8,** 7
12. Thompson, R. E., Liu, X., Ripoll-Rozada, J., Alonso-García, N., Parker, B. L., Pereira, P. J. B., and Payne, R. J. (2017) Tyrosine sulfation modulates activity of tick-derived thrombin inhibitors. *Nat. Chem.* 10.1038/nchem.2744
13. Bachelerie, F., Ben-Baruch, A., Burkhardt, A. M., Combadiere, C., Farber, J. M., Graham, G. J., Horuk, R., Sparre-Ulrich, A. H., Locati, M., Luster, A. D., Mantovani, A., Matsushima, K., Murphy, P. M., Nibbs, R., Nomiyama, H., *et al.* (2014) International Union of Basic and Clinical Pharmacology. [corrected]. LXXXIX. Update on the extended family of chemokine receptors and introducing a new nomenclature for atypical chemokine receptors. *Pharmacol. Rev.* **66,** 1–79
14. Bonvin, P., Power, C. A., and Proudfoot, A. E. (2016) Evasins: therapeutic potential of a new family of chemokine-binding proteins from ticks. *Front. Immunol.* **7,** 208
15. Frauenschuh, A., Power, C. A., Déruaz, M., Ferreira, B. R., Silva, J. S., Teixeira, M. M., Dias, J. M., Martin, T., Wells, T. N., and Proudfoot, A. E. (2007) Molecular cloning and characterization of a highly selective chemokine-binding protein from the tick *Rhipicephalus sanguineus*. *J. Biol. Chem.* **282,** 27250–27258
16. Déruaz, M., Frauenschuh, A., Alessandri, A. L., Dias, J. M., Coelho, F. M., Russo, R. C., Ferreira, B. R., Graham, G. J., Shaw, J. P., Wells, T. N., Teixeira, M. M., Power, C. A., and Proudfoot, A. E. (2008) Ticks produce highly selective chemokine binding proteins with antiinflammatory activity. *J. Exp. Med.* **205,** 2019–2031
17. Anatriello, E., Ribeiro, J. M., de Miranda-Santos, I. K., Brandão, L. G., Anderson, J. M., Valenzuela, J. G., Maruyama, S. R., Silva, J. S., and Ferreira, B. R. (2010) An insight into the sialotranscriptome of the brown dog tick, *Rhipicephalus sanguineus*. *BMC Genomics* **11,** 450
18. Déruaz, M., Bonvin, P., Severin, I. C., Johnson, Z., Krohn, S., Power, C. A., and Proudfoot, A. E. (2013) Evasin-4, a tick-derived chemokine-binding protein with broad selectivity can be modified for use in preclinical disease models. *FEBS J.* **280,** 4876–4887
19. Radulovic, Ž. M., Kim, T. K., Porter, L. M., Sze, S. H., Lewis, L., and Mulenga, A. (2014) A 24–48 h fed *Amblyomma americanum* tick saliva immuno-proteome. *BMC Genomics* **15,** 518
20. Karim, S., and Ribeiro, J. M. (2015) An insight into the sialome of the lone star tick, *Amblyomma americanum*, with a glimpse on its time dependent gene expression. *PLoS One* **10,** e0131292
21. Garcia, G. R., Gardinassi, L. G., Ribeiro, J. M., Anatriello, E., Ferreira, B. R., Moreira, H. N., Mafra, C., Martins, M. M., Szabó, M. P., de Miranda-Santos, I. K., and Maruyama, S. R. (2014) The sialotranscriptome of *Amblyomma triste*, *Amblyomma parvum* and *Amblyomma cajennense* ticks, uncovered by 454-based RNA-seq. *Parasit. Vectors* **7,** 430
22. Karim, S., Singh, P., and Ribeiro, J. M. (2011) A deep insight into the sialotranscriptome of the gulf coast tick, *Amblyomma maculatum*. *PLoS One* **6,** e28525
23. Tan, A. W., Francischetti, I. M., Slovak, M., Kini, R. M., and Ribeiro, J. M. (2015) Sexual differences in the sialomes of the zebra tick, *Rhipicephalus pulchellus*. *J. Proteomics* **117,** 120–144
24. de Castro, M. H., de Klerk, D., Pienaar, R., Latif, A. A., Rees, D. J., and Mans, B. J. (2016) *De novo* assembly and annotation of the salivary gland transcriptome *of Rhipicephalus appendiculatus* male and female ticks during blood feeding. *Ticks Tick Borne Dis.* **7,** 536–548
25. Vancová, I., Hajnická, V., Slovák, M., Kocáková, P., Paesen, G. C., and Nuttall, P. A. (2010) Evasin-3-like anti-chemokine activity in salivary gland extracts of ixodid ticks during blood-feeding: a new target for tick control. *Parasite Immunol.* **32,** 460–463
26. Proudfoot, A. E. (2002) Chemokine receptors: multifaceted therapeutic targets. *Nat. Rev. Immunol.* **2,** 106–115
27. Proudfoot, A. E., Power, C. A., and Wells, T. N. (2000) The strategy of blocking the chemokine system to combat disease. *Immunol. Rev.* **177,** 246–256
28. Russo, R. C., Alessandri, A. L., Garcia, C. C., Cordeiro, B. F., Pinho, V., Cassali, G. D., Proudfoot, A. E., and Teixeira, M. M. (2011) Therapeutic effects of evasin-1, a chemokine binding protein, in bleomycin-induced pulmonary fibrosis. *Am. J. Respir. Cell Mol. Biol.* **45,** 72–80
29. Vieira, A. T., Fagundes, C. T., Alessandri, A. L., Castor, M. G., Guabiraba, R., Borges, V. O., Silveira, K. D., Vieira, E. L., Gonçalves, J. L., Silva, T. A., Deruaz, M., Proudfoot, A. E., Sousa, L. P., and Teixeira, M. M. (2009) Treatment with a novel chemokine-binding protein or eosinophil lineage-ablation protects mice from experimental colitis. *Am. J. Pathol.* **175,** 2382–2391
30. Copin, J. C., da Silva, R. F., Fraga-Silva, R. A., Capettini, L., Quintao, S., Lenglet, S., Pelli, G., Galan, K., Burger, F., Braunersreuther, V., Schaller, K., Deruaz, M., Proudfoot, A. E., Dallegri, F., Stergiopulos, N., *et al.* (2013) Treatment with Evasin-3 reduces atherosclerotic vulnerability for ischemic stroke, but not brain injury in mice. *J. Cereb. Blood Flow Metab.* **33,** 490–498
31. Stone, M. J., and Payne, R. J. (2015) Homogeneous sulfopeptides and sulfoproteins: synthetic approaches and applications to characterize the effects of tyrosine sulfation on biochemical function. *Acc. Chem. Res.* **48,** 2251–2261
32. Wang, X., Sanchez, J., Stone, M. J., and Payne, R. J. (2017) Sulfation of the human cytomegalovirus protein UL22A enhances binding to the chemokine RANTES. *Angew. Chem. Int. Ed. Engl.* **56,** 8490–8494
33. Ludeman, J. P., Nazarí-Robati, M., Wilkinson, B. L., Huang, C., Payne, R. J., and Stone, M. J. (2015) Phosphate modulates receptor sulfotyrosine recognition by the chemokine monocyte chemoattractant protein-1 (MCP-1/CCL2). *Org. Biomol. Chem.* **13,** 2162–2169
34. Singh, K., Davies, G., Alenazi, Y., Eaton, J. R. O., Kawamura, A., and Bhattacharya, S. (2017) Yeast surface display identifies a family of evasins from ticks with novel polyvalent CC chemokine-binding activities. *Sci. Rep.* **7,** 4267
35. Proudfoot, A. E., Handel, T. M., Johnson, Z., Lau, E. K., LiWang, P., Clark-Lewis, I., Borlat, F., Wells, T. N., and Kosco-Vilbois, M. H. (2003) Glycosaminoglycan binding and oligomerization are essential for the *in vivo* activity of certain chemokines. *Proc. Natl. Acad. Sci. U.S.A.* **100,** 1885–1890
36. Bonvin, P., Dunn, S. M., Rousseau, F., Dyer, D. P., Shaw, J., Power, C. A., Handel, T. M., and Proudfoot, A. E. (2014) Identification of the pharmacophore of the CC chemokine-binding proteins Evasin-1 and -4 using phage display. *J. Biol. Chem.* **289,** 31846–31855
37. Dias, J. M., Losberger, C., Déruaz, M., Power, C. A., Proudfoot, A. E., and Shaw, J. P. (2009) Structural basis of chemokine sequestration by a tick chemokine binding protein: the crystal structure of the complex between Evasin-1 and CCL3. *PLoS One* **4,** e8514
38. Ogden, N. H., Maarouf, A., Barker, I. K., Bigras-Poulin, M., Lindsay, L. R., Morshed, M. G., O'callaghan, C. J., Ramay, F., Waltner-Toews, D., and Charron, D. F. (2006) Climate change and the potential for range expansion of the Lyme disease vector *Ixodes scapularis* in Canada. *Int. J. Parasitol.* **36,** 63–70
39. Hovius, J. W. (2009) Spitting image: tick saliva assists the causative agent of Lyme disease in evading host skin's innate immune response. *J. Invest. Dermatol.* **129,** 2337–2339
40. Gulia-Nuss, M., Nuss, A. B., Meyer, J. M., Sonenshine, D. E., Roe, R. M., Waterhouse, R. M., Sattelle, D. B., de la Fuente, J., Ribeiro, J. M., Megy, K., Thimmapuram, J., Miller, J. R., Walenz, B. P., Koren, S., Hostetler, J. B., *et al.* (2016) Genomic insights into the *Ixodes scapularis* tick vector of Lyme disease. *Nat. Commun.* **7,** 10507
41. Jonsson, N. N., Davis, R., and De Witt, M. (2001) An estimate of the economic effects of cattle tick (*Boophilus microplus*) infestation on Queensland dairy farms. *Aust. Vet. J.* **79,** 826–831
42. Jonsson, N. N. (2006) The productivity effects of cattle tick (*Boophilus microplus*) infestation on cattle, with particular reference to *Bos indicus* cattle and their crosses. *Vet. Parasitol.* **137,** 1–10
43. Altschul, S. F., Gish, W., Miller, W., Myers, E. W., and Lipman, D. J. (1990) Basic local alignment search tool. *J. Mol. Biol.* **215,** 403–410
44. Giraldo-Calderón, G. I., Emrich, S. J., MacCallum, R. M., Maslen, G., Dialynas, E., Topalis, P., Ho, N., Gesing, S., VectorBase Consortium, Madey, G., Collins, F. H., and Lawson, D. (2015) VectorBase: an updated bioinformatics resource for invertebrate vectors and other organisms related with human diseases. *Nucleic Acids Res.* **43,** D707–D713
45. Sievers, F., Wilm, A., Dineen, D., Gibson, T. J., Karplus, K., Li, W., Lopez, R., McWilliam, H., Remmert, M., Söding, J., Thompson, J. D., and Higgins,

D. G. (2011) Fast, scalable generation of high-quality protein multiple sequence alignments using Clustal Omega. *Mol. Syst. Biol.* **7,** 539–539
46. Petersen, T. N., Brunak, S., von Heijne, G., and Nielsen, H. (2011) SignalP 4.0: discriminating signal peptides from transmembrane regions. *Nat. Methods* **8,** 785–786
47. Monigatti, F., Gasteiger, E., Bairoch, A., and Jung, E. (2002) The Sulfinator: predicting tyrosine sulfation sites in protein sequences. *Bioinformatics* **18,** 769–770
48. Edgar, R. C. (2004) MUSCLE: multiple sequence alignment with high accuracy and high throughput. *Nucleic Acids Res.* **32,** 1792–1797
49. Finn, R. D., Clements, J., Arndt, W., Miller, B. L., Wheeler, T. J., Schreiber, F., Bateman, A., and Eddy, S. R. (2015) HMMER web server: 2015 update. *Nucleic Acids Res.* **43,** W30–W38
50. Haas, B. J., Papanicolaou, A., Yassour, M., Grabherr, M., Blood, P. D., Bowden, J., Couger, M. B., Eccles, D., Li, B., Lieber, M., MacManes, M. D., Ott, M., Orvis, J., Pochet, N., Strozzi, F., *et al.* (2013) *De novo* transcript sequence reconstruction from RNA-Seq: reference generation and analysis with Trinity. *Nat. Protoc.* **8,** 1494–1512
51. Huff, S., Matsuka, Y. V., McGavin, M. J., and Ingham, K. C. (1994) Interaction of N-terminal fragments of fibronectin with synthetic and recombinant D motifs from its binding protein on *Staphylococcus aureus* studied using fluorescence anisotropy. *J. Biol. Chem.* **269,** 15563–15570
52. Thompson, G. L., Lane, J. R., Coudrat, T., Sexton, P. M., Christopoulos, A., and Canals, M. (2015) Biased agonism of endogenous opioid peptides at the μ-opioid receptor. *Mol. Pharmacol.* **88,** 335–346
53. Jiang, L. I., Collins, J., Davis, R., Lin, K. M., DeCamp, D., Roach, T., Hsueh, R., Rebres, R. A., Ross, E. M., Taussig, R., Fraser, I., and Sternweis, P. C. (2007) Use of a cAMP BRET sensor to characterize a novel regulation of cAMP by the sphingosine 1-phosphate/G_{13} pathway. *J. Biol. Chem.* **282,** 10576–10584

Ticks from diverse genera encode chemokine-inhibitory evasin proteins

Jenni Hayward, Julie Sanchez, Andrew Perry, Cheng Huang, Manuel Rodriguez Valle, Meritxell Canals, Richard J. Payne and Martin J. Stone

J. Biol. Chem. 2017, 292:15670-15680.
doi: 10.1074/jbc.M117.807255 originally published online August 4, 2017

Chapter 6. General Discussion and Conclusion

6.1. Thesis Summary

Chemokines and chemokine receptors constitute a crucial part of our immune system [9, 309]. They play major roles in leukocyte recruitment in both inflammatory and homeostatic processes. For this reason, chemokines and their receptors have been involved in countless diseases such as HIV [50, 51, 55], cancer [310-312] and diabetes [313] but especially in inflammatory and autoimmune diseases such as multiple sclerosis [314-316], rheumatoid arthritis [317] and atherosclerosis [46, 318]. This has provided a strong incentive to develop therapeutics targeting chemokine receptors and over the last thirty years, a variety of chemokine receptor antagonists have been developed. Nevertheless, only two small molecule inhibitors are currently approved as drugs, due to an apparent lack of efficacy in clinical trials of most other antagonists [230, 301]. This apparent lack of efficacy can be explained, at least in part, by the complexity of the chemokine:receptor network. Around 50 chemokines and 25 chemokine receptors have been identified in humans to date and most receptors and chemokines are promiscuous. Therefore, inhibiting leukocyte recruitment by blocking only one receptor may be unsuccessful because chemokines can activate other receptors expressed on the leukocyte surface and still promote chemotaxis.

Considering the low success rates targeting chemokine receptors, targeting chemokines may represent a favourable alternative approach [319, 320]. Development of chemokine antagonists has been considered and a few chemokine antagonists have been developed. Although synthetic small molecule-based strategies are possible, such molecules may not be highly selective for their targets. On the other hand, in nature, several viruses and parasites have evolved to be able to disrupt or invade our immune system by interacting with either chemokines or their receptors [307]. Chemokine-inhibitory activity was detected in tick saliva and linked to proteins named evasins, of which three proteins (evasin-1, -3 and -4) were identified in the brown dog tick species [256, 308]. Thus, we set out to identify and characterise new evasin proteins. In Chapter 5, which was recently published in *The Journal of Biological Chemistry* [321], we used sequence-based searches and bioinformatic tools to identify evasin candidates from several tick species. We expressed and partially purified the most promising candidates and screened them for chemokine-binding activity before fully purifying and characterising four new evasins (from different tick genera) that could bind and inhibit chemokines. Our results are discussed at the end of the Chapter 5 article and will not be discussed further. However, it is worth mentioning that the ultimate goal of this project is to engineer highly selective evasins. To pursue this aim and improve our knowledge of chemokine recognition by evasins, it will be necessary to identify evasins with varied chemokine selectivity, solve structures of their chemokine complexes and evaluate the contributions of interface residues to binding affinity and selectivity. In addition, and similarly to chemokine receptors, evasins can be post-translationally modified and present several glycosylation as well as tyrosine sulfation sites. The influence of post-translational modifications on chemokine recognition by evasins is also of interest in our laboratory.

Although this relatively new approach is promising, chemokine antagonists, just like chemokine receptor antagonists, may suffer from an apparent lack of efficacy due to the high promiscuity in the

chemokine:receptor network. To avoid this shortcoming, it is essential to improve our understanding of the structural basis of chemokine recognition by chemokine receptors. Thus, in Chapters 3 and 4, we focused on the mechanisms of activation of chemokine receptor CCR1. In Chapter 3, we described CCR1 biased agonism when activated by HCC-2, MCP-2 and MCP-3. We found that receptor tyrosine sulfation did not seem to have an influence on responses to chemokines and the observed bias did not depend on the Gα subtype. However, N-terminal modifications of chemokines had substantial influences on their ability to activate CCR1. Truncated and HCC-2/MCP-3 chimeric chemokines were expressed, purified and tested for CCR1 activation. This showed that the chemokine N-terminus does have an impact on receptor activation but is not the only region of the chemokine that controls receptor activation. As the results of this Chapter suggested that the two-site model of receptor activation may not be entirely applicable for CCR1, in Chapter 4, we decided to explore this model further. To investigate the two-site model, we examined one site at a time. For site 1, which is postulated to control binding only, we used a set of sulfopeptides with the CCR1 N-terminal sequence and compared their ability to bind chemokines to the full-length CCR1. We developed a fluorescence anisotropy assay to measure binding between sulfopeptides and chemokines and a radioligand displacement assay in cell membranes to measure binding between the whole CCR1 protein and chemokines. This demonstrated that the receptor N-terminus is not the only receptor region involved in binding as the peptide binding affinities and selectivities did not correlate to the receptor ones. For site 2, which is postulated to control activation only, we designed, expressed and purified a series of ten chimeric chemokines between MCP-3, a CCR1 agonist and MCP-1, which is not a CCR1 agonist. By swapping regions between MCP-1 and -3 and testing the chimeras for CCR1 activation using several different readouts, we could assess the involvement of each chemokine region, i.e. N-terminus, N-loop and β3-turn. The results confirmed that the chemokine N-terminus plays a crucial role in receptor activation. However, just like in Chapter 3, it also showed that the chemokine N-terminus is not sufficient to restore full activation of the receptor and that the N-loop also influences receptor activation. In this section, we discuss the results from Chapters 3 and 4 further and propose a more detailed version of the two-site model that accounts for our results.

6.2. Elaboration of the Two-site Model

6.2.1. Introduction of an Additional Chemokine:Receptor State

As described previously, numerous structural and mutational studies have been performed on chemokines and chemokine receptors [298] and a model based on these studies was proposed in 1997 by Crump *et al.* [280]. An important aspect of this model, is the definition of two sites that are distinct both spatially and functionally. As drawn in Figure 6.1A, site 1 (black circle) involves the receptor N-terminus and the chemokine N-loop and β3 regions and accounts for chemokine:receptor binding. Site 2 (orange circle) involves the chemokine N-terminus and some receptor transmembrane helices and is responsible for receptor activation. Although this simple model has proven very useful over the years, recent results from our laboratory as well as other laboratories are either not accounted for or in contradiction with the two-site model [299]. Therefore, there is a need to elaborate this model and to reconcile it with more recent data.

The comparison of chemokine binding selectivity by CCR1 N-terminal peptides and full-length CCR1 (Chapter 4) showed that the receptor N-terminus does not completely account for all the binding interactions. This implies that other regions are involved in chemokine binding by CCR1. This conclusion is consistent with previous results from our laboratory where chemokine N-termini were found to contribute to the affinity of MCP-1 and MCP-3 for CCR2 [287]. In addition, this hypothesis is supported by the fact that peptide binding is much weaker than receptor binding, so interactions from outside site 1 are needed to achieve full-strength binding. Adding another intermediate species in the traditional two-site model (Figure 6.1B, state c) where the receptor is still in an inactive state but is fully interacting with the chemokine allows for other binding interactions to be made after the core of the chemokine attaches to the receptor N-terminus. The first equilibrium in Figure 6.1B, which describes site 1 interactions, would be a low affinity binding and could occur for cognate and non-cognate chemokines. This initial binding would then be followed by a high affinity binding (second equilibrium) involving other regions of the chemokine and receptor, including but maybe not limited to the chemokine N-terminus interacting with residues in the receptor transmembrane helices. The high affinity binding would occur only for cognate chemokines and receptor antagonists and would be responsible, in large part, for the chemokine selectivity of the receptor. Thus, if the selectivity is no longer believed to be driven by the receptor N-terminus, it would not be surprising that the N-terminal peptides did not reflect the receptor selectivity. This proposed extended model is in agreement with our results, however it directly challenges the original spatial separation between binding and activation, as binding interactions would now be occurring in site 2.

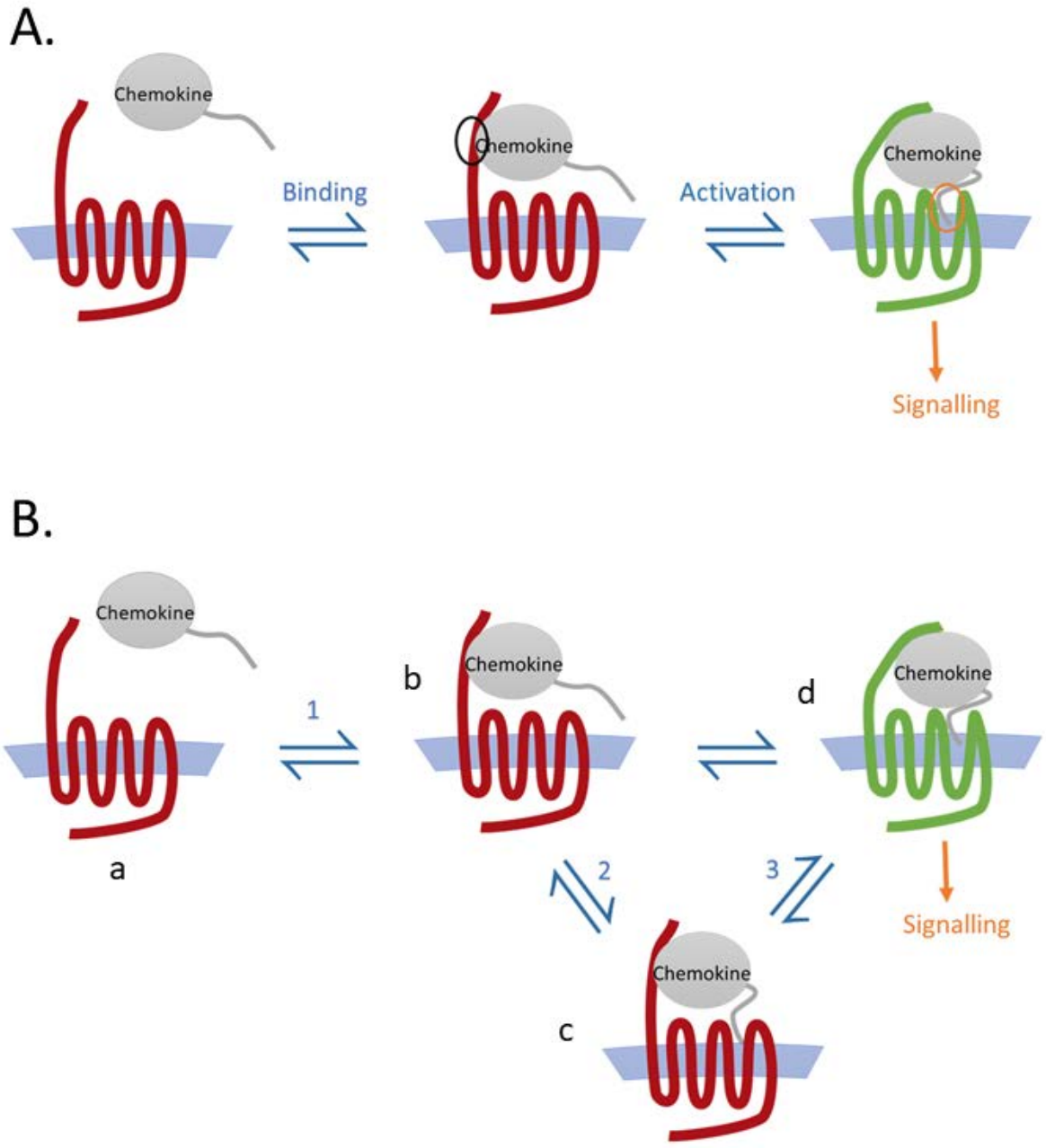

Figure 6.1: Traditional and Extended Two-site Model. (A) Schematic representation of the original two-site model proposed by Crump *et al.* This model contains two distinct steps, one for binding (site 1 circled in black) and one for activation (site 2 circled in orange). **(B)** Schematic representation of the proposed extended two-site model. Each receptor state is labelled from a to d. In this model, an additional state is present (state c). Binding occurs in the first two equilibria, equilibrium 1 representing a low affinity binding and equilibrium 2 representing a second binding site, which, together with site 1 leads to high affinity binding. At this stage, the receptor is still in an inactive conformation (red). The third equilibrium represents a change in receptor conformation which leads to the receptor being activated (green) and generating further downstream signalling.

The existence of a high affinity complex between a chemokine and an inactive receptor is supported by two recent high-resolution structures. In the CXCR4:vMIPII [166] and CCR5:5P7-CCL5 [167] structures, we know that the receptors are in inactive conformations as they are bound to receptor antagonists. This proves that a high affinity, inactive state of the complex exists. Importantly, in both of these structures, the chemokine N-terminus is inserted into the TM bundle of the receptor forming the site 2 interactions proposed above, consistent with the representation in Figure 6.1B, state c.

Knowing that the high affinity, inactive state of the complex exists for bound antagonists and that a high affinity, active state complex exists for bound agonists (because agonists are able to initiate signalling), the only missing piece of this model is a direct proof of the existence of an inactive receptor fully bound to a cognate chemokine agonist. It will not be easy to solve a structure of such a complex because its population is likely to be low or comparable to that of the activated complex. Therefore, other methods will be needed to demonstrate its existence. In particular, a method is required that reports on the populations of different structural states of the receptor. Various fluorescence techniques that enable measurement of intramolecular distances may be suitable. For example, FRET has been used to assess distances between GPCR helices [322, 323] and direct measurement of GPCR activation has been accomplished using FRET between CFP introduced into ICL3 and YFP in the C-terminus of α_2 adrenergic receptor [324]. Similar approaches could be applied to chemokine receptors. It may be necessary to apply these approaches in single molecule measurements to observe the populations of receptor molecules in distinct conformations (different FRET efficiencies).

Once the receptor is fully bound to its cognate chemokine, conformational changes can occur enabling the receptor to transition from an inactive to an active state and initiate signalling. In this extended model, site 1 interactions could potentially be involved in controlling activation. This is consistent with our results from Chapters 3 and 4 where we first showed that the N-terminus was not sufficient to restore full activation (Chapter 4, section 4.3.2), then identified the N-loop as another chemokine region involved in receptor activation (Chapter 4, section 4.3.2). As previously mentioned, the major difference between the traditional and extended models is the spatial separation between binding and activation sites. In the proposed extended model, sites 1 and 2 are still spatially distinct but could partake in both functions.

6.2.2. The Extended Two-site Model for Agonists, Antagonists, Partial Agonists and Inverse Agonists

It is important to note that both the traditional and amended versions of the two-site model are thermodynamic models and that they do not describe any kinetic aspect. These thermodynamic models all assume that the chemokine:receptor interactions are at equilibrium which may not always be entirely true. The hypothesis that binding occurs prior to the receptor being activated is derived from indirect evidence such as the fact that N-terminally truncated chemokines can still bind to their receptor without activating it [325, 326]. Kinetic studies would be of high interest because they could help in testing the various models of receptor activation. Moreover, reaction rates could play a crucial role in differential agonism as reported by Shonberg *et al.* for the dopamine D_2 receptor [284].

An advantage of the proposed amended two-site model is that it can account for several different types of ligands, including full, partial and inverse agonists and antagonists. Each type of ligand would stabilise the complexes formed with the receptor to different extents and thus differ in their ability to shift the equilibria presented in Figure 6.2A, particularly between the bound (high affinity) inactive state (state c) and the bound (high affinity) activated state (state d). A speculative free energy diagram is provided in Figure 6.2B to help interpret the extended model. Of course, the details of the free energy diagram would depend on the precise values of the various equilibrium constants and the ligand concentration. Figure 6.2B represents the typical situation expected for a ligand concentration of ~10-100 nM, intermediate between the K_d for receptor binding (typically ~1 nM or less) and the K_d for site 1 binding (typically ~1 μM or more). The free energy diagram can be used to compare the relative energy levels and deduce which species is more likely to be the dominant one in the receptor population for different types of ligands.

When there is no ligand bound (Figure 6.2B, black curve), the receptor can either be in an inactive or active conformation. No interaction can be made to stabilise the active conformation which makes it relatively unstable and rare in the receptor population, although occasional population of this state could result in basal signalling activity. When a ligand is present, it can bind to the receptor and generate the low affinity inactive complex (state b). The interactions involved are weak and do not account for ligand selectivity, so the free energy of this state is likely to be similar regardless of the ligand type, including for non-cognate chemokines. The differences materialise in the last two states. A non-cognate chemokine (neither an agonist nor an antagonist, yellow curve) is unlikely to form a high affinity complex with the receptor and the equilibrium will tend to favour state a. For a full agonist (green curve), the high affinity inactive state (state c) is more stable than the low affinity state (state b) but less stable than the bound, active state, which is why the energy level of state c is higher than that of state d. For an antagonist (red curve) or an inverse agonist (purple curve), it will be the opposite. The interactions made between the antagonist or inverse agonist and the receptor will be in favour of the inactive state c, thus lowering its energy level compare to the active state d. In the case of a partial agonist (blue curve), the energy levels are likely to be similar between active and inactive conformations. This will generate a mixed receptor population reflective of a weaker overall signalling outcome.

The extended model presented in Figure 6.2 does not explicitly incorporate the influence of tyrosine sulfation (or other post-translational modifications) on chemokine receptor activation. However, the effects of receptor sulfation could be incorporated into this model, essentially by treating the modified receptor as a different receptor from the non-modified one. For CCR1, we found (Chapter 4) that tyrosine sulfation enhanced the binding affinity of chemokines to N-terminal receptor peptides but did not appear to influence high affinity CCR1 binding and activation. In the extended two-site model these effects could be represented by stabilisation of state b without altering the free energy of states c and d. On the other hand, sulfation has previously been shown to enhance high affinity chemokine binding in several chemokine receptors [144]. In those cases, it is likely that both states b and c as well as possibly state d) would be stabilised in the sulfated form of the receptor compared to the non-sulfated form.

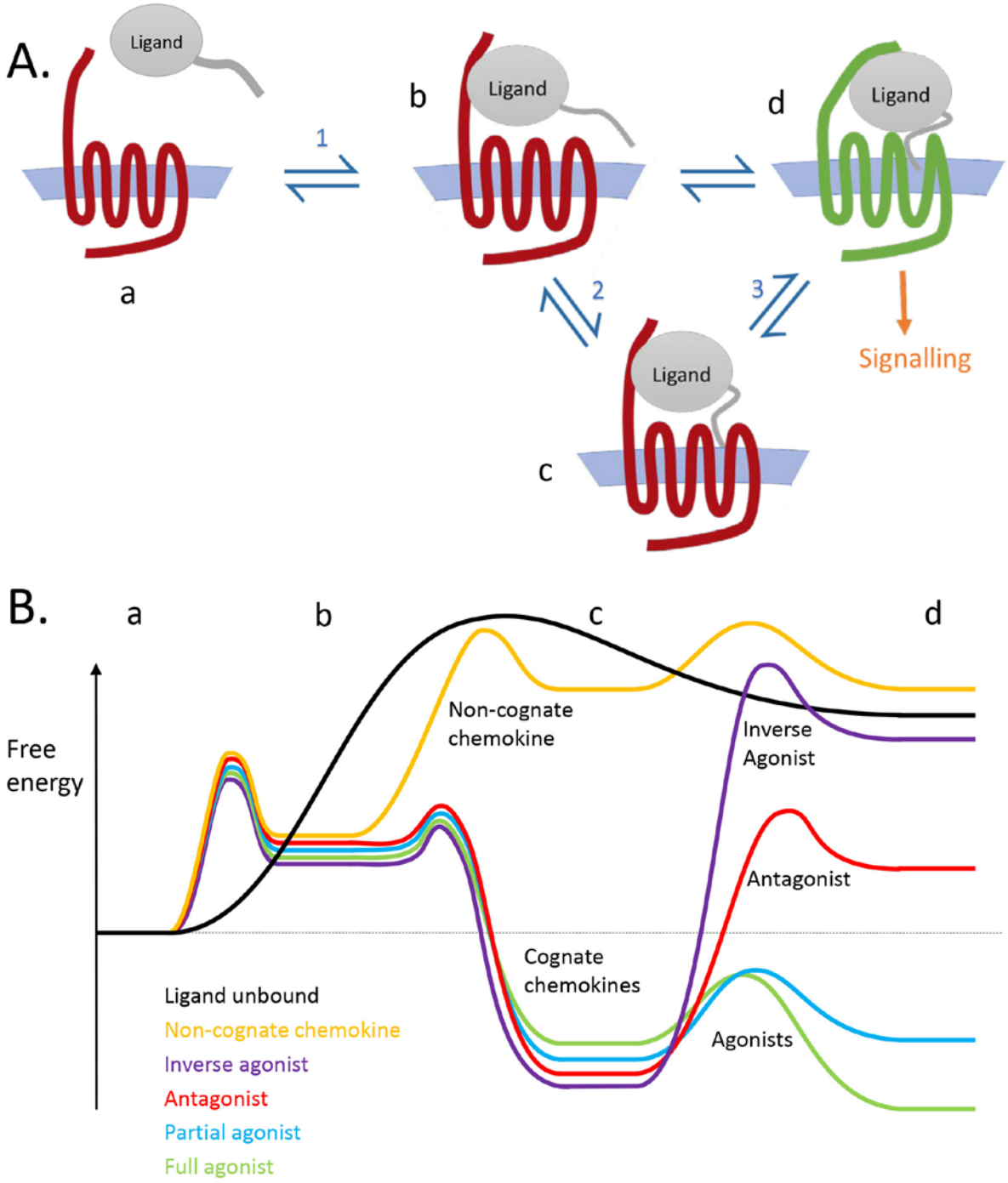

Figure 6.2: Extended Two-site Model for Differential Agonism. (A) Schematic representation of the proposed extended two-site model. In this model, an additional equilibrium is present. Each receptor state is labelled from a to d. **(B)** Hypothetical free energy diagram expected for a ligand concentration of ~10-100 nM, intermediate between the K_d for receptor binding (typically ~1 nM or less) and the K_d for site 1 binding (typically ~1 µM). Activation energy barriers are shown at arbitrary heights. The relative energy levels of each receptor state are represented by various colours, depending on what type of ligand the receptor is interacting with.

6.2.3. Further Extension of the Model to Account for Biased Agonism

The extended model presented above is more versatile than the traditional two-site model as it can account for various types of agonism and antagonism. However, biased agonism is not represented in Figure 6.2 as it includes only one active form of the receptor. Nevertheless, by considering different active conformations corresponding to the activation of different pathways, it would be possible to represent biased agonism as well. For example, a ligand biased towards β-arrestin recruitment and away from cAMP inhibition would lower the free energy level of the receptor conformation (state d) that couples to the β-arrestin pathway relative to the receptor conformation (state d) that couples to the cAMP inhibition pathway. In the simplest model consistent with biased agonism, both active states would be derived from the same high affinity agonist-bound inactive state, similar to state c in Figure 6.2.

Another aspect that is not described in the proposed model in Figure 6.2 is the structural dynamics of chemokine and receptor and how this could affect the receptor's activation and biased agonism. It is indeed likely that upon binding, both chemokine and receptor structures change, particularly for the N-termini that are usually flexible and disordered but are likely to transition towards more ordered states when complexes are formed. The chemokine N-terminus induces structural changes within the core of the receptor and becomes visible in crystal structures which is usually not the case in free chemokine structures. Similarly, binding between the receptor N-terminus and the chemokine core is likely to induce subtle structural changes within the chemokine, which could be responsible for subtle changes observed in signalling. Once again, structural and other biophysical information would be critical to understand the different interactions giving rise to the alternative active states of the receptor.

6.2.4. Towards a Multi-site Model

All results obtained during this project can be interpreted using the extended models discussed above in which the interactions between the chemokine and receptor occur within the two physically distinct and discrete sites defined previously. However, we cannot exclude the possibility that there are significant influences of interactions outside these two sites. In this regard, the structure of vMIP-II bound to CXCR4 indicated the presence of interactions in a site called site 1.5 [166]. As its name suggests, this site is located between site 1 and site 2 and includes regions that could not be attributed to site 1 or 2, i.e. interactions between the cysteine residues in the CC or CXC motif of the chemokine and the base of the receptor N-terminus. Moreover, as new structural studies were published, further interactions were observed that did not belong to site 1, 2 or 1.5, particularly in the extracellular loops of the receptor [327]. Although the observation of these structural interactions does not necessarily imply that they are energetically or mechanistically significant, it does suggest that a model with two spatially separated sites may not be sufficient to account for the complexity of the interactions. Therefore, some groups are now considering a more complex multi-site model [328]. Validation of such models will require more structures of chemokine-receptor complexes to be solved and the importance of the additional interactions will need to be tested using mutational approaches. More broadly, we should consider that there may not be a general model that is applicable to all chemokine:receptor interactions

and that each chemokine:receptor pair may follow a slightly different mechanistic pathway leading to the variety of signalling outcomes needed to selectively recruit different types of leukocytes.

6.3. Potential CCR1 and MCP Chemokine Mutants to Identify Detailed Site 2 Interactions

In the extended two-site model proposed above, critical interactions for both high affinity binding and receptor activation are located in site 2, i.e. the chemokine N-terminus and the TM bundle of the receptor. In Chapter 4, we showed that replacing the N-terminus of MCP-3 by that of MCP-1 (in the MCP3-133 chimera) *reduced* the ability of the chemokine to activate CCR1. However, in a recent study in our laboratory [287], we found that the same modification *increased* the ability of the chemokine to activate CCR2. Thus, it appears that, in comparison to MCP-3, the N-terminus of MCP-1 forms unfavourable interactions with residues in the TM bundle of CCR1 and favourable interactions with the corresponding residues in the TM bundle of CCR2. It would be interesting to identify the specific chemokine and receptor residues that could be responsible for these differential interactions.

Comparison of MCP-3 and MCP-1 indicates that their N-terminal sequences differ at only five residues separated into two clusters. Residues $V^{3}G^{4}$ in MCP-3 are substituted by $D^{3}A^{4}$ in MCP-1 and residues $T^{7}S^{8}T^{9}$ in MCP-3 are substituted by $A^{7}A^{8}V^{9}$ in MCP-1. It may be informative to examine a series of mutants in which each residue or each cluster is swapped between the two chemokines in order to identify those contributing most to the differential effects at CCR1 and CCR2.

For identifying the receptor residues influencing the differential interactions with these chemokine N-terminal residues, it is noteworthy that MCP-1 is a potent agonist of CCR2, CCR3 and CCR5 but is much less potent at CCR1, which is nonetheless closely related to the other three CC chemokine receptors. A recent review on the structural analysis of chemokine receptor:ligand interactions reported that the binding site of CCR1 shares 68, 86 and 81% sequence similarity with the binding sites of CCR2, CCR3 and CCR5, respectively [329]. Considering these high levels of similarity, and that there is no CCR1 structure available to date, we have used a sequence alignment of the four CC chemokine receptors as well as a homology model of CCR2 bound to MCP-1 previously developed in our laboratory [287] to investigate and identify residues that could be critical for the differential interactions of the chemokine N-termini. Figure 6.3 shows in red the residues that are hypothesised to have an influence on MCP-1:CCR1 interactions. Several residues were chosen according to three criteria. First, the sequence alignment (Figure 6.3A) was used to identify residues that are conserved in CCR2, CCR3 and CCR5 but differ in CCR1. Second, the locations of these residues on the structure were considered and residues that were not close to the binding site were excluded, although they could still have an indirect influence on MCP-1:CCR1 interactions. Finally, residues that were previously identified as important through mutagenesis were also included [329], as long as the location criteria were met. This approach led to the identification of seven residues that are proposed to contribute to the differential interactions with chemokine N-termini and would therefore be good candidates for CCR1 mutational studies: F^{32} (TM1), D^{92} (TM2), Y^{114} (TM3), Y^{170} (TM4), A^{200} (TM5), L^{203} (TM5) and V^{264} (TM6). Although the side

chains of some residues are pointing outside the helical bundle in the CCR2 model, it is hard to predict the exact orientation of each helix in CCR1, so these residues were not excluded. Five of the seven residues were conserved in the other three sequences and different in the CCR1 sequence: F^{32} (TM1) corresponds to isoleucine or leucine residues in the other receptors; D^{92} (TM2) corresponds to a conserved histidine residue; Y^{170} (TM4) corresponds to a conserved isoleucine residue; A^{200} (TM5) corresponds to a conserved threonine residue and V^{264} (TM6) corresponds to serine or threonine residues. Other than these five, Y^{114} (TM3) is located just next to another tyrosine residue that is highly conserved in chemokine receptors and is known to be interacting with chemokines (Y^{116} belongs to the signal initiation residues in CXCR4 [330] and Y^{120} in CCR2 was also identified as a critical position by our laboratory). In the other receptors, this position is either a histidine (CCR2 and CCR3) or a phenylalanine (CCR5) residue. Although this residue is a less obvious choice, the two tyrosines could interact with each other, preventing other interactions from happening. Finally, L^{203} (TM5) corresponds to a variable position. However, the corresponding R^{206} in CCR2 was identified as crucial for MCP-1 binding and activation by our laboratory and its side chain is pointing inside the helical bundle, towards the first residues of MCP-1.

To summarise, these sequence and structural comparisons have identified a series of residues in the N-termini of MCP chemokines and CC chemokine receptors that may form critical interactions with each other. It would be informative to mutate these residues of CCR1 to corresponding residues in CCR2 (and vice versa) and compare the ability of these mutants to bind and be activated by the wild type chemokines as well as the N-terminus swap mutants suggested above. Such studies may identify critical interactions contributing to chemokine:receptor specificity.

A.

```
CCR1   --------METPNTTEDYDTTTEFDYGDATPCQKVNERAFGAQLLPPLYSLVFVIGLVGNI
CCR3   --------MTTSLDTVETFGTTSYYDDVGLLCEKADTRALMAQFVPPLYSLVFTVGLLGNV
CCR2   MLSTSRSRFIRNTNESGEEVTTFFDYDYGAPCHKFDVKQIGAQLLPPLYSLVFIFGFVGNM
CCR5   ------------MDYQVSSPIYDINYYTSEPCQKINVKQIAARLLPPLYSLVFIFGFVGNM

CCR1   LVVLVLVQYKRLKNMTSIYLLNLAISDLLFLFTLPFWIDYKLKDDWVFGDAMCKILSGFYY
CCR3   VVVMILIKYRRLRIMTNIYLLNLAISDLLFLVTLPFWIHYVRGHNWVFGHGMCKLLSGFYH
CCR2   LVVLILINCKKLKCLTDIYLLNLAISDLLFLITLPLWAHSAAN-EWVFGNAMCKLFTGLYH
CCR5   LVILILINCKRLKSMTDIYLLNLAISDLFFLLTVPFWAHYAAA-QWDFGNTMCQLLTGLYF

CCR1   TGLYSEIFFIILLTIDRYLAIVHAVFALRARTVTFGVITSIIIWALAILASMPGLYFSKTQ
CCR3   TGLYSEIFFIILLTIDRYLAIVHAVFALRARTVTFGVITSIVTWGLAVLAALPEFIFYETE
CCR2   IGYFGGIFFIILLTIDRYLAIVHAVFALKARTVTFGVVTSVITWLVAVFASVPGIIFTKCQ
CCR5   IGFFSGIFFIILLTIDRYLAVVHAVFALKARTVTFGVVTSVITWVVAVFASLPGIIFTRSQ

CCR1   WEFTHHTCSLHFPHESLREWKLFQALKLNLFGLVLPLLVMIICYTGIIKILLRRPNEKK-S
CCR3   ELFEETLCSALYPEDTVYSWRHFHTLRMTIFCLVLPLLVMAICYTGIIKTLLRCPSKKK-Y
CCR2   KEDSVYVCGPYFPR----GWNNFHTIMRNILGLVLPLLIMVICYSGILKTLLRCRNEKKRH
CCR5   KEGLHYTCSSHFPYSQYQFWKNFQTLKIVILGLVLPLLVMVICYSGILKTLLRCRNEKKRH

CCR1   KAVRLIFVIMIIFFLFWTPYNLTILISVFQDFLFTHECEQSRHLDLAVQVTEVIAYTHCCV
CCR3   KAIRLIFVIMAVFFIFWTPYNVAILLSSYQSILFGNDCERSKHLDLVMLVTEVIAYSHCCM
CCR2   RAVRVIFTIMIVYFLFWTPYNIVILLNTFQEFFGLSNCESTSQLDQATQVTETLGMTHCCI
CCR5   RAVRLIFTIMIVYFLFWAPYNIVLLLNTFQEFFGLNNCSSSNRLDQAMQVTETLGMTHCCI

CCR1   NPVIYAFVGERFRKYLRQLFHRRVAVHLVKWLPFLSVDRLERVSSTSP-STGEHELSAGF
CCR3   NPVIYAFVGERFRKYLRHFFHRHLLMHLGRYIPFLPSEKLERTSSVSP-STAEPELSIVF
CCR2   NPIIYAFVGEKFRRYLSVFFRKHITKRFCKQCPVFYRETVDGVTSTNTPSTGEQEVSAGL
CCR5   NPIIYAFVGEKFRNYLLVFFQKHIAKRFCKCCSIFQQEAPERASSVYTRSTGEQEISVGL
```

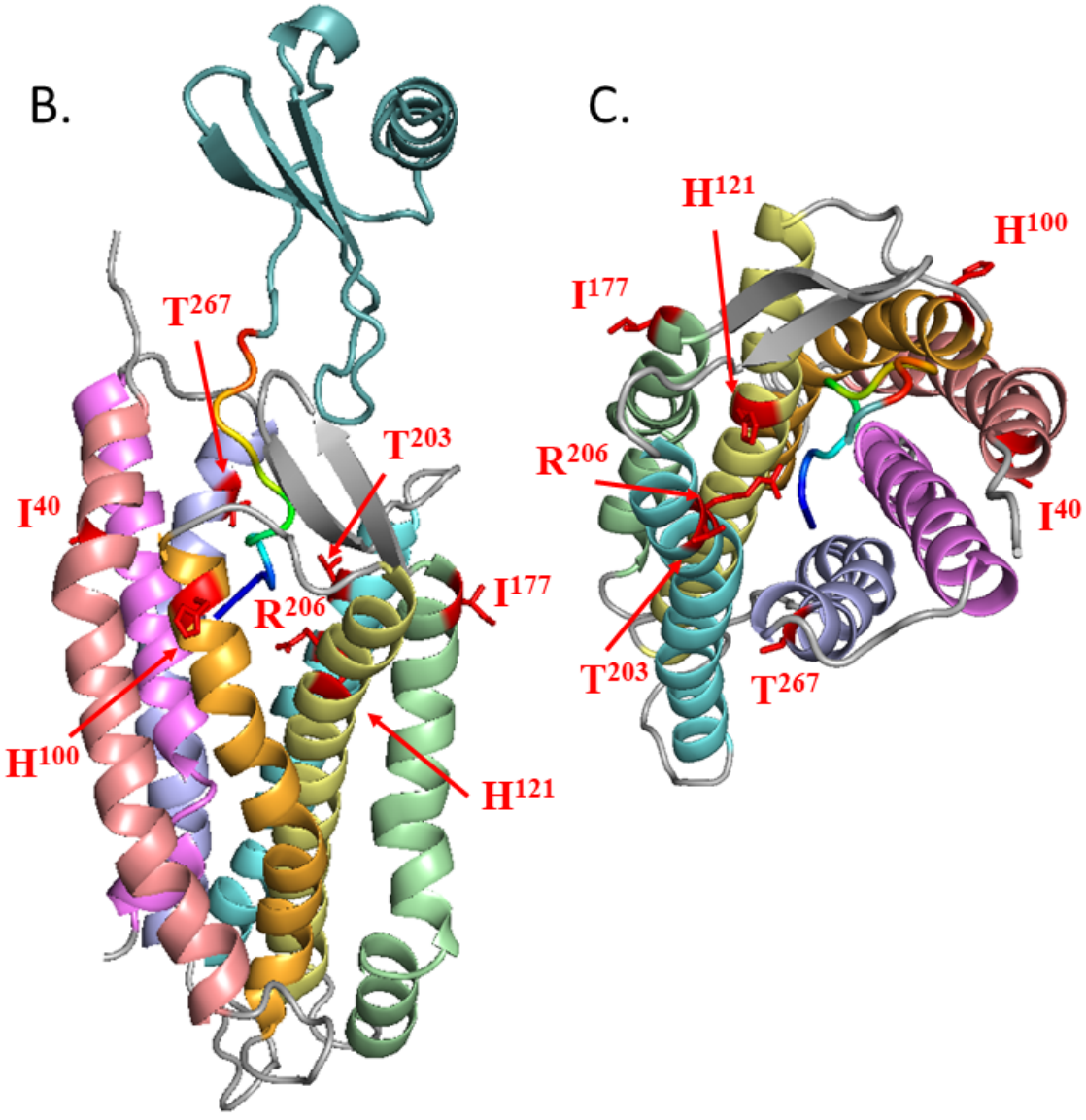

Figure 6.3: Potential CCR1 Mutations for MCP-1 Activation. (A) Sequence alignment of CCR1, 2, 3 and 5. CCR1 is the only receptor that is not activated by MCP-1. Potential mutations are highlighted in red and the residues with side chains pointing towards the inside of the receptor bundle are highlighted in bold. **(B)** Full view showing the homology model of CCR2 (grey background, helices coloured in salmon (TM1), orange (TM2), pale yellow (TM3), pale green (TM4), cyan (TM5), violet (TM6) and magenta (TM7)) bound to MCP-1 (light blue with rainbow N-terminus). The potential mutations are shown in red with their side chains and amino acid numbers. **(C)** Top view of the picture shown in (B). MCP-1 is not shown except for its N-terminus (rainbow).

6.4. Conclusion

To summarise, this project was designed to investigate chemokine recognition by the CC chemokine receptor CCR1. By measuring several signalling readouts, we showed that CCR1 exhibits biased agonism when activated by several cognate chemokines and that the chemokine N-terminus is not the only chemokine region regulating receptor activation. This unpredicted result prompted us to explore in more details the model describing chemokine:receptor interactions. We studied both sites of this two-site model using peptide models for site 1 and chimeric proteins for site 2. Our results revealed that the site 1 interactions were not sufficient to account for full-strength binding, suggesting that regions other than the receptor N-terminus contribute to high affinity chemokine binding. Results from site 2 also proved that regions other than the chemokine N-terminus are needed to fully control receptor activation, in particular the chemokine N-loop. Thus, we proposed an amended version of the two-site model that could reconcile our results and also account for subtle changes and fine-tuned mechanisms. Together with recent structural data on chemokine receptors, our findings contribute to ongoing efforts to elucidate the molecular mechanisms of chemokine receptor activation and provide insights towards understanding the functional selectivity of different chemokines.

In addition to the mechanistic aspect of this project, we sought an alternative to small molecule antagonists targeting chemokine receptors. Increasing our structural knowledge is indeed crucial to designing better drugs and overcoming the complexity of the chemokine:receptor network. However, it is also essential to look for alternative strategies in the meantime. Thus, we used bioinformatics to identify new chemokine-inhibitory evasins from a variety of tick species. Evasins, unlike other types of chemokine antagonists have already shown some selectivity in the subset of chemokines that they can bind and inhibit. This makes them ideal candidates to modify and engineer in order to create highly specific chemokine inhibitors that could be used as treatments for many diseases.

References

1. Lawrence, T., D.A. Willoughby, and D.W. Gilroy, Anti-Inflammatory Lipid Mediators and Insights into the Resolution of Inflammation. *Nat. Rev. Immunol.*, 2002. **2**: 787-95.
2. Han, J. and R.J. Ulevitch, Limiting Inflammatory Responses During Activation of Innate Immunity. *Nat. Immunol.*, 2005. **6**: 1198-205.
3. Davidson, A. and B. Diamond, Autoimmune Diseases. *N. Engl. J. Med.*, 2001. **345**: 340-50.
4. Rajagopalan, L. and K. Rajarathnam, Structural Basis of Chemokine Receptor Function--a Model for Binding Affinity and Ligand Selectivity. *Biosci. Rep.*, 2006. **26**: 325-39.
5. Kunkel, E.J. and E.C. Butcher, Plasma-Cell Homing. *Nat. Rev. Immunol.*, 2003. **3**: 822-9.
6. Lau, E.K., C.D. Paavola, Z. Johnson, J.P. Gaudry, E. Geretti, F. Borlat, A.J. Kungl, A.E. Proudfoot, and T.M. Handel, Identification of the Glycosaminoglycan Binding Site of the Cc Chemokine, Mcp-1: Implications for Structure and Function in Vivo. *J. Biol. Chem.*, 2004. **279**: 22294-305.
7. Poluri, K.M., P.R. Joseph, K.V. Sawant, and K. Rajarathnam, Molecular Basis of Glycosaminoglycan Heparin Binding to the Chemokine Cxcl1 Dimer. *J. Biol. Chem.*, 2013. **288**: 25143-53.
8. Yu, Y., M.D. Sweeney, O.M. Saad, S.E. Crown, A.R. Hsu, T.M. Handel, and J.A. Leary, Chemokine-Glycosaminoglycan Binding: Specificity for Ccr2 Ligand Binding to Highly Sulfated Oligosaccharides Using Fticr Mass Spectrometry. *J. Biol. Chem.*, 2005. **280**: 32200-8.
9. Baggiolini, M., Chemokines and Leukocyte Traffic. *Nature*, 1998. **392**: 565-8.
10. Horuk, R., Chemokines. *Sci. World J.*, 2007. **7**: 224-32.
11. Nguyen, L.T. and H.J. Vogel, Structural Perspectives on Antimicrobial Chemokines. *Front. Immunol.*, 2012. **3**: 384.
12. Ren, M., Q. Guo, L. Guo, M. Lenz, F. Qian, R.R. Koenen, H. Xu, A.B. Schilling, C. Weber, R.D. Ye, A.R. Dinner, and W.J. Tang, Polymerization of Mip-1 Chemokine (Ccl3 and Ccl4) and Clearance of Mip-1 by Insulin-Degrading Enzyme. *EMBO J.*, 2010. **29**: 3952-66.
13. Mackay, C.R., Chemokines: Immunology's High Impact Factors. *Nat. Immunol.*, 2001. **2**: 95-101.
14. Walz, D.A., V.Y. Wu, R. de Lamo, H. Dene, and L.E. McCoy, Primary Structure of Human Platelet Factor 4. *Thromb. Res.*, 1977. **11**: 893-8.
15. Zlotnik, A. and O. Yoshie, Chemokines: A New Classification System and Their Role in Immunity. *Immunity.*, 2000. **12**: 121-127.
16. Moser, B. and P. Loetscher, Lymphocyte Traffic Control by Chemokines. *Nat. Immunol.*, 2001. **2**: 123-8.
17. Moser, B., M. Wolf, A. Walz, and P. Loetscher, Chemokines: Multiple Levels of Leukocyte Migration Control. *Trends Immunol.*, 2004. **25**: 75-84.
18. Weber, C. and R.R. Koenen, Fine-Tuning Leukocyte Responses: Towards a Chemokine 'Interactome'. *Trends Immunol.*, 2006. **27**: 268-73.
19. Baldwin, E.T., I.T. Weber, R. St Charles, J.C. Xuan, E. Appella, M. Yamada, K. Matsushima, B.F. Edwards, G.M. Clore, A.M. Gronenborn, and et al., Crystal Structure of Interleukin 8: Symbiosis of Nmr and Crystallography. *Proc Natl Acad Sci U S A*, 1991. **88**: 502-6.
20. Grygiel, T.L., A. Teplyakov, G. Obmolova, N. Stowell, R. Holland, J.F. Nemeth, S.C. Pomerantz, M. Kruszynski, and G.L. Gilliland, Synthesis by Native Chemical Ligation and Crystal Structure of Human Ccl2. *Biopolymers*, 2010. **94**: 350-9.
21. Blain, K.Y., et al., Structural and Functional Characterization of Cc Chemokine Ccl14. *Biochemistry*, 2007. **46**: 10008-10015.
22. Paavola, C.D., S. Hemmerich, D. Grunberger, I. Polsky, A. Bloom, R. Freedman, M. Mulkins, S. Bhakta, D. McCarley, L. Wiesent, B. Wong, K. Jarnagin, and T.M. Handel, Monomeric Monocyte Chemoattractant Protein-1 (Mcp-1) Binds and Activates the Mcp-1 Receptor Ccr2b. *J. Biol. Chem.*, 1998. **273**: 33157-65.
23. Proudfoot, A.E., T.M. Handel, Z. Johnson, E.K. Lau, P. LiWang, I. Clark-Lewis, F. Borlat, T.N. Wells, and M.H. Kosco-Vilbois, Glycosaminoglycan Binding and Oligomerization Are Essential for the *in Vivo* Activity of Certain Chemokines. *Proc Natl Acad Sci U S A*, 2003. **100**: 1885-90.

24. Gangavarapu, P., L. Rajagopalan, D. Kolli, A. Guerrero-Plata, R.P. Garofalo, and K. Rajarathnam, The Monomer-Dimer Equilibrium and Glycosaminoglycan Interactions of Chemokine Cxcl8 Regulate Tissue-Specific Neutrophil Recruitment. *J Leukoc Biol*, 2012. **91**: 259-65.
25. Meunier, S., J.M. Bernassau, J.C. Guillemot, P. Ferrara, and H. Darbon, Determination of the Three-Dimensional Structure of Cc Chemokine Monocyte Chemoattractant Protein 3 by 1h Two-Dimensional Nmr Spectroscopy. *Biochemistry*, 1997. **36**: 4412-22.
26. Stone, M.J., J.A. Hayward, C. Huang, E.H. Z, and J. Sanchez, Mechanisms of Regulation of the Chemokine-Receptor Network. *Int. J. Mol. Sci.*, 2017. **18**.
27. Noso, N., J. Bartels, A.I. Mallet, M. Mochizuki, E. Christophers, and J.M. Schroder, Delayed Production of Biologically Active O-Glycosylated Forms of Human Eotaxin by Tumor-Necrosis-Factor-α-Stimulated Dermal Fibroblasts. *Eur. J. Biochem.*, 1998. **253**: 114-22.
28. Hermand, P., F. Pincet, S. Carvalho, H. Ansanay, E. Trinquet, M. Daoudi, C. Combadiere, and P. Deterre, Functional Adhesiveness of the Cx3cl1 Chemokine Requires Its Aggregation. Role of the Transmembrane Domain. *J. Biol. Chem.*, 2008. **283**: 30225-34.
29. Kameyoshi, Y., A. Dorschner, A.I. Mallet, E. Christophers, and J.M. Schroder, Cytokine Rantes Released by Thrombin-Stimulated Platelets Is a Potent Attractant for Human Eosinophils. *J. Exp. Med.*, 1992. **176**: 587-92.
30. Barker, C.E., S. Ali, G. O'Boyle, and J.A. Kirby, Transplantation and Inflammation: Implications for the Modification of Chemokine Function. *Immunology*, 2014. **143**: 138-45.
31. Proost, P., T. Loos, A. Mortier, E. Schutyser, M. Gouwy, S. Noppen, C. Dillen, I. Ronsse, R. Conings, S. Struyf, G. Opdenakker, P.C. Maudgal, and J. Van Damme, Citrullination of Cxcl8 by Peptidylarginine Deiminase Alters Receptor Usage, Prevents Proteolysis, and Dampens Tissue Inflammation. *J. Exp. Med.*, 2008. **205**: 2085-97.
32. Molon, B., et al., Chemokine Nitration Prevents Intratumoral Infiltration of Antigen-Specific T Cells. *J. Exp. Med.*, 2011. **208**: 1949-62.
33. Moelants, E.A., A. Mortier, J. Van Damme, and P. Proost, *In Vivo* Regulation of Chemokine Activity by Post-Translational Modification. *Immunol. Cell Biol.*, 2013. **91**: 402-7.
34. Mortier, A., J. Van Damme, and P. Proost, Regulation of Chemokine Activity by Posttranslational Modification. *Pharmacol Ther*, 2008. **120**: 197-217.
35. Ott, T.R., F.M. Lio, D. Olshefski, X.J. Liu, R.S. Struthers, and N. Ling, Determinants of High-Affinity Binding and Receptor Activation in the N-Terminus of Ccl-19 (Mip-3β). *Biochemistry*, 2004. **43**: 3670-8.
36. Chevigne, A., V. Fievez, J.C. Schmit, and S. Deroo, Engineering and Screening the N-Terminus of Chemokines for Drug Discovery. *Biochem Pharmacol*, 2011. **82**: 1438-56.
37. Dong, C.Z., S. Tian, W.T. Choi, S. Kumar, D. Liu, Y. Xu, X. Han, Z. Huang, and J. An, Critical Role in Cxcr4 Signaling and Internalization of the Polypeptide Main Chain in the Amino Terminus of Sdf-1α Probed by Novel N-Methylated Synthetically and Modularly Modified Chemokine Analogues. *Biochemistry*, 2012. **51**: 5951-7.
38. Panzer, U., A. Schneider, J. Wilken, D.A. Thompson, S.B. Kent, and R.A. Stahl, The Chemokine Receptor Antagonist Aop-Rantes Reduces Monocyte Infiltration in Experimental Glomerulonephritis. *Kidney Int.*, 1999. **56**: 2107-15.
39. Matsui, M., J. Weaver, A.E. Proudfoot, J.R. Wujek, T. Wei, E. Richer, B.D. Trapp, A. Rao, and R.M. Ransohoff, Treatment of Experimental Autoimmune Encephalomyelitis with the Chemokine Receptor Antagonist Met-Rantes. *J. Neuroimmunol.*, 2002. **128**: 16-22.
40. Detheux, M., L. Standker, J. Vakili, J. Munch, U. Forssmann, K. Adermann, S. Pohlmann, G. Vassart, F. Kirchhoff, M. Parmentier, and W.G. Forssmann, Natural Proteolytic Processing of Hemofiltrate Cc Chemokine 1 Generates a Potent Cc Chemokine Receptor (Ccr)1 and Ccr5 Agonist with Anti-Hiv Properties. *J. Exp. Med.*, 2000. **192**: 1501-8.
41. Escher, S.E., U. Forssmann, A. Frimpong-Boateng, K. Adermann, J. Vakili, H. Sticht, and M. Detheux, Functional Analysis of Chemically Synthesized Derivatives of the Human Cc Chemokine Ccl15/Hcc-2, a High Affinity Ccr1 Ligand. *J. Pept. Res.*, 2004. **63**: 36-47.
42. Forssmann, U., I. Hartung, R. Balder, B. Fuchs, S.E. Escher, N. Spodsberg, Y. Dulkys, M. Walden, A. Heitland, A. Braun, W.G. Forssmann, and J. Elsner, N-Nonanoyl-Cc Chemokine Ligand 14, a Potent

Cc Chemokine Ligand 14 Analogue That Prevents the Recruitment of Eosinophils in Allergic Airway Inflammation. *J. Immunol.*, 2004. **173**: 3456-66.
43. Jeffrey K. Harrison and N.W. Lukacs, The Chemokine Receptors. 2007.
44. Holmes, W.E., J. Lee, W.J. Kuang, G.C. Rice, and W.I. Wood, Structure and Functional Expression of a Human Interleukin-8 Receptor. *Science*, 1991. **253**: 1278-80.
45. O'Hayre, M., C.L. Salanga, T.M. Handel, and S.J. Allen, Chemokines and Cancer: Migration, Intracellular Signalling and Intercellular Communication in the Microenvironment. *Biochem. J.*, 2008. **409**: 635-49.
46. Koenen, R.R. and C. Weber, Therapeutic Targeting of Chemokine Interactions in Atherosclerosis. *Nat. Rev. Drug. Discov.*, 2010. **9**: 141-53.
47. Cameron, M.J., G.A. Arreaza, M. Grattan, C. Meagher, S. Sharif, M.D. Burdick, R.M. Strieter, D.N. Cook, and T.L. Delovitch, Differential Expression of Cc Chemokines and the Ccr5 Receptor in the Pancreas Is Associated with Progression to Type I Diabetes. *J. Immunol. (Baltimore, Md. : 1950)*, 2000. **165**: 1102.
48. Rossi, D. and A. Zlotnik, The Biology of Chemokines and Their Receptors. *Annu. Rev. Immunol.*, 2000. **18**: 217-42.
49. Jin, H., I. Kagiampakis, P. Li, and P.J. Liwang, Structural and Functional Studies of the Potent Anti-Hiv Chemokine Variant P2-Rantes. *Proteins*, 2010. **78**: 295-308.
50. Cashin, K., M. Roche, J. Sterjovski, A. Ellett, L.R. Gray, A.L. Cunningham, P.A. Ramsland, M.J. Churchill, and P.R. Gorry, Alternative Coreceptor Requirements for Efficient Ccr5- and Cxcr4-Mediated Hiv-1 Entry into Macrophages. *J. Virol.*, 2011. **85**: 10699-709.
51. Liu, R., W.A. Paxton, S. Choe, D. Ceradini, S.R. Martin, R. Horuk, M.E. MacDonald, H. Stuhlmann, R.A. Koup, and N.R. Landau, Homozygous Defect in Hiv-1 Coreceptor Accounts for Resistance of Some Multiply-Exposed Individuals to Hiv-1 Infection. *Cell*, 1996. **86**: 367-77.
52. Wu, L., N.P. Gerard, R. Wyatt, H. Choe, C. Parolin, N. Ruffing, A. Borsetti, A.A. Cardoso, E. Desjardin, W. Newman, C. Gerard, and J. Sodroski, Cd4-Induced Interaction of Primary Hiv-1 Gp120 Glycoproteins with the Chemokine Receptor Ccr-5. *Nature*, 1996. **384**: 179-83.
53. Deng, H., et al., Identification of a Major Co-Receptor for Primary Isolates of Hiv-1. *Nature*, 1996. **381**: 661-6.
54. Pease, J. and R. Horuk, Chemokine Receptor Antagonists. *J. Med. Chem.*, 2012. **55**: 9363-92.
55. Duan, Y., Hiv Co-Receptor Ccr5: Structure and Interactions with Inhibitors. *Infectious Disorders - Drug Targets*, 2009. **9**: 279-288.
56. Murphy, P.M., M. Baggiolini, I.F. Charo, C.A. Hebert, R. Horuk, K. Matsushima, L.H. Miller, J.J. Oppenheim, and C.A. Power, International Union of Pharmacology. Xxii. Nomenclature for Chemokine Receptors. *Pharmacol. Rev.*, 2000. **52**: 145-76.
57. Ulvmar, M.H., E. Hub, and A. Rot, Atypical Chemokine Receptors. *Exp. Cell Res.*, 2011. **317**: 556-68.
58. Alexander, J.M., C.A. Nelson, V. van Berkel, E.K. Lau, J.M. Studts, T.J. Brett, S.H. Speck, T.M. Handel, H.W. Virgin, and D.H. Fremont, Structural Basis of Chemokine Sequestration by a Herpesvirus Decoy Receptor. *Cell*, 2002. **111**: 343-56.
59. Murphy, P.M., Chemokine Receptors: Structure, Function and Role in Microbial Pathogenesis. *Cyto. & Growth Fact. Rev.*, 1996. **7**: 47 - 64.
60. Katritch, V., V. Cherezov, and R.C. Stevens, Structure-Function of the G Protein-Coupled Receptor Superfamily. *Annu. Rev. Pharmacol. Toxicol.*, 2013. **53**: 531-56.
61. Pierce, K.L., R.T. Premont, and R.J. Lefkowitz, Seven-Transmembrane Receptors. *Nat. Rev. Mol. Cell Biol.*, 2002. **3**: 639-50.
62. Kobilka, B.K., G Protein Coupled Receptor Structure and Activation. *Biochim. Biophys. Acta.*, 2007. **1768**: 794-807.
63. Kaushal, S., K.D. Ridge, and H.G. Khorana, Structure and Function in Rhodopsin: The Role of Asparagine-Linked Glycosylation. *Proc. Natl. Acad. Sci. U S A*, 1994. **91**: 4024-8.
64. Fredriksson, R., M.C. Lagerstrom, L.G. Lundin, and H.B. Schioth, The G-Protein-Coupled Receptors in the Human Genome Form Five Main Families. Phylogenetic Analysis, Paralogon Groups, and Fingerprints. *Mol. Pharmacol.*, 2003. **63**: 1256-72.

65. Grace, C.R., M.H. Perrin, M.R. DiGruccio, C.L. Miller, J.E. Rivier, W.W. Vale, and R. Riek, Nmr Structure and Peptide Hormone Binding Site of the First Extracellular Domain of a Type B1 G Protein-Coupled Receptor. *Proc. Natl. Acad. Sci. U S A*, 2004. **101**: 12836-41.
66. Perrin, M.H., S. Sutton, D.L. Bain, W.T. Berggren, and W.W. Vale, The First Extracellular Domain of Corticotropin Releasing Factor-R1 Contains Major Binding Determinants for Urocortin and Astressin. *Endocrinology*, 1998. **139**: 566-70.
67. Okamoto, T., N. Sekiyama, M. Otsu, Y. Shimada, A. Sato, S. Nakanishi, and H. Jingami, Expression and Purification of the Extracellular Ligand Binding Region of Metabotropic Glutamate Receptor Subtype 1. *J. Biol. Chem.*, 1998. **273**: 13089-96.
68. Langenhan, T., G. Aust, and J. Hamann, Sticky Signaling--Adhesion Class G Protein-Coupled Receptors Take the Stage. *Sci. Signal.*, 2013. **6**: re3.
69. Lee, J., R. Horuk, G.C. Rice, G.L. Bennett, T. Camerato, and W.I. Wood, Characterization of Two High Affinity Human Interleukin-8 Receptors. *J. Biol. Chem.*, 1992. **267**: 16283-7.
70. Dohlman, H.G., M.G. Caron, and R.J. Lefkowitz, Structure and Function of the β2-Adrenergic Receptor--Homology with Rhodopsin. *Kidney Int. Suppl.*, 1987. **23**: S2-13.
71. Cherezov, V., D.M. Rosenbaum, M.A. Hanson, S.G. Rasmussen, F.S. Thian, T.S. Kobilka, H.J. Choi, P. Kuhn, W.I. Weis, B.K. Kobilka, and R.C. Stevens, High-Resolution Crystal Structure of an Engineered Human β2-Adrenergic G Protein-Coupled Receptor. *Science*, 2007. **318**: 1258-65.
72. Palczewski, K., T. Kumasaka, T. Hori, C.A. Behnke, H. Motoshima, B.A. Fox, I. Le Trong, D.C. Teller, T. Okada, R.E. Stenkamp, M. Yamamoto, and M. Miyano, Crystal Structure of Rhodopsin: A G Protein-Coupled Receptor. *Science*, 2000. **289**: 739-45.
73. Venkatakrishnan, A.J., X. Deupi, G. Lebon, C.G. Tate, G.F. Schertler, and M.M. Babu, Molecular Signatures of G-Protein-Coupled Receptors. *Nature*, 2013. **494**: 185-94.
74. Kobilka, B.K., T.S. Kobilka, K. Daniel, J.W. Regan, M.G. Caron, and R.J. Lefkowitz, Chimeric α2-,β2-Adrenergic Receptors: Delineation of Domains Involved in Effector Coupling and Ligand Binding Specificity. *Science*, 1988. **240**: 1310-6.
75. Dixon, R.A., I.S. Sigal, E. Rands, R.B. Register, M.R. Candelore, A.D. Blake, and C.D. Strader, Ligand Binding to the B-Adrenergic Receptor Involves Its Rhodopsin-Like Core. *Nature*, 1987. **326**: 73-7.
76. Havlickova, M., J. Blahos, I. Brabet, J. Liu, B. Hruskova, L. Prezeau, and J.P. Pin, The Second Intracellular Loop of Metabotropic Glutamate Receptors Recognizes C Termini of G-Protein α-Subunits. *J. Biol. Chem.*, 2003. **278**: 35063-70.
77. Rasmussen, S.G., et al., Crystal Structure of the β2 Adrenergic Receptor-Gs Protein Complex. *Nature*, 2011. **477**: 549-55.
78. Gilman, A.G., G Proteins: Transducers of Receptor-Generated Signals. *Annu. Rev. Biochem.*, 1987. **56**: 615-49.
79. Brandt, D.R. and E.M. Ross, Gtpase Activity of the Stimulatory Gtp-Binding Regulatory Protein of Adenylate Cyclase, Gs. Accumulation and Turnover of Enzyme-Nucleotide Intermediates. *J. Biol. Chem.*, 1985. **260**: 266-72.
80. Cassel, D. and Z. Selinger, Mechanism of Adenylate Cyclase Activation through the β-Adrenergic Receptor: Catecholamine-Induced Displacement of Bound Gdp by Gtp. *Proc. Natl. Acad. Sci. U S A*, 1978. **75**: 4155-9.
81. Wettschureck, N. and S. Offermanns, Mammalian G Proteins and Their Cell Type Specific Functions. *Physiol Rev*, 2005. **85**: 1159-204.
82. Wall, M.A., B.A. Posner, and S.R. Sprang, Structural Basis of Activity and Subunit Recognition in G Protein Heterotrimers. *Structure*, 1998. **6**: 1169-83.
83. Musnier, A., B. Blanchot, E. Reiter, and P. Crepieux, Gpcr Signalling to the Translation Machinery. *Cell Signal.*, 2010. **22**: 707-16.
84. Sutherland, E.W., T.W. Rall, and T. Menon, Adenyl Cylase. I. Distribution, Preparation, and Properties. *J. Biol. Chem.*, 1962. **237**: 1220.
85. Pfeuffer, T., Gtp-Binding Proteins in Membranes and the Control of Adenylate Cyclase Activity. *J. Biol. Chem.*, 1977. **252**: 7224-34.

References

86. Codina, J., J. Hildebrandt, R. Iyengar, L. Birnbaumer, R.D. Sekura, and C.R. Manclark, Pertussis Toxin Substrate, the Putative Ni Component of Adenylyl Cyclases, Is an αβ Heterodimer Regulated by Guanine Nucleotide and Magnesium. *Proc. Natl. Acad. Sci. U S A*, 1983. **80**: 4276-80.
87. Taylor, S.J. and J.H. Exton, Two α Subunits of the Gq Class of G Proteins Stimulate Phosphoinositide Phospholipase C-β 1 Activity. *FEBS Lett.*, 1991. **286**: 214-6.
88. Berridge, M.J., Inositol Trisphosphate and Calcium Signalling. *Nature*, 1993. **361**: 315-25.
89. Ridley, A.J. and A. Hall, The Small Gtp-Binding Protein Rho Regulates the Assembly of Focal Adhesions and Actin Stress Fibers in Response to Growth Factors. *Cell*, 1992. **70**: 389-99.
90. Hart, M.J., X. Jiang, T. Kozasa, W. Roscoe, W.D. Singer, A.G. Gilman, P.C. Sternweis, and G. Bollag, Direct Stimulation of the Guanine Nucleotide Exchange Activity of P115 Rhogef by Gα13. *Science*, 1998. **280**: 2112-4.
91. Tan, Q., et al., Structure of the Ccr5 Chemokine Receptor-Hiv Entry Inhibitor Maraviroc Complex. *Science*, 2013. **341**: 1387-90.
92. Lefkowitz, R.J., Historical Review: A Brief History and Personal Retrospective of Seven-Transmembrane Receptors. *Trends Pharmacol. Sci.*, 2004. **25**: 413-22.
93. Logothetis, D.E., Y. Kurachi, J. Galper, E.J. Neer, and D.E. Clapham, The βγ ubunits of Gtp-Binding Proteins Activate the Muscarinic K+ Channel in Heart. *Nature*, 1987. **325**: 321-6.
94. DeWire, S.M., S. Ahn, R.J. Lefkowitz, and S.K. Shenoy, β-Arrestins and Cell Signaling. *Annu. Rev. Physiol.*, 2007. **69**: 483-510.
95. Homan, K.T. and J.J. Tesmer, Structural Insights into G Protein-Coupled Receptor Kinase Function. *Curr. Opin. Cell Biol.*, 2014. **27**: 25-31.
96. Harden, T.K., Y.F. Su, and J.P. Perkins, Catecholamine-Induced Desensitization Involves an Uncoupling of β-Adrenergic Receptors and Adenylate Cyclase. *J. Cycl. Nucl. Res.*, 1979. **5**: 99-106.
97. Attramadal, H., J.L. Arriza, C. Aoki, T.M. Dawson, J. Codina, M.M. Kwatra, S.H. Snyder, M.G. Caron, and R.J. Lefkowitz, β-Arrestin2, a Novel Member of the Arrestin/β-Arrestin Gene Family. *J. Biol. Chem.*, 1992. **267**: 17882-90.
98. Benovic, J.L., H. Kuhn, I. Weyand, J. Codina, M.G. Caron, and R.J. Lefkowitz, Functional Desensitization of the Isolated B-Adrenergic Receptor by the β-Adrenergic Receptor Kinase: Potential Role of an Analog of the Retinal Protein Arrestin (48-Kda Protein). *Proc. Natl. Acad. Sci. U S A*, 1987. **84**: 8879-82.
99. Luttrell, L.M., S.S. Ferguson, Y. Daaka, W.E. Miller, S. Maudsley, G.J. Della Rocca, F. Lin, H. Kawakatsu, K. Owada, D.K. Luttrell, M.G. Caron, and R.J. Lefkowitz, β-Arrestin-Dependent Formation of β2 Adrenergic Receptor-Src Protein Kinase Complexes *Science*, 1999. **283**: 655-61.
100. Miller, W.E., D.A. Houtz, C.D. Nelson, P.E. Kolattukudy, and R.J. Lefkowitz, G-Protein-Coupled Receptor (Gpcr) Kinase Phosphorylation and β-Arrestin Recruitment Regulate the Constitutive Signaling Activity of the Human Cytomegalovirus Us28 Gpcr. *J. Biol. Chem.*, 2003. **278**: 21663-71.
101. Chong, H., H.G. Vikis, and K.L. Guan, Mechanisms of Regulating the Raf Kinase Family. *Cell Signal.*, 2003. **15**: 463-9.
102. Thomas, W.G., T.J. Thekkumkara, and K.M. Baker, Molecular Mechanisms of Angiotensin II (At1a) Receptor Endocytosis. *Clin. Exp. Pharmacol. Physiol.*, 1996. **23**: S74-80.
103. Lefkowitz, R.J. and S.K. Shenoy, Transduction of Receptor Signals by β-Arrestins. *Science*, 2005. **308**: 512-7.
104. Hamm, H.E., The Mainy Faces of G Protein Signaling. *J Biol Chem*, 1998. **273**: 669-672.
105. Stewart, A. and R.A. Fisher, Introduction: G Protein-Coupled Receptors and Rgs Proteins. *Prog Mol Biol Transl Sci*, 2015. **133**: 1-11.
106. Berman, D.M., T.M. Wilkie, and A.G. Gilman, Gaip and Rgs4 Are Gtpase-Activating Proteins for the Gi Subfamily of G Protein Alpha Subunits. *Cell*, 1996. **86**: 445-52.
107. Ross, E.M. and T.M. Wilkie, Gtpase-Activating Proteins for Heterotrimeric G Proteins: Regulators of G Protein Signaling (Rgs) and Rgs-Like Proteins. *Annu Rev Biochem*, 2000. **69**: 795-827.
108. Chini, B. and M. Parenti, G-Protein Coupled Receptors in Lipid Rafts and Caveolae: How, When and Why Do They Go There? *J Mol Endocrinol*, 2004. **32**: 325-38.

109. Escriba, P.V., P.B. Wedegaertner, F.M. Goni, and O. Vogler, Lipid-Protein Interactions in Gpcr-Associated Signaling. *Biochim Biophys Acta*, 2007. **1768**: 836-52.
110. Ogilvie, P., G. Bardi, I. Clark-Lewis, M. Baggiolini, and M. Uguccioni, Eotaxin Is a Natural Antagonist for Ccr2 and an Agonist for Ccr5. *Blood*, 2001. **97**: 1920-4.
111. Martinelli, R., I. Sabroe, G. LaRosa, T.J. Williams, and J.E. Pease, The Cc Chemokine Eotaxin (Ccl11) Is a Partial Agonist of Cc Chemokine Receptor 2b. *J. of Biol. Chem.*, 2001. **276**: 42957-64.
112. Parody, T.R. and M.J. Stone, High Level Expression, Activation, and Antagonism of Cc Chemokine Receptors Ccr2 and Ccr3 in Chinese Hamster Ovary Cells. *Cytokine*, 2004. **27**: 38-46.
113. Gurwitz, D., R. Haring, E. Heldman, C.M. Fraser, D. Manor, and A. Fisher, Discrete Activation of Transduction Pathways Associated with Acetylcholine M1 Receptor by Several Muscarinic Ligands. *Eur. J. Pharmacol.*, 1994. **267**: 21-31.
114. Shonberg, J., L. Lopez, P.J. Scammells, A. Christopoulos, B. Capuano, and J.R. Lane, Biased Agonism at G Protein-Coupled Receptors: The Promise and the Challenges--a Medicinal Chemistry Perspective. *Med Res Rev*, 2014. **34**: 1286-330.
115. Sternini, C., M. Spann, B. Anton, D.E. Keith, Jr., N.W. Bunnett, M. von Zastrow, C. Evans, and N.C. Brecha, Agonist-Selective Endocytosis of μ Opioid Receptor by Neurons in Vivo. *Proc. Natl. Acad. Sci. U S A*, 1996. **93**: 9241-6.
116. Keith, D.E., S.R. Murray, P.A. Zaki, P.C. Chu, D.V. Lissin, L. Kang, C.J. Evans, and M. von Zastrow, Morphine Activates Opioid Receptors without Causing Their Rapid Internalization. *J. Biol. Chem.*, 1996. **271**: 19021-4.
117. Stallaert, W., J.F. Dorn, E. van der Westhuizen, M. Audet, and M. Bouvier, Impedance Responses Reveal B(2)-Adrenergic Receptor Signaling Pluridimensionality and Allow Classification of Ligands with Distinct Signaling Profiles. *PLoS One*, 2012. **7**: e29420.
118. Urban, J.D., G.A. Vargas, M. von Zastrow, and R.B. Mailman, Aripiprazole Has Functionally Selective Actions at Dopamine D2 Receptor-Mediated Signaling Pathways. *Neuropsycho.*, 2007. **32**: 67-77.
119. Newman-Tancredi, A., J.C. Martel, M.B. Assie, J. Buritova, E. Lauressergues, C. Cosi, P. Heusler, L. Bruins Slot, F.C. Colpaert, B. Vacher, and D. Cussac, Signal Transduction and Functional Selectivity of F15599, a Preferential Post-Synaptic 5-Ht1a Receptor Agonist. *Br. J. Pharmacol.*, 2009. **156**: 338-53.
120. Berg, K.A., S. Maayani, J. Goldfarb, C. Scaramellini, P. Leff, and W.P. Clarke, Effector Pathway-Dependent Relative Efficacy at Serotonin Type 2a and 2c Receptors: Evidence for Agonist-Directed Trafficking of Receptor Stimulus. *Mol. Pharmacol.*, 1998. **54**: 94-104.
121. Wei, H., S. Ahn, S.K. Shenoy, S.S. Karnik, L. Hunyady, L.M. Luttrell, and R.J. Lefkowitz, Independent β-Arrestin 2 and G Protein-Mediated Pathways for Angiotensin Ii Activation of Extracellular Signal-Regulated Kinases 1 and 2. *Proc. Natl. Acad. Sci. U S A*, 2003. **100**: 10782-7.
122. Urban, J.D., W.P. Clarke, M. von Zastrow, D.E. Nichols, B. Kobilka, H. Weinstein, J.A. Javitch, B.L. Roth, A. Christopoulos, P.M. Sexton, K.J. Miller, M. Spedding, and R.B. Mailman, Functional Selectivity and Classical Concepts of Quantitative Pharmacology. *J. Pharmacol. Exp. Ther.*, 2007. **320**: 1-13.
123. Rajagopal, S., K. Rajagopal, and R.J. Lefkowitz, Teaching Old Receptors New Tricks: Biasing Seven-Transmembrane Receptors. *Nat. Rev. Drug Discov.*, 2010. **9**: 373-86.
124. Kenakin, T., C. Watson, V. Muniz-Medina, A. Christopoulos, and S. Novick, A Simple Method for Quantifying Functional Selectivity and Agonist Bias. *ACS Chem. Neurosci.*, 2012. **3**: 193-203.
125. Rajagopal, S., S. Ahn, D.H. Rominger, W. Gowen-MacDonald, C.M. Lam, S.M. Dewire, J.D. Violin, and R.J. Lefkowitz, Quantifying Ligand Bias at Seven-Transmembrane Receptors. *Mol. Pharmacol.*, 2011. **80**: 367-77.
126. Kohout, T.A., S.L. Nicholas, S.J. Perry, G. Reinhart, S. Junger, and R.S. Struthers, Differential Desensitization, Receptor Phosphorylation, B-Arrestin Recruitment, and Erk1/2 Activation by the Two Endogenous Ligands for the Cc Chemokine Receptor 7. *J. Biol. Chem.*, 2004. **279**: 23214-22.
127. Rajagopal, S., D.L. Bassoni, J.J. Campbell, N.P. Gerard, C. Gerard, and T.S. Wehrman, Biased Agonism as a Mechanism for Differential Signaling by Chemokine Receptors. *J. Biol. Chem.*, 2013. **288**: 35039-48.

References

128. Corbisier, J., C. Gales, A. Huszagh, M. Parmentier, and J.Y. Springael, Biased Signaling at Chemokine Receptors. *J. Biol. Chem.*, 2015. **290**: 9542-54.
129. Nørskov - Lauritsen, L., S. Jørgensen, and H. Bräuner - Osborne, N ‐ Glycosylation and Disulfide Bonding Affects Gprc6a Receptor Expression, Function, and Dimerization. *FEBS Letters*, 2015. **589**: 588-597.
130. Pu, Q. and C. Yu, Glycosyltransferases, Glycosylation and Atherosclerosis. *Glycoconj. J.*, 2014. **31**: 605-11.
131. Neel, N.F., E. Schutyser, J. Sai, G.H. Fan, and A. Richmond, Chemokine Receptor Internalization and Intracellular Trafficking. *Cytokine Growth Factor Rev*, 2005. **16**: 637-58.
132. Maeda, A., K. Okano, P.S. Park, J. Lem, R.K. Crouch, T. Maeda, and K. Palczewski, Palmitoylation Stabilizes Unliganded Rhodopsin. *Proc Natl Acad Sci U S A*, 2010. **107**: 8428-33.
133. Jean-Charles, P.Y., J.C. Snyder, and S.K. Shenoy, Chapter One - Ubiquitination and Deubiquitination of G Protein-Coupled Receptors. *Prog. Mol. Biol. Transl. Sci.*, 2016. **141**: 1-55.
134. Gao, J., H. Choe, D. Bota, P.L. Wright, C. Gerard, and N.P. Gerard, Sulfation of Tyrosine 174 in the Human C3a Receptor Is Essential for Binding of C3a Anaphylatoxin. *J. Biol. Chem.*, 2003. **278**: 37902-8.
135. Huttner, W.B., Sulphation of Tyrosine Residues-a Widespread Modification of Proteins. *Nature*, 1982. **299**: 273-6.
136. Lee, R.W. and W.B. Huttner, Tyrosine-O-Sulfated Proteins of Pc12 Pheochromocytoma Cells and Their Sulfation by a Tyrosylprotein Sulfotransferase. *J. Biol. Chem.*, 1983. **258**: 11326-34.
137. Stone, M.J., S. Chuang, X. Hou, M. Shoham, and J.Z. Zhu, Tyrosine Sulfation: An Increasingly Recognised Post-Translational Modification of Secreted Proteins. *New Biotech.*, 2009. **25**: 299-317.
138. Ludeman, J.P. and M.J. Stone, The Structural Role of Receptor Tyrosine Sulfation in Chemokine Recognition. *Br. J. Pharmacol.*, 2014. **171**: 1167-79.
139. Kehoe, J.W. and C.R. Bertozzi, Tyrosine Sulfation: A Modulator of Extracellular Protein-Protein Interactions. *Chem. Biol.*, 2000. **7**: R57-61.
140. Simpson, L.S., J.Z. Zhu, T.S. Widlanski, and M.J. Stone, Regulation of Chemokine Recognition by Site-Specific Tyrosine Sulfation of Receptor Peptides. *Chem. Biol.*, 2009. **16**: 153-61.
141. Zhu, J.Z., C.J. Millard, J.P. Ludeman, L.S. Simpson, D.J. Clayton, R.J. Payne, T.S. Widlanski, and M.J. Stone, Tyrosine Sulfation Influences the Chemokine Binding Selectivity of Peptides Derived from Chemokine Receptor Ccr3. *Biochemistry*, 2011. **50**: 1524-34.
142. Veldkamp, C.T., C. Seibert, F.C. Peterson, T.P. Sakmar, and B.F. Volkman, Recognition of a Cxcr4 Sulfotyrosine by the Chemokine Stromal Cell-Derived Factor-1α (Sdf-1α/Cxcl12). *J. Mol. Biol.*, 2006. **359**: 1400-9.
143. Tan, J.H., M. Canals, J.P. Ludeman, J. Wedderburn, C. Boston, S.J. Butler, A.M. Carrick, T.R. Parody, D. Taleski, A. Christopoulos, R.J. Payne, and M.J. Stone, Design and Receptor Interactions of Obligate Dimeric Mutant of Chemokine Monocyte Chemoattractant Protein-1 (Mcp-1). *J. Biol. Chem.*, 2012. **287**: 14692-702.
144. Duma, L., D. Haussinger, M. Rogowski, P. Lusso, and S. Grzesiek, Recognition of Rantes by Extracellular Parts of the Ccr5 Receptor. *J. Mol. Biol.*, 2007. **365**: 1063-75.
145. Tan, J.H., J.P. Ludeman, J. Wedderburn, M. Canals, P. Hall, S.J. Butler, D. Taleski, A. Christopoulos, M.J. Hickey, R.J. Payne, and M.J. Stone, Tyrosine Sulfation of Chemokine Receptor Ccr2 Enhances Interactions with Both Monomeric and Dimeric Forms of the Chemokine Monocyte Chemoattractant Protein-1 (Mcp-1). *J. Biol. Chem.*, 2013. **288**: 10024-34.
146. Jen, C.H. and J.A. Leary, A Competitive Binding Study of Chemokine, Sulfated Receptor, and Glycosaminoglycan Interactions by Nano-Electrospray Ionization Mass Spectrometry. *Anal. Biochem.*, 2010. **407**: 134-40.
147. Taleski, D., S.J. Butler, M.J. Stone, and R.J. Payne, Divergent and Site-Selective Solid-Phase Synthesis of Sulfopeptides. *Chem. Asian J.*, 2011. **6**: 1316-1320.
148. Preobrazhensky, A.A., S. Dragan, T. Kawano, M.A. Gavrilin, I.V. Gulina, L. Chakravarty, and P.E. Kolattukudy, Monocyte Chemotactic Protein-1 Receptor Ccr2b Is a Glycoprotein That Has Tyrosine Sulfation in a Conserved Extracellular N-Terminal Region. *J. Immunol.*, 2000. **165**: 5295-303.

149. Millard, C.J., J.P. Ludeman, M. Canals, J.L. Bridgford, M.G. Hinds, D.J. Clayton, A. Christopoulos, R.J. Payne, and M.J. Stone, Structural Basis of Receptor Sulfotyrosine Recognition by a Cc Chemokine: The N-Terminal Region of Ccr3 Bound to Ccl11/Eotaxin-1. *Structure*, 2014. **22**: 1571-81.
150. Farzan, M., T. Mirzabekov, P. Kolchinsky, R. Wyatt, M. Cayabyab, N.P. Gerard, C. Gerard, J. Sodroski, and H. Choe, Tyrosine Sulfation of the Amino Terminus of Ccr5 Facilitates Hiv-1 Entry. *Cell*, 1999. **96**: 667-76.
151. Gutierrez, J., L. Kremer, A. Zaballos, I. Goya, A.C. Martinez, and G. Marquez, Analysis of Post-Translational Ccr8 Modifications and Their Influence on Receptor Activity. *J. Biol. Chem.*, 2004. **279**: 14726-33.
152. Colvin, R.A., G.S. Campanella, L.A. Manice, and A.D. Luster, Cxcr3 Requires Tyrosine Sulfation for Ligand Binding and a Second Extracellular Loop Arginine Residue for Ligand-Induced Chemotaxis. *Mol. Cell. Biol.*, 2006. **26**: 5838-49.
153. Gao, J.M., R.L. Xiang, L. Jiang, W.H. Li, Q.P. Feng, Z.J. Guo, Q. Sun, Z.P. Zeng, and F.D. Fang, Sulfated Tyrosines 27 and 29 in the N-Terminus of Human Cxcr3 Participate in Binding Native Ip-10. *Acta. Pharmacol. Sin.*, 2009. **30**: 193-201.
154. Farzan, M., G.J. Babcock, N. Vasilieva, P.L. Wright, E. Kiprilov, T. Mirzabekov, and H. Choe, The Role of Post-Translational Modifications of the Cxcr4 Amino Terminus in Stromal-Derived Factor 1 α Association and Hiv-1 Entry. *J. Biol. Chem.*, 2002. **277**: 29484-9.
155. Fong, A.M., S.M. Alam, T. Imai, B. Haribabu, and D.D. Patel, Cx3cr1 Tyrosine Sulfation Enhances Fractalkine-Induced Cell Adhesion. *J. Biol. Chem.*, 2002. **277**: 19418-23.
156. Choe, H., M.J. Moore, C.M. Owens, P.L. Wright, N. Vasilieva, W. Li, A.P. Singh, R. Shakri, C.E. Chitnis, and M. Farzan, Sulphated Tyrosines Mediate Association of Chemokines and Plasmodium Vivax Duffy Binding Protein with the Duffy Antigen/Receptor for Chemokines (Darc). *Mol. Microbiol.*, 2005. **55**: 1413-22.
157. Szpakowska, M., V. Fievez, K. Arumugan, N. van Nuland, J.C. Schmit, and A. Chevigne, Function, Diversity and Therapeutic Potential of the N-Terminal Domain of Human Chemokine Receptors. *Biochem. Pharmacol.*, 2012. **84**: 1366-1380.
158. Palczewski, K., T. Kumasaka, T. Hori, C.A. Behnke, H. Motoshima, B.A. Fox, I. Le Trong, D.C. Teller, T. Okada, R.E. Stenkamp, M. Yamamoto, and M. Miyano, Crystal Structure of Rhodopsin: A G Protein-Coupled Receptor. *Science*, 2000. **289**: 739-745.
159. Ai, L.S. and F. Liao, Mutating the Four Extracellular Cysteines in the Chemokine Receptor Ccr6 Reveals Their Differing Roles in Receptor Trafficking, Ligand Binding, and Signaling. *Biochemistry*, 2002. **41**: 8332-41.
160. Samanta, A.K., S. Dutta, and E. Ali, Modification of Sulfhydryl Groups of Interleukin-8 (Il-8) Receptor Impairs Binding of Il-8 and Il-8-Mediated Chemotactic Response of Human Polymorphonuclear Neutrophils. *J. Biol. Chem.*, 1993. **268**: 6147-53.
161. Karnik, S.S., C. Gogonea, S. Patil, Y. Saad, and T. Takezako, Activation of G-Protein-Coupled Receptors: A Common Molecular Mechanism. *Trends Endocrinol. Metab.*, 2003. **14**: 431-7.
162. Park, S.H., B.B. Das, F. Casagrande, Y. Tian, H.J. Nothnagel, M. Chu, H. Kiefer, K. Maier, A.A. De Angelis, F.M. Marassi, and S.J. Opella, Structure of the Chemokine Receptor Cxcr1 in Phospholipid Bilayers. *Nature*, 2012. **491**: 779-83.
163. Wu, B.L., et al., Structures of the Cxcr4 Chemokine Gpcr with Small-Molecule and Cyclic Peptide Antagonists. *Science*, 2010. **330**: 1066-1071.
164. Zheng, Y., et al., Structure of Cc Chemokine Receptor 2 with Orthosteric and Allosteric Antagonists. *Nature*, 2016. **540**: 458-461.
165. Oswald, C., M. Rappas, J. Kean, A.S. Dore, J.C. Errey, K. Bennett, F. Deflorian, J.A. Christopher, A. Jazayeri, J.S. Mason, M. Congreve, R.M. Cooke, and F.H. Marshall, Intracellular Allosteric Antagonism of the Ccr9 Receptor. *Nature*, 2016. **540**: 462-465.
166. Qin, L., I. Kufareva, L.G. Holden, C. Wang, Y. Zheng, C. Zhao, G. Fenalti, H. Wu, G.W. Han, V. Cherezov, R. Abagyan, R.C. Stevens, and T.M. Handel, Structural Biology. Crystal Structure of the Chemokine Receptor Cxcr4 in Complex with a Viral Chemokine. *Science*, 2015. **347**: 1117-22.

References

167. Zheng, Y., G.W. Han, R. Abagyan, B. Wu, R.C. Stevens, V. Cherezov, I. Kufareva, and T.M. Handel, Structure of Cc Chemokine Receptor 5 with a Potent Chemokine Antagonist Reveals Mechanisms of Chemokine Recognition and Molecular Mimicry by Hiv. *Immunity*, 2017. **46**: 1005-1017 e5.
168. Burg, J.S., J.R. Ingram, A.J. Venkatakrishnan, K.M. Jude, A. Dukkipati, E.N. Feinberg, A. Angelini, D. Waghray, R.O. Dror, H.L. Ploegh, and K.C. Garcia, Structural Biology. Structural Basis for Chemokine Recognition and Activation of a Viral G Protein-Coupled Receptor. *Science*, 2015. **347**: 1113-7.
169. Rajagopalan, L. and K. Rajarathnam, Ligand Selectivity and Affinity of Chemokine Receptor Cxcr1. Role of N-Terminal Domain. *J. Biol. Chem.*, 2004. **279**: 30000-8.
170. Pease, J.E., J. Wang, P.D. Ponath, and P.M. Murphy, The N-Terminal Extracellular Segments of the Chemokine Receptors Ccr1 and Ccr3 Are Determinants for Mip-1α and Eotaxin Binding, Respectively, but a Second Domain Is Essential for Efficient Receptor Activation. *J. Biol. Chem.*, 1998. **273**: 19972-19976.
171. Crump, M.P., J.H. Gong, P. Loetscher, K. Rajarathnam, A. Amara, F. Arenzana-Seisdedos, J.L. Virelizier, M. Baggiolini, B.D. Sykes, and I. Clark-Lewis, Solution Structure and Basis for Functional Activity of Stromal Cell-Derived Factor-1; Dissociation of Cxcr4 Activation from Binding and Inhibition of Hiv-1. *EMBO Journal*, 1997. **16**: 6996-7007.
172. Wescott, M.P., I. Kufareva, C. Paes, J.R. Goodman, Y. Thaker, B.A. Puffer, E. Berdougo, J.B. Rucker, T.M. Handel, and B.J. Doranz, Signal Transmission through the Cxc Chemokine Receptor 4 (Cxcr4) Transmembrane Helices. *Proc Natl Acad Sci USA*, 2016. **113**: 9928-33.
173. Burg, J.S., J.R. Ingram, A.J. Venkatakrishnan, K.M. Jude, A. Dukkipati, E.N. Feinberg, A. Angelini, D. Waghray, R.O. Dror, H.L. Ploegh, and K.C. Garcia, Structural Basis for Chemokine Recognition and Activation of a Viral G Protein–Coupled Receptor. *Science*, 2015. **347**: 1113-1117.
174. Skelton, N.J., C. Quan, D. Reilly, and H. Lowman, Structure of a Cxc Chemokine-Receptor Fragment in Complex with Interleukin-8. *Structure*, 1999. **7**: 157-68.
175. Veldkamp, C.T., C. Seibert, F.C. Peterson, N.B. De la Cruz, J.C. Haugner, 3rd, H. Basnet, T.P. Sakmar, and B.F. Volkman, Structural Basis of Cxcr4 Sulfotyrosine Recognition by the Chemokine Sdf-1/Cxcl12. *Science Signaling*, 2008. **1**: ra4.
176. Matthew P.Crump, Jiang-Hong Gong, Pius Loetscher, Krishna Rajarathnam, Ali Amara, Fernando Arenzana-Seisdedos, Jean-Louis Virelizier, Marco Baggiolini, Brian D.Sykes, and I. Clark-Lewis, Solution Structure and Basis for Functional Activity of Stromal Cell-Derived Factor-1; Dissociation of Cxcr4 Activation from Binding and Inhibition of Hiv-1. *EMBO J.*, 1997. **16**: 6996 - 7007.
177. Gao, J.L., D.B. Kuhns, H.L. Tiffany, D. McDermott, X. Li, U. Francke, and P.M. Murphy, Structure and Functional Expression of the Human Macrophage Inflammatory Protein 1 α/Rantes Receptor. *J. Exp. Med.*, 1993. **177**: 1421-7.
178. Mantovani, A., R. Bonecchi, and M. Locati, Tuning Inflammation and Immunity by Chemokine Sequestration: Decoys and More. *Nat. Rev. Immunol.*, 2006. **6**: 907-18.
179. Proudfoot, A.E., Chemokine Receptors: Multifaceted Therapeutic Targets. *Nat. Rev. Immunol.*, 2002. **2**: 106-15.
180. Tak, P.P., A. Balanescu, V. Tseluyko, S. Bojin, E. Drescher, D. Dairaghi, S. Miao, V. Marchesin, J. Jaen, T.J. Schall, and P. Bekker, Chemokine Receptor Ccr1 Antagonist Ccx354-C Treatment for Rheumatoid Arthritis: Carat-2, a Randomised, Placebo Controlled Clinical Trial. *Ann. Rheum. Dis.*, 2013. **72**: 337-44.
181. Trebst, C., T.L. Sorensen, P. Kivisakk, M.K. Cathcart, J. Hesselgesser, R. Horuk, F. Sellebjerg, H. Lassmann, and R.M. Ransohoff, Ccr1+/Ccr5+ Mononuclear Phagocytes Accumulate in the Central Nervous System of Patients with Multiple Sclerosis. *Am. J. Pathol.*, 2001. **159**: 1701-10.
182. Karash, A.R. and A. Gilchrist, Therapeutic Potential of Ccr1 Antagonists for Multiple Myeloma. *Fut. Med. Chem.*, 2011. **3**: 1889-908.
183. Vallet, S. and K.C. Anderson, Ccr1 as a Target for Multiple Myeloma. *Expert Opin. Ther. Targets.*, 2011. **15**: 1037-47.
184. Horuk, R., et al., A Non-Peptide Functional Antagonist of the Ccr1 Chemokine Receptor Is Effective in Rat Heart Transplant Rejection. *J. Biol. Chem.*, 2001. **276**: 4199-204.
185. Ribeiro, S. and R. Horuk, The Clinical Potential of Chemokine Receptor Antagonists. *Pharmacol. Ther.*, 2005. **107**: 44-58.

186. Hoshino, A., et al., Deficiency of Chemokine Receptor Ccr1 Causes Osteopenia Due to Impaired Functions of Osteoclasts and Osteoblasts. *J. Biol. Chem.*, 2010. **285**: 28826.
187. Ninichuk, V. and H.J. Anders, Chemokine Receptor Ccr1: A New Target for Progressive Kidney Disease. *Am. J. Nephrol.*, 2005. **25**: 365-72.
188. Chuan-Chu Chou, Jay S. Fine, Catherine Pugliese-Sivo, Waldemar Gonsiorek, Liza Davies, Gregory Deno, Mary Petro, Martin Schwarz, Paul J. Zavodny, and R.W. Hipkin, Pharmacological Characterization of the Chemokine Receptor, Hccr1 in a Stable Transfectant and Differentiated Hl-60 Cells: Antagonism of Hccr1 Activation by Mip-1b. *Br. J. Pharmacol.*, 2002. **137**: 663 ± 675.
189. Mortier, A., J. Van Damme, and P. Proost, Regulation of Chemokine Activity by Posttranslational Modification. *Pharmacol. Ther.*, 2008. **120**: 197-217.
190. Allen, S.J., S. Ribeiro, R. Horuk, and T.M. Handel, Expression, Purification and in Vitro Functional Reconstitution of the Chemokine Receptor Ccr1. *Protein Expr. Purif.*, 2009. **66**: 73-81.
191. Vaidehi, N., et al., Predictions of Ccr1 Chemokine Receptor Structure and Bx 471 Antagonist Binding Followed by Experimental Validation. *J. Biol. Chem.*, 2006. **281**: 27613-20.
192. Dorr, P., et al., Maraviroc (Uk-427,857), a Potent, Orally Bioavailable, and Selective Small-Molecule Inhibitor of Chemokine Receptor Ccr5 with Broad-Spectrum Anti-Human Immunodeficiency Virus Type 1 Activity. *Antimicrobial Agents and Chemotherapy*, 2005. **49**: 4721-4732.
193. Saita, Y., E. Kodama, M. Orita, M. Kondo, T. Miyazaki, K. Sudo, K. Kajiwara, M. Matsuoka, and Y. Shimizu, Structural Basis for the Interaction of Ccr5 with a Small Molecule, Functionally Selective Ccr5 Agonist. *J. Immunol.*, 2006. **177**: 3116-22.
194. Uy, G.L., M.P. Rettig, and A.F. Cashen, Plerixafor, a Cxcr4 Antagonist for the Mobilization of Hematopoietic Stem Cells. *Expert Opin. Biol. Ther.*, 2008. **8**: 1797-804.
195. Allen, S.J., S.E. Crown, and T.M. Handel, Chemokine: Receptor Structure, Interactions, and Antagonism. *Ann. Rev. Immunol.*, 2007. **25**: 787.
196. Gilliland, C.T., C.L. Salanga, T. Kawamura, J. Trejo, and T.M. Handel, The Chemokine Receptor Ccr1 Is Constitutively Active, Which Leads to G Protein-Independent, B-Arrestin-Mediated Internalization. *J. Biol. Chem.*, 2013. **288**: 32194.
197. Gao, W., P.S. Topham, J.A. King, S.T. Smiley, V. Csizmadia, B. Lu, C.J. Gerard, and W.W. Hancock, Targeting of the Chemokine Receptor Ccr1 Suppresses Development of Acute and Chronic Cardiac Allograft Rejection. *J. Clin. Invest.*, 2000. **105**: 35-44.
198. Saeki, T. and A. Naya, Ccr1 Chemokine Receptor Antagonist. *Curr. Pharm. Des.*, 2003. **9**: 1201-8.
199. Liang, M., et al., Identification and Characterization of a Potent, Selective, and Orally Active Antagonist of the Cc Chemokine Receptor-1. *J. Biol. Chem.*, 2000. **275**: 19000.
200. Anders, H.J., et al., Late Onset of Treatment with a Chemokine Receptor Ccr1 Antagonist Prevents Progression of Lupus Nephritis in Mrl-Fas(Lpr) Mice. *J. Am. Soc. Nephrol.*, 2004. **15**: 1504-13.
201. Anders, H.J., et al., A Chemokine Receptor Ccr-1 Antagonist Reduces Renal Fibrosis after Unilateral Ureter Ligation. *J. Clin. Invest.*, 2002. **109**: 251-9.
202. Kitamura, T., T. Fujishita, P. Loetscher, L. Revesz, H. Hashida, S. Kizaka-Kondoh, M. Aoki, and M.M. Taketo, Inactivation of Chemokine (C-C Motif) Receptor I (Ccr1) Suppresses Colon Cancer Liver Metastasis by Blocking Accumulation of Immature Myeloid Cells in a Mouse Model. *Proc. Natl. Acad. Sci. U S A*, 2010. **107**: 13063.
203. Lebre, M.C., C.E. Vergunst, I.Y. Choi, S. Aarrass, A.S. Oliveira, T. Wyant, R. Horuk, K.A. Reedquist, and P.P. Tak, Why Ccr2 and Ccr5 Blockade Failed and Why Ccr1 Blockade Might Still Be Effective in the Treatment of Rheumatoid Arthritis. *PLoS One*, 2011. **6**: e21772.
204. Dairaghi, D.J., B.O. Oyajobi, A. Gupta, B. McCluskey, S. Miao, J.P. Powers, L.C. Seitz, Y. Wang, Y. Zeng, P. Zhang, T.J. Schall, and J.C. Jaen, Ccr1 Blockade Reduces Tumor Burden and Osteolysis in Vivo in a Mouse Model of Myeloma Bone Disease. *Blood*, 2012. **120**: 1449-57.
205. Sabroe, I., M.J. Peck, B.J. Van Keulen, A. Jorritsma, G. Simmons, P.R. Clapham, T.J. Williams, and J.E. Pease, A Small Molecule Antagonist of Chemokine Receptors Ccr1 and Ccr3 - Potent Inhibition of Eosinophil Function and Ccr3-Mediated Hiv-1 Entry. *J. Biol. Chem.*, 2000. **275**: 25985-25992.
206. Gladue, R.P., et al., Cp-481,715, a Potent and Selective Ccr1 Antagonist with Potential Therapeutic Implications for Inflammatory Diseases. *J. Biol. Chem.*, 2003. **278**: 40473-80.

References

207. Gladue, R.P., S.H. Zwillich, A.T. Clucas, and M.F. Brown, Ccr1 Antagonists for the Treatment of Autoimmune Diseases. *Curr. Opin. Investig. Drugs*, 2004. **5**: 499-504.
208. Zipp, F., H.P. Hartung, J. Hillert, S. Schimrigk, C. Trebst, M. Stangel, C. Infante-Duarte, P. Jakobs, C. Wolf, R. Sandbrink, C. Pohl, M. Filippi, and C.C.R.A.S. Group, Blockade of Chemokine Signaling in Patients with Multiple Sclerosis. *Neurology*, 2006. **67**: 1880-3.
209. Gladue, R.P., M.F. Brown, and S.H. Zwillich, Ccr1 Antagonists: What Have We Learned from Clinical Trials. *Curr. Top. Med. Chem.*, 2010. **10**: 1268-77.
210. SchulzKnappe, P., et al., Hcc-1, a Novel Chemokine from Human Plasma. *J. Exp. Med.*, 1996. **183**: 295-299.
211. Richter, R., P. Schulz-Knappe, H. John, and W.G. Forssmann, Posttranslationally Processed Forms of the Human Chemokine Hcc-1. *Biochemistry*, 2000. **39**: 10799-805.
212. Tsou, C.L., R.P. Gladue, L.A. Carroll, T. Paradis, J.G. Boyd, R.T. Nelson, K. Neote, and I.F. Charo, Identification of C-C Chemokine Receptor 1 (Ccr1) as the Monocyte Hemofiltrate C-C Chemokine (Hcc)-1 Receptor. *J. Exp. Med.*, 1998. **188**: 603-8.
213. Pardigol, A., U. Forssmann, H.D. Zucht, P. Loetscher, P. Schulz-Knappe, M. Baggiolini, W.G. Forssmann, and H.J. Magert, Hcc-2, a Human Chemokine: Gene Structure, Expression Pattern, and Biological Activity. *Proc. Natl. Acad. Sci. U S A* 1998. **95**: 6308-6313.
214. Sticht, H., S.E. Escher, K. Schweimer, W.G. Forssmann, P. Rosch, and K. Adermann, Solution Structure of the Human Cc Chemokine 2: A Monomeric Representative of the Cc Chemokine Subtype. *Biochemistry*, 1999. **38**: 5995-6002.
215. Lee, J.K., E.H. Lee, Y.P. Yun, K. Kim, K. Kwack, D.S. Na, B.S. Kwon, and C.K. Lee, Truncation of Nh2-Terminal Amino Acid Residues Increases Agonistic Potency of Leukotactin-1 on Cc Chemokine Receptors 1 and 3. *J. Biol. Chem.*, 2002. **277**: 14757-63.
216. Patel, V.P., B.L. Kreider, Y. Li, H. Li, K. Leung, T. Salcedo, B. Nardelli, V. Pippalla, S. Gentz, R. Thotakura, D. Parmelee, R. Gentz, and G. Garotta, Molecular and Functional Characterization of Two Novel Human C-C Chemokines as Inhibitors of Two Distinct Classes of Myeloid Progenitors. *J. Exp. Med.*, 1997. **185**: 1163-72.
217. Rajarathnam, K., Y. Li, T. Rohrer, and R. Gentz, Solution Structure and Dynamics of Myeloid Progenitor Inhibitory Factor-1 (Mpif-1), a Novel Monomeric Cc Chemokine. *J. Biol. Chem.*, 2001. **276**: 4909-16.
218. Shin, Y.H., G.W. Lee, K.N. Son, S.M. Lee, C.J. Kang, B.S. Kwon, and J. Kim, Promoter Analysis of Human Cc Chemokine Ccl23 Gene in U937 Monocytoid Cells. *Biochim. Biophys. Acta.*, 2007. **1769**: 204-8.
219. Nardelli, B., H.L. Tiffany, G.W. Bong, P.A. Yourey, D.K. Morahan, Y. Li, P.M. Murphy, and R.F. Alderson, Characterization of the Signal Transduction Pathway Activated in Human Monocytes and Dendritic Cells by Mpif-1, a Specific Ligand for Cc Chemokine Receptor 1. *J. Immunol.*, 1999. **162**: 435-44.
220. Van Damme, J., P. Proost, J.P. Lenaerts, and G. Opdenakker, Structural and Functional Identification of Two Human, Tumor-Derived Monocyte Chemotactic Proteins (Mcp-2 and Mcp-3) Belonging to the Chemokine Family. *J. Exp. Med.*, 1992. **176**: 59-65.
221. Minty, A., P. Chalon, J.C. Guillemot, M. Kaghad, P. Liauzun, M. Magazin, B. Miloux, C. Minty, P. Ramond, N. Vita, and et al., Molecular Cloning of the Mcp-3 Chemokine Gene and Regulation of Its Expression. *Eur. Cytokine Netw.*, 1993. **4**: 99-110.
222. Proost, P., A. Wuyts, and J. Van Damme, Human Monocyte Chemotactic Proteins-2 and -3: Structural and Functional Comparison with Mcp-1. *J. Leukoc. Biol.*, 1996. **59**: 67-74.
223. Kim, K.S., K. Rajarathnam, I. Clark-Lewis, and B.D. Sykes, Structural Characterization of a Monomeric Chemokine: Monocyte Chemoattractant Protein-3. *FEBS Lett.*, 1996. **395**: 277-82.
224. Els Van Coillie, Jo Van Damme, and G. Opdenakker, The Mcp/Eotaxin Subfamily of Cc Chemokines. *Cytokine & Growth Factor Reviews*, 1999. **10**: 61 - 86.
225. Pease, J. and R. Horuk, Chemokine Receptor Antagonists. *Journal of Medicinal Chemistry*, 2012. **55**: 9363-9392.

226. Scholten, D.J., M. Canals, D. Maussang, L. Roumen, M.J. Smit, M. Wijtmans, C. de Graaf, H.F. Vischer, and R. Leurs, Pharmacological Modulation of Chemokine Receptor Function. *Br. J. Pharmacol.*, 2012. **165**: 1617-1643.
227. Duvic, M., M. Evans, and C. Wang, Mogamulizumab for the Treatment of Cutaneous T-Cell Lymphoma: Recent Advances and Clinical Potential. *Therapeutic Advances in Hematology*, 2016. **7**: 171-174.
228. Griffiths, K., et al., I-Bodies, Human Single Domain Antibodies That Antagonize Chemokine Receptor Cxcr4. *Journal of Biological Chemistry*, 2016. **291**: 12641-12657.
229. Sozzani, S., et al., The Viral Chemokine Macrophage Inflammatory Protein-II Is a Selective Th2 Chemoattractant. *Blood*, 1998. **92**: 4036-4039.
230. Solari, R. and J.E. Pease, Targeting Chemokine Receptors in Disease--a Case Study of Ccr4. *Eur. J. Pharmacol.*, 2015. **763**: 169-77.
231. Morokata, T., et al., A Novel, Selective, and Orally Available Antagonist for Cc Chemokine Receptor 3. *J. Pharmacol. Exp. Ther.*, 2006. **317**: 244-50.
232. Karpus, W.J., N.W. Lukacs, B.L. McRae, R.M. Strieter, S.L. Kunkel, and S.D. Miller, An Important Role for the Chemokine Macrophage Inflammatory Protein-1 Alpha in the Pathogenesis of the T Cell-Mediated Autoimmune Disease, Experimental Autoimmune Encephalomyelitis. *J. Immunol.*, 1995. **155**: 5003-10.
233. Smith, E.W., Y. Liu, A.E. Getschman, F.C. Peterson, J.J. Ziarek, R. Li, B.F. Volkman, and Y. Chen, Structural Analysis of a Novel Small Molecule Ligand Bound to the Cxcl12 Chemokine. *J. Med. Chem.*, 2014. **57**: 9693-9.
234. Rivera-Delgado, E., Z. Sadeghi, N.X. Wang, J. Kenyon, S. Satyanarayan, M. Kavran, C. Flask, A.Z. Hijaz, and H.A. von Recum, Local Release from Affinity-Based Polymers Increases Urethral Concentration of the Stem Cell Chemokine Ccl7 in Rats. *Biomed. Mater.*, 2016. **11**: 025022.
235. Isahak, N., J. Sanchez, S. Perrier, M.J. Stone, and R.J. Payne, Synthesis of Polymers and Nanoparticles Bearing Polystyrene Sulfonate Brushes for Chemokine Binding. *Org. Biomol. Chem.*, 2016. **14**: 5652-8.
236. Popova, T.G., A. Teunis, R. Magni, A. Luchini, V. Espina, L.A. Liotta, and S.G. Popov, Chemokine-Releasing Nanoparticles for Manipulation of the Lymph Node Microenvironment. *Nanomaterials (Basel)*, 2015. **5**: 298-320.
237. Mao-Yu, Z., L. Jin-Jian, L. Wang, G. Zi-Chao, H. Hu, U. Carolina Oi Lam, and W. Yi-Tao, Development of Monoclonal Antibodies in China: Overview and Prospects. *BioMed Research International*, 2015.
238. Klarenbeek, A., D. Maussang, C. Blanchetot, M. Saunders, S. van der Woning, M. Smit, H. de Haard, and E. Hofman, Targeting Chemokines and Chemokine Receptors with Antibodies. *Drug Discovery Today: Technologies*, 2012. **9**: e237-e244.
239. Oberthür, D., J. Achenbach, A. Gabdulkhakov, K. Buchner, C. Maasch, S. Falke, D. Rehders, S. Klussmann, and C. Betzel, Crystal Structure of a Mirror-Image L-Rna Aptamer (Spiegelmer) in Complex with the Natural L-Protein Target Ccl2. *Nature Communications*, 2015. **6**: 6923.
240. Montaner, S., I. Kufareva, R. Abagyan, and S.J. Gutkind, Molecular Mechanisms Deployed by Virally Encoded G Protein–Coupled Receptors in Human Diseases. *Annual Review of Pharmacology and Toxicology*, 2013. **53**: 331-354.
241. Dagna, L. and P. Lusso, Virus-Encoded Chemokines, Chemokine Receptors and Chemokine-Binding Proteins: New Paradigms for Future Therapy. *Future Virology*, 2007. **2**: 353-368.
242. Vischer, H.F., M. Siderius, R. Leurs, and M.J. Smit, Herpesvirus-Encoded Gpcrs: Neglected Players in Inflammatory and Proliferative Diseases? *Nature Reviews. Drug Discovery*, 2014. **13**: 123-39.
243. Wang, X., J. Sanchez, M.J. Stone, and R.J. Payne, Sulfation of the Human Cytomegalovirus Protein Ul22a Enhances Binding to the Chemokine Rantes. *Angew. Chem. Int. Ed. Engl.*, 2017.
244. Wang, D., W. Bresnahan, and T. Shenk, Human Cytomegalovirus Encodes a Highly Specific Rantes Decoy Receptor. *Proc. Natl. Acad. Sci. U S A*, 2004. **101**: 16642-7.
245. Burns, J.M., D.J. Dairaghi, M. Deitz, M. Tsang, and T.J. Schall, Comprehensive Mapping of Poxvirus Vcci Chemokine-Binding Protein. Expanded Range of Ligand Interactions and Unusual Dissociation Kinetics. *J. Biol. Chem.*, 2002. **277**: 2785-9.

References

246. Carfi, A., C.A. Smith, P.J. Smolak, J. McGrew, and D.C. Wiley, Structure of a Soluble Secreted Chemokine Inhibitor Vcci (P35) from Cowpox Virus. *Proc. Natl. Acad. Sci. U S A*, 1999. **96**: 12379-83.
247. Zhang, L., M. Derider, M.A. McCornack, S.C. Jao, N. Isern, T. Ness, R. Moyer, and P.J. LiWang, Solution Structure of the Complex between Poxvirus-Encoded Cc Chemokine Inhibitor Vcci and Human Mip-1β. *Proc. Natl. Acad. Sci. U S A*, 2006. **103**: 13985-90.
248. Bahar, M.W., J.C. Kenyon, M.M. Putz, N.G. Abrescia, J.E. Pease, E.L. Wise, D.I. Stuart, G.L. Smith, and J.M. Grimes, Structure and Function of A41, a Vaccinia Virus Chemokine Binding Protein. *PLoS Pathog.*, 2008. **4**: e5.
249. Xue, X., Q. Lu, H. Wei, D. Wang, D. Chen, G. He, L. Huang, H. Wang, and X. Wang, Structural Basis of Chemokine Sequestration by Crmd, a Poxvirus-Encoded Tumor Necrosis Factor Receptor. *PLoS Pathog.*, 2011. **7**: e1002162.
250. Smith, P., R.E. Fallon, N.E. Mangan, C.M. Walsh, M. Saraiva, J.R. Sayers, A.N. McKenzie, A. Alcami, and P.G. Fallon, Schistosoma Mansoni Secretes a Chemokine Binding Protein with Antiinflammatory Activity. *J. Exp. Med.*, 2005. **202**: 1319-25.
251. Mans, B.J., D. de Klerk, R. Pienaar, M.H. de Castro, and A.A. Latif, The Mitochondrial Genomes of Nuttalliella Namaqua (Ixodoidea: Nuttalliellidae) and Argas Africolumbae (Ixodoidae: Argasidae): Estimation of Divergence Dates for the Major Tick Lineages and Reconstruction of Ancestral Blood-Feeding Characters. *PLoS One*, 2012. **7**: e49461.
252. Guglielmone, A.A.a., The Hard Ticks of the World : (Acari: Ixodida: Ixodidae). 2014: Dordrecht : Springer.
253. Hovius, J.W., Spitting Image: Tick Saliva Assists the Causative Agent of Lyme Disease in Evading Host Skin's Innate Immune Response. *J. Invest. Dermatol.*, 2009. **129**: 2337-9.
254. Kazimirova, M. and I. Stibraniova, Tick Salivary Compounds: Their Role in Modulation of Host Defences and Pathogen Transmission. *Front. Cell Infect. Microbiol.*, 2013. **3**: 43.
255. Anatriello, E., J.M. Ribeiro, I.K. de Miranda-Santos, L.G. Brandao, J.M. Anderson, J.G. Valenzuela, S.R. Maruyama, J.S. Silva, and B.R. Ferreira, An Insight into the Sialotranscriptome of the Brown Dog Tick, Rhipicephalus Sanguineus. *BMC Genomics*, 2010. **11**: 450.
256. Deruaz, M., A. Frauenschuh, A.L. Alessandri, J.M. Dias, F.M. Coelho, R.C. Russo, B.R. Ferreira, G.J. Graham, J.P. Shaw, T.N. Wells, M.M. Teixeira, C.A. Power, and A.E. Proudfoot, Ticks Produce Highly Selective Chemokine Binding Proteins with Antiinflammatory Activity. *J. Exp. Med.*, 2008. **205**: 2019-31.
257. Frauenschuh, A., C.A. Power, M. Deruaz, B.R. Ferreira, J.S. Silva, M.M. Teixeira, J.M. Dias, T. Martin, T.N. Wells, and A.E. Proudfoot, Molecular Cloning and Characterization of a Highly Selective Chemokine-Binding Protein from the Tick Rhipicephalus Sanguineus. *J. Biol. Chem.*, 2007. **282**: 27250-8.
258. Bachelerie, F., et al., International Union of Basic and Clinical Pharmacology. [Corrected]. Lxxxix. Update on the Extended Family of Chemokine Receptors and Introducing a New Nomenclature for Atypical Chemokine Receptors. *Pharmacol. Rev.*, 2014. **66**: 1-79.
259. Dias, J.M., C. Losberger, M. Deruaz, C.A. Power, A.E. Proudfoot, and J.P. Shaw, Structural Basis of Chemokine Sequestration by a Tick Chemokine Binding Protein: The Crystal Structure of the Complex between Evasin-1 and Ccl3. *PLoS One*, 2009. **4**: e8514.
260. Nonaka, E., G.D. Ebel, and H.J. Wearing, Persistence of Pathogens with Short Infectious Periods in Seasonal Tick Populations: The Relative Importance of Three Transmission Routes. *PLoS One*, 2010. **5**: e11745.
261. Hai, V.V., L. Almeras, C. Socolovschi, D. Raoult, P. Parola, and F. Pages, Monitoring Human Tick-Borne Disease Risk and Tick Bite Exposure in Europe: Available Tools and Promising Future Methods. *Ticks Tick Borne Dis.*, 2014. **5**: 607-19.
262. Russo, R.C., A.L. Alessandri, C.C. Garcia, B.F. Cordeiro, V. Pinho, G.D. Cassali, A.E. Proudfoot, and M.M. Teixeira, Therapeutic Effects of Evasin-1, a Chemokine Binding Protein, in Bleomycin-Induced Pulmonary Fibrosis. *Am. J. Respir. Cell Mol. Biol.*, 2011. **45**: 72-80.
263. Vieira, A.T., et al., Treatment with a Novel Chemokine-Binding Protein or Eosinophil Lineage-Ablation Protects Mice from Experimental Colitis. *Am. J. Pathol.*, 2009. **175**: 2382-91.

264. Montecucco, F., F. Mach, S. Lenglet, A. Vonlaufen, A.L. Gomes Quindere, G. Pelli, F. Burger, K. Galan, F. Dallegri, F. Carbone, A.E. Proudfoot, N. Vuilleumier, and J.L. Frossard, Treatment with Evasin-3 Abrogates Neutrophil-Mediated Inflammation in Mouse Acute Pancreatitis. *Eur. J. Clin. Invest.*, 2014. **44**: 940-50.
265. Bonvin, P., C.A. Power, and A.E. Proudfoot, Evasins: Therapeutic Potential of a New Family of Chemokine-Binding Proteins from Ticks. *Front. Immunol.*, 2016. **7**: 208.
266. Abboud, D. and J. Hanson, Chemokine Neutralization as an Innovative Therapeutic Strategy for Atopic Dermatitis. *Drug Discov Today*, 2017. **22**: 702-711.
267. Hartman, M.H.T., H.E. Groot, I.M. Leach, J.C. Karper, and P. van der Harst, Translational Overview of Cytokine Inhibition in Acute Myocardial Infarction and Chronic Heart Failure. *Trends Cardiovasc Med*, 2018.
268. Scholten, D.J., M. Canals, M. Wijtmans, S. de Munnik, P. Nguyen, D. Verzijl, I.J. de Esch, H.F. Vischer, M.J. Smit, and R. Leurs, Pharmacological Characterization of a Small-Molecule Agonist for the Chemokine Receptor Cxcr3. *Br. J. Pharmacol.*, 2012. **166**: 898-911.
269. Hollins, B., S. Kuravi, G.J. Digby, and N.A. Lambert, The C-Terminus of Grk3 Indicates Rapid Dissociation of G Protein Heterotrimers. *Cell Signal*, 2009. **21**: 1015-21.
270. Zweemer, A.J., I. Nederpelt, H. Vrieling, S. Hafith, M.L. Doornbos, H. de Vries, J. Abt, R. Gross, D. Stamos, J. Saunders, M.J. Smit, A.P. Ijzerman, and L.H. Heitman, Multiple Binding Sites for Small-Molecule Antagonists at the Cc Chemokine Receptor 2. *Mol. Pharmacol.*, 2013. **84**: 551-61.
271. Smith, P.K., R.I. Krohn, G.T. Hermanson, A.K. Mallia, F.H. Gartner, M.D. Provenzano, E.K. Fujimoto, N.M. Goeke, B.J. Olson, and D.C. Klenk, Measurement of Protein Using Bicinchoninic Acid. *Anal. Biochem.*, 1985. **150**: 76-85.
272. Huff, S., Y.V. Matsuka, M.J. McGavin, and K.C. Ingham, Interaction of N-Terminal Fragments of Fibronectin with Synthetic and Recombinant D Motifs from Its Binding Protein on Staphylococcus Aureus Studied Using Fluorescence Anisotropy. *J. Biol. Chem.*, 1994. **269**: 15563-70.
273. Black, J.W., P. Leff, N.P. Shankley, and J. Wood, An Operational Model of Pharmacological Agonism: The Effect of E/[a] Curve Shape on Agonist Dissociation Constant Estimation. *Br. J. Pharmacol.*, 1985. **84**: 561-71.
274. Christopoulos, A., Assessing the Distribution of Parameters in Models of Ligand-Receptor Interaction: To Log or Not to Log. *Trends Pharmacol. Sci.*, 1998. **19**: 351-7.
275. Robinson, S.C., K.A. Scott, J.L. Wilson, R.G. Thompson, A.E. Proudfoot, and F.R. Balkwill, A Chemokine Receptor Antagonist Inhibits Experimental Breast Tumor Growth. *Cancer Res*, 2003. **63**: 8360-5.
276. O'Hayre, M., C.L. Salanga, T.M. Handel, and D.J. Hamel, Emerging Concepts and Approaches for Chemokine-Receptor Drug Discovery. *Expert Opin. Drug Discov.*, 2010. **5**: 1109-22.
277. Yoshie, O., Chemokine Receptors as Therapeutic Targets. *Nihon Rinsho Meneki Gakkai Kaishi*, 2013. **36**: 189-96.
278. Kenakin, T., Biased Agonism. *F1000 Biol. Rep.*, 2009. **1**: 87.
279. Zidar, D.A., Endogenous Ligand Bias by Chemokines: Implications at the Front Lines of Infection and Leukocyte Trafficking. *Endocr. Metab. Immune Disord. Drug Targets*, 2011. **11**: 120-31.
280. Crump, M.P., J.H. Gong, P. Loetscher, K. Rajarathnam, A. Amara, F. Arenzana-Seisdedos, J.L. Virelizier, M. Baggiolini, B.D. Sykes, and I. Clark-Lewis, Solution Structure and Basis for Functional Activity of Stromal Cell-Derived Factor-1; Dissociation of Cxcr4 Activation from Binding and Inhibition of Hiv-1. *EMBO J.*, 1997. **16**: 6996-7007.
281. Kenakin, T., Quantifying Biological Activity in Chemical Terms: A Pharmacology Primer to Describe Drug Effect. *ACS Chem. Biol.*, 2009. **4**: 249-60.
282. Berchiche, Y.A., S. Gravel, M.E. Pelletier, G. St-Onge, and N. Heveker, Different Effects of the Different Natural Cc Chemokine Receptor 2b Ligands on β-Arrestin Recruitment, Gαi Signaling, and Receptor Internalization. *Mol. Pharmacol.*, 2011. **79**: 488-98.
283. Klaassen, C.D. and J.W. Boles, Sulfation and Sulfotransferases 5: The Importance of 3'-Phosphoadenosine 5'-Phosphosulfate (Paps) in the Regulation of Sulfation. *FASEB J.*, 1997. **11**: 404-18.

References

284. Klein Herenbrink, C., D.A. Sykes, P. Donthamsetti, M. Canals, T. Coudrat, J. Shonberg, P.J. Scammells, B. Capuano, P.M. Sexton, S.J. Charlton, J.A. Javitch, A. Christopoulos, and J.R. Lane, The Role of Kinetic Context in Apparent Biased Agonism at Gpcrs. *Nat. Commun.*, 2016. **7**: 10842.
285. Starr, A.E., A. Dufour, J. Maier, and C.M. Overall, Biochemical Analysis of Matrix Metalloproteinase Activation of Chemokines Ccl15 and Ccl23 and Increased Glycosaminoglycan Binding of Ccl16. *J. Biol. Chem.*, 2012. **287**: 5848-60.
286. Gladue, R.P., S.H. Zwillich, A.T. Clucas, and M.F. Brown, Ccr1 Antagonists for the Treatment of Autoimmune Diseases. *Curr Opin Investig Drugs*, 2004. **5**: 499-504.
287. Huma, Z.E., J. Sanchez, H.D. Lim, J.L. Bridgford, C. Huang, B.J. Parker, J.G. Pazhamalil, B.T. Porebski, K.D.G. Pfleger, J.R. Lane, M. Canals, and M.J. Stone, Key Determinants of Selective Binding and Activation by the Monocyte Chemoattractant Proteins at the Chemokine Receptor Ccr2. *Sci. Signal.*, 2017. **10**.
288. Jarnagin, K., et al., Identification of Surface Residues of the Monocyte Chemotactic Protein 1 That Affect Signaling through the Receptor Ccr2. *Biochemistry*, 1999. **38**: 16167-77.
289. Clark-Lewis, I., B. Dewald, M. Loetscher, B. Moser, and M. Baggiolini, Structural Requirements for Interleukin-8 Function Identified by Design of Analogs and Cxc Chemokine Hybrids. *J. Biol. Chem.*, 1994. **269**: 16075-81.
290. Fonseca, N.A., C.P. Vieira, and J. Vieira, Gene Classification Based on Amino Acid Motifs and Residues: The Dlx (Distal-Less) Test Case. *PLoS One*, 2009. **4**: e5748.
291. Ludeman, J.P., M. Nazari-Robati, B.L. Wilkinson, C. Huang, R.J. Payne, and M.J. Stone, Phosphate Modulates Receptor Sulfotyrosine Recognition by the Chemokine Monocyte Chemoattractant Protein-1 (Mcp-1/Ccl2). *Org. Biomol. Chem.*, 2015. **13**: 2162-9.
292. Lakowicz, J.R., Principles of Fluorescence Spectroscopy. 3rd ed. ed, ed. SpringerLink. 2006, New York: New York : Springer.
293. Ho, H.H., D. Du, and M.C. Gershengorn, The N Terminus of Kaposi's Sarcoma-Associated Herpesvirus G Protein-Coupled Receptor Is Necessary for High Affinity Chemokine Binding but Not for Constitutive Activity. *J Biol Chem*, 1999. **274**: 31327-32.
294. Hemmerich, S., et al., Identification of Residues in the Monocyte Chemotactic Protein-1 That Contact the Mcp-1 Receptor, Ccr2. *Biochemistry*, 1999. **38**: 13013-25.
295. Zlotnik, A. and O. Yoshie, The Chemokine Superfamily Revisited. *Immunity*, 2012. **36**: 705-16.
296. Anderson, C.A., R. Solari, and J.E. Pease, Biased Agonism at Chemokine Receptors: Obstacles or Opportunities for Drug Discovery? *J. Leukoc. Biol.*, 2016. **99**: 901-9.
297. Steen, A., O. Larsen, S. Thiele, and M.M. Rosenkilde, Biased and G Protein-Independent Signaling of Chemokine Receptors. *Front. Immunol.*, 2014. **5**: 277.
298. Monteclaro, F.S. and I.F. Charo, The Amino-Terminal Extracellular Domain of the Mcp-1 Receptor, but Not the Rantes/Mip-1α Receptor, Confers Chemokine Selectivity. Evidence for a Two-Step Mechanism for Mcp-1 Receptor Activation. *J. Biol. Chem.*, 1996. **271**: 19084-92.
299. Yoshiura, C., T. Ueda, Y. Kofuku, M. Matsumoto, J. Okude, K. Kondo, Y. Shiraishi, and I. Shimada, Elucidation of the Ccr1- and Ccr5-Binding Modes of Mip-1α by Application of an Nmr Spectra Reconstruction Method to the Transferred Cross-Saturation Experiments. *J. Biomol. NMR.*, 2015. **63**: 333-40.
300. Mishiro, E., Y. Sakakibara, M.C. Liu, and M. Suiko, Differential Enzymatic Characteristics and Tissue-Specific Expression of Human Tpst-1 and Tpst-2. *J. Biol. Chem.*, 2006. **140**: 731-7.
301. Solari, R., J.E. Pease, and M. Begg, "Chemokine Receptors as Therapeutic Targets: Why Aren't There More Drugs?". *Eur. J. Pharmacol.*, 2015. **746**: 363-7.
302. Allegretti, M., M.C. Cesta, A. Garin, and A.E. Proudfoot, Current Status of Chemokine Receptor Inhibitors in Development. *Immunol. Lett.*, 2012. **145**: 68-78.
303. Proudfoot, A.E., C.A. Power, and M.K. Schwarz, Anti-Chemokine Small Molecule Drugs: A Promising Future? *Expert. Opin. Investig. Drugs.*, 2010. **19**: 345-55.
304. Wells, T.N., C.A. Power, J.P. Shaw, and A.E. Proudfoot, Chemokine Blockers--Therapeutics in the Making? *Trends Pharmacol. Sci.*, 2006. **27**: 41-7.
305. Seet, B.T. and G. McFadden, Viral Chemokine-Binding Proteins. *J. Leukoc. Biol.*, 2002. **72**: 24-34.

306. Heidarieh, H., B. Hernaez, and A. Alcami, Immune Modulation by Virus-Encoded Secreted Chemokine Binding Proteins. *Virus Res.*, 2015. **209**: 67-75.
307. Proudfoot, A.E., P. Bonvin, and C.A. Power, Targeting Chemokines: Pathogens Can, Why Can't We? *Cytokine*, 2015. **74**: 259-67.
308. Frauenschuh, A., C.A. Power, M. Deruaz, B.R. Ferreira, J.S. Silva, M.M. Teixeira, J.M. Dias, T. Martin, T.N. Wells, and A.E. Proudfoot, Molecular Cloning and Characterization of a Highly Selective Chemokine-Binding Protein from the Tick Rhipicephalus Sanguineus. *J Biol Chem*, 2007. **282**: 27250-8.
309. Butcher, E.C. and L.J. Picker, Lymphocyte Homing and Homeostasis. *Science*, 1996. **272**: 60-6.
310. Mantovani, A., B. Savino, M. Locati, L. Zammataro, P. Allavena, and R. Bonecchi, The Chemokine System in Cancer Biology and Therapy. *Cytokine Growth Factor Rev.*, 2010. **21**: 27-39.
311. Van Damme, J., S. Struyf, and G. Opdenakker, Chemokine-Protease Interactions in Cancer. *Semin. Cancer Biol.*, 2004. **14**: 201-8.
312. Vandercappellen, J., J. Van Damme, and S. Struyf, The Role of Cxc Chemokines and Their Receptors in Cancer. *Cancer Lett.*, 2008. **267**: 226-44.
313. Awad, A.S., G.R. Kinsey, K. Khutsishvili, T. Gao, W.K. Bolton, and M.D. Okusa, Monocyte/Macrophage Chemokine Receptor Ccr2 Mediates Diabetic Renal Injury. *Am. J. Physiol. Renal Physiol.*, 2011. **301**: F1358-66.
314. Sorensen, T.L., M. Tani, J. Jensen, V. Pierce, C. Lucchinetti, V.A. Folcik, S. Qin, J. Rottman, F. Sellebjerg, R.M. Strieter, J.L. Frederiksen, and R.M. Ransohoff, Expression of Specific Chemokines and Chemokine Receptors in the Central Nervous System of Multiple Sclerosis Patients. *J. Clin. Invest.*, 1999. **103**: 807-15.
315. Zhang, G.X., C.M. Baker, D.L. Kolson, and A.M. Rostami, Chemokines and Chemokine Receptors in the Pathogenesis of Multiple Sclerosis. *Mult. Scler.*, 2000. **6**: 3-13.
316. Kipp, M., P. van der Valk, and S. Amor, Pathology of Multiple Sclerosis. *CNS Neurol. Disord. Drug Targets*, 2012. **11**: 506-17.
317. Szekanecz, Z., J. Kim, and A.E. Koch, Chemokines and Chemokine Receptors in Rheumatoid Arthritis. *Semin. Immunol.*, 2003. **15**: 15-21.
318. Libby, P., Inflammation in Atherosclerosis. *Arterioscl. Thromb. Vasc. Biol.*, 2012. **32**: 2045-51.
319. Wells, T.N., C.A. Power, J.P. Shaw, and A.E. Proudfoot, Chemokine Blockers--Therapeutics in the Making? *Trends Pharmacol Sci*, 2006. **27**: 41-7.
320. Proudfoot, A.E., C.A. Power, C. Rommel, and T.N. Wells, Strategies for Chemokine Antagonists as Therapeutics. *Semin. Immunol.*, 2003. **15**: 57-65.
321. Hayward, J., J. Sanchez, A. Perry, C. Huang, M. Rodriguez Valle, M. Canals, R.J. Payne, and M.J. Stone, Ticks from Diverse Genera Encode Chemokine-Inhibitory Evasin Proteins. *J. Biol. Chem.*, 2017. **292**: 15670-15680.
322. Hoffmann, C., A. Zurn, M. Bunemann, and M.J. Lohse, Conformational Changes in G-Protein-Coupled Receptors-the Quest for Functionally Selective Conformations Is Open. *Br. J. Pharmacol.*, 2008. **153 Suppl 1**: S358-66.
323. Sridharan, R., J. Zuber, S.M. Connelly, E. Mathew, and M.E. Dumont, Fluorescent Approaches for Understanding Interactions of Ligands with G Protein-Coupled Receptors. *Biochim. Biophys. Acta.*, 2014. **1838**: 15-33.
324. Vilardaga, J.P., M. Bunemann, C. Krasel, M. Castro, and M.J. Lohse, Measurement of the Millisecond Activation Switch of G Protein-Coupled Receptors in Living Cells. *Nat. Biotechnol.*, 2003. **21**: 807-12.
325. Gong, J.H. and I. Clark-Lewis, Antagonists of Monocyte Chemoattractant Protein 1 Identified by Modification of Functionally Critical Nh2-Terminal Residues. *J. Exp. Med.*, 1995. **181**: 631-40.
326. Clark-Lewis, I., I. Mattioli, J.H. Gong, and P. Loetscher, Structure-Function Relationship between the Human Chemokine Receptor Cxcr3 and Its Ligands. *J. Biol. Chem.*, 2003. **278**: 289-95.
327. Zoffmann, S., A. Chollet, and J.L. Galzi, Identification of the Extracellular Loop 2 as the Point of Interaction between the N Terminus of the Chemokine Mip-1α and Its Ccr1 Receptor. *Mol. Pharmacol.*, 2002. **62**: 729-36.

References

328. Kleist, A.B., A.E. Getschman, J.J. Ziarek, A.M. Nevins, P.A. Gauthier, A. Chevigne, M. Szpakowska, and B.F. Volkman, New Paradigms in Chemokine Receptor Signal Transduction: Moving Beyond the Two-Site Model. *Biochem. Pharmacol.*, 2016. **114**: 53-68.
329. Arimont, M., S.L. Sun, R. Leurs, M. Smit, I.J.P. de Esch, and C. de Graaf, Structural Analysis of Chemokine Receptor-Ligand Interactions. *J. Med. Chem.*, 2017. **60**: 4735-4779.
330. Wescott, M.P., I. Kufareva, C. Paes, J.R. Goodman, Y. Thaker, B.A. Puffer, E. Berdougo, J.B. Rucker, T.M. Handel, and B.J. Doranz, Signal Transmission through the Cxc Chemokine Receptor 4 (Cxcr4) Transmembrane Helices. *Proc. Natl. Acad. Sci. U S A*, 2016. **113**: 9928-33.

Appendices

Appendix I

Correspondence table showing systematic names, abbreviated names and full common names of chemokines mentioned in this thesis

Appendix II

G protein activation screen and timecourse at CCR1 (full data set for Chapter 3, section 3.5)

Appendix III

CCR1 activation by MCP-1/3 chimeras (full data set for Chapter 4, section 4.3.2)

Appendix IV

Oligonucleotide sequences for chemokine and chemokine receptor cloning

Appendix V

Supplementary material for “Tick from Diverse Genera Encode Chemokine-Inhibitory Evasin Proteins” (Chapter 5) [Hayward J.*, **Sanchez J**.*, Perry A., Huang C., Valle M. R., Canals M., Payne R. J. and Stone M. J., Ticks from Diverse Genera Encode Chemokine-Inhibitory Evasin Proteins. J. Biol. Chem. 2017; DOI: 10.1074/jbc.M117.807255; *, these authors contributed equally to this work]

Appendix I: Correspondence Table for Systematic and Common Chemokine Names

Systematic Names	Abbreviated Names	Common Names
CCL1	I-309	T Lymphocyte-Secreted Protein I-309
CCL2	MCP-1	Monocyte Chemoattractant Protein 1
CCL3	MIP-1α	Macrophage Inflammatory Protein 1α
CCL4	MIP-1β	Macrophage Inflammatory Protein 1β
CCL5	RANTES	Regulated upon Activation, Normally T cell Expressed And Secreted
CCL7	MCP-3	Monocyte Chemoattractant Protein 3
CCL8	MCP-2	Monocyte Chemoattractant Protein 2
CCL11	Eotaxin-1	Eotaxin 1
CCL13	MCP-4	Monocyte Chemoattractant Protein 4
CCL14	HCC-1	Hemofiltrate CC Chemokine 1
CCL15	HCC-2/Lkn-1	Hemofiltrate CC Chemokine 2/Leukotactin 1
CCL16	HCC-4	Hemofiltrate CC Chemokine 4
CCL17	TARC	Thymus And Activation-Regulated Chemokine
CCL18	PARC	Pulmonary And Activation-Regulated Chemokine
CCL19	ELC/MIP-3β	Epstein-Barr Virus-Induced Molecule 1 Ligand Chemokine/Macrophage Inflammatory Protein 3β
CCL20	MIP-3α	Macrophage Inflammatory Protein 3α
CCL21	SLC	Secondary Lymphoid Tissue Chemokine
CCL22	MDC	Macrophage-Derived Chemokine
CCL23	MPIF-1	Myeloid Progenitor Inhibitory Factor 1
CCL24	Eotaxin-2	Eotaxin 2
CCL25	TECK	Thymus Expressed Chemokine
CCL26	Eotaxin-3	Eotaxin 3
CCL27	CTACK	Cutaneous T-Cell Attracting Chemokine
CCL28	MEC	Mucosae-Associated Epithelial Chemokine
CXCL1	Gro-α	Melanoma Growth Stimulatory Activity α
CXCL2	Gro-β	Melanoma Growth Stimulatory Activity β
CXCL3	Gro-γ	Melanoma Growth Stimulatory Activity γ
CXCL4	PF4	Platelet Factor 4
CXCL5	ENA78	Epithelial-Derived Neutrophil-Activating Protein 78
CXCL6	GCP-2	Granulocyte Chemotactic Protein 2
CXCL7	PPBP	Pro-Platelet Basic Protein
CXCL8	IL-8	Interleukin 8
CXCL9	MIG	Monokine Induced By Interferon-Gamma
CXCL10	IP-10	10 kDa Interferon Gamma-Induced Protein
CXCL11	I-TAC	Interferon-Inducible T-Cell Alpha Chemoattractant
CXCL12	SDF-1	Stromal Cell-Derived Factor 1
CXCL13	BLC	B Lymphocyte Chemoattractant
CXCL14	BRAK	Breast and Kidney-Expressed Chemokine
CXCL16	SRPSOX	Scavenger Receptor For Phosphatidylserine And Oxidized Low Density Lipoprotein
CXCL17	vCC1	VEGF Coregulated Chemokine 1
CX_3CL1	Fractalkine	Fractalkine
XCL1	SCM-1α	Single Cysteine Motif 1α / Lymphotactin
XCL2	SCM-1β	Single Cysteine Motif 1β

Table I.1: Correspondence Table between Common and Systematic Chemokine Names. The systematic name, abbreviated names and common name are provided for each chemokine mentioned in this thesis.

Appendix II: Gα Screen and Timecourse

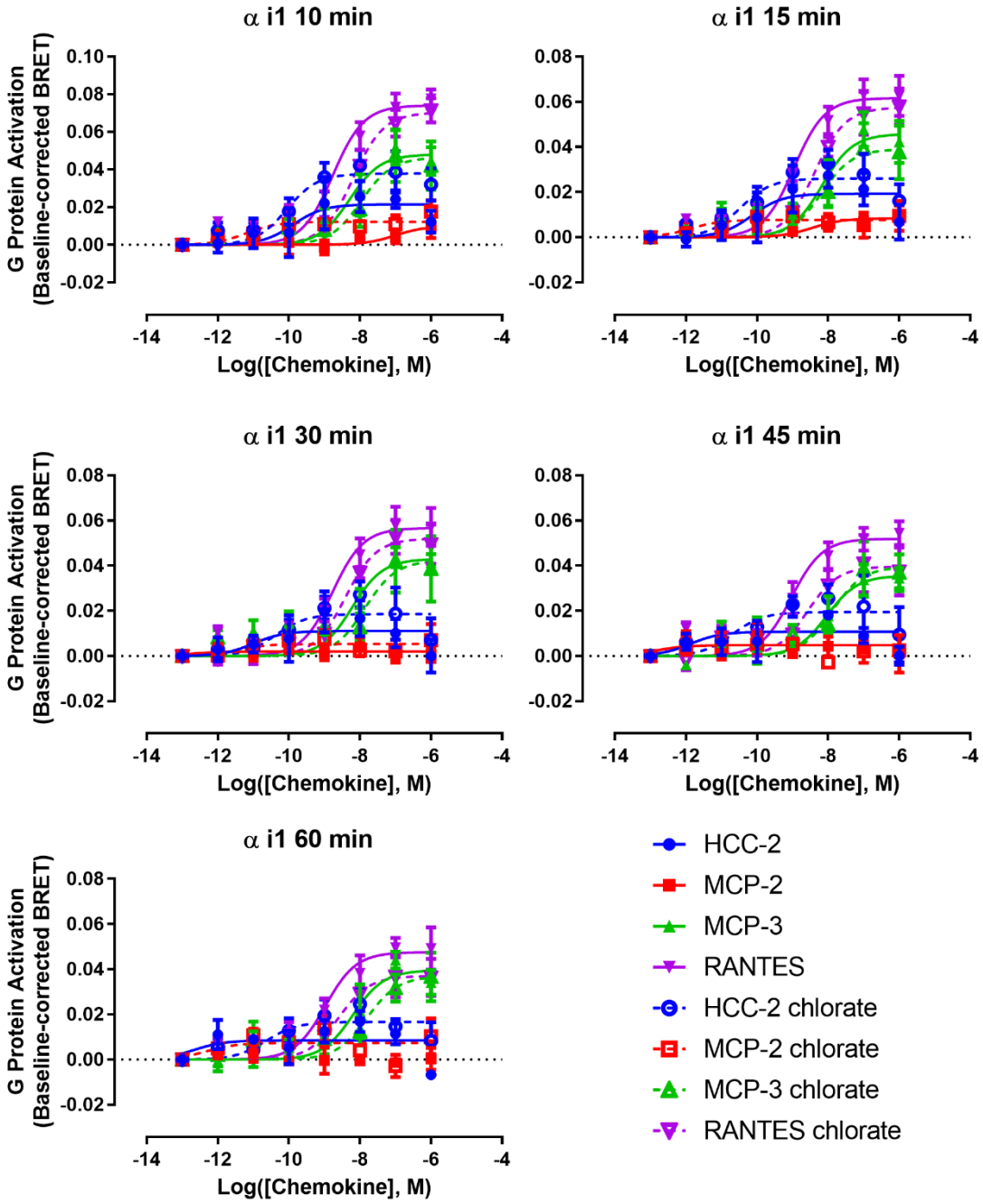

Figure II.1: $G\alpha_{i1}$ Concentration-response Curves and Timecourse. GPA was measured using His_6-c-Myc-CCR1 Flp-In T-REx HEK 293 cells and $G\alpha_{i1}$. Transfections were performed as described in Chapter 2, section 2.7.6. Each graph shows, for a given time after addition of chemokines, the concentration-response data for four chemokines HCC-2, MCP-2, MCP-3 and RANTES using non-treated or chlorate-treated cells. Data points represent means ± SEM of at least three independent experiments performed in duplicate.

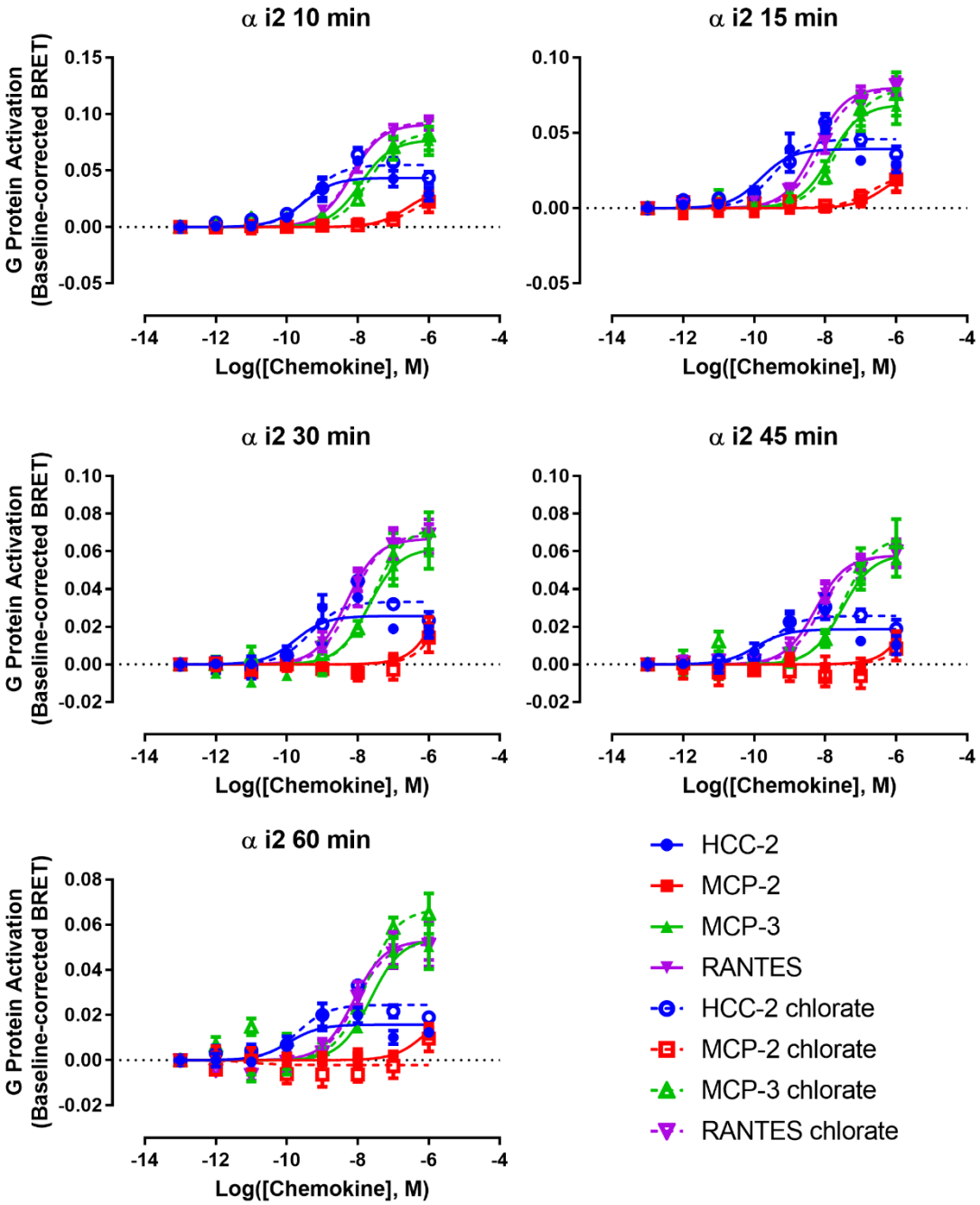

Figure II.2: $G\alpha_{i2}$ Concentration-response Curves and Timecourse. GPA was measured using His_6-c-Myc-CCR1 Flp-In T-REx HEK 293 cells and $G\alpha_{i2}$. Transfections were performed as described in Chapter 2, section 2.7.6. Each graph shows, for a given time after addition of chemokines, the concentration-response data for four chemokines HCC-2, MCP-2, MCP-3 and RANTES using non-treated or chlorate-treated cells. Data points represent means ± SEM of at least three independent experiments performed in duplicate.

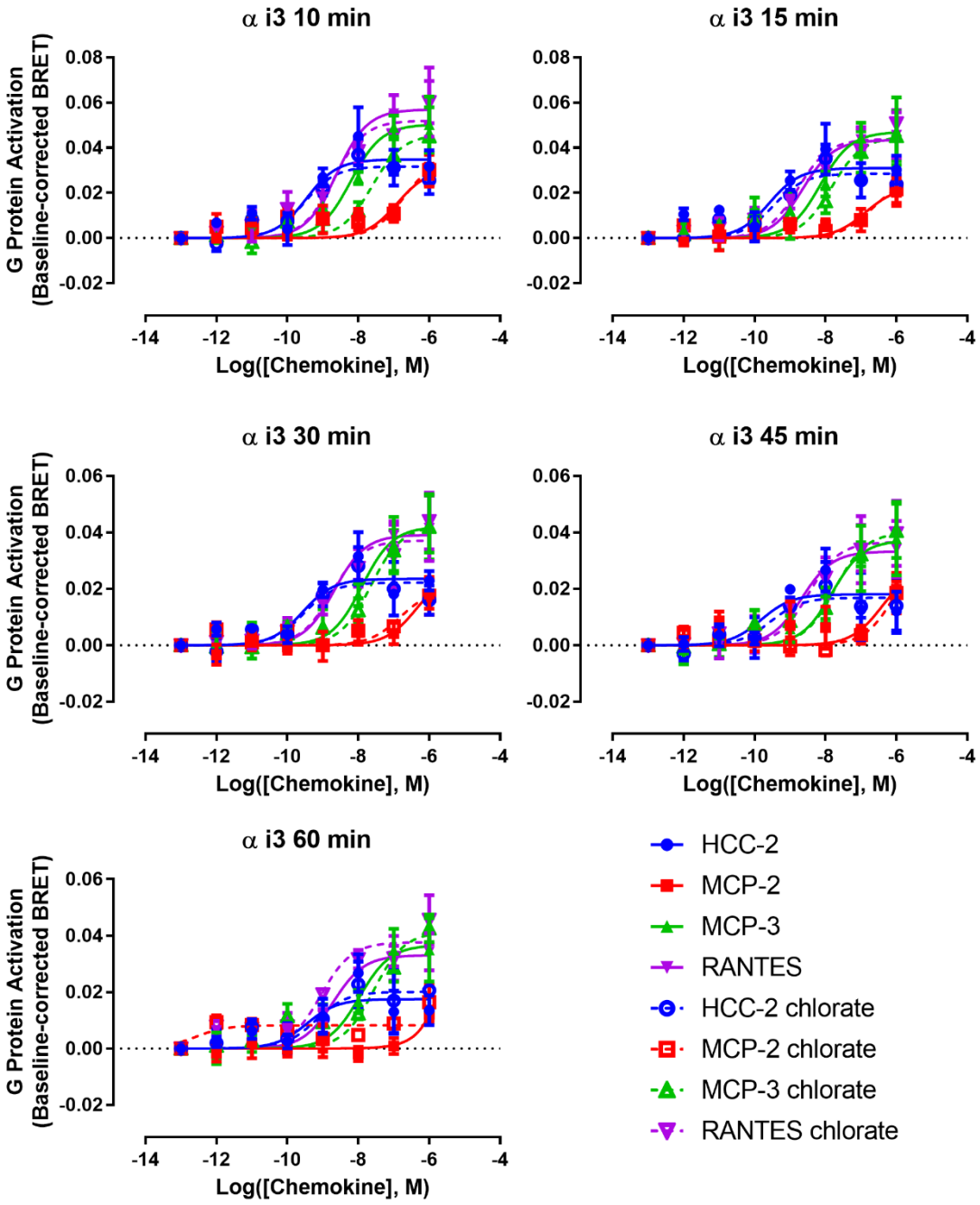

Figure II.3: $G\alpha_{i3}$ Concentration-response Curves and Timecourse. GPA was measured using His_6-c-Myc-CCR1 Flp-In T-REx HEK 293 cells and $G\alpha_{i3}$. Transfections were performed as described in Chapter 2, section 2.7.6. Each graph shows, for a given time after addition of chemokines, the concentration-response data for four chemokines HCC-2, MCP-2, MCP-3 and RANTES using non-treated or chlorate-treated cells. Data points represent means ± SEM of at least three independent experiments performed in duplicate.

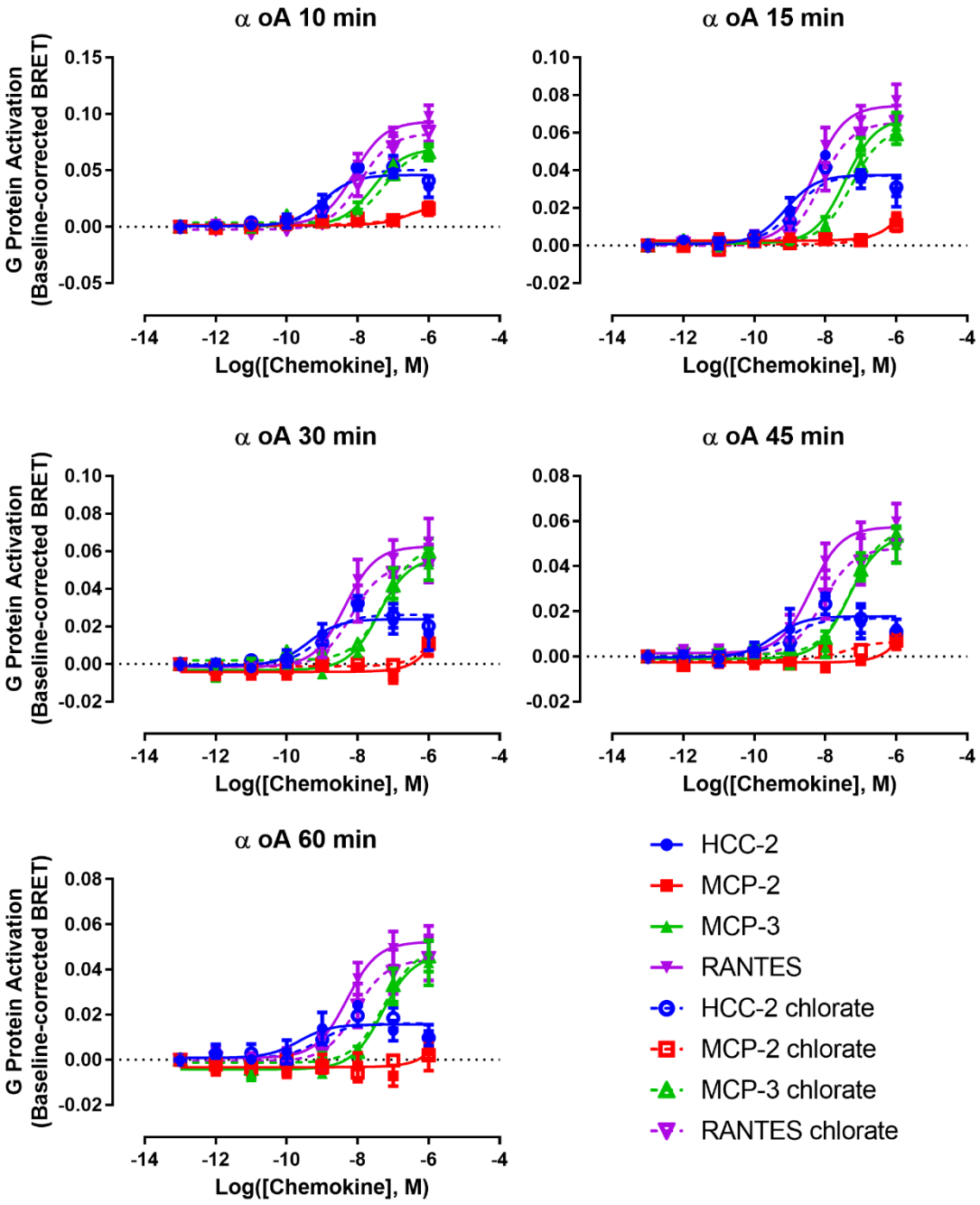

Figure II.4: $G\alpha_{oA}$ Concentration-response Curves and Timecourse. GPA was measured using His_6-c-Myc-CCR1 Flp-In T-REx HEK 293 cells and $G\alpha_{oA}$. Transfections were performed as described in Chapter 2, section 2.7.6. Each graph shows, for a given time after addition of chemokines, the concentration-response data for four chemokines HCC-2, MCP-2, MCP-3 and RANTES using non-treated or chlorate-treated cells. Data points represent means ± SEM of at least three independent experiments performed in duplicate.

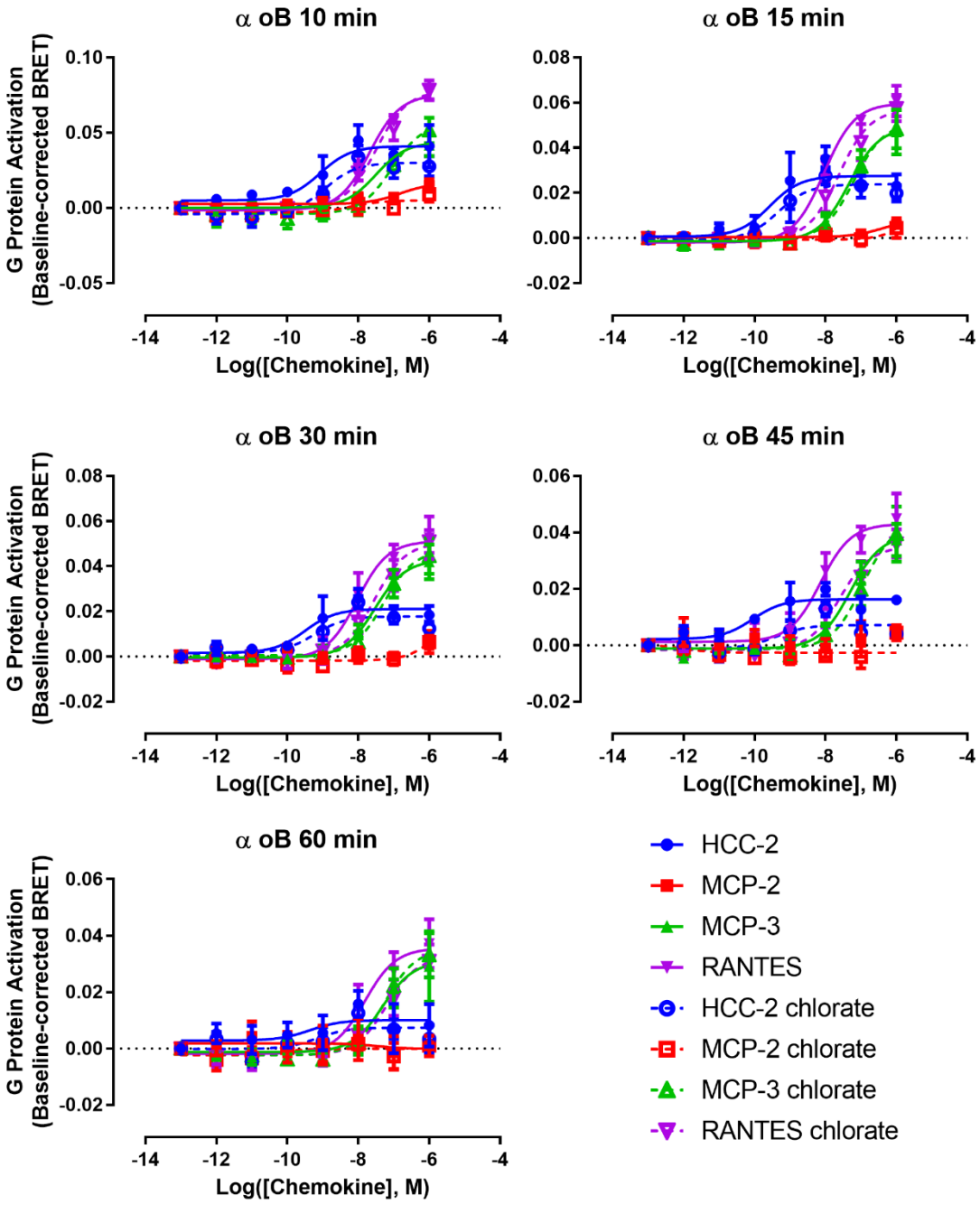

Figure II.5: $G\alpha_{oB}$ Concentration-response Curves and Timecourse. GPA was measured using His_6-c-Myc-CCR1 Flp-In T-REx HEK 293 cells and $G\alpha_{oB}$. Transfections were performed as described in Chapter 2, section 2.7.6. Each graph shows, for a given time after addition of chemokines, the concentration-response data for four chemokines HCC-2, MCP-2, MCP-3 and RANTES using non-treated or chlorate-treated cells. Data points represent means ± SEM of at least three independent experiments performed in duplicate.

Appendix III: CCR1 Activation by MCP-1/3 Chimeras

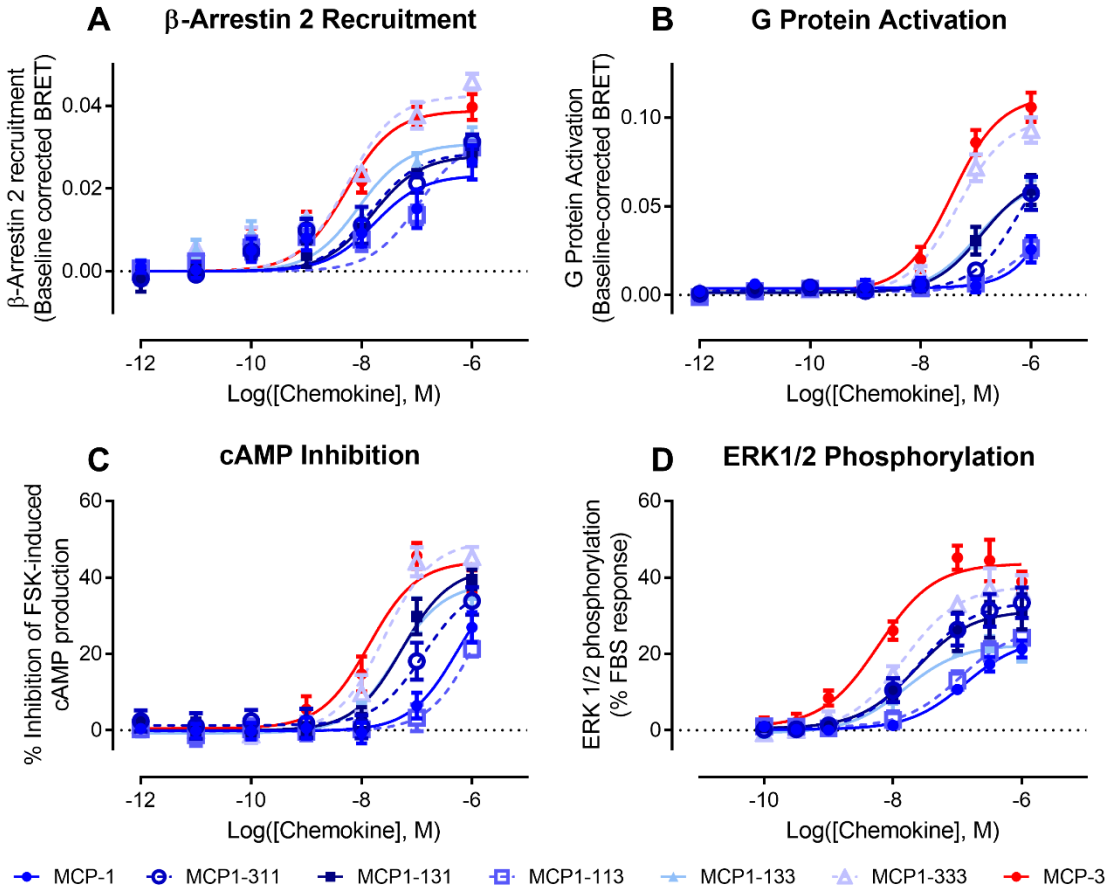

Figure III.1: Activation of CCR1 by MCP-1 Background Chimeras. (A) β-arr2 recruitment was measured using parental HEK 293 cells transiently transfected with plasmids encoding CCR1-RLuc8 and β-arr2-YFP. **(B)** GPA was measured using His_6-c-Myc-CCR1 Flp-In T-REx HEK 293 cells and several G proteins and a GRK3 constructs (as described in Chapter 2, section 2.7.6), transiently transfected. **(C)** cAMP inhibition was measured using His_6-c-Myc-CCR1 Flp-In T-REx 293 cells transiently transfected with a BRET-based cAMP biosensor. **(D)** ERK1/2 phosphorylation assay was performed using His_6-c-Myc-CCR1 Flp-In T-REx HEK 293 cells and the amount of phosphorylated ERK1/2 was measured by AlphaScreen detection. Data points represent means ± SEM of at least three independent experiments performed in duplicate.

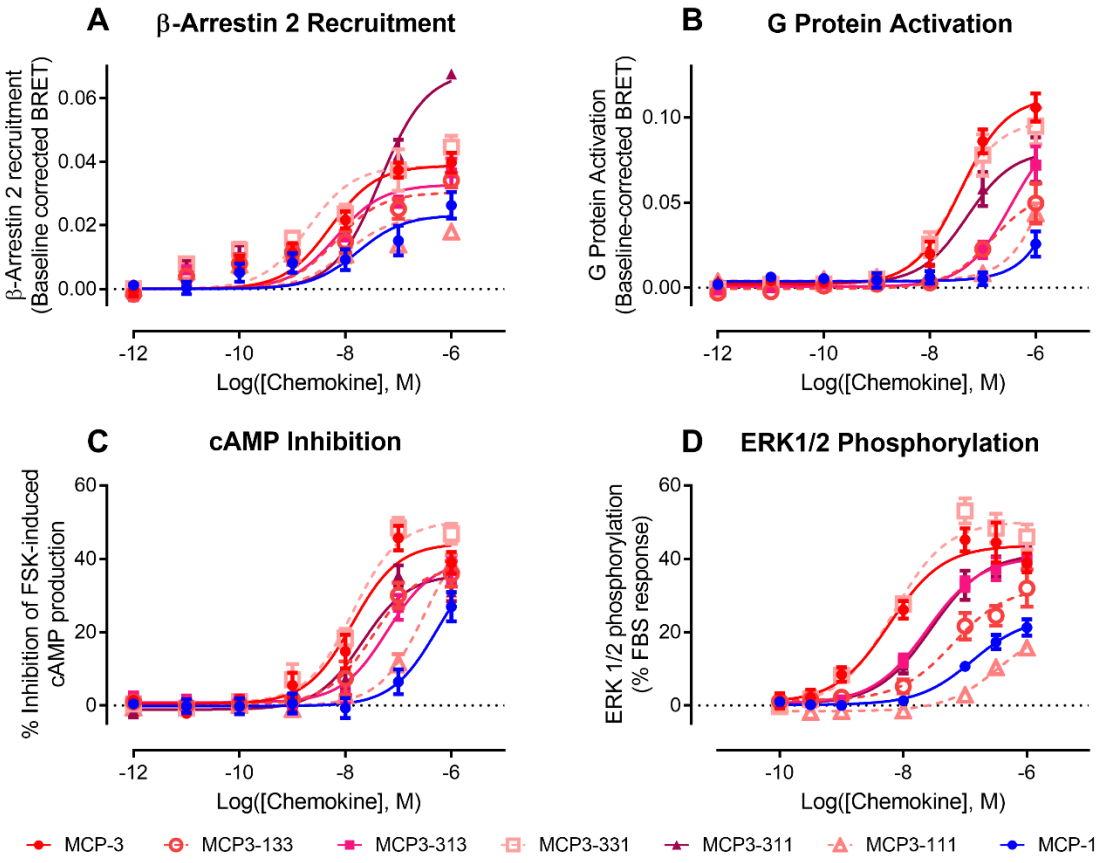

Figure III.2: Activation of CCR1 by MCP-3 Background Chimeras. (A) β-arr2 recruitment was measured using parental HEK 293 cells transiently transfected with plasmids encoding CCR1-RLuc8 and β-arr2-YFP. **(B)** GPA was measured using His_6-c-Myc-CCR1 Flp-In T-REx HEK 293 cells and several G proteins and a GRK3 constructs (as described in Chapter 2, section 2.7.6), transiently transfected. **(C)** cAMP inhibition was measured using His_6-c-Myc-CCR1 Flp-In T-REx 293 cells transiently transfected with a BRET-based cAMP biosensor. **(D)** ERK1/2 phosphorylation assay was performed using His_6-c-Myc-CCR1 Flp-In T-REx HEK 293 cells and the amount of phosphorylated ERK1/2 was measured by AlphaScreen detection. Data points represent means ± SEM of at least three independent experiments performed in duplicate.

Appendix IV: Oligonucleotide Sequences

Oligo Label	Description	Oligo Sequence	Oligo Length
HCC1-1 JS-14-01	Oligo for recursive PCR to make HCC1/CCL14 gene	5'-GGCGATATTCATATGGAGAACCTGTACTTCCAGGGCCCGTATCATCCGTCCGAATGTTGC- 3'	60
HCC1-2 JS-14-02	Oligo for recursive PCR to make HCC1/CCL14 gene	5'-CCCGTATCATCCGTCCGAATGTTGCTTCACCTATACCACGTACAAGATTCCGCGCCAGCGC- 3'	61
HCC1-3 JS-14-03	Oligo for recursive PCR to make HCC1/CCL14 gene	5'-CAAGATTCCGCGCCAGCGCATTATGGATTACTATGAAACCAATTCCCAGTGCAGCAAACCGGGC- 3'	64
HCC1-4 JS-14-04	Oligo for recursive PCR to make HCC1/CCL14 gene	5'-GGTGCACACGCTATGGCCGCGTTTCGTGATGAAGACAATGCCCGGTTTGCTGCACTGG- 3'	58
HCC1-5 JS-14-05	Oligo for recursive PCR to make HCC1/CCL14 gene	5'-CCTTGATGTAATCCTGCACCCACTTGTCGCTCGGATTGGTGCACACGCTATGGCCGC- 3'	57
HCC1-6 JS-14-06	Oligo for recursive PCR to make HCC1/CCL14 gene	5'-CGTCGGCAGCTCGAGTTAGTTTTCTTTCATATCCTTGATGTAATCCTGCACCCACTTGTCG- 3'	61
HCC2-1 JS-14-07	Oligo for recursive PCR to make HCC2/CCL15 gene	5'-GGCGATATTCATATGGAGAACCTGTACTTCCAGCATTTTGCCGCGGATTGTTGCACCAGC- 3'	60
HCC2-2 JS-14-08	Oligo for recursive PCR to make HCC2/CCL15 gene	5'-CCGCGGATTGTTGCACCAGCTACATCAGCCAGAGCATTCCGTGCAGCCTGATGAAAAGC- 3'	59
HCC2-3 JS-14-09	Oligo for recursive PCR to make HCC2/CCL15 gene	5'-GCATTCCGTGCAGCCTGATGAAAAGCTACTTCGAAACGTCCAGCGAATGCAGCAAACCGGGCG- 3'	63
HCC2-4 JS-14-10	Oligo for recursive PCR to make HCC2/CCL15 gene	5'-CGCGCACACCTGGCGGCCTTTCTTGGTCAGGAAGATGACGCCCGGTTTGCTGCATTCGC- 3'	59
HCC2-5 JS-14-11	Oligo for recursive PCR to make HCC2/CCL15 gene	5'-CAGTTTCTTCATGCAATCCTGCACGCCCGGGCCGCTCGGTTTCGCGCACACCTGGCGG- 3'	58
HCC2-6 JS-14-12	Oligo for recursive PCR to make HCC2/CCL15 gene	5'-CGTCGGCAGCTCGAGTTAAATGGAATACGGTTTCAGTTTCTTCATGCAATCCTGCACGCCC- 3'	61

MPIF1-0 JS-14-13	Oligo for recursive PCR to make MPIF1/CCL23 gene	5'-GGCGATATTCATATGGAGAACCTGTACTTCCAGATGGATCGCTTCCATGCCACGTC- 3'	56
MPIF1-1 JS-14-14	Oligo for recursive PCR to make MPIF1/CCL23 gene	5'-GGATCGCTTCCATGCCACGTCGGCGGATTGTTGCATTAGCTATACCCCGCG- 3'	51
MPIF1-2 JS-14-15	Oligo for recursive PCR to make MPIF1/CCL23 gene	5'-GGATTGTTGCATTAGCTATACCCCGCGCTCCATTCCGTGCAGCCTGCTGGAGAGCTACTTCGAGACC- 3'	67
MPIF1-3 JS-14-16	Oligo for recursive PCR to make MPIF1/CCL23 gene	5'-CCTGCTGGAGAGCTACTTCGAGACCAATAGCGAATGCAGCAAACCGGGCGTGATCTTCCTGAC- 3'	63
MPIF1-4 JS-14-17	Oligo for recursive PCR to make MPIF1/CCL23 gene	5'-CCTGCTTGTCGCTCGGATTCGCGCAGAAGCGGCGGCCTTTCTTGGTCAGGAAGATCACGCCCGG- 3'	64
MPIF1-5 JS-14-18	Oligo for recursive PCR to make MPIF1/CCL23 gene	5'-GCGGGTATCCAGTTTCAGCATACGCATACAGACCTGCACCTGCTTGTCGCTCGGATTCG- 3'	59
MPIF1-6 JS-14-19	Oligo for recursive PCR to make MPIF1/CCL23 gene	5'-CGTCGGCAGCTCGAGTTAGTTCTTGCGCGTCTTGATGCGGGTATCCAGTTTCAGCATACGC-3'	61
CCR1/5-0 JS-14-20	Oligo for recursive PCR to make His_6-c-Myc-CCR1/5 gene	5'-AGCGCGGGCAAGCTTATGGGCGAGCAGAAACTTATCTCTGAAGAAGATCTGGGCAGCGCGCACC-3'	64
CCR1-1 JS-14-21	Oligo for recursive PCR to make His_6-c-Myc-CCR1 gene	5'-GGGCAGCGCGCACCATCATCATCATCACAGCGGCGCAATGGAAACTCCAAACACCACAGAGGACTATG-3'	68
CCR1-2 JS-14-22	Oligo for recursive PCR to make His_6-c-Myc-CCR1 gene	5'-CCCTCTAGACTCGAGTCAGAACCCAGCAGAGAGTTCATGCTCCCC-3'	45

Table IV.1: Oligonucleotide List for HCC-1, HCC-2, MPIF-1 and CCR1 Cloning. The ordering name, description, sequence and length of each oligo used in this thesis are provided.

Appendix V: Supplementary Material for Chapter 5

Supplementary Material for:

Ticks from Diverse Genera Encode Chemokine-Inhibitory Evasin Proteins

Jenni Hayward, **Julie Sanchez**, **Andrew Perry**, **Cheng Huang**, **Manuel Rodriguez Valle**, **Meritxell Canals**, **Richard J. Payne** and **Martin J. Stone**

Supplementary Table

Supplementary Figures

Table S1: Accession numbers of all sequences in the final evasin database

Sequence ID	Database	Species
iho_saliv_g12712t000003	*I. holocyclus* transcriptome	*Ixodes holocyclus*
iho_saliv_g1036t000001	*I. holocyclus* transcriptome	*Ixodes holocyclus*
iho_saliv_g24745t000001	*I. holocyclus* transcriptome	*Ixodes holocyclus*
rmi_SG_T5290	*R. microplus* transcriptome	*Rhipicephalus microplus*
JAA60714.1	Genbank	*Rhipicephalus pulchellus*
G3MSV3_9ACAR	UniprotKB	*Amblyomma maculatum*
G3ML03_9ACAR	UniprotKB	*Amblyomma maculatum*
G3MSV4_9ACAR	UniprotKB	*Amblyomma maculatum*
JAA57173.1	Genbank	*Rhipicephalus pulchellus*
JAG92275.1	Genbank	*Amblyomma americanum*
JAA60749.1	Genbank	*Rhipicephalus pulchellus*
JAA71836.1	Genbank	*Ixodes ricinus*
JAA70458.1	Genbank	*Ixodes ricinus*
JAA65577.1	Genbank	*Ixodes ricinus*
JAA67769.1	Genbank	*Ixodes ricinus*
JAA67752.1	Genbank	*Ixodes ricinus*
JAA67622.1	Genbank	*Ixodes ricinus*
JAB77289.1	Genbank	*Ixodes ricinus*
JAA67762.1	Genbank	*Ixodes ricinus*
JAA67760.1	Genbank	*Ixodes ricinus*
JAB76903.1	Genbank	*Ixodes ricinus*
JAC18893.1	Genbank	*Amblyomma cajennense*
JAC24826.1	Genbank	*Amblyomma parvum*
JAC27776.1	Genbank	*Amblyomma triste*
JAC27143.1	Genbank	*Amblyomma parvum*
JAC27149.1	Genbank	*Amblyomma parvum*
JAG91851.1	Genbank	*Amblyomma americanum*
JAC18902.1	Genbank	*Amblyomma cajennense*
JAG91726.1	Genbank	*Amblyomma americanum*
JAC19610.1	Genbank	*Amblyomma cajennense*
JAC18918.1	Genbank	*Amblyomma cajennense*
JAC18937.1	Genbank	*Amblyomma cajennense*
JAC19608.1	Genbank	*Amblyomma cajennense*
JAC19605.1	Genbank	*Amblyomma cajennense*
JAC19611.1	Genbank	*Amblyomma cajennense*
JAC19604.1	Genbank	*Amblyomma cajennense*
JAA60767.1	Genbank	*Rhipicephalus pulchellus*
JAC28501.1	Genbank	*Amblyomma triste*
JAC27742.1	Genbank	*Amblyomma triste*
JAC19000.1	Genbank	*Amblyomma cajennense*
JAC18987.1	Genbank	*Amblyomma cajennense*

JAC27176.1	Genbank	*Amblyomma parvum*
JAC27182.1	Genbank	*Amblyomma parvum*
JAC19683.1	Genbank	*Amblyomma cajennense*
JAC19684.1	Genbank	*Amblyomma cajennense*
JAC19139.1	Genbank	*Amblyomma cajennense*
JAC19681.1	Genbank	*Amblyomma cajennense*
JAC19128.1	Genbank	*Amblyomma cajennense*
JAC19685.1	Genbank	*Amblyomma cajennense*
JAC27265.1	Genbank	*Amblyomma parvum*
JAC27987.1	Genbank	*Amblyomma triste*
JAC23907.1	Genbank	*Amblyomma cajennense*
JAC27222.1	Genbank	*Amblyomma parvum*
JAG92131.1	Genbank	*Amblyomma americanum*
JAA60809.1	Genbank	*Rhipicephalus pulchellus*
G3MSY7	UniprotKB	*Amblyomma maculatum*
JAC30584.1	Genbank	*Amblyomma triste*
G3MSY6	UniprotKB	*Amblyomma maculatum*
JAC30583.1	Genbank	*Amblyomma triste*
G3MSY5	UniprotKB	*Amblyomma maculatum*
JAC23894.1	Genbank	*Amblyomma cajennense*
JAC23897.1	Genbank	*Amblyomma cajennense*
JAC23881.1	Genbank	*Amblyomma cajennense*
JAC23884.1	Genbank	*Amblyomma cajennense*
JAC23883.1	Genbank	*Amblyomma cajennense*
JAC23886.1	Genbank	*Amblyomma cajennense*
JAC23882.1	Genbank	*Amblyomma cajennense*
JAC23885.1	Genbank	*Amblyomma cajennense*
JAC23887.1	Genbank	*Amblyomma cajennense*
JAG92204.1	Genbank	*Amblyomma americanum*
JAG92196.1	Genbank	*Amblyomma americanum*
JAC23903.1	Genbank	*Amblyomma cajennense*
JAC23898.1	Genbank	*Amblyomma cajennense*
JAC26565.1	Genbank	*Amblyomma parvum*
JAC30582.1	Genbank	*Amblyomma triste*
JAC30579.1	Genbank	*Amblyomma triste*
JAC30580.1	Genbank	*Amblyomma triste*
JAC30575.1	Genbank	*Amblyomma triste*
JAC30578.1	Genbank	*Amblyomma triste*
JAC30574.1	Genbank	*Amblyomma triste*
JAC30577.1	Genbank	*Amblyomma triste*
JAC30576.1	Genbank	*Amblyomma triste*
JAA56354.1	Genbank	*Rhipicephalus pulchellus*
C9W1Q9	UniprotKB	*Rhipicephalus sanguineus*
rmi_SG_T727	*R. microplus* transciptome	*Rhipicephalus microplus*
rmi_SG_T822	*R. microplus* transciptome	*Rhipicephalus microplus*

JAA60776.1	Genbank	*Rhipicephalus pulchellus*
JAA60817.1	Genbank	*Rhipicephalus pulchellus*
JAA60787.1	Genbank	*Rhipicephalus pulchellus*
JAA60785.1	Genbank	*Rhipicephalus pulchellus*
JAA60838.1	Genbank	*Rhipicephalus pulchellus*
JAA65011.1	Genbank	*Rhipicephalus pulchellus*
GADI01004698.1/1-98	VectorBase	*Ixodes ricinus*
GADI01004698.1/1-98	VectorBase	*Ixodes ricinus*
GADI01007577.1/1-100	VectorBase	*Ixodes ricinus*
GADI01007577.1/1-100	VectorBase	*Ixodes ricinus*
Q09JP0	UniprotKB	*Argas monolakensis (Mono lake bird tick)*
JAG92081.1	Genbank	*Amblyomma americanum*
JAC27926.1	Genbank	*Amblyomma triste*
JAC19108.1	Genbank	*Amblyomma cajennense*
JAC27217.1	Genbank	*Amblyomma parvum*
GBIH01002127.1/1-69	VectorBase	*Ixodes ricinus*
GBIH01002127.1/1-69	VectorBase	*Ixodes ricinus*
JAC19007.1	Genbank	*Amblyomma cajennense*
JAG92086.1	Genbank	*Amblyomma americanum*
rmi_SG_T6156	*R. microplus* transciptome	*Rhipicephalus microplus*
JAC26686.1	Genbank	*Amblyomma parvum*
JAC26685.1	Genbank	*Amblyomma parvum*
JAA60747.1	Genbank	*Rhipicephalus pulchellus*
JAA53866.1	Genbank	*Rhipicephalus pulchellus*
JAA64989.1	Genbank	*Rhipicephalus pulchellus*
JAA54118.1	Genbank	*Rhipicephalus pulchellus*
JAC30561.1	Genbank	*Amblyomma triste*
G3MKY5_9ACAR	UniprotKB	*Amblyomma maculatum*
JAC23850.1	Genbank	*Amblyomma cajennense*
JAC30571.1	Genbank	*Amblyomma triste*
JAC30557.1	Genbank	*Amblyomma triste*
JAC30565.1	Genbank	*Amblyomma triste*
JAC30564.1	Genbank	*Amblyomma triste*
JAC30567.1	Genbank	*Amblyomma triste*
G3ML31_9ACAR	UniprotKB	*Amblyomma maculatum*
JAC24466.1	Genbank	*Amblyomma cajennense*
JAC24465.1	Genbank	*Amblyomma cajennense*
JAC27213.1	Genbank	*Amblyomma parvum*
JAC26564.1	Genbank	*Amblyomma parvum*
JAC23849.1	Genbank	*Amblyomma cajennense*
JAC23848.1	Genbank	*Amblyomma cajennense*
JAC23847.1	Genbank	*Amblyomma cajennense*
JAG92108.1	Genbank	*Amblyomma americanum*
JAC27053.1	Genbank	*Amblyomma parvum*

JAC27057.1	Genbank	*Amblyomma parvum*
JAC27055.1	Genbank	*Amblyomma parvum*
JAC24473.1	Genbank	*Amblyomma cajennense*
JAC24470.1	Genbank	*Amblyomma cajennense*
JAC24468.1	Genbank	*Amblyomma cajennense*
JAC24471.1	Genbank	*Amblyomma cajennense*
JAC24464.1	Genbank	*Amblyomma cajennense*
JAC24462.1	Genbank	*Amblyomma cajennense*
JAC24461.1	Genbank	*Amblyomma cajennense*
JAC24463.1	Genbank	*Amblyomma cajennense*
JAC24472.1	Genbank	*Amblyomma cajennense*
JAC24467.1	Genbank	*Amblyomma cajennense*
JAC27054.1	Genbank	*Amblyomma parvum*
JAC24469.1	Genbank	*Amblyomma cajennense*
G3MKY4	UniprotKB	*Amblyomma maculatum*
JAC30696.1	Genbank	*Amblyomma triste*
JAC30698.1	Genbank	*Amblyomma triste*
JAC30697.1	Genbank	*Amblyomma triste*
JAC26666.1	Genbank	*Amblyomma parvum*
G3MKK4	UniprotKB	*Amblyomma maculatum*
G3MFD0_9ACAR	UniprotKB	*Amblyomma maculatum*
JAC30642.1	Genbank	*Amblyomma triste*
JAC23986.1	Genbank	*Amblyomma cajennense*
JAC23985.1	Genbank	*Amblyomma cajennense*
JAG92346.1	Genbank	*Amblyomma americanum*
JAC23940.1	Genbank	*Amblyomma cajennense*
JAC23941.1	Genbank	*Amblyomma cajennense*
JAG92343.1	Genbank	*Amblyomma americanum*
JAC29290.1	Genbank	*Amblyomma triste*
JAC29289.1	Genbank	*Amblyomma triste*
rmi_SG_T6169	*R. microplus* transciptome	*Rhipicephalus microplus*
JAB70277.1	Genbank	*Ixodes ricinus*
JAA71053.1	Genbank	*Ixodes ricinus*
JAA70397.1	Genbank	*Ixodes ricinus*
iho_VISC_g29118t000004_1	*I. holocyclus* transcriptome	*Ixodes holocyclus*
iho_SG_g24826t000001_3	*I. holocyclus* transcriptome	*Ixodes holocyclus*
iho_saliv_g3982t000001	*I. holocyclus* transcriptome	*Ixodes holocyclus*
iho_VISC_g12895t000001_1	*I. holocyclus* transcriptome	*Ixodes holocyclus*
iho_VISC_g21431t000002_4	*I. holocyclus* transcriptome	*Ixodes holocyclus*
iho_saliv_g40346t000001	*I. holocyclus* transcriptome	*Ixodes holocyclus*
iho_saliv_g7041t000006	*I. holocyclus* transcriptome	*Ixodes holocyclus*
JAA60771.1	Genbank	*Rhipicephalus pulchellus*
P0C8E9	UniprotKB	*Rhipicephalus sanguineus*
JAA54802.1	Genbank	*Rhipicephalus pulchellus*
JAA60789.1	Genbank	*Rhipicephalus pulchellus*

JAA60818.1	Genbank	*Rhipicephalus pulchellus*
C9W1C3	UniprotKB	*Rhipicephalus sanguineus*
JAA60799.1	Genbank	*Rhipicephalus pulchellus*
JAA60777.1	Genbank	*Rhipicephalus pulchellus*
C9W1D9	UniprotKB	*Rhipicephalus sanguineus*
iho_saliv_g33416t000001	*I. holocyclus* transcriptome	*Ixodes holocyclus*
transcriptome	*I. holocyclus* transcriptome	*Ixodes holocyclus*
JAC93358.1	Genbank	*Ixodes ricinus*
GBIH01001339.1/1-150	VectorBase	*Ixodes ricinus*
GBIH01001339.1/1-150	VectorBase	*Ixodes ricinus*
GBIH01001345.1/1-143	VectorBase	*Ixodes ricinus*
GBIH01001345.1/1-143	VectorBase	*Ixodes ricinus*
JAA65551.1	Genbank	*Ixodes ricinus*
JAC92770.1	Genbank	*Ixodes ricinus*
GBIH01001335.1/1-152	VectorBase	*Ixodes ricinus*
GBIH01001335.1/1-152	VectorBase	*Ixodes ricinus*
GADI01003281.1/1-157	VectorBase	*Ixodes ricinus*
GADI01003281.1/1-157	VectorBase	*Ixodes ricinus*
JAA67927.1	Genbank	*Ixodes ricinus*
GADI01006018.1/1-162	VectorBase	*Ixodes ricinus*
GADI01006018.1/1-162	VectorBase	*Ixodes ricinus*
JAC93377.1	Genbank	*Ixodes ricinus*
GADI01003252.1/1-154	VectorBase	*Ixodes ricinus*
GADI01003252.1/1-154	VectorBase	*Ixodes ricinus*
GADI01003291.1/1-158	VectorBase	*Ixodes ricinus*
GADI01003291.1/1-158	VectorBase	*Ixodes ricinus*
JAC93372.1	Genbank	*Ixodes ricinus*
JAC93373.1	Genbank	*Ixodes ricinus*
GBBN01015718.1/1-151	VectorBase	*Ixodes scapularis*
GBBN01015718.1/1-151	VectorBase	*Ixodes scapularis*
JAA67835.1	Genbank	*Ixodes ricinus*
JAA65508.1	Genbank	*Ixodes ricinus*
JAC93369.1	Genbank	*Ixodes ricinus*
JAA71946.1	Genbank	*Ixodes ricinus*
JAC93366.1	Genbank	*Ixodes ricinus*
GBIH01001350.1/1-141	VectorBase	*Ixodes ricinus*
GBIH01001350.1/1-141	VectorBase	*Ixodes ricinus*
JAC93364.1	Genbank	*Ixodes ricinus*
JAC93379.1	Genbank	*Ixodes ricinus*
JAC93396.1	Genbank	*Ixodes ricinus*
JAA65581.1	Genbank	*Ixodes ricinus*
JAC93383.1	Genbank	*Ixodes ricinus*
JAA68201.1	Genbank	*Ixodes ricinus*
JAA67791.1	Genbank	*Ixodes ricinus*
JAA65625.1	Genbank	*Ixodes ricinus*

GBIH01001355.1/1-133	VectorBase	*Ixodes ricinus*
GBIH01001355.1/1-133	VectorBase	*Ixodes ricinus*
JAA70749.1	Genbank	*Ixodes ricinus*
GBIH01001354.1/1-133	VectorBase	*Ixodes ricinus*
GBIH01001354.1/1-133	VectorBase	*Ixodes ricinus*
JAC93374.1	Genbank	*Ixodes ricinus*
JAA67827.1	Genbank	*Ixodes ricinus*
GADI01003397.1/1-173	VectorBase	*Ixodes ricinus*
GADI01003397.1/1-173	VectorBase	*Ixodes ricinus*
JAG92134.1	Genbank	*Amblyomma americanum*
JAA55737.1	Genbank	*Rhipicephalus pulchellus*
JAA68608.1	Genbank	*Ixodes ricinus*
JAB75472.1	Genbank	*Ixodes ricinus*
JAG92019.1	Genbank	*Amblyomma americanum*
A0A0C9R596	UniprotKB	*Amblyomma americanum*
iho_visc_g26315t000006	*I. holocyclus* transcriptome	*Ixodes holocyclus*
JAG91989.1	Genbank	*Amblyomma americanum*
JAC19654.1	Genbank	*Amblyomma cajennense*
JAC24842.1	Genbank	*Amblyomma parvum*
JAC27912.1	Genbank	*Amblyomma triste*
JAC27939.1	Genbank	*Amblyomma triste*
JAC27940.1	Genbank	*Amblyomma triste*
JAB71388.1	Genbank	*Ixodes ricinus*
JAA68126.1	Genbank	*Ixodes ricinus*
JAB70275.1	Genbank	*Ixodes ricinus*
JAC92340.1	Genbank	*Ixodes ricinus*
JAB71160.1	Genbank	*Ixodes ricinus*
P0C8E7	UniprotKB	*Rhipicephalus sanguineus*
C9W1N8	UniprotKB	*Rhipicephalus sanguineus*
JAA60786.1	Genbank	*Rhipicephalus pulchellus*
JAC19009.1	Genbank	*Amblyomma cajennense*
JAG92268.1	Genbank	*Amblyomma americanum*
JAC27175.1	Genbank	*Amblyomma parvum*
JAC27188.1	Genbank	*Amblyomma parvum*
JAC27189.1	Genbank	*Amblyomma parvum*
JAC27187.1	Genbank	*Amblyomma parvum*
JAC18992.1	Genbank	*Amblyomma cajennense*
JAC18993.1	Genbank	*Amblyomma cajennense*
JAC19634.1	Genbank	*Amblyomma cajennense*
JAG91729.1	Genbank	*Amblyomma americanum*
JAG91744.1	Genbank	*Amblyomma americanum*
JAG91651.1	Genbank	*Amblyomma americanum*
JAC27763.1	Genbank	*Amblyomma triste*
JAC27735.1	Genbank	*Amblyomma triste*
JAG92120.1	Genbank	*Amblyomma americanum*

JAC27963.1	Genbank	*Amblyomma triste*
JAC19052.1	Genbank	*Amblyomma cajennense*
JAG92333.1	Genbank	*Amblyomma americanum*
JAC27944.1	Genbank	*Amblyomma triste*
JAG92380.1	Genbank	*Amblyomma americanum*
JAC19034.1	Genbank	*Amblyomma cajennense*
JAC19650.1	Genbank	*Amblyomma cajennense*
JAC19663.1	Genbank	*Amblyomma cajennense*
JAC19655.1	Genbank	*Amblyomma cajennense*
JAC19653.1	Genbank	*Amblyomma cajennense*
JAC19651.1	Genbank	*Amblyomma cajennense*
JAC19652.1	Genbank	*Amblyomma cajennense*

Figure S1. Simulated fluorescence anisotropy binding curves. Shown are the fluorescence anisotropy competitive displacement curves simulated for binding of evasins to chemokines with 10 different K_d values (in the range 1-1000 nM, different curves on the same panel) and for four different binding affinities between the chemokine and the fluorescent peptide (Fl-Pep) in the four panels (20 nM, top panel; 50 nM, second panel; 100 nM, third panel; and 200 nM, bottom panel). In all simulations the concentrations of chemokine (100 nM) and Fl-Pep (10 nM) are held constant.

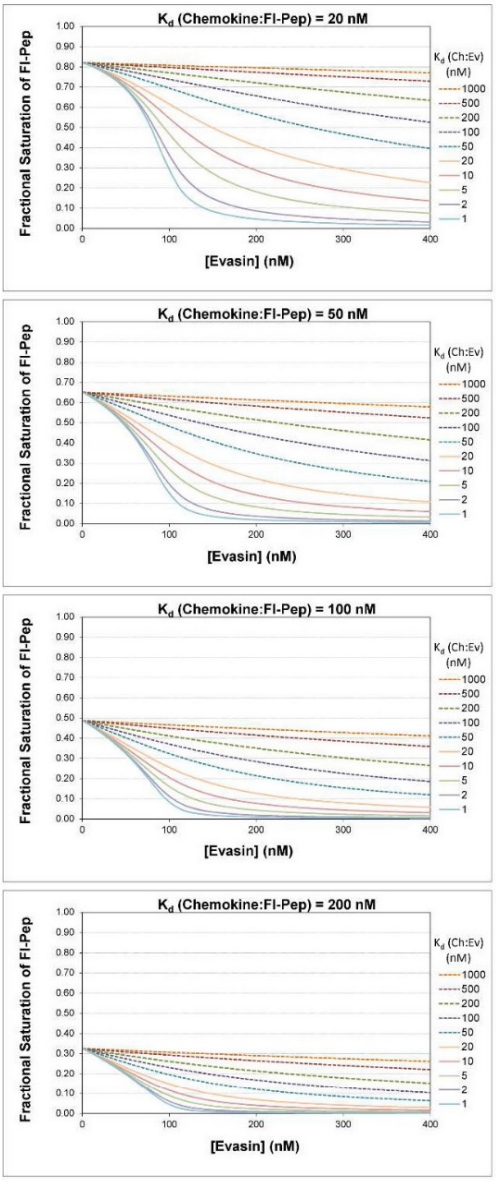

Figure S2. Chemokine binding curves of candidate evasins. Shown are the fluorescence anisotropy competitive displacement curves obtained for binding of nine evasin candidates against a panel of 6 human CC chemokines. Data points represent the mean anisotropy ± SEM from duplicate assays performed three times independently. Solid lines are the best fits to a competitive displacement model (see *Experimental Procedures* for details).

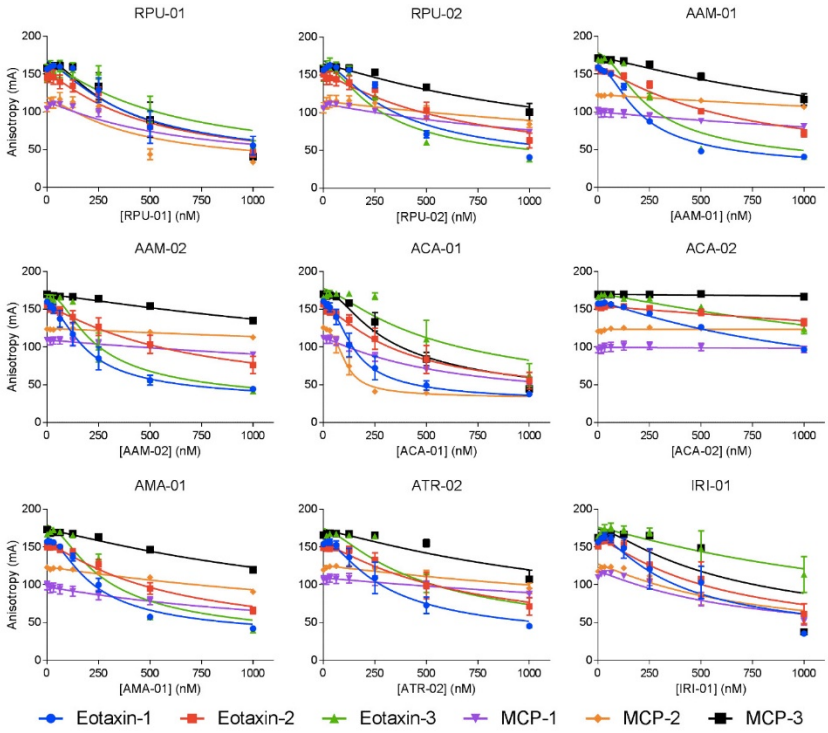

Figure S3. Chemokine binding affinity profiles of purified evasins. *(A-E)*Affinities (pK_d values), derived from the competitive fluorescence anisotropy binding curves (Figs. 3 and 4) for binding of purified evasins to each of five CC chemokines. Each panel shows the binding profile for one evasin: *(A)* RSA evasin-4, *(B)* RPU-01, *(C)* ACA-01, *(D)* IRI-01, and *(E)* IHO-01. Data represent the average ± SEM of values from three independent experiments, each recorded in duplicate. Significance (multiple t-tests) is shown as * p< 0.05, ** p<0.01 and *** p < 0.001.

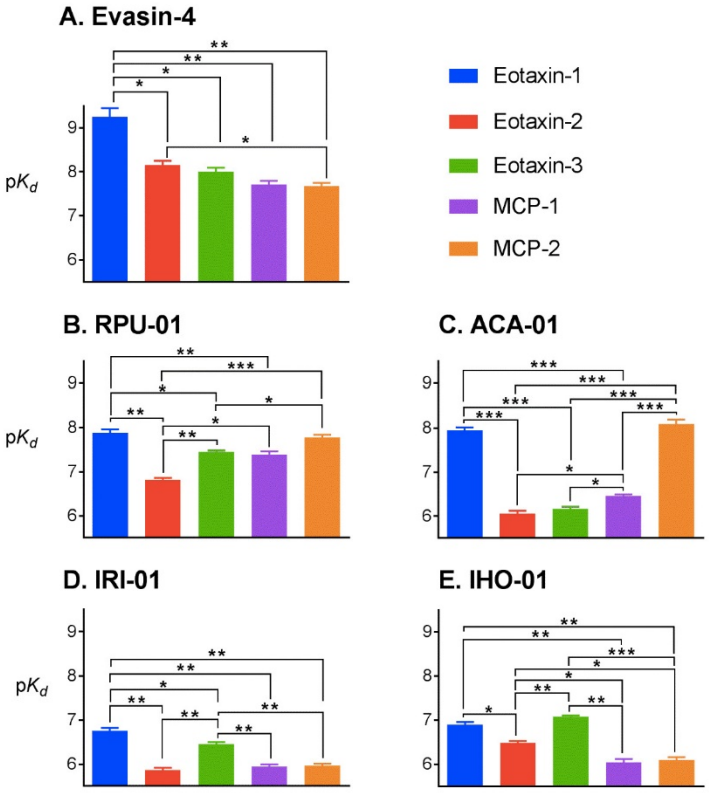

Figure S4. Chemokine inhibition of forskolin-induced cAMP production. Shown are concentration-response curves for inhibition of forskolin (10 µM)-induced production of cAMP in: *(A)* cMyc-FLAG-CCR2 TREx HEK293 cells by the chemokines MCP-1 and MCP-2; or *(B)* cMyc-FLAG-CCR3 FlpIn TREx HEK293 cells by the chemokines eotaxin-1 and eotaxin-2. cAMP was detected via a BRET biosensor, as described in the *Experimental Procedures*. Data points represent the average ± SEM of values from three independent experiments, each recorded in duplicate.